Development of a Novel Technology of Atomic Layer Epitaxy for III-V Compound Semiconductors and Study on its Growth Mechanism

Yoshiki Sakuma

OSAKA UNIVERSITY
GRADUATE SCHOOL OF ENGINEERING SCIENCE
DEPARTMENT OF PHYSICAL SCIENCE
DIVISION OF MATERIALS PHYSICS

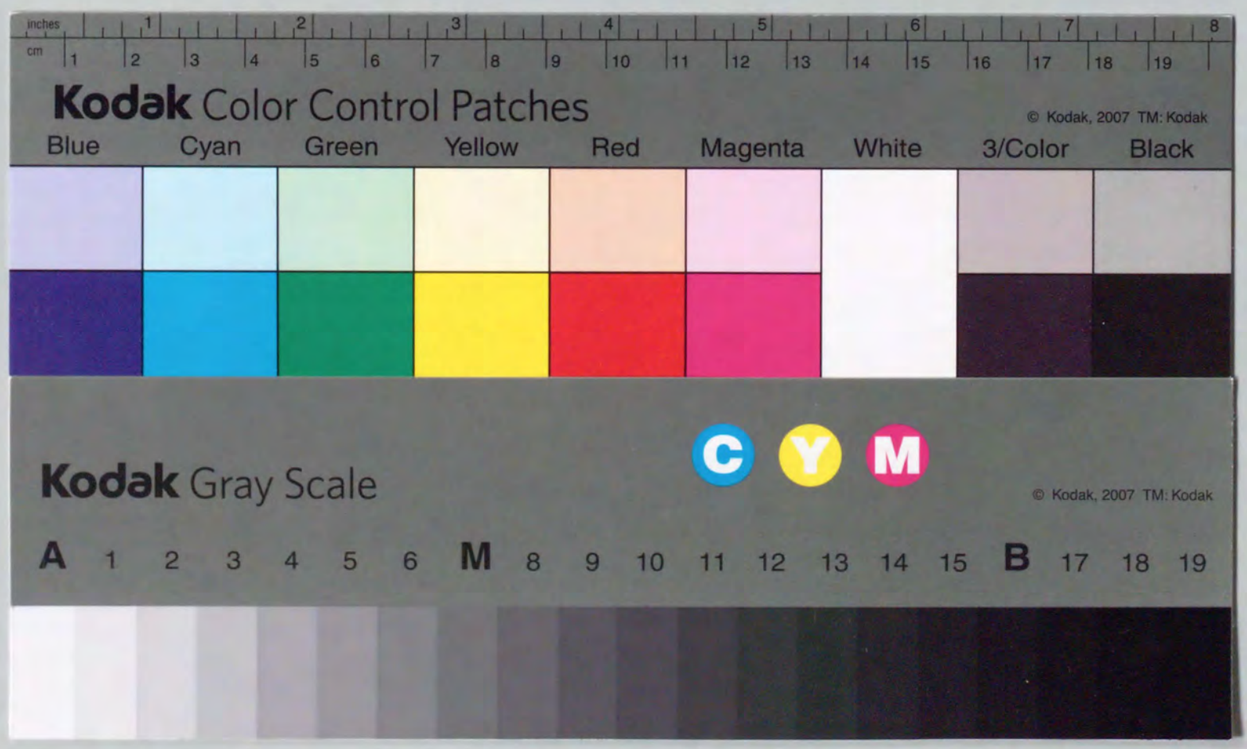

Development of a Novel Technology of Atomic Layer Epitaxy for III-V Compound Semiconductors and Study on its Growth Mechanism

Yoshiki Sakuma

Fujitsu Laboratories Ltd.
10-1 Morinosato-Wakamiya, Atsugi 243-01, Japan

October 22, 1997

OSAKA UNIVERSITY
GRADUATE SCHOOL OF ENGINEERING SCIENCE
DEPARTMENT OF PHYSICAL SCIENCE
DIVISION OF MATERIALS PHYSICS

ABSTRACT

This thesis provides detailed studies on a "Pulsed-Jet Epitaxy" (PJE), a novel technology of atomic layer epitaxy (ALE) of III-V compound semiconductors based on low-pressure metalorganic vapor phase epitaxy. ALE or PJE is a fascinating growth method in which growth proceeds in a layer-by-layer fashion due to the inherent self-limiting growth mechanism. The course of research and development of PJE, the mechanism of self-limiting growth, and the applications to device fabrication process are described. This thesis is a review of the work performed at Fujitsu Laboratories Ltd. in the 8 years between 1987 and 1994. It consists of nine chapters.

Chapter 1 describes the background and purpose of this study. First, in order to clarify the technological importance of ALE or PJE, the limitations and disadvantages of the well-known, state-of-the-art growth techniques are discussed. Then, the principles of ALE and self-limiting growth are explained. Finally, some ALE methods reported so far are introduced and the inevitable problems in each method are revealed.

In Chapter 2, fundamentals of the PJE technique are reported. First, a definition of PJE is given and some advantages of this novel ALE method are clarified. Then, the growth apparatus of PJE is described in detail. Finally, the experimental procedure in this work is described.

In Chapter 3, self-limiting growth of III-V binary compounds using PJE is described. Experimental results on GaAs, GaP, InAs, and InP growth are shown in detail. For some materials, results are compared with horizontal-type and chimney-type reactors. From these studies, it is discussed that how the "ALE window", which is the range of growth conditions leading to self-limiting, is affected by the reactor design.

Chapter 4 elucidates the mechanism of the self-limiting process. Important results on the *in-situ* analyses of surface adsorbates during PJE are shown using X-ray photoelectron spectroscopy. A "selective adsorption model" is proposed to explain the self-limiting deposition

of nonvolatile group-III atoms such as Ga and In. Finally, several experimental facts that support the proposed selective adsorption model are stated.

The role of group-III precursors on the self-limiting growth mechanism is discussed in Chapter 5. Growth results are shown with some organometals, such as trimethylgallium (TMGa), triethylgallium (TEGa), ethyldimethylgallium (EDMGa), triisobutylgallium (TiBGa), and galliumtrichloride ($GaCl_3$). It is clearly shown that the site selectivity of Ga precursors between Ga and As atoms on the growth surface is important to understand the self-limiting growth. A useful method is proposed to evaluate the site selectivity. The self-limiting deposition of Ga is reviewed in terms of both Lewis acid-base reactions and of the polarization of precursors and the GaAs surface.

In contrast, the adsorption and desorption of group-V atoms during PJE are discussed in Chapter 6. First, it is clarified that there is an unprecedented problem of the reevaporation of group-V atoms from the outermost growth surface during purge periods. It is shown that the saturated growth rate changes if the H_2 purge time during PJE is not controlled accurately. Then, it is pointed out that GaAs growth rate increases over 1 ML/cycle if a sufficient amount of AsH_3 is supplied. Finally, it is explained that these problems of group-V atoms are related to stable surface reconstructed structures and their surface coverage of group-V atoms.

In Chapter 7, heteroepitaxial growth by PJE is described. First, results of the heteroepitaxy of binary materials are systematically reported. The effect of lattice mismatch and surface free energy on the self-limiting characteristic is discussed. Then, the PJE growth of ternary materials such as InGaAs and InGaP is shown. Some interesting phenomena are described: compositional latching, phase separation and the surface segregation of In atoms, which occur during PJE. Moreover, the fabrication of strained-layer superlattices such as InGaAs/GaAs, GaAs/GaP, and InAs/InP are reported, and the X-ray diffraction profiles showing the superstructures are shown. Finally, some key technical points in fabricating abrupt heterointerfaces using PJE are discussed. It is revealed that suppressing the desorption of group-V atoms from the growth surface is indispensable.

Chapter 8 describes some applications of PJE. It is explained that some features of PJE, such as excellent thickness uniformity and controllability, low temperature growth, high-

concentration doping, and selective epitaxy, are useful for device fabrication. As practical applications, results on the regrowth of highly n-type doped GaAs and InGaAs to make non-alloyed ohmic contacting layer on the processed substrates are shown. In addition, a PJE/MOVPE hybrid process to fabricate InGaAs/InP heterojunction bipolar transistors (HBTs) is reported.

Finally in Chapter 9, this thesis is summarized and the technical and scientific significance of this study on PJE is clarified. Some unsolved problems in PJE are also considered and future possibilities for this technology are described.

ACKNOWLEDGEMENTS

The author would like to express gratitude to Professor Satoshi Hiyamizu of the Faculty of Engineering Science at Osaka University, for helpful discussions and for continuing guidance and encouragement.

The author would also like to express appreciation to Professors Saburo Nasu and Hisao Nakashima at Osaka University for their helpful advice and discussions.

The author wishes to extend thanks to Dr. Shigeru Sato, President, and Dr. Hajime Ishikawa of Fujitsu Laboratories Ltd. for their helpful suggestions and support during the course of this work.

Further thanks to Professor Osamu Ohtsuki of Wakayama University and Dr. Masashi Ozeki of the Joint Research Center for Atom Technology for their stimulating discussions and heartily support at Fujitsu Laboratories.

Thanks also to Dr. Naoki Yokoyama, Dr. Kazuo Nakajima, Dr. Osamu Ueda, Dr. Yuji Awano, and Mr. Toshiro Futatsugi of Fujitsu Laboratories Ltd., and Professor Shunichi Muto of Hokkaido University, for their strong support.

The author is also grateful to Dr. Yoshiyasu Kanno, Dr. Masahisa Suzuki, and Mr. Teruo Yokoyama of Fujitsu Quantum Device Ltd., for trying and discussing the application of PJE to ohmic contacts for a FET.

Extended thanks to Dr. Kunihiko Kodama and Mr. Toshihiko Ashino for XPS, PL, and Raman spectroscopy, Messrs. Koji Mochizuki, Nobuyuki Ohtsuka, and Yasuo Matsumiya for discussing growth technologies, Dr. Kuninori Kitahara for instructing electrical property measurements of epitaxial layers, Messrs. Hiroshi Yamada and Hisao Shigematsu for HBTs process and their electrical characterization, Dr. Teruo Yagishita for NMR spectroscopy of organometals, and Mr. Tadashi Ishino for AES analyses.

Finally, the author thanks Messrs. Eiji Taguchi and Hirokazu Hosoi for technical assistance in growth experiments.

CONTENTS

Chapter 1. Introduction 1
1.1 Preliminaries 1
1.2 Background 1
1.2.1 Historical overview of crystal growth technology 1
1.2.2 Principle of ALE 5
1.2.3 Self-limiting mechanism 7
1.2.4 Some methods for ALE 9
1.2.4.1 MOMBE-type ALE 9
1.2.4.2 MOVPE-type ALE 11
1.2.4.3 Hydride VPE-type ALE 14
1.2.4.4 Laser-assisted ALE 14
1.3 Purpose of This Study 17
1.4 Outline of This Study 17
References 20

Chapter 2. Development of Pulsed-Jet Epitaxy 22
2.1 Preliminaries 22
2.2 Definition of PJE 22
2.3 Requirements for PJE 23
2.4 Advantages of PJE 25
2.5 Growth Apparatus for PJE 32
2.5.1 Gas handling system 33
2.5.2 Gas-switching valves 33
2.5.3 Reactors 36
2.5.4 Heating methods 36
2.6 Experimental Procedure 38
2.6.1 Growth procedure 38
2.6.2 Procedure for thickness measurement 41
2.7 Summary 42
References 43

Chapter 3. Growth of III-V Binary Compounds 44
3.1 Preliminaries 44
3.2 Structure and Properties of III-V Semiconductors 45
3.3 PJE of Binary Compounds 48
3.3.1 Results in horizontal reactor 48
3.3.1.1 InP 48
3.3.1.2 GaAs 56
3.3.1.3 GaP 56
3.3.1.4 InAs 59
3.3.2 Some problems in horizontal reactor 61

3.3.3 Results in chimney reactor 63
3.3.3.1 GaAs 63
3.3.3.2 InAs 66
3.4 Dependence of Growth Rate on Surface Orientations 67
3.4.1 GaAs 69
3.4.2 InP 74
3.5 Electrical and Optical Properties of PJE-Grown Layers 74
3.6 Summary 78
References 79

Chapter 4. Self-Limiting Growth Mechanism 81
4.1 Preliminaries 81
4.2 In-Situ Study of Surface Adsorbates by XPS 82
4.2.1 Apparatus 82
4.2.2 Experiment 82
4.2.3 Results and implications 84
4.2.3.1 GaAs 84
4.2.3.2 GaP 86
4.2.3.3 InP 86
4.3 Mechanism of Self-Limiting Growth 89
4.3.1 Selective adsorption model 89
4.3.2 Comparison with other models 92
4.3.2.1 Radical inhibition (site blocking) model 92
4.3.2.2 Selective decomposition model 92
4.3.2.3 Flux balance model 94
4.4 Rate Equations for Selective Adsorption Model 94
4.4.1 Theory 94
4.4.2 Simulation of growth kinetics 97
4.4.2.1 Dependence on TMGa pulse duration 97
4.4.2.2 Dependence on TMGa flow rate 99
4.5 Evidences of Selective Adsorption Model 100
4.5.1 Growth by consecutive supply of TMGa 102
4.5.2 Growth by sequential supply of TEGa and TMGa 103
4.6 Summary 106
References 108

Chapter 5. Role of Group-III Precursors 110
5.1 Preliminaries 110
5.2 Chemistry of Ga Precursors 111
5.3 GaAs Growth using Several Ga Precursors 113
5.3.1 TEGa 114
5.3.1.1 Growth results 114
5.3.1.2 Growth model using TEGa source 114
5.3.1.3 Theory 116

5.3.1.4 Simulation 118
5.3.2 EDMGa 121
5.3.2.1 NMR study for synthesis 121
5.3.2.2 Growth results 124
5.3.2.3 Implications 127
5.3.3 TiBGa 128
5.3.3.1 Background 128
5.3.3.2 Growth results 128
5.3.4 $GaCl_3$ 128
5.3.4.1 Background 130
5.3.4.2 Growth results 130
5.4 Evaluation of "Site Selectivity" of Ga Precursors 132
5.4.1 Theory 132
5.4.2 Comparison of TMGa, EDMGa, and TEGa 135
5.5 Elucidation for Role of Ligands in Self-Limiting Mechanism 136
5.5.1 Crystal growth via Lewis acid and Lewis base reaction 136
5.5.2 Crystal growth via molecular and surface polarization 138
5.5.3 Role of ligands in self-limiting 141
5.6 Novel Approaches to Self-Limiting 142
5.6.1 TMGa plus TEGa 142
5.6.1.1 TEGa, TMGa consecutive supply 142
5.6.1.2 TEGa, TMGa simultaneous supply 144
5.6.2 TEGa plus CCl_4 148
5.7 Summary 150
References 152

Chapter 6. Influence of Adsorption and Desorption of Group-V Atoms 153
6.1 Preliminaries 153
6.2 Role of H_2 Purge in PJE Gas Sequence 154
6.3 Growth Rate Dependence on H_2 Purge Time 156
6.3.1 InAs (001) 156
6.3.1.1 Experiment 158
6.3.1.2 Kinetics during H_2 purge 158
6.3.1.3 Surface morphologies 161
6.3.1.4 Implications 162
6.3.1.5 Achievement in monolayer growth 165
6.3.2 InP (001) 167
6.3.2.1 Experiment 167
6.3.2.2 Effect of H_2 purge 167
6.3.3 Relationship between growth temperatures and congruent temperatures 168
6.4 As-Related Problems at GaAs (001) 168
6.4.1 Experiment 170
6.4.2 As adsorption 170
6.4.3 As desorption 172
6.5 Growth Mechanism Considering Surface Reconstructions 176

6.5.1 Surface reconstructions of GaAs (001) 176
6.5.2 Surface stoichiometric problem at GaAs (001) during ALE 177
6.5.3 Growth model including surface reconstructions 177
6.5.3.1 Model for As adsorption at GaAs (001) 179
6.5.3.2 Model for As desorption from GaAs (001) 183
6.5.3.3 Others 187
6.6 Explanation for Orientation Dependence of Growth Rate 190
6.7 Summary 194
References 195

Chapter 7. Heteroepitaxy 198
7.1 Preliminaries 198
7.2 Binary Materials 199
7.2.1 Growth results 199
7.2.1.1 GaAs on InAs 199
7.2.1.2 GaAs on InP 199
7.2.1.3 GaAs on GaP 201
7.2.1.4 GaAs on InGaP 201
7.2.1.5 GaP on GaAs 201
7.2.1.6 GaP on InP 204
7.2.2 Effect of lattice mismatch and surface free energy 204
7.3 Ternary Systems 209
7.3.1 InGaP on GaAs 210
7.3.1.1 Growth schemes 210
7.3.1.2 Phase separation and effect of growth temperature 212
7.3.1.3 Growth model 218
7.3.2 InGaAs on InP 218
7.3.2.1 Gas sequence and experimental 219
7.3.2.2 Composition latching 219
(a) TMIn-TMGa system 219
(b) TMIn-TEGa system 227
(c) AES analysis of composition latching 227
(d) Growth model 227
7.3.3 InGaAs on GaAs 231
7.3.3.1 Growth behavior 231
7.3.3.2 Growth model 234
7.4 Strained-Layer Superlattices 236
7.4.1 (InGaAs)(GaAs)/GaAs 236
7.4.2 (InAs)(InP)/InAs 238
7.4.2.1 Experiment 239
7.4.2.2 InAs and InP homoepitaxy 239
7.4.2.3 InAs/InP short-period superlattices 239
7.4.3 (GaP)(GaAs)/GaAs 246
7.5 Fabrication of Sharp Heterointerfaces by PJE 246
7.5.1 InAs/InP short-period superlattice 248

7.5.2 InAs/InP single quantum well 250
7.6 Summary 256
References 257

Chapter 8. Device Applications 259
8.1 Preliminaries 259
8.2 Summary of PJE 260
8.3 Elemental Factors Applicable to Device Process 260
8.3.1 Thickness uniformity 262
8.3.2 Interface controllability 262
8.3.3 Band engineering 265
8.3.4 Low-temperature growth and high-concentration doping 265
8.3.4.1 Se doping into GaAs 265
8.3.4.2 Be doping into InGaAs 267
8.3.5 Selective epitaxy 272
8.3.5.1 Nucleation on mask 272
8.3.5.2 Growth rate enhancement at mask edge 273
8.3.5.3 Mask pattern dependence of growth rate 276
8.3.5.4 Shape of selective-grown layers 276
8.3.5.5 Model for selective epitaxy 281
8.4 Practical Application 283
8.4.1 InGaAs/InP HBT 283
8.4.2 Ohmic contacting layer 287
8.4.2.1 InAs/InGaAs/GaAs graded layer 288
8.4.2.2 GaAs selective regrowth layer 291
8.5 Summary 293
References 294

Chapter 9. Conclusions 296

List of Publications and Presentations 302

CHAPTER 1
Introduction

1.1 Preliminaries

In this chapter, we give an introduction to this thesis. We explain the background, the purpose and the outline of this study. First, to clarify the technical significance of atomic layer epitaxy (ALE) or pulsed-jet epitaxy (PJE), we review the history of growth technology for III-V compound semiconductors, taking the history of device development into consideration. We consider the limitations of better known techniques such as liquid-phase epitaxy (LPE), chloride or hydride vapor-phase epitaxy (VPE), metalorganic vapor-phase epitaxy (MOVPE), and molecular beam epitaxy (MBE). Then, we explain the principle of ALE and "self-limiting growth", the most fundamental and outstanding feature of ALE. To date, several novel growth methods have been proposed and demonstrated to achieve the clear self-limiting. We explain these reported ALE methods and try to reveal the inevitable problems in each method. Finally, we describe the purpose of our study and give an outline of this thesis.

1.2 Background

1.2.1 Historical overview of crystal growth technology

The importance of growing epitaxial layers is widely recognized in the semiconductor industry. Especially for III-V compound semiconductors, epitaxial growth is a key technology used to fabricate some high performance electrical and optical devices. There are several reasons for this. One is that the epitaxial layer can be grown at much lower temperatures than with the melt growth technique. Therefore, we can obtain nearly stoichiometric, high quality III-V layers. The non-stoichiometric problem, which is severe for III-V compounds, is strongly related to the defects of the crystal and leads to the unexpected worsening of material

characteristics. Other advantages of epitaxial growth are the capabilities of growing uniform, thin films and of preparing multiple layers and heterostructures. In addition, the easy control of impurity doping and the possibility of selective growth and the growth on non-planar substrates are promising. Thus, the development of epitaxial growth techniques for III-V compounds is stimulated and enhanced by the need to improve the device performance or to fabricate new device structures.

Let us review the history of epitaxial growth techniques for III-V compounds. In the early stages, both LPE [1] and halogen-transported VPEs [2, 3] were widely used to grow structures for light-emitting diodes (LEDs), laser diodes (LDs), Gunn diodes, field effect transistors (FETs), and so on. These techniques provided the high purity epitaxial layers for device researchers. Note that LPE made possible the first room-temperature continuous wave (CW) operation of a LD with a double heterostructure (DH) in 1970 [4]. The advantages of LPE and VPE are summarized as follows:

•Advantages of LPE: LPE needs only simple equipment and provides us with very high-purity epilayers of high growth rate. A wide variety of materials can be grown using the same apparatus.

•Advantages of VPE: multilayers with abrupt interfaces can be grown easier than in LPE. Control over the thin-film thickness is also better. In addition, selective epitaxy is expected.

However, after the proposal of a superlattice by Esaki *et al.* in 1970 [5], research into quantum effect devices began. Since the thickness of the layer period and interface abruptness required for the superlattice was far beyond the control of LPE and VPE, a strong need to develop a new growth technology with extremely precise thickness and composition control arose. Here we show the disadvantages or limitations of LPE and VPE.

•Disadvantages of LPE: the limitations of LPE are the poor thickness uniformity of the grown layers and the difficulty in growing multilayer structures with abrupt interfaces. This is due to the high growth rate and the inherent meltback phenomena. Growth on large-area substrates is difficult, so mass production is limited. In addition, due to the large distribution coefficient of aluminum (Al), it is difficult to grow alloys of high indium (In) composition in the case of alloys containing both Al and In.

•Disadvantages of VPE: although VPE has been used to fabricate some commercial devices such as GaAsP LEDs and InGaAs photodetectors, it is difficult to grow Al-containing materials due to the inefficient formation of AlCl or $AlCl_3$. Auto doping into the epilayer is also a severe problem because the etching of the substrate by HCl gas is tied with the growth reaction. It is extremely difficult, if not impossible, to grow superlattice structures. Alternating layers are normally obtained by physically moving the substrate back and forth between reactor tubes. This is not a promising method.

The development of MBE started toward the end of the 1960s [6]. MBE was the first growth technique to realize superlattices because it had the ability to grow layers several tens angstroms thick [7]. Then the quantum well (QW) laser, proposed by van der Ziel *et al.*, was realized for the first time using MBE in 1975 [8]. In fact, the multiple QW laser [9], modulation-doped structures [10], and high electron-mobility transistors (HEMT) [11, 12] were all successfully realized by MBE. Thus, for many years MBE was the only technique capable of producing perfectly abrupt interfaces and the MBE-grown novel quantum effect structures contributed to the drastic improvement in semiconductor devices. The advantages of MBE are summarized as:

•Advantages of MBE: since MBE is carried out under ultra-high vacuum (UHV) conditions, the purity of epitaxial layers is very high. The growth process can be monitored in situ by several diagnostic techniques such as reflection high-energy electron diffraction (RHEED), Auger electron spectroscopy (AES) and low-energy electron

diffraction (LEED). Therefore, MBE is capable of growing with extremely precise control over layer thickness, composition, and doping profile.

Meanwhile, MOVPE [13] had been studied as another candidate for fabricating quantum structures. Initially, it was thought to be difficult to make high-purity epilayers using MOVPE due to the severe contamination from source gases [14, 15]. However, since Dupuis *et al.* reported the high performance room temperature operation of a GaAs QW laser using MOVPE in 1978 [16], research into MOVPE has become active. MOVPE was established as a useful growth technology for making certain commercial optical devices, such as QW lasers and photodiodes. The advantages of MOVPE are as follows:

•Advantages of MOVPE: a major advantage of MOVPE is its versatility. We can grow various kinds of binary compounds, and ternary and quaternary alloys. It is of great benefit in growing phosphorus (P)-containing materials. The suitability for large scale and multiple wafer production is superior. The thickness and interface abruptness is now controllable to within a few atomic layers.

Up to now, both MBE and MOVPE have made impressive advances in their ability to grow semiconductor layers with ultra-low thickness and abrupt interfaces. Thus, both techniques have been exclusively used to grow many sophisticated electrical and optical device structures. However, the general disadvantages of MBE and MOVPE are considered to be as follows:

•Disadvantages of MBE: the MBE apparatus is very expensive because of the need for an ultra-high vacuum (UHV) system and *in-situ* surface analytical equipment. Frequent shutdowns are required to replenish the source materials, and opening the UHV apparatus requires bake-out before returning to the growth of very high-purity materials. Another major problem is the difficulty in growing P-containing materials such as InP and GaInAsP.

•Disadvantages of MOVPE: the main drawback of MOVPE is the use of large quantities of arsine (AsH_3) and phosphine (PH_3) which are toxic gases. Compared to MBE, it is difficult to perform *in-situ* characterization during MOVPE.

Although we recognize the technical importance of both MBE and MOVPE, we still have to control a large number of parameters carefully during growth to obtain the necessary uniformity and reproducibility. In the 1980s, some researchers began to develop a novel growth technique offering better growth control than MBE and MOVPE. At that time, new quantum devices such as resonant-tunneling devices [17-19] and strained-layer QW lasers [20] strongly required the ultimate controllability of thickness and interface sharpness with monolayer precision. If we can get a novel growth technique in which the growth process proceeds stepwise, *i.e.*, monolayer by monolayer in a self-regulated fashion, we don't have to control the growth parameters precisely and this process leads to the ultimate uniformity within atomic fluctuation over a large area of the substrate. Atomic layer epitaxy (ALE) provides this.

1.2.2 Principle of ALE

ALE was proposed by Suntola and Antson in Finland in 1974 [21, 22]. ALE can be briefly described as an epitaxial growth method where the source materials (reactants) are alternately supplied into the reaction chamber and onto the substrate surface. In this case, the growth of thin films proceeds based on the alternating chemisorption, surface reaction, and desorption steps of the reactants. The basic model representing the ALE process is shown in Fig. 1-1. First, when the gas source "AX" is injected, the reactor contains an excess of the reactant in the gas phase but the temperature of the substrate and the partial pressure of the gas "AX" are adjusted so that the only one monolayer (ML) of the reactant "AX" is chemisorbed on the substrate "BA" (Fig. 1-1 (a)). Next, the excess reactant "AX", which is in the gas phase or physisorbed on the surface, is purged or evacuated before dosing with the other reactant (Fig. 1-1 (b)). The latter reactant "BY" chemisorbs and reacts with the first reactant on the substrate surface (Fig. 1-1 (c)), resulting in the formation (growth) of a solid molecular film "AB" and a

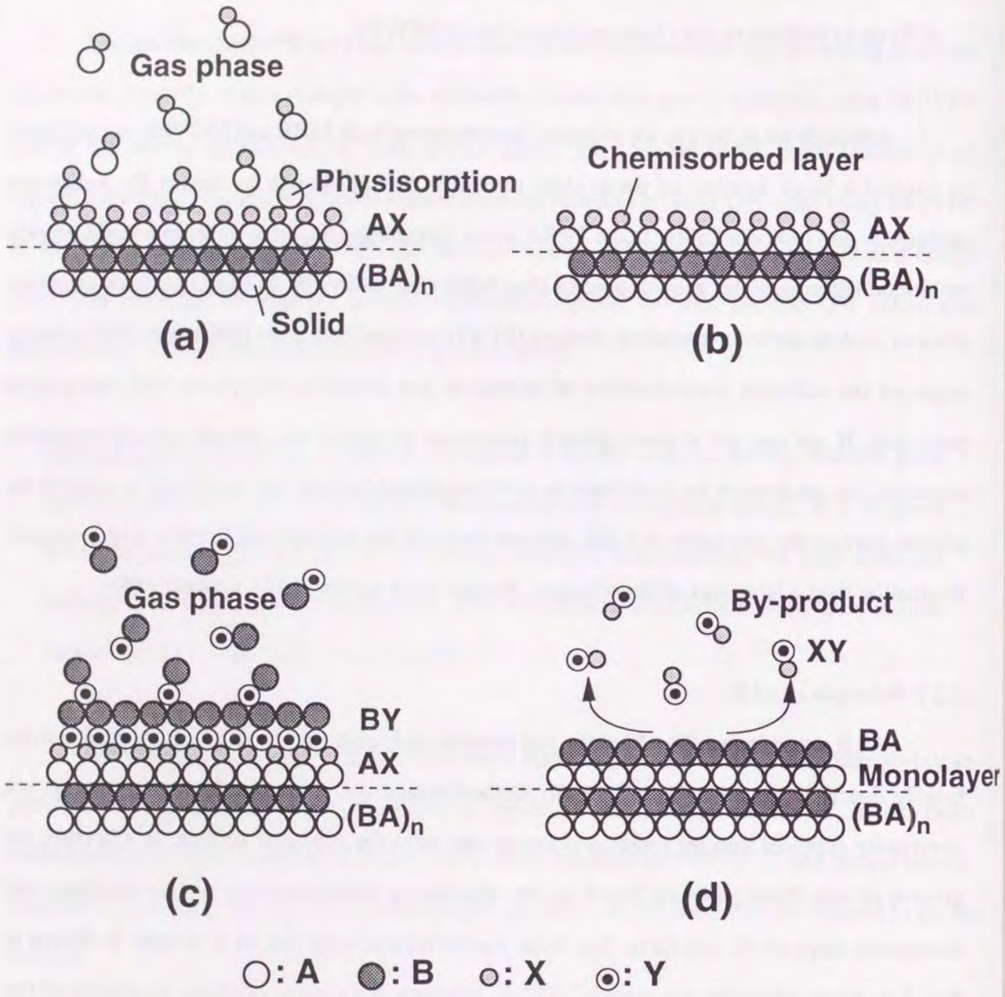

Figure 1-1. Principle of atomic layer epitaxy during one cycle of gas introduction.

gaseous by-product "XY" is removed from the surface and the gas phase with the following purge duration or evacuation (Fig. 1-1 (d)). Repeating this reaction cycle leads to the controlled layer-by-layer growth of "AB".

As a result, the next two major kinds of surface reactions occur at the gas (g)/solid (s) interface during the ALE of binary compounds, and these reactions lead to the monolayer-limited growth of the epitaxial layers.

$$AX(g)+(BA)_n(s) \rightarrow XA\bullet(BA)_n(s) \quad (1\text{-}1)$$

$$BY(g)+XA\bullet(BA)_n(s) \rightarrow (BA)_{n+1}(s)+XY(g) \quad (1\text{-}2)$$

1.2.3 Self-limiting mechanism

In the ALE process, the most important and attractive phenomenon is that the surface coverage by each source reactant should be virtually unity independent of the normal growth parameters such as reactant partial pressures, exposure times, and growth temperatures, over a wide range of growth conditions. When this situation occurs, a *"self-limiting mechanism"* is said to be present. This situation has also been called digital epitaxy because no control of analogous growth parameters is required. This *"self-limiting"* feature is a fundamental aspect of ALE, from which ALE's desirable features such as ultrathin epitaxial layers with extremely good uniformity, atomically abrupt heterointerfaces, and perfect selective epitaxy, are derived.

One consequence of self-limiting growth is that the final thickness is dependent only upon the number of deposition cycles (or gas exposure cycles) and the lattice constant of the material, and can be controlled and reproduced extremely well. This is in contrast to pseudo-ALE schemes which employ source switching (or modulation) but do not have a real self-limiting mechanism. Several pseudo-ALE techniques such as migration-enhanced epitaxy (MEE) and flow rate modulation epitaxy (FME) have been reported [23, 24]. In these cases the growth rate has been adjusted to equal approximately 1 ML/cycle. As expected with the pseudo-ALE process, the precise control of growth conditions, *i.e.* the reactant partial pressures, total

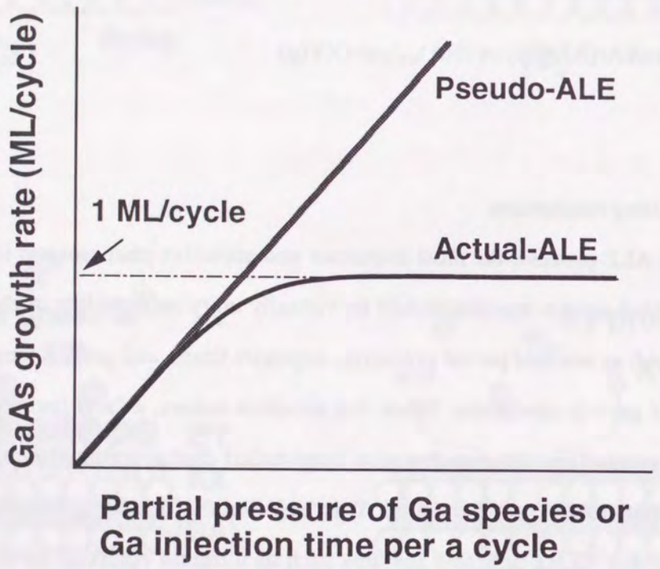

Figure 1-2. Comparison of GaAs growth rate between pseudo-ALE and actual-ALE as a function of partial pressure (injection time) of Ga-containing species.

gas flow rate, and exposure times as well as hydrodynamic considerations, is necessary to achieve approximately 1 ML per gas cycle. The difference is shown in Fig. 1-2 with respect to the partial pressure or the injected time of gallium (Ga) species for the growth of GaAs. No accurate control of the Ga flux is needed in ALE to achieve monolayer deposition. In contrast, the Ga flux must be precisely controlled in the pseudo-ALE scheme so as to realize a monolayer growth.

Since the self-limiting behavior is a fundamental aspect of ALE, understanding its underlying mechanism is very important and necessary for the future exploitation of more useful growth methods. Unfortunately, a microscopic, chemically specific description has not been fully realized yet. At the present stage, a number of growth models have been proposed, but none of them can explain satisfactorily all the experimental results ever reported.

1.2.4 Some methods for ALE

This section will review the various reported approaches to the self-limiting growth or ALE of III-V compounds, including system descriptions and typical experimental results which show the self-limiting growth. Here, we will describe the four kinds of methods, each based on the conventional growth techniques such as metalorganic molecular beam epitaxy (MOMBE), hydride VPE, and MOVPE, respectively. These methods were proposed during the early stages of the development of ALE.

1.2.4.1 MOMBE-type ALE

The MOMBE-type method has been adapted for the growth of GaAs ALE by Nishizawa *et al.* under the name of molecular layer epitaxy (MLE) [25, 26]. They demonstrated the clear self-limiting GaAs epitaxial growth for the first time. Their work strongly influenced research into this field and increased the population of ALE researchers. Figure 1-3 shows a schematic of the Nishizawa's group's system. Their apparatus consists of an ultra high-vacuum MBE-type chamber, but with a gas injection system for metalorganics and hydride sources as in an MOVPE system. The substrate is lamp heated. A typical gas sequence for GaAs growth consists of an AsH_3 exposure of 20 s, a 3 s evacuation, a 4 s trimethylgallium (TMGa)

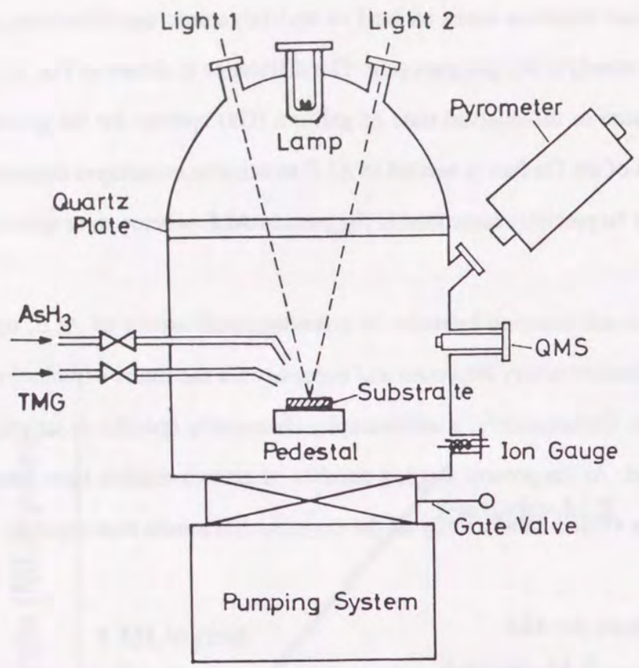

Figure 1-3. Schematics of growth apparatus for molecular layer epitaxy (MLE).

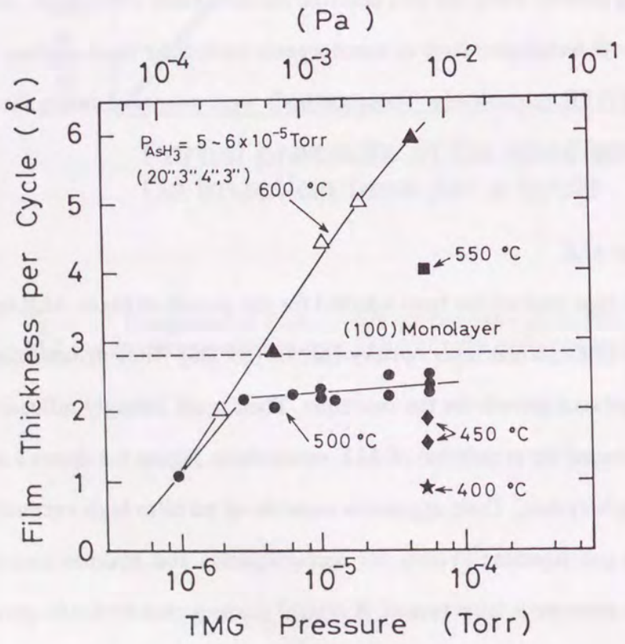

Figure 1-4. GaAs growth rate dependence on TMGa partial pressure in MLE.

exposure and a 3 s evacuation (20 s, 3 s, 4 s, 3 s). A plot of the thickness of the epitaxial layer per cycle versus the TMGa partial pressure is shown in Fig. 1-4. A self-limiting mechanism appears to be present at 500°C and at a TMGa pressure greater than about $3x10^{-6}$ Torr.

The drawbacks of the MOMBE-type method are summarized as follows:

1) It is difficult to apply this method to P-containing materials because the growth is carried out in a UHV chamber.

2) The temperature range for realizing self-limiting is limited between 490°C and 510°C. The so-called "ALE window" seems to be narrow.

3) The saturated growth rate per cycle is below 1 ML/cycle. This will be related to the stable GaAs (001) surface reconstructed structure under a UHV environment. A detailed explanation is given in Chapter 6.

4) It is difficult to exchange reactants within a short time in the chamber because the gas exchange is conducted by evacuation. This is inconvenient for suppressing the re-evaporation problem of surface group-V atoms, as described in Chapter 6, which lead to the decrease in the saturated growth rate.

1.2.4.2 MOVPE-type ALE

Bedair *et al.* demonstrated the GaAs ALE in a modified atmospheric-pressure MOVPE system [27, 28]. The major modifications were in the design of the reactor and susceptor. Figure 1-5 (a) shows a schematic of their reactor. The quartz reactor has three inlets. For the growth of GaAs, streams of AsH_3+H_2 and $TMGa+H_2$ are introduced through the separated inlet tubes. A large flow of H_2 in the middle tube is designed to prevent the mixing of AsH_3 and TMGa. The susceptor shown in Fig. 1-5 (b) is made of SiC-coated graphite and is radio-frequency (RF) heated. It consists of a fixed and a rotating part. The substrate sits in a recess of the rotating part and can be positioned directly under the gas inlet tubes supplying either group-III and group-V species. The growth is done by rotating the susceptor. Figure 1-6 shows the thickness per cycle as a function of the TMGa flow at various growth temperatures, AsH_3 flows, and substrate orientations. From these results, they concluded that the self-limiting growth of GaAs is achieved.

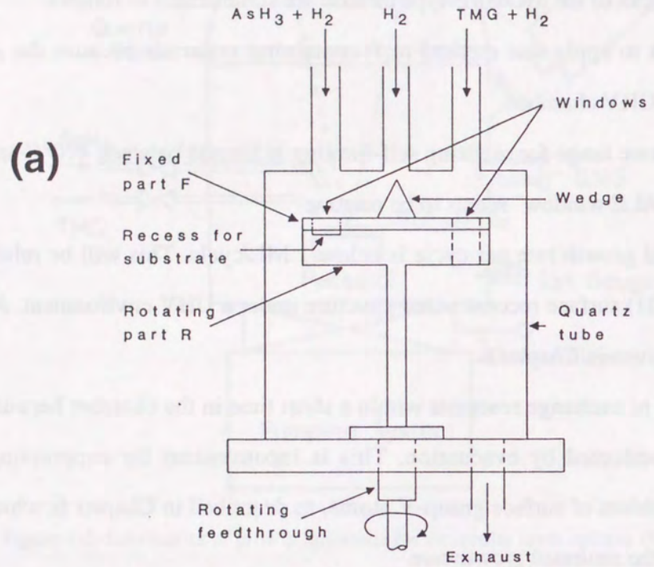

Figure 1-5. Schematics of growth apparatus with a rotating susceptor in MOVPE. (a) The growth chamber and susceptor and (b) a detailed diagram of the susceptor.

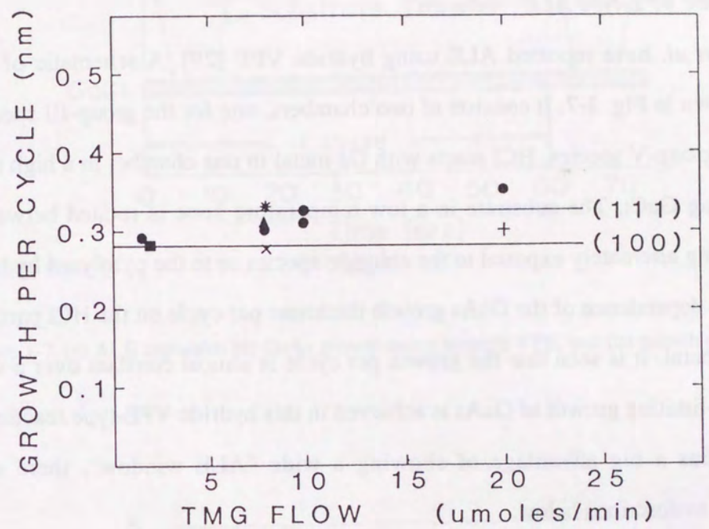

(100)
- ● Ts: 630°C, AsH_3: 52 μmol/min
- ■ Ts: 450°C, AsH_3: 156 μmol/min
- \+ Ts: 450°C, AsH_3: 410 μmol/min
- ∗ Ts: 630°C, AsH_3: 410 μmol/min
- × Ts: 700°C, AsH_3: 52 μmol/min

(111)
- ▲ Ts: 630°C, AsH_3: 52 μmol/min

Figure 1-6. Growth thickness of GaAs per cycle versus TMGa flow rate under various growth conditions. Horizontal lines show the ideal ALE growth rate for (100) and (111) orientations.

The disadvantages of this method are:

1) The reactor is complex. Therefore, it is inconvenient for growth on large scale wafers and multiple wafers for mass production.

2) It is difficult to grow multi-layered heterostructures and combine with the conventional MOVPE growth mode. This also originates from the complex growth system.

1.2.4.3 Hydride VPE-type ALE

Usui *et al.* have reported ALE using hydride VPE [29]. A schematic of the growth system is shown in Fig. 1-7. It consists of two chambers, one for the group-III species and the other for the group-V species. HCl reacts with Ga metal in one chamber in a high temperature zone producing GaCl. The substrate in a low temperature zone is rotated between the two chambers, being alternately exposed to the chloride species or to the pyrolysed hydride. Figure 1-8 shows the dependence of the GaAs growth thickness per cycle on the HCl partial pressure over the Ga metal. It is seen that the growth per cycle is almost constant over a wide range. Thus, the self-limiting growth of GaAs is achieved in this hydride VPE-type reactor. Although this method has a big advantage of showing a wide "ALE window", there are several disadvantages as described below:

1) Because of the complex reactor, it is inconvenient for growth on large scale wafers and multiple wafers.

2) It is difficult to grow multi-layered heterostructures.

3) It takes a long time to grow thick films due to the slow substrate transfer between the two chambers.

4) Due to the hydride VPE, the growth of Al-containing materials is difficult. Therefore, the variation of growth materials is limited.

1.2.4.4 Laser-assisted ALE

Laser-assisted ALE has been reported by Doi *et al.* [30, 31]. In this technique the source gases, TMGa and AsH_3, are separately introduced into the growth chamber while a laser beam is irradiated on the substrate at some point during the growth cycle. The sequence is shown in

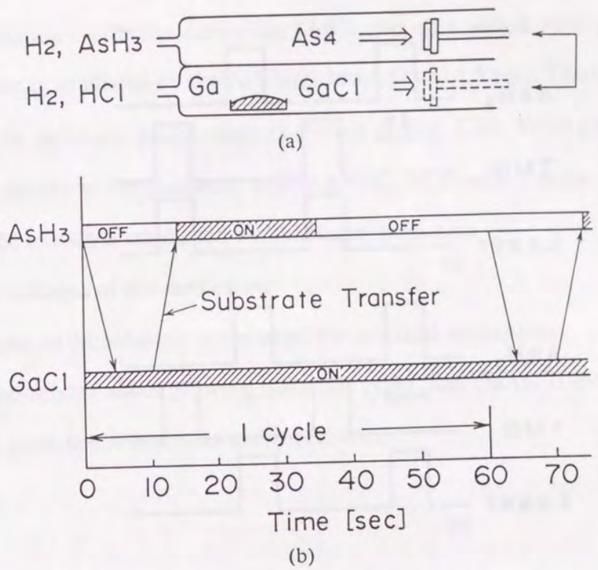

Figure 1-7. (a) ALE apparatus for GaAs growth using hydride VPE, and (b) growth procedure.

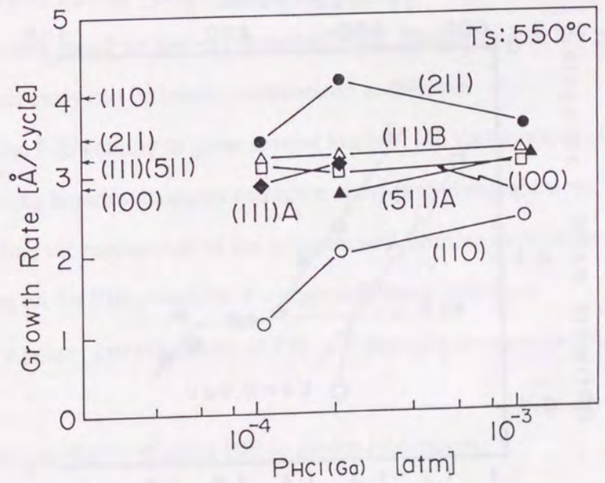

Figure 1-8. Dependence of GaAs growth rate on injected HCl partial pressure.

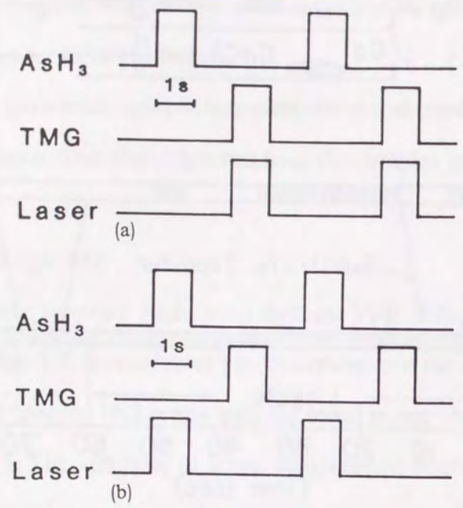

Figure 1-9. Gas sequence of laser-assisted ALE. Ar laser irradiation occurs concurrently with the introduction of (a) TMGa and (b) AsH_3.

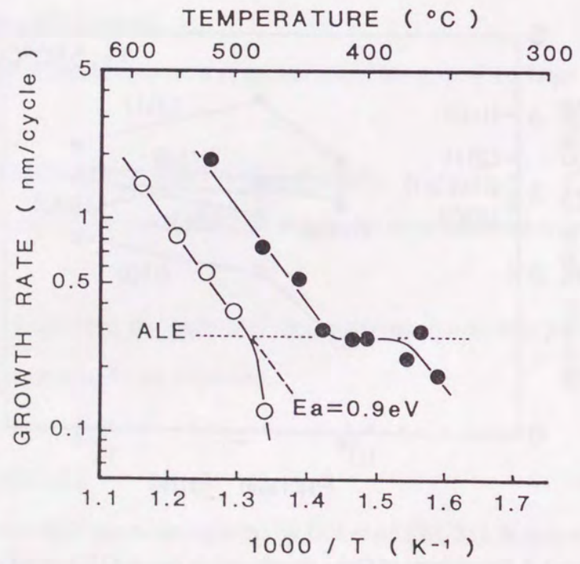

Figure 1-10. Temperature dependence of GaAs growth rate in laser-assisted ALE. Solid circles refer to treatment under laser irradiation and open circles to that without laser irradiation.

Fig. 1-9. The laser is turned on during the TMGa or AsH_3 exposure time. Doi *et al.* reported that the laser irradiation is effective during the TMGa exposure period. ALE growth occurs only where the substrate is irradiated by the Ar^+ laser beam (λ=514.5 nm). The GaAs growth rate's dependence on the substrate temperature is shown in Fig. 1-10. With irradiation, the self-limiting growth occurs at temperatures below 430°C. In contrast, there is no self-limiting condition when the growth is conducted without laser irradiation.

The disadvantages of this method are:

1) The ALE area on the substrate is too small for practical application.

2) There are no reports about growing materials other than GaAs. Therefore, it seems to be difficult to grow heterostructures and superlattices.

1.3 Purpose of This Study

As mentioned-above, there are still some problems with the various ALE techniques proposed at the early stages. Therefore, we have proposed and developed a novel ALE technique, "Pulsed-jet Epitaxy" (PJE), for the growth of III-V compound semiconductors. Our technique is basically based on low-pressure MOVPE. Details of PJE are given in Chapter 2. The purpose of this study can be briefly summarized as follows:

1) Clarifying the PJE's ability to grow several kinds of III-V compounds in a self-limiting manner, including binaries, ternaries and some short-period superlattices.

2) Understanding the mechanism of the inherent self-limiting deposition of group-III and group-V atoms on the PJE-grown III-V compound semiconductors.

3) Proposing a proper growth model of PJE and showing some experimental support for the model.

4) Showing the possibility of using PJE in device fabrication.

1.4 Outline of This Study

An outline of this thesis is as follows.

In Chapter 2, we describe the development of PJE and the experimental procedure in this study. First, we explain the definition of PJE and discuss some advantages of this novel ALE method. Then, we show growth apparatus including reactors, a gas handling system, a gas switching valve, and heating systems. Finally, we explain the experimental procedure such as thickness measurement in this work.

In Chapter 3, we describe the self-limiting growth of III-V binary compounds using PJE. We show the detailed experimental results on GaAs, GaP, InAs, and InP growth. For some materials, we compare the growth reactor designs between the horizontal type and the chimney type. From these results, we discuss how the "ALE window", which is a range of growth conditions leading to self-limiting, is affected by the reactors.

In Chapter 4, the mechanism of the self-limiting process is discussed. We show the results of the *in-situ* analyses of the surface adsorbates during PJE using X-ray photoelectron spectroscopy (XPS). We propose a "selective adsorption model" explaining the self-limiting deposition of nonvolatile group-III atoms such as Ga and In. Finally, we show several growth results which support the proposed selective adsorption model.

In Chapter 5, we discuss the role of group-III precursors in the self-limiting growth mechanism. We deal with some organometals, such as trimethylgallium (TMGa), triethylgallium (TEGa), ethyldimethylgallium (EDMGa), triisobutylgallium (TiBGa), and galliumtrichloride ($GaCl_3$). We show that the site selectivity of the Ga precursors between the Ga and As atoms on the growth surface is important in understanding the self-limiting growth. We propose a method to evaluate the site selectivity. We discuss the self-limiting deposition of Ga from the viewpoint of Lewis acid-base reactions and from the polarization of the precursors and GaAs surface.

In Chapter 6, we discuss the self-limited monolayer deposition of group-V atoms on the growth surface. First, we deal with the unprecedented problem of the reevaporation of group-V atoms from the outermost growth surface during the H_2 purge periods. We show that the saturated growth rate changes if we do not control the H_2 purge time during PJE. Then, we point out that the GaAs growth rate increases over 1 ML/cycle if sufficient amounts of AsH_3 are

supplied. We explain these problems related to the group-V atoms from the viewpoint of the stable surface-reconstructed structures and their surface coverage of group-V atoms.

In Chapter 7, the heteroepitaxial growth by PJE is described. First, we systematically describe the results of the heteroepitaxy of binary materials. We discuss the effect of lattice mismatch and the surface free energy on the self-limiting characteristic. Then, we deal with the PJE growth of ternary materials such as InGaAs and InGaP. We describe that some interesting phenomena, such as compositional latching, phase separation, and the surface segregation of In atoms, occur during PJE. Moreover, we describe the fabrication of strained-layer superlattices such as InGaAs/GaAs, GaAs/GaP, and InAs/InP. We show the X-ray diffraction profiles showing the superstructures. Finally, we discuss technical issues in fabricating the sharp heterointerfaces using PJE. We reveal that it is essential to suppress the desorption of group-V atoms from the growth surface.

In Chapter 8, some applications of PJE are described. We explain some features of PJE that are useful for device fabrication: excellent thickness uniformity and controllability, low temperature growth, high-concentration doping, and selective epitaxy. As practical applications, we show results of the regrowth of highly n-type doped GaAs and InGaAs to make a non-alloyed ohmic contacting layer on the processed substrates. In addition, we explain a PJE/MOVPE hybrid process to fabricate InGaAs/InP heterojunction bipolar transistors (HBTs).

Finally in Chapter 9, we summarize this study and clarify the technical and scientific significance of this study into PJE. Then, we consider some unresolved problems in the PJE technique and future possibilities for this technology.

REFERENCES (Chap. 1)

[1] H. Nelson, RCA Rev. (1963) 603.

[2] J.R. Knight, D. Effer, and P.R. Evans, Solid State Electron. **8** (1965) 178.

[3] J.J. Tietjen and J.A. Amick, J. Electrochem. Soc. **113** (1966) 724.

[4] I. Hayashi, M.B. Panish, P.W. Foy, and S. Sumski, Appl. Phys. Lett. **17** (1970) 109.

[5] L. Esaki and R. Tsu, IBM J. Res. Develop. **14** (1970) 61.

[6] J.R. Arthur, J. Appl. Phys. **39** (1968) 4032.

[7] L.L. Chang, L. Esaki, W.E. Howard, R. Ludeke, and G. Schul, J. Vac. Sci. Technol. **10** (1973) 655.

[8] J.P. van der Ziel, R. Dingle, R.C. Miller, W. Wiegmann, and W.A. Nordland Jr., Appl. Phys. Lett. **26** (1975) 463.

[9] W.T. Tsang, Appl. Phys. Lett. **39** (1981) 786.

[10] R. Dingle, H.L. Stormer, A.C. Gossard, and W. Wiegmann, Appl. Phys. Lett. **33** (1978) 665.

[11] T. Mimura, S. Hiyamizu, T. Fujii, and K. Nanbu, Jpn. J. Appl. Phys. **19** (1980) L225.

[12] S. Hiyamizu, T. Mimura, T. Fujii, K. Nanbu, and H. Hashimoto, Jpn. J. Appl. Phys. **20** (1981) L245.

[13] H.M. Manasevit, Appl. Phys. Lett. **12** (1968) 156.

[14] P. Rai-Choudhury, J. Electrochem. Soc. **116** (1969) 1745.

[15] S. Ito, T. Shinohara, and Y. Seki, J. Electrochem. Soc. **120** (1973) 1419.

[16] R.D. Dupuis and P.D. Dapkus, Appl. Phys. Lett. **32** (1978) 473.

[17] T.C.L.G. Sollner, W.D. Goodhue, P.E. Tannenwald, C.D. Parker, and D.D. Peck, Appl. Phys. Lett. **43** (1983) 588.

[18] F. Capasso and R.A. Kiehl, J. Appl. Phys. **58** (1985) 1366.

[19] N. Yokoyama, K. Imamura, S. Muto, S. Hiyamizu, and H. Nishi, Jpn. J. Appl. Phys. **24** (1985) L853.

[20] D. Fekete, K.T. Chan, J.M. Ballantyne, and L.F. Eastman, Appl. Phys. Lett. **49** (1986) 1659.

[21] T. Suntola and J. Antson, Finnish Patent No. 52359 (1974).

[22] T. Suntola, Extended Abstracts of Int. Conf. on Solid State Devices and Materials, Kobe (1984) 647.

[23] Y. Horikoshi, M. Kawashima, and H. Yamaguchi, Jpn. J. Appl. Phys. **25** (1986) L868.

[24] N. Kobayashi, T. Makimoto, Y. Yamauchi, and Y. Horikoshi, J. Appl. Phys. **66** (1989) 640.

[25] J. Nishizawa, H. Abe, and T. Kurabayashi, J. Electrochem. Soc. **132** (1985) 1197.

[26] J. Nishizawa, T. Kurabayashi, H. Abe, and N. Sakurai, J. Electrochem. Soc. **134** (1987) 945.

[27] S.M. Bedair, M.A. Tischler, T. Katsuyama, and N.A. El-Masry, Appl. Phys. Lett. **47** (1985) 51.

[28] M.A. Tischler and S.M. Bedair, Appl. Phys. Lett. **48** (1986) 1681.

[29] A. Usui and H. Sunakawa, Jpn. J. Appl. Phys. **25** (1986) L212.

[30] A. Doi, Y. Aoyagi, and S. Namba, Appl. Phys. Lett. **48** (1986) 1787.

[31] A. Doi, Y. Aoyagi, and S. Namba, Appl. Phys. Lett. **49** (1986) 785.

CHAPTER 2
Development of Pulsed-Jet Epitaxy

2.1 Preliminaries

As mentioned in Chapter 1, there are several methods for realizing self-limiting growth, which is a unique characteristic of ALE, for semiconductor thin films. As a novel method of ALE, we have proposed and developed "Pulsed-jet epitaxy" (PJE) to grow III-V compound semiconductors.

In this chapter, we first give a definition of PJE. Second, the requirements for PJE are described. Third, some technical advantages of PJE are clarified. Fourth, the growth apparatus of PJE is explained in detail. Finally, the procedure of growth experiments is described.

2.2 Definition of PJE

PJE can be classified as a kind of ALE. It is based on a modified low-pressure (LP) MOVPE and has a special reactor design as described later. Figure 2-1 illustrates the fundamental concept of PJE. The substrates placed on a stationary, heated susceptor are alternately exposed to the gas pulses containing reactants. As the precursors, organometals of group-III atoms and hydrides of group-V atoms are typically used. These precursors are carried with a Pd-diffused H_2 gas into the reactor. Each gas pulse containing either a group-III or group-V precursor is separated by a H_2 purge pulse to prevent the gas-phase mixing reaction between the two reactants. The gas pulses are generated by switching the air-operated valves which will also be explained later. The operative growth pressure and the total flow rate in the reactor are kept constant during growth. These parameters, as well as the growth temperatures, must be optimized to suppress the excess deposition of the constituent atoms in the growth materials on the substrate surface. To achieve self-limiting growth under

a LP-MOVPE environment, we have to use a considerably faster gas stream in the reactor compared to the conventional MOVPE. This is the key to realizing self-limiting, and is also the reason for naming our method "pulsed-jet".

2.3 Requirements for PJE

In the first successful attempt at applying ALE to GaAs growth, Nishizawa *et al.* used an ultra-high vacuum (UHV) growth system [1]. They used TMGa and AsH_3 as sources and these gases were directly injected into the chamber without any carrier gas. To obtain a clear self-limiting growth, it was considered that the pyrolysis of TMGa must be prevented prior to reaching the substrate surface. Since the vapor pressure of Ga atoms is low (*e.g.*, 1 Torr at 1349°C), the Ga atoms will be continuously deposited on the GaAs surface if the precursors are decomposed into nonvolatile Ga in the gas phase. A UHV system is of benefit to avoid the precracking of Ga precursors because they impinge directly on the hot substrate surface in a so-called "molecular beam" form. Conversely, in an MOVPE process, the precursor such as TMGa was thought to be decomposed perfectly into nonvolatile species such as Ga while diffusing through a boundary (or stagnant flow) layer formed at the vicinity of substrate surface [2-4]. Therefore, it seemed difficult to achieve self-limiting growth in an MOVPE environment.

Despite the above-mentioned consideration, Ozeki *et al.* tried to realize the self-limiting growth of GaAs and AlAs in LP-MOVPE [5]. They employed a pulsed vapor-phase method in a chimney-type reactor. At the beginning, they observed no clear self-limiting, even when using TMGa and AsH_3 as sources. This was probably due to the unexpected, excess Ga deposition on the GaAs substrate caused by the unoptimal flow conditions in the reactor. Later, however, they achieved clear self-limiting growth of GaAs by modifying the design and arrangement of the reactor and susceptor [6]. They called the new configuration a "pulsed-jet" reactor. "Pulsed-jet" is, however, a slightly conceptual expression, and this was not the only reactor they used. The requirements for PJE can be summarized as follows:

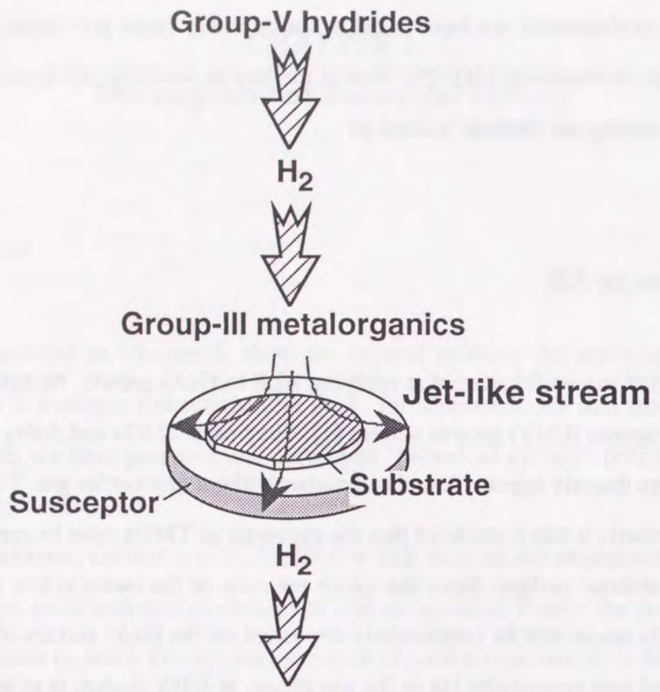

Figure 2-1. Illustration of basic concept of pulsed-jet epitaxy.

Table 2-1: Comparison of available III-V binaries among various ALE techniques.

Laboratories	Systems	Materials				
		GaAs	AlAs	InAs	GaP	InP
Nishizawa et al.	MOMBE in UHV	Yes				
Bedair et al.	MOVPE with rotating substrate	Yes	Yes	Yes		
Usui et al.	Hydride VPE	Yes		Yes	Yes	Yes
Doi et al.	Laser-assisted MOVPE	Yes				
This work	Pulsed-jet	Yes	Yes	Yes	Yes	Yes

(1) The most important feature of PJE is that the source gases are supplied toward the substrates as a fast gas stream from a jet nozzle with a small inner diameter. It is difficult to accurately evaluate the gas velocity at the substrate surface. However, we can roughly estimate from the dimensions of the reactor tube, the total flow rate, and the growth pressure, that the gas velocity is at least several tens of meters per second. Clear self-limiting is obtained with increasing gas velocity. Under this situation, the temperature of the injected gas will not be in equilibrium with that of the heated substrates. Therefore, the precursors will be supplied to the substrate without thermal decomposition, as in a UHV system.

(2) Attention must be paid so that vortices and turbulent flows do not occur in the reactor. They are usually caused by the thermal buoyancy effect from a heated susceptor and convection. These factors cause the gas-phase mixing reaction between group-III and group-V precursors, and the self-limiting growth fails. We have to try to maintain the laminar flow in the reactor.

(3) The gas-switching valves must be carefully designed. A three-way valve with a minimum dead space should be used. These valves should be mounted on a compact manifold. The pressure-balanced, vent/run motion is highly recommended. Unless we pay careful attention to the structure and the arrangement of the valves, the gas-phase mixing reaction will inevitably occur. Furthermore, both the fast-switching speed and its reliability are also important factors to strictly control the surface reactions involved in the PJE.

2.4 Advantages of PJE

In this section, we clarify the distinctive features of PJE, which are superior to other methods for III-V's ALE from the technical point of view. We can expect the following points as the advantages of PJE.

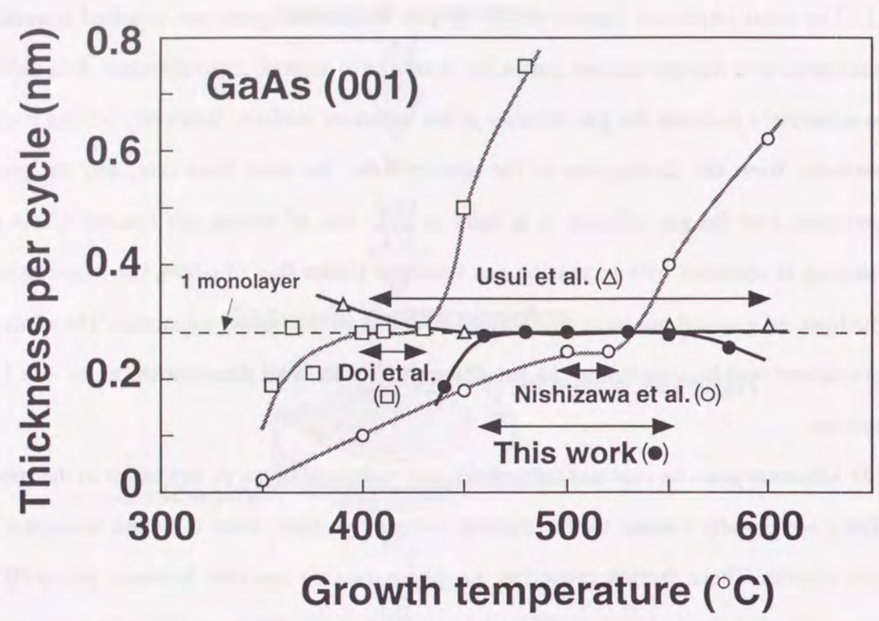

Figure 2-2. Temperature range of GaAs (001) growth rate in various ALE methods.

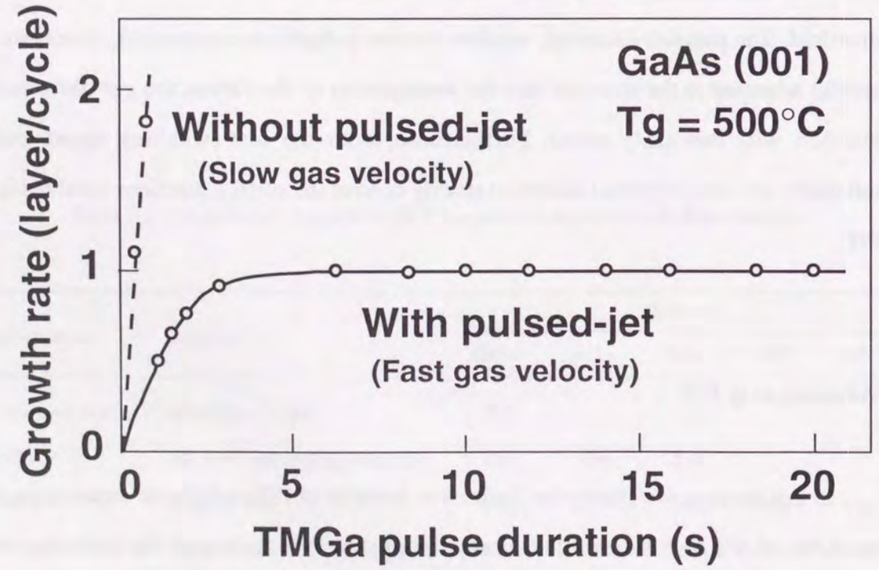

Figure 2-3. GaAs growth rate as a function of TMGa pulse duration.

(1) PJE can be used to grow a larger variety of materials in a self-limiting manner. Table 2-1 summarizes the reported III-V binary materials that can be grown by various ALE methods. In particular, PJE can be used to grow phosphorus (P)-containing materials, *e.g.* InP and GaP [7, 8]. It is difficult to grow these materials in a UHV condition such as that which Nishizawa *et al.* employed [1]. PJE also offers unlimited growth of Al-containing materials, which is a major problem with the method based on hydride VPE as employed by Usui *et al.* [9].

(2) In spite of the use of organometal sources in PJE, a clear self-limiting growth can be attained under a wide range of growth conditions. Figure 2-2 compares the temperature dependence of GaAs (001) growth rate among several ALE methods. It should be natural that the GaCl+AsH_3 system, which was employed by Usui *et al.*, gives the self-limiting over a wide range of growth temperatures because the thermal stability of GaCl in the gas phase is much higher than TMGa [9]. Unlike the other methods using organometal sources, we can realize the self-limiting over a wide rage of growth temperatures with PJE. In addition, it is for the first time that clear self-limiting growth of GaAs was observed for the change of TMGa pulse durations, as shown in Fig. 2-3 [6]. These results show that adopting the extremely fast gas stream ("pulsed-jet") of sources is effective in avoiding the excess Ga atoms deposition over a monolayer coverage. Detailed explanation for the growth experiments is presented in Chapter 3.

(3) High quality epitaxial layers with low residual impurities can be obtained by PJE. Table 2-2 lists the reported electrical properties of undoped GaAs (001) layers grown by several ALE methods. The major problem for the ALE using metalorganic sources has been the unintentional carbon (C) incorporation into GaAs epitaxial layers. Carbon contamination yields inevitable p-type layers. We found for the first time that the careful optimization of the PJE growth cycle yields n-type layer with a carrier concentration of $2x10^{14}$ cm^{-3} and a mobility of $6.5x10^4$ cm^2/Vs at 77 K [6, 10]. As seen in Fig. 2-4, the layer also exhibited sharp emission peaks due to the free and bound excitons near its band gap energy but no emissions associated with the carbon acceptor, which reflects the high optical quality of the PJE-grown epitaxial layer [10]. This is the best result among the

Table 2-2: Electrical properties of GaAs epitaxial layers prepared by various ALE methods.

Laboratories	Systems	Carrier concentration (cm^{-3})	Mobility (cm^2/Vs)	Sources
Nishizawa et al.	MOMBE in UHV	p: 10^{18} - 10^{20} (300K)	less than 100 (300K)	TMGa + AsH_3
Bedair et al.	MOVPE with rotating substrate	p: 2.8 x 10^{17} (77K)	290 (77K)	TMGa + AsH_3
Usui et al.	Hydride VPE	n: 6 x 10^{15} (77K)	16,000 (77K)	GaCl + AsH_3
This work (*)	Pulsed-jet	n: 2 x 10^{14} (77K)	65,000 (77K)	TMGa + AsH_3

*: The electrical property is sensitive to growth conditions. This data is from the best result in our experiments.

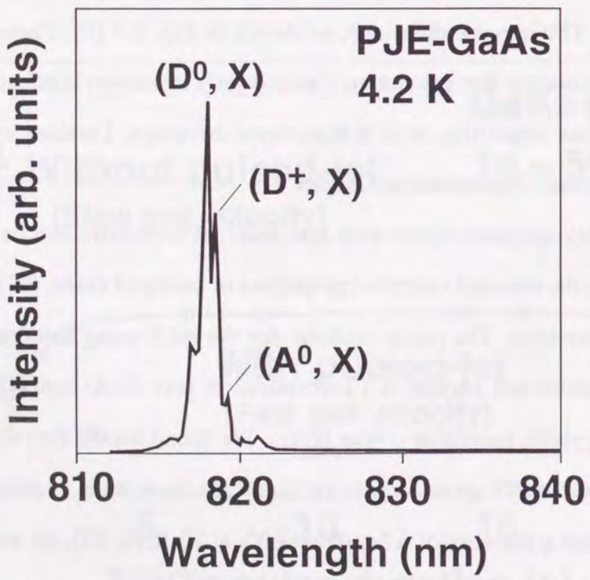

Figure 2-4. PL spectrum from the best, ALE-grown GaAs (001) epitaxial layer.

ALE-grown GaAs ever reported. The shorter TMGa exposure time and the subsequent surface exposure to a sufficient AsH_3 flow are important to obtain high quality materials. As mentioned above, PJE allows the growth to be carried out at higher growth temperatures above 500°C. Therefore, we can use a shorter TMGa pulse to achieve a monolayer growth. Much higher AsH_3 partial pressure in the PJE environment than that in a UHV case also help us obtain GaAs layers with lower C level. Thus, it is easier for PJE to accomplish the growth conditions leading to the epilayers of high purity. The detail procedure for obtaining high quality epitaxial layers is described in Section 3.5.

(4) Extremely uniform thickness profile of grown layers is the most pronounced feature in ALE process. Also in PJE, it is easy to grow epitaxial films with excellent uniformity due to the distinct self-limiting growth behavior. Figure 2-5 shows the thickness variations of PJE and MOVPE-grown GaAs layers on 2-inch diameter substrates [10, 11]. Both epilayers were obtained in the same growth chamber and without any rotation of the substrates. The thickness variation for PJE case is within 1.5% over 2-inch wafer, which is comparable to the error in the thickness measurement. The doping concentration is also extremely uniform in PJE. Figure 2-6 shows the distribution of carrier concentration over 2-inch GaAs wafer doped with selenium (Se) [12]. The electron concentration is normalized by 8.4x10^{18} cm^{-3}. The variation is only 2%, probably within the measurement error. Thus, PJE process is not sensitive to the gas flow pattern in the reactor. These results clearly show that PJE is very useful to the practical device fabrication process.

(5) Ideal selective growth is possible. There is no deposition on the dielectric mask such as SiO_2. Figure 2-7 compares the thickness variation of GaAs epitaxial layers from the SiO_2 mask edge between PJE an MOVPE [13]. The thickness of PJE remains the same surface level, while that of MOVPE gradually decreases due to the enhanced supply of growth species at the mask edge. Thus, there is no so-called "edge effect" in PJE. This is important for a precise masking process in planar technology. The selective epitaxy is explained in detail in Chapter 8.

(6) The growth of heterostructures and superlattices is one of the important purpose of ALE. However, there are few reports on the successful superlattice fabrication of high

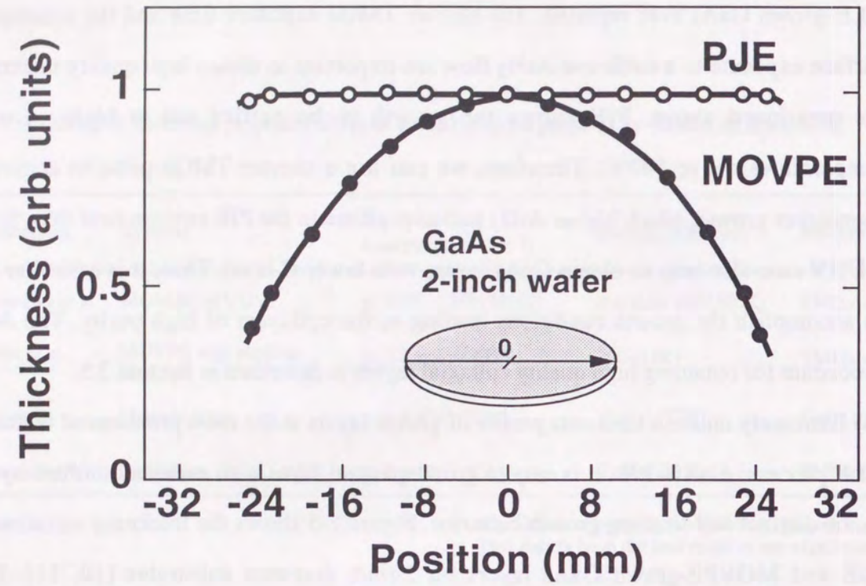

Figure 2-5. Comparison of thickness variations of GaAs epitaxial layers grown by PJE and MOVPE in the same reactor.

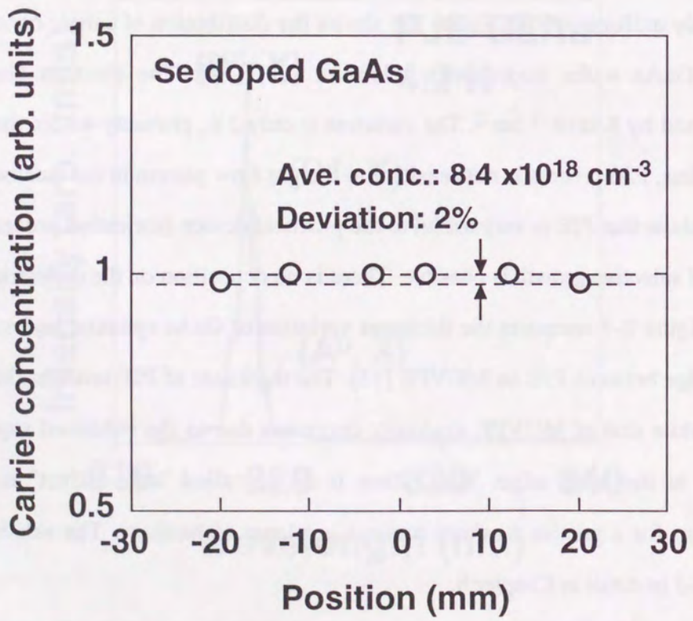

Figure 2-6. Distribution of electron concentration of Se-doped GaAs over 2-inch wafer.

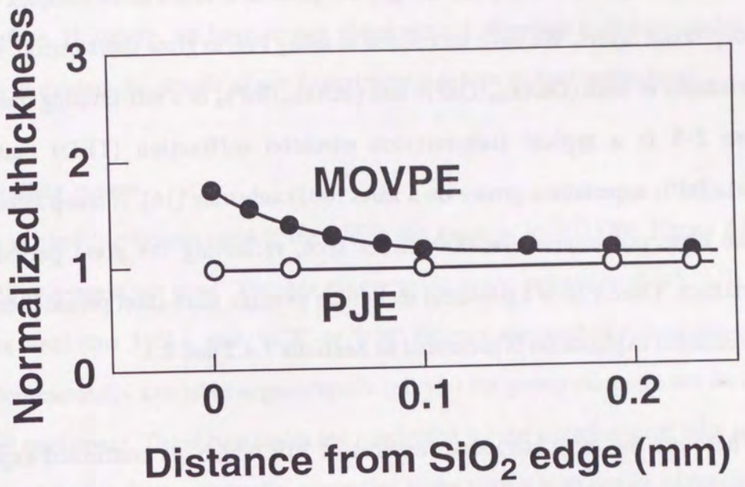

Figure 2-7. Thickness variation of PJE and MOVPE-grown GaAs from SiO_2 edge.

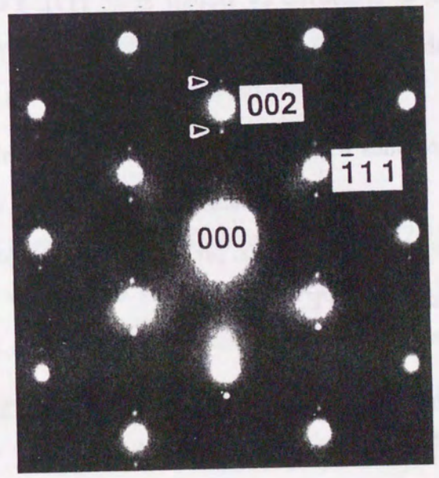

Figure 2-8. A TED pattern from (110) cross-section of $(InAs)_4(InP)_1$ sample.

structural quality. This is because the growth process is much more complex than growing homoepitaxial layers. We have succeeded in using PJE to grow short-period, strained-layer superlattices of both $(GaAs)_m(GaP)_n$ and $(InAs)_m(InP)_n$ in a self-limiting manner [14, 15]. Figure 2-8 is a typical transmission electron diffraction (TED) pattern for the $(InAs)_4(InP)_1$ superlattice grown on a InAs (001) substrate [16]. A sharp satellite-spot pair can be observed around the 000 direct spot, reflecting the good periodicity of the superlattice. Thus, PJE is a powerful technique to make ultra-short period heterostructures. More detailed explanation is presented in Sections 7.4.2 and 8.3.

These are the most attractive features of PJE which we confirmed experimentally. Besides these things, the following things are also expected as the merits of PJE.

(7) PJE is expected to be suitable for mass production. This is because MOVPE growth can be easily done in the same reactor by simply changing the gas sequence so as to simultaneously supply the group-III and group-V sources. Such an advantage is due to the use of switching valves for exchanging the gases in the reactor. In the method using a rotating susceptor, as employed by Bedair *et al.* [17], a complicated machine will be needed to deal with multiple wafers. Compatibility with MOVPE is also difficult with this method.

(8) As MOVPE becomes widespread, a huge base of technical and scientific know-how has accumulated. Since PJE is based on LP-MOVPE, we can use the progressive development of the growth machines, precursors, and the basic understanding of growth mechanisms related to MOVPE.

Thus, PJE is the most flexible approach among the methods proposed for the ALE of III-V compounds.

2.5 Growth Apparatus for PJE

The growth apparatus used for PJE is basically the same as that for LP-MOVPE, as mentioned before. However, we have to pay some special attention to designing the growth system. We will explain the details of our experimental setups in four major parts.

2.5.1 Gas handling system

The gas handling system used in the PJE is the same as in MOVPE. Figure 2-9 shows the gas handling system we used. The gas pipework is made primarily of 1/8, 1/4, and 3/8 inch stainless steel (sus 316L), and 'VCR' or 'UJR' fittings are used to ensure the system is leak-tight. Commercially available organometals (alkyls) for group-III atoms are delivered in stainless-steel containers. These containers are connected by the stainless-steel inlet and outlet tubes, and are bathed in thermostatically-controlled baths with a high degree of precision (less than 0.1°C). High-purity Pd-diffused H_2 is passed through the diptube and is bubbled inside the container. The inner pressure of the containers is kept at constant (1520 Torr) by a pressure regulator. The H_2 flow is accurately metered by mass flow controllers (MFC). Using this equipment, the alkyls with a stable concentration are transported into the reactor with H_2 flow. As the group-V precursors, we used AsH_3 and PH_3. These hydrides are diluted with pure H_2 and filled in cylinders. The concentration is 10% for AsH_3 and 20% for PH_3 in cylinders. The flows of these gases are precisely controlled by MFC.

2.5.2 Gas-switching valves

The role of gas-switching valves is crucial in PJE. In Fig. 2-10, we have shown the schematic of the switching valves. The source gas pulses are generated by switching the individual pneumatic valves on-and-off. It is necessary to switch gases abruptly with a high precision of timing. Elimination of the mixing between group-III and group-V sources at the upstream of the susceptor is also strongly needed. To achieve these requirements, the three-way pneumatic valves with an extremely small dead volume were arranged on a manifold in a vent/run configuration [18]. The pressures in both vent and run lines were balanced to eliminate the spikes in the gas-phase concentration of the reactants [19]. As a valve element, we employed NUPRO SS-4BY-V35 as seen in Fig. 2-11. This valve acts in a three-way

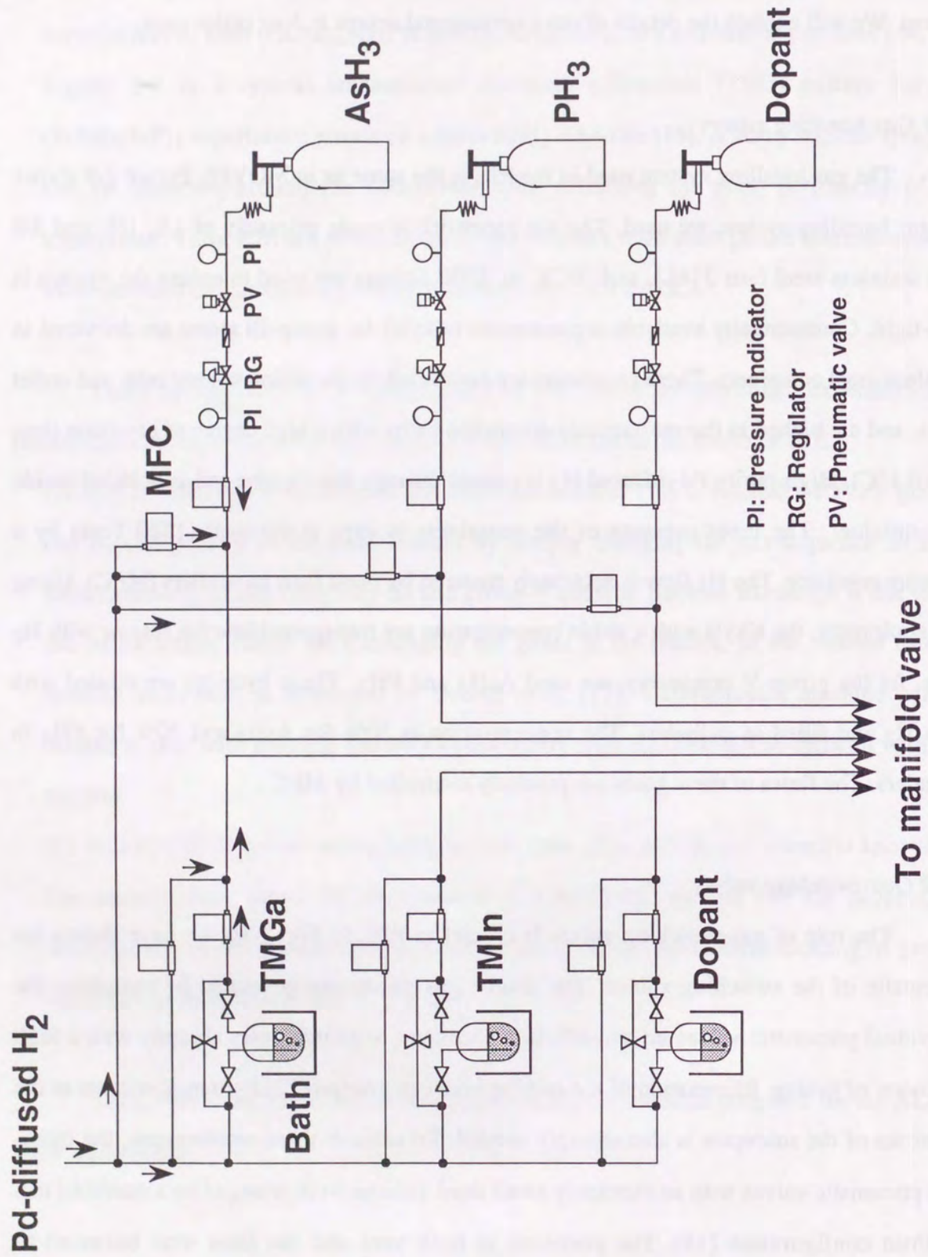

Figure 2-9. Schematics of gas handling system.

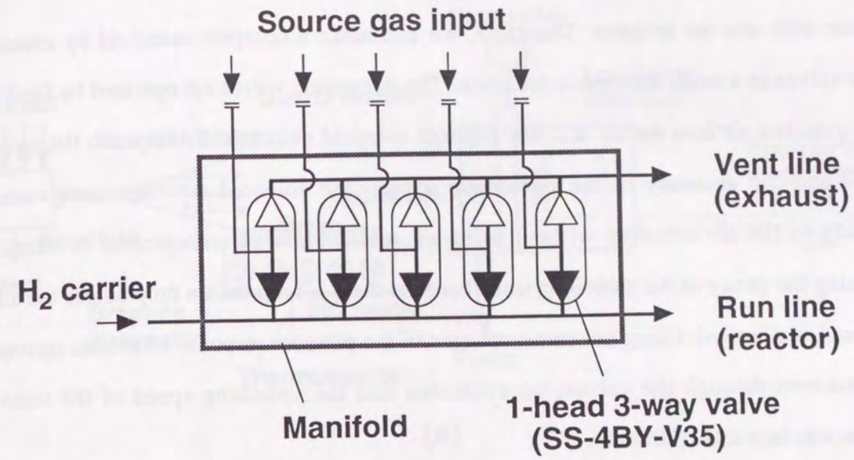

Figure 2-10. Schematic diagram of gas switching valves.

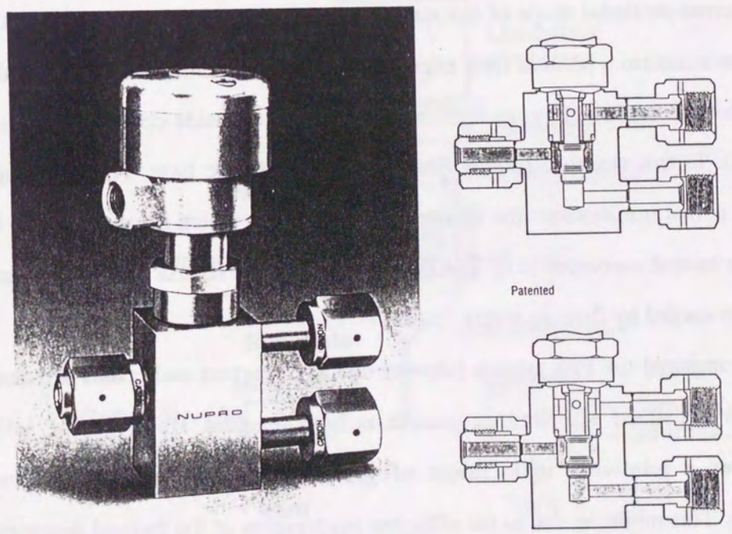

Figure 2-11. Schematic diagram of three-way pneumatic valve.

motion with one air actuator. Therefore, we can make a compact manifold by assembling these valves in a small stainless-steel block. The pneumatic valves are operated by feeding the high-pressure air into the air actuator through solenoid switches. To improve the switching speed and the accuracy of the pneumatic valves, the solenoid switches were connected directly to the air actuators without using air tubes. Such an arrangement is effective in reducing the decay of the switching time, because there is no pressure drop across the air tube conventionally used. Using our measurements of the pressure response time from upstream to downstream through the valves, we estimated that the switching speed of the individual valves was less than 100 msec.

2.5.3 Reactors

We used two types of reactors in our growth experiments. Both reactors were made of the fused quartz tubes. One is the horizontal design seen in Fig. 2-12 (a), widely used in the conventional MOVPE [20, 21]. The gas flow is parallel to the substrate surface for this design. The cross-sectional shape of our reactor is rectangular. The inlet portion of the reactor is designed to maintain a laminar flow even if the gas has expanded after entering the reactor [22]. The other reactor is a chimney-type reactor, or vertical upside-down reactor, as shown in Fig. 2-12 (b). In this reactor, the gas flows upward from the base. The advantage of this arrangement is that it minimizes the recirculation of the gas which is caused by the buoyancy effects of the heated susceptor [23]. The cross section of the reactor tube is circular, and the reactor wall is cooled by flowing water.

We compared the PJE growth between the two reactors and results are described in Chapter 3. We realized self-limiting growth in both reactors. However, the self-limiting occurred over a relatively wide range of growth conditions with the chimney-type configuration. This might be due to the effective suppression of the thermal decomposition of the group-III precursors in the gas phase. Thus, the chimney reactor is better than the horizontal one in achieving self-limiting growth.

2.5.4 Heating methods

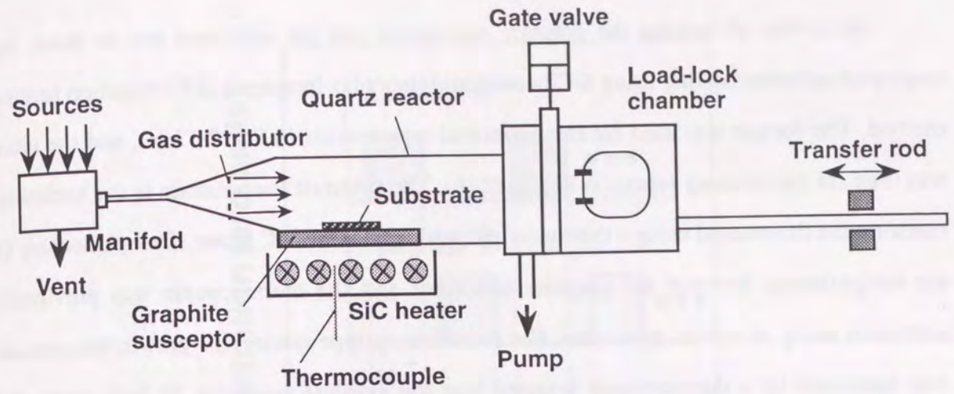

Figure 2-12. PJE reactors: (a) horizontal type, and (b) chimney type.

As a way of heating the graphite susceptors and the substrates put on them, we employed radiative heating using SiC heaters and the radio-frequency (RF) induction heating method. The former was used for the horizontal-type reactor in Fig. 2-12 (a), and the latter was used for the chimney reactor in Fig. 2-12 (b). The substrate temperatures in the horizontal reactor were determined using a thermocouple setting near the SiC heater. The relationship of the temperatures between the graphite susceptor and the thermocouple was previously calibrated using an optical pyrometer. For the chimney-type reactor, the growth temperature was measured by a thermocouple inserted into the graphite susceptor. In both cases, the growth temperature was controlled to an accuracy of 0.1°C.

2.6 Experimental Procedure

2.6.1 Growth procedure

Epitaxial growth was carried out by alternately feeding the group-III and group-V precursors into the reactor. Figure 2-13 represents the gas flow sequence used for III-V epitaxial layers. The alternating pulses of the organometals for group-III atoms and hydrides for group-V are separated by H_2 purge pulses which prevent the mixing of the reaction gases. We defined one gas cycle during PJE as shown in the figure. The duration of individual gas pulses and the concentration of the reactants contained in the H_2 carrier gas were varied to study the growth kinetics. We grew several kinds of III-V materials (GaAs, GaP, InAs, and InP) by repeating the gas cycles several hundred times. The precursors used in our experiments and several of their properties are summarized in Table 2-3.

The total H_2 flow rate in the reactor, f_{total}, was kept at 1000 or 2000 sccm (standard cubic centimeters per minute). The growth pressure, p_{total}, was typically 15 or 20 Torr. If the group-III precursor is used under its vapor pressure of $vp_{group\text{-}III}$ (Torr) and the H_2 flow rate through the container is $f_{group\text{-}III}$ (sccm), the mole fraction of the group-III precursors, $mf_{group\text{-}III}$, in the gas pulse is given by,

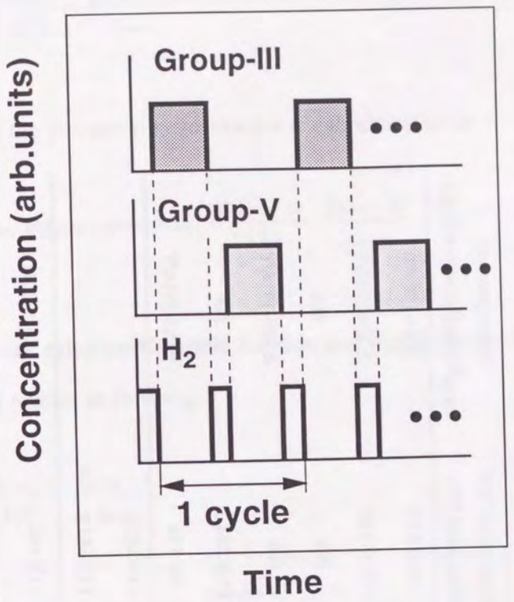

Figure 2-13. Gas sequence of PJE.

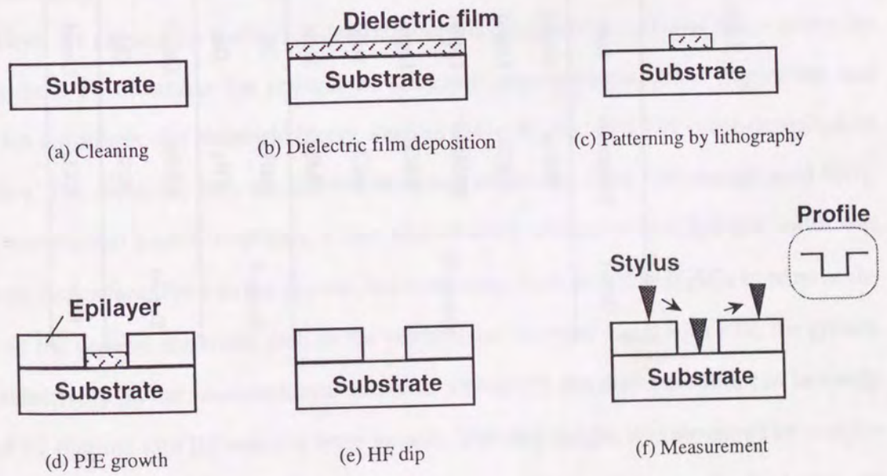

Figure 2-14. Procedure for growth thickness measurement.

Table 2-3: Precursors for PJE and their properties.

Group	Compound	State	Molecular weight	Melting point (°C)/ Boiling point (°C)	Vapor pressure $\log_{10}P$ (mmHg) = B-A/T (K)
Group-III	TMGa	Liquid	114.82	-15.8/ 55.7	8.07-1703/T
	TEGa	Liquid	156.91	-82.5/ 143	8.224-2222/T
	EDMGa	Liquid	128.85	NA	NA
	TiBGa	Liquid	240.93	NA	4.769-1718/T
	$GaCl_3$	Solid	176.03	77.9/ 201.3	NA
	TMIn	Solid	159.93	88/ 134	10.52-3014/T
Group-V	AsH_3	Gas	77.95	-117/ -62.5	
	PH_3	Gas	34.00	-133/ -87.8	
Dopant	DEBe	Liquid	67.05	-12/ 194	14.5-5102/T
	H_2Se	Gas	80.98	-64/ -47.3	
Other	CCl_4	Liquid	153.84	-23/ 76.7	5.991-1202.9/(T-48.01)

NA: Not available

$$mf_{group-III} = \frac{vp_{group-III}}{1520} \cdot \frac{f_{group-III}}{f_{total}} \tag{2-1}$$

The partial pressure of the precursor in the reactor is calculated to be

$$p_{group-III} = p_{total} \cdot mf_{group-III} = p_{total} \cdot \frac{vp_{group-III}}{1520} \cdot \frac{f_{group-III}}{f_{total}} \tag{2-2}$$

Similarly, we can calculate the mole fraction and the partial pressure for the group-V hydride sources in the reactor as follows:

$$mf_{group-V} = \frac{c_{group-V}}{100} \cdot \frac{f_{group-V}}{f_{total}} \tag{2-3}$$

$$p_{group-V} = p_{total} \cdot mf_{group-V} = p_{total} \cdot \frac{c_{group-V}}{100} \cdot \frac{f_{group-V}}{f_{total}} \tag{2-4}$$

where the $c_{group\text{-}V}$ is the volume-percent concentration of the hydrides in the cylinders.

2.6.2 Procedure for thickness measurement

Here, we explain the method of determining the thickness of epitaxial layers grown by PJE. Figure 2-14 illustrates the process of thickness measurement. After degreasing and etching the substrates, the dielectric layers, such as SiO_2, Si_3N_4, or SiON, were deposited on the surface. The dielectric film was several thousand angstroms thick. We mainly used SiO_2. Using conventional photolithography, a line-shaped SiO_2 pattern with a 500 μm width was formed on the surface. Prior to the growth, the substrates were rinsed in H_2SO_4 to remove the residue of the organic materials such as the photoresist. In most cases with PJE, the growth occurs selectively on the semiconductor surfaces. Therefore, the dielectric film can be easily removed by dipping into HF solution after growth. The step height was measured by a stylus profilometer (DEKTAK 3030). This height corresponds to the growth thickness. In

calculating the growth rate per gas cycle, the thickness was divided by the number of the injected gas cycles. The accuracy of the thickness measurement was about 1%.

2.7 Summary

We have explained the details of pulsed-jet epitaxy, or PJE, which enables us to grow III-V compound semiconductor's thin films in a self-limiting manner. First, we defined PJE. Then, we described the requirements for PJE in terms of the growth conditions and the growth apparatus. Although PJE is based on LP-MOVPE, achieving clear self-limiting growth is difficult under the normal MOVPE growth conditions with conventional machines. We must employ a fast gas velocity to suppress the gas-phase decomposition of group-III precursors. We also have to pay special attention to the design of reactors and the gas switching valves to ensure both a laminar flow and abruptly-switched gas pulses. These are the key factors to attain the self-limiting growth. Comparing with other reported ALE methods, we have described the inherent advantages of PJE in detail. Finally, we explained the growth procedure and the method of thickness measurement.

REFERENCES (Chap. 2)

[1] J. Nishizawa, H. Abe, and T. Kurabayashi, J. Electrochem. Soc. **132** (1985) 1197.

[2] M.R. Leys and H. Veenvliet, J. Cryst. Growth **55** (1981) 145.

[3] J. Nishizawa and T. Kurabayashi, J. Electrochem. Soc. **130** (1983) 413.

[4] M. Yoshida, H. Watanabe, and F. Uesugi, J. Electrochem. Soc. **132** (1985) 677.

[5] M. Ozeki, K. Mochizuki, N. Ohtsuka, and K. Kodama, J. Vac. Sci. Technol. **B5** (1987) 1184.

[6] M. Ozeki, K. Mochizuki, N. Ohtsuka, and K. Kodama, Appl. Phys. Lett. **53** (1988) 1509.

[7] Y. Sakuma, K. Kodama, and M. Ozeki, Jpn. J. Appl. Phys. **27** (1988) L2189.

[8] Y. Sakuma, K. Kodama, and M. Ozeki, Appl. Phys. Lett. **56** (1990) 827.

[9] A. Usui and H. Sunakawa, Jpn. J. Appl. Phys. **25** (1986) L212.

[10] M. Ozeki, N. Ohtsuka, Y. Sakuma, and K. Kodama, J. Cryst. Growth **107** (1991) 102.

[11] Y. Sakuma, M. Ozeki, N. Ohtsuka, Y. Matsumiya, H. Shigematsu, O. Ueda, S. Muto, K. Nakajima, and N. Yokoyama, Appl. Surf. Sci. **82/83** (1994) 46.

[12] T. Takanohashi, K. Mochizuki, and M. Ozeki, Inst. Phys. Conf. Ser. **106** (1990) 39.

[13] M. Ozeki, K. Mochizuki, N. Ohtsuka, and K. Kodama, Thin Solid Films **174** (1989) 63.

[14] M. Ozeki, K. Kodama, Y. Sakuma, N. Ohtsuka, and T. Takanohashi, J. Vac. Sci. Technol. **B8** (1990) 741.

[15] Y. Sakuma, M. Ozeki, K. Kodama, and N. Ohtsuka, J. Cryst. Growth **115** (1991) 324.

[16] O. Ueda, Y. Sakuma, M. Ozeki, N. Ohtsuka, and K. Nakajima, Proceedings of 1st International Symposium on Control of Semiconductor Interfaces, p. 531 (1993).

[17] S.M. Bedair, M.A. Tischler, T. Katsuyama, and N.A. El-Masry, Appl. Phys. Lett. **47** (1985) 51.

[18] J.S. Roberts, N.J. Mason, and M. Robinson, J. Cryst. Growth **68** (1984) 422.

[19] R.S. Sillmon, N. Bottka, J.E. Butler, and D.K. Gaskill, J. Cryst. Growth **77** (1986) 73.

[20] S.J. Bass, J. Cryst. Growth **31** (1975) 172.

[21] H. Beneking, A. Escobosa, and H. Kraute, J. Electron. Mater. **10** (1981) 473.

[22] A. Okamoto, H. Sunakawa, H. Terao, and H. Watanabe, J. Cryst. Growth **70** (1984) 140.

[23] M.R. Leys, C. Van Opdorp, M.P.A. Viegers, and H.J. Talen-Van Der Mheen, J. Cryst. Growth **68** (1984) 431.

CHAPTER 3
Growth of III-V Binary Compounds

3.1 Preliminaries

As described in the previous chapter, the concept of PJE was first proposed and demonstrated by Ozeki *et al.* in 1987 [1]. From the beginning of their research, they used a chimney-type reactor and tried to grow GaAs and AlAs. In their first attempt, however, they didn't observe the clear self-limiting growth. Meanwhile, they found that by both increasing the gas velocity and creating a laminar flow at the substrates by optimizing the arrangement of the susceptor in the chimney reactor, it was possible to achieve distinct self-limiting growth [2]. At the same time, we began to expand the range of materials we can grow by developing a PJE for phosphorus (P)-containing materials. The capability of growing P-containing materials is one of the attributes of PJE. We also wanted to know if we could use a horizontal-type reactor for PJE. Thus, the first experiment for the self-limiting growth of InP and GaP by PJE was conducted using a horizontal reactor shown in Fig. 2-12 (a) [3, 4]. Naturally, we could also grow GaAs and InAs in the same horizontal reactor. However, we found that the so-called "ALE window", the range of growth conditions for self-limiting growth, is narrower than that obtained in the chimney-type configuration. Therefore, the use of the horizontal-type reactor was limited at the beginning of our studies.

In this chapter, we describe the homoepitaxial growth results for III-V binary compounds on (001) substrates. First, we show the preliminary results obtained in the simple horizontal reactor. We clarify some drawbacks leading to the narrow "ALE window" inherent in the horizontal-type reactor. Next, the results obtained in the chimney-type reactor are shown. Using this reactor, we were able to grow epitaxial layers of III-V compounds in a self-limiting manner over a relatively wide range of growth conditions. Then, we show the dependence of the growth rates for both GaAs and InP on the specific substrate orientations:

(111)A, (111)B, and (011). Furthermore, some electrical and optical properties of the PJE-grown epitaxial layers are shown.

3.2 Structure and Properties of III-V Semiconductors

Figure 3-1 shows a zinc-blende crystal structure of III-V compound semiconductor, where a_o is a lattice parameter of the material. In this structure, the group-III and group-V atoms have an average of four valence electrons per atom available for binding. It is usually considered that the covalent bonds are formed through tetrahedral *sp3* hybrid orbitals. For example, for GaAs, the reaction is written as:

$$\mathrm{Ga}(4s^24p) + \mathrm{As}(4s^24p^3) \rightarrow \mathrm{Ga}(4s4p^3)^- + \mathrm{As}(4s4p^3)^+ \qquad (3\text{-}1)$$

In this consideration of covalent bonding, each group-V atom donates an electron to a group-III atom, so that V^+ and III^- ions having four valence electrons are formed.

However, another explanation, based on the ionic bonding formation, is very important. In this consideration, the bonds are caused by the Coulomb attractive force between the excess positive and negative charges of ions. The excess charges are generated by the transfer of electrons from the metallic group-III atom to the nonmetallic group-V atom. For GaAs, the reaction pathway is shown as:

$$\mathrm{Ga}(3d^{10}4s^24p) + \mathrm{As}(3d^{10}4s^24p^3) \rightarrow \mathrm{Ga}(3d^{10})^{+3} + \mathrm{As}(3d^{10}4s^24p^6)^{-3} \qquad (3\text{-}2)$$

The bonds of most III-V compounds are not described by these extreme models, but usually have intermediate characteristics between the "covalent" and "ionic" bonds. Anyway, the polarity of III-V compounds seems to play a significant role in the surface reaction during PJE growth.

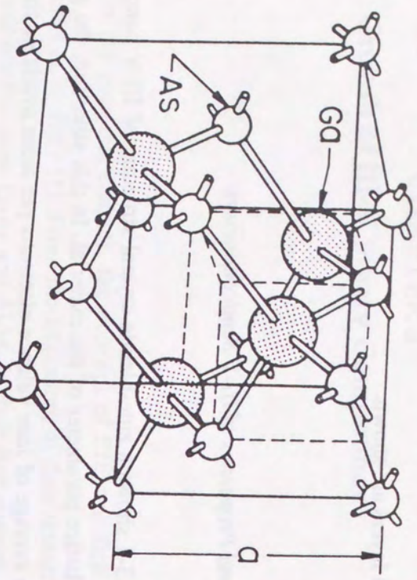

Figure 3-1. Zinc-blende crystal structures.

Figure 3-2. Atomic arrangements of III-V crystals for various orientations.

Table 3-1: Physical properties of III-V binary compounds.

Material	Density (g/cm^3)	Lattice constant at 300 K (nm)	Melting point (°C)	Band gap (eV)	Effective mass (m^*/m_o)	Mobility (cm^2/Vs)	
				77 K/ 300 K	$m_e^*/ m_{hh}^*/ m_{lh}^*$	μ_e 77 K/ 300 K	μ_h 300 K
AlAs	3.598	0.5661	1740	2.25/ 2.13 (X)	0.15/ 0.76/ 0.15	/ 180	
GaAs	5.307	0.5653	1238	1.522/ 1.428 (Γ)	0.067/ 0.50/ 0.093	244000/ 8500	420
InAs	5.667	0.6058	943	0.410/ 0.356 (Γ)	0.023/ 0.41/ 0.025	120000/ 33000	460
GaP	4.129	0.5451	1467	2.34/ 2.24 (X)	0.17/ 0.54/ 0.10	2100/ 200	120
InP	4.787	0.5868	1070	1.420/ 1.351 (Γ)	0.080/ 0.60/ 0.12	140220/ 6060	150

In Fig. 3-2, we show the schematic side views of the atomic arrangement of the III-V crystals toward the crystallographic orientation of (001), (011), (111)A and (111)B. It should be noted that the monolayer thickness is different among the growth orientations. The monolayer thickness, d, is obtained as follows.

$$d = \frac{a_o}{2} \text{ for (001), } \frac{a_o}{2\sqrt{2}} \text{ for (011), and } \frac{a_o}{\sqrt{3}} \text{ for (111)A, (111)B} \qquad (3\text{-}3)$$

where a_o is a lattice parameter. For instance, for GaAs, a_o is 0.5653 nm.

We summarize the physical properties for several binary compounds in Table 3-1.

3.3 PJE of Binary Compounds

3.3.1 Results in horizontal reactor

3.3.1.1 InP

As a typical example of PJE conducted in the horizontal reactor, we explain the growth of InP in detail. For the first time, we successfully achieved the self-limited InP epitaxial growth using PJE [3]. At that time, little work had been done on the ALE of InP. For experiments, we used the horizontal reactor seen in Fig. 2-12 (a). The substrates were heated by the SiC heater placed outside the reactor, as explained in Section 2.5.4. We employed trimethylindium (TMIn) and PH_3 as sources. The total flow rate in the reactor was 1000 sccm at all times. The total pressure inside the reactor ranged from 15 to 23 Torr. The substrates were Sn-doped and Fe-doped InP (001). The mirror etching of the substrates was done by a Br_2-ethanol solution. We determined the growth rates according to the method described in Section 2.6.2.

Figure 3-3 shows the dependence of the InP (001) growth rate (expressed in units of monolayers per cycle) on the TMIn mole fraction. The mole fraction was varied by changing the vapor pressure of the TMIn in the container and the H_2 flow rate through it. Since we didn't know the appropriate growth temperatures for the self-limiting growth of InP, we

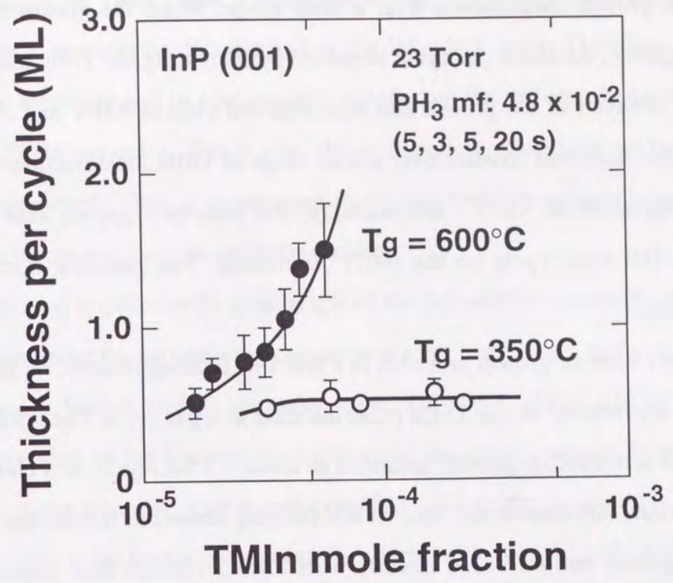

Figure 3-3. Dependence of InP (001) growth rate as a function of TMIn mole fraction. (5, 3, 5, 20 s) is the gas supply mode; 5 s purge with H_2, 3 s TMIn supply, 5 s H_2 purge, and 20 s PH_3 injection.

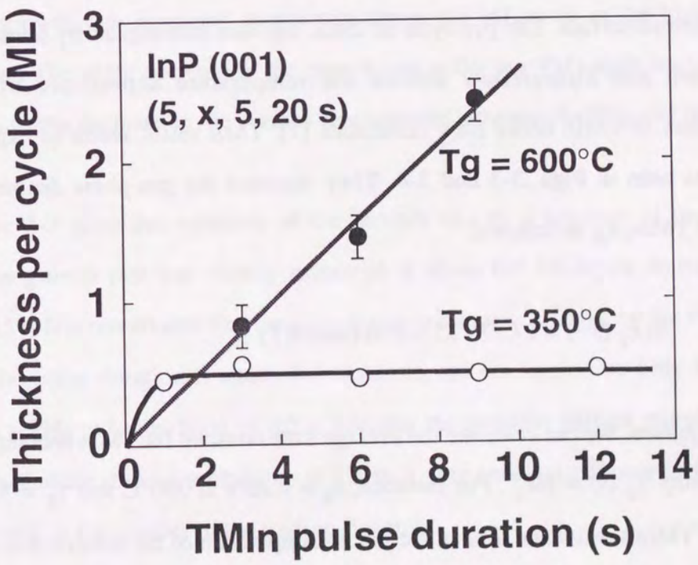

Figure 3-4. Dependence of InP (001) growth rate as a function of TMIn pulse duration.

changed the growth temperatures over a wide range. When the growth temperature was 600°C, the growth thickness per cycle increased by increasing the TMIn mole fraction. This unsaturated behavior of the growth rate was observed even at 400°C and 375°C. However, the growth rate remained constant over a wide range of TMIn mole fractions by lowering the growth temperature to 350°C. Interestingly, the saturated growth rate was about 0.5 monolayers (ML) per cycle on the (001) orientation. The plausible mechanism will be discussed later.

To test whether growth proceeds in a real self-limiting manner, we have to study the growth rate dependence on the TMIn pulse duration in a gas cycle. The results are shown in Fig. 3-4. The self-limiting growth, saturated at about 0.5 ML/cycle, was clearly observed at 350°C. We could not observe any distinct self-limiting above this temperature. As seen in the figure, the growth rate increased linearly with TMIn exposure time, especially at around 600°C. Thus, the growth temperature is an important parameter to be controlled for achieving the self-limiting growth of InP.

Based on the results in Figs. 3-3 and 3-4, we can conclude that the self-limiting mechanism is related to the thermal decomposition rate of TMIn in the boundary layer formed near the substrate surface. The pyrolysis of TMIn has been investigated by several researchers [5-7]. Larsen and Stringfellow studied the temperature dependence of the percent decomposition of TMIn under flow conditions [7]. Their result seems to explain well our observations seen in Figs. 3-3 and 3-4. They reported the gas-phase decomposition rate constant for TMIn, k_g, as follows:

$$\ln k_g\ (s^{-1}) = 27.57 - 35.9\ \text{kcal/(mol•RT)} \qquad (3\text{-}4)$$

From this equation, we can calculate the average time constant for TMIn decomposition using the relationship τ_g (s) = $1/k_g$. For instance, τ_g = 4.23 s at 350°C and $\tau_g = 1.04\text{x}10^{-3}$ s at 600°C. The TMIn's residence time at the hot zone upstream of the substrates is calculated to be about 50 ms, considering our flow condition and the dimensions of the reactor. Comparing this residence time with the time constants of TMIn decomposition, it is clear that the

pyrolysis of TMIn in the vapor phase is negligible at 350°C. Contrary to this, at 600°C, most of the TMIn molecules will be decomposed in the boundary layer. Therefore, nonvolatile products such as atomic In will be continuously supplied on the surface while the substrate is exposed to the TMIn gas pulse. This is why the self-limiting growth cannot be obtained at high growth temperatures. Thus, it is important that TMIn is not decomposed completely into such an In atom before reaching the substrate surface.

Figure 3-5 (a) is a Nomarski photograph of the InP surface grown by PJE at 350°C. The layers grown under the self-limiting condition always had smooth surfaces independent of the TMIn mole faction and its exposure time. However, above 350°C, the surface morphology depended on the TMIn mole fraction and the pulse duration. In particular, the surface became rough when the growth rate exceeded 1 ML/cycle, as shown in Fig. 3-5 (b). This is probably due to the formation of many In islands on the growth surface after excess In atoms were supplied from the vapor phase. This suggests that In overlayers on the InP (001) surface grow under the Stranski-Krastanov mode [8], *i.e.*, two-dimensional growth occurs at a coverage of up to 1 ML, followed by island formation, then three-dimensional growth.

Figure 3-6 shows the dependence of the growth rate on the PH_3 mole fraction at 350°C. The growth rate remained constant at about 0.5 ML/cycle in the high-PH_3 mole fraction region. The slight decrease in the growth rate at the low-PH_3 mole fraction region is probably due to the decrease in the surface reaction rate between the PH_3 and the surface In species.

Figure 3-7 plots the variation of the growth rate as a function of the PH_3 pulse duration. The growth rate was clearly saturated at about 0.5 ML/cycle above PH_3 pulse duration of 15 s. It is remarkable that the growth rate is strongly affected by the PH_3 exposure time when the pulse duration is short. For example, we could observe little InP epitaxial growth with a PH_3 pulse duration of 0.5 s, keeping the specular surface morphology. This result implies that the sticking probability of TMIn is very small on a P-poor surface, and that it is proportional to the number of the surface P atoms.

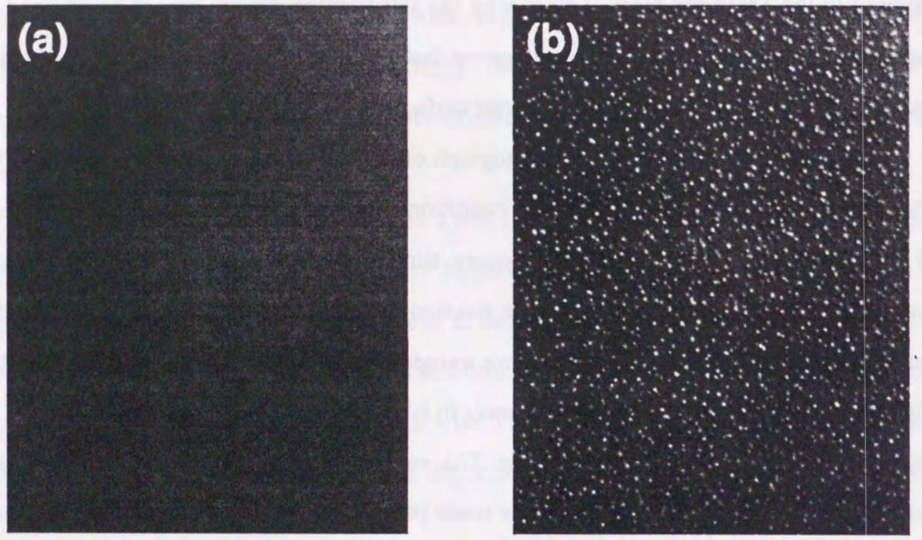

Figure 3-5. Nomarski micrographs of InP epilayers grown at (a) 350°C with thickness of 75 nm and (b) 600°C with thickness of 120 nm.

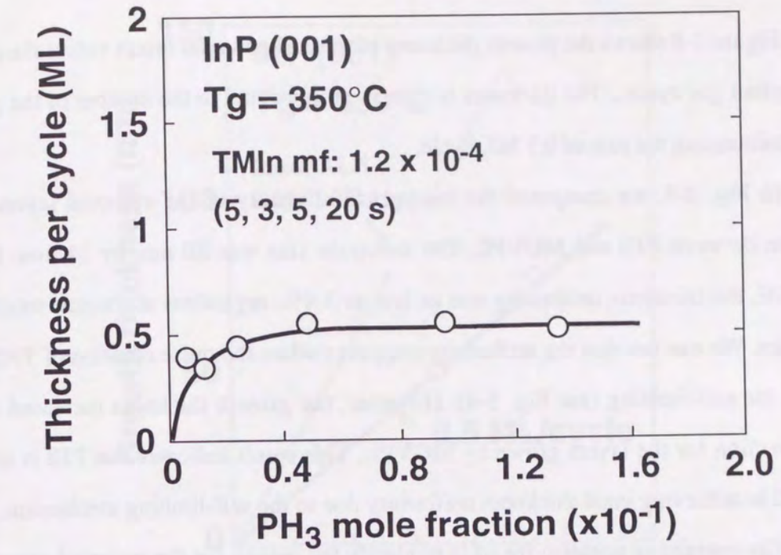

Figure 3-6. Dependence of InP (001) growth rate on PH_3 mole fraction.

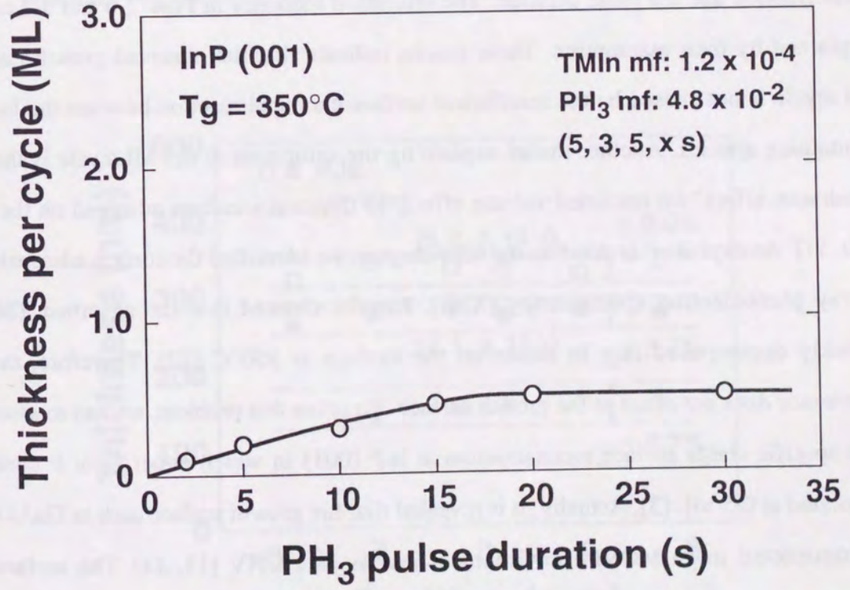

Figure 3-7. Variation of InP growth rate as a function of PH_3 pulse duration.

Figure 3-8 shows the growth thickness of the InP epitaxial layers versus the number of the supplied gas cycles. The thickness is clearly proportional to the number of the gas cycles when maintaining the rate of 0.5 ML/cycle.

In Fig. 3-9, we compared the thickness uniformity of the epitaxial layers over the substrate between PJE and MOVPE. The substrate size was 20 mm by 14 mm. In growth using PJE, the thickness uniformity was as low as 3-4%, regardless of the non-rotation of the substrates. We can see that the uniformity improves when the pulse duration of TMIn is long enough for self-limiting (see Fig. 3-4). However, the growth thickness increased along the flow direction for the layers grown by MOVPE. This result indicates that PJE is superior to MOVPE in achieving good thickness uniformity due to the self-limiting mechanism.

The remaining problem for us is to clarify the reason for the saturated growth rate of 0.5 ML/cycle observed in PJE-grown InP. Usui *et al.* pointed out that the lack of the PH_3 cracking at the low growth temperature (350°C) is likely to be the main reason for this [9]. If this is true, we could observe the gradual increase in the growth rates as we increase the PH_3 mole fraction and the pulse duration. The saturation tendency in Figs. 3-6 and 3-7 cannot be explained by their assumption. These results indicate that the observed growth rate of 0.5 ML/cycle is not caused by the insufficient surface chemical reaction between the In- and P-containing species. Another model explaining the saturation at 0.5 ML/cycle is the "steric hindrance effect" (or excluded volume effect) of the methylindium adsorbed on the surface [10, 11]. As explained in detail in the next chapter, we identified the surface adsorbates using X-ray photoelectron spectroscopy (XPS). Results showed that the adsorbed TMIn was quickly decomposed into In atoms on the surface at 350°C [12]. Therefore, the steric hindrance does not occur at the growth surface. To solve this problem, we had to assume that the specific stable surface reconstruction at InP (001) in which either In or P coverage is saturated at 0.5 ML [3]. Actually, it is revealed that the growth surface such as GaAs (001) is reconstructed in an MOVPE environment just as in a UHV [13, 14]. The surface is not necessarily stable when the reconstructed surfaces have a monolayer coverage of Ga or As, *i.e.* 6.3×10^{14} cm^{-2}. The relationship between the self-limiting value of the ALE growth rate and the surface stoichiometry of the reconstructed surface is a current topic [15].

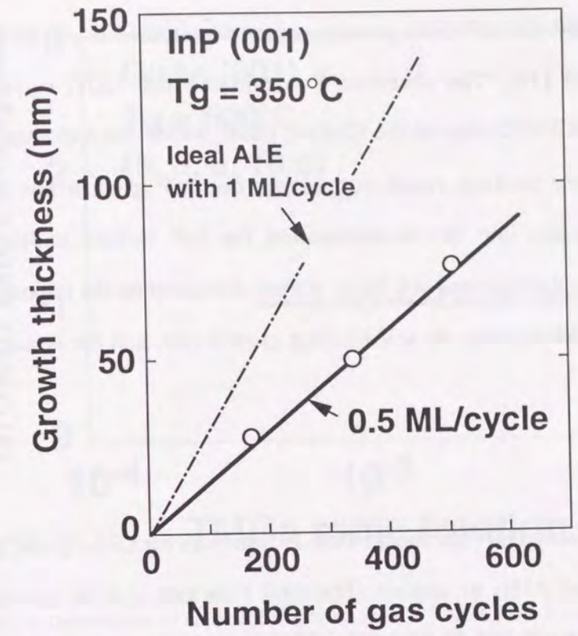

Figure 3-8. Growth thickness of InP epitaxial layers versus the number of gas cycles. Growth was done under 15 Torr with a gas sequence of (5, 3, 5, 20 s). The mole fraction of TMIn and PH_3 was 1.2×10^{-4} and 9.6×10^{-2}, respectively.

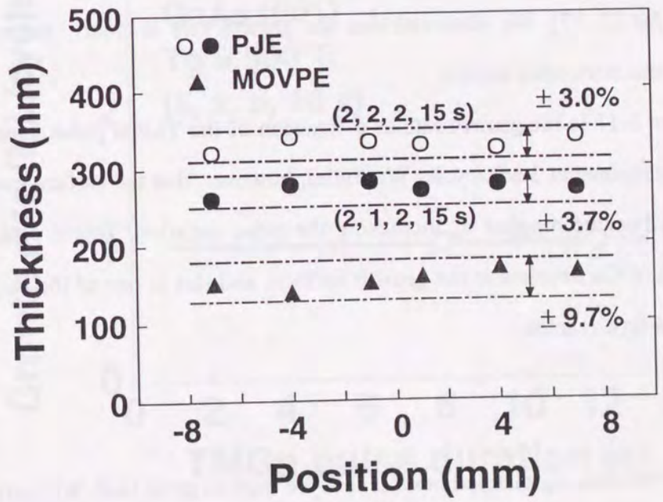

Figure 3-9. Comparison of thickness uniformity between PJE and MOVPE mode. The PJE was done at 350°C and MOVPE at 500°C. The left-hand side of position corresponds to the upstream.

Very recently, the InP (001) growth surface was studied *in-situ* by scanning tunneling microscopy (STM) [16]. The observed P-terminated InP (001) surface under a UHV condition at around 350°C showed the (2x4)-α phase which has a surface P coverage of 0.5 ML. This is a very striking result supporting our InP growth rate of 0.5 ML/cycle. Unfortunately, studies into the reconstruction for InP surface under the low-pressure environment have not progressed yet. Here, we just comment on the importance of the surface reconstruction for determining the self-limiting growth rate, and the details will be discussed again in Chapter 6.

3.3.1.2 GaAs

Prior to growing GaP, we checked the PJE growth for GaAs in the horizontal reactor. We used TMGa and AsH_3 as sources. The total flow rate and the growth pressure in the reactor were 1000 sccm and 15 Torr. The TMGa bubbler was held at 3.0°C, providing a TMGa vapor pressure of 79.4 Torr. The substrates were CrO-doped, semi-insulating GaAs (001).

Figure 3-10 shows the dependence of the GaAs growth rate on the TMGa mole fraction at 500°C. This is a typical growth temperature for achieving the self-limiting growth reported so far [2, 17]. We observed that the growth rate is clearly saturated at nearly 1 ML/cycle in our horizontal reactor.

Figure 3-11 is the growth rate as a function of the TMGa pulse duration. Again, the growth rate remained at 1 ML/cycle. We found, however, that the surface morphology of the grown layers became rougher by increasing the pulse duration. This is probably due to the accumulation of Ga droplets at the growth surface, and this is one of the major problems of the horizontal-type reactor.

3.3.1.3 GaP

As a P-containing material besides InP, we tried to grow GaP. We carried out the ALE of GaP for the first time, in a horizontal PJE reactor [4]. The sources we used were TMGa and PH_3. The flow condition and the growth pressure were the same as those for

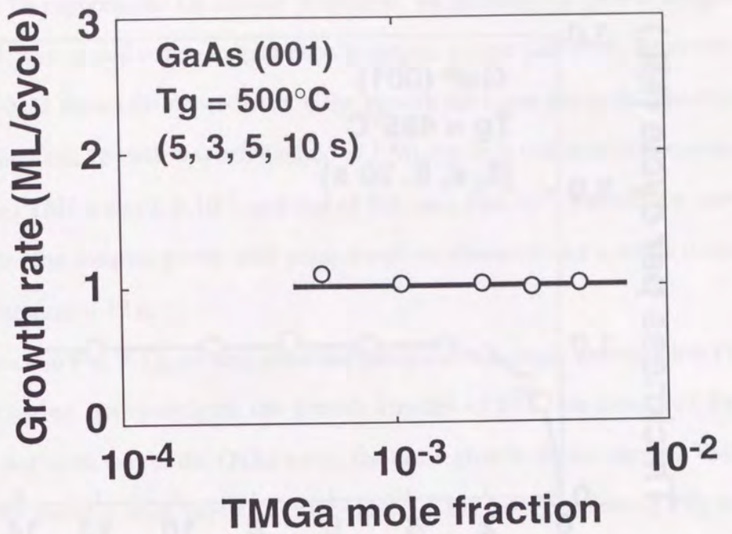

Figure 3-10. Dependence of GaAs (001) growth rate on TMGa mole fraction. (5, 3, 5, 10 s) shows gas sequence; 5 s H_2 purge, 3 s TMGa pulse, 5 s H_2, and 10 s AsH_3 supply. AsH_3 mole fraction was 4.8×10^{-2}.

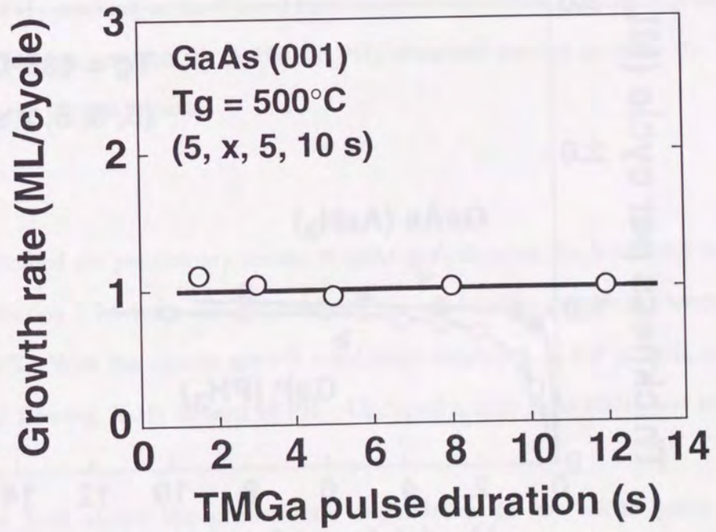

Figure 3-11. Dependence of GaAs (001) growth rate on TMGa pulse duration. The mole fraction of TMGa and AsH_3 was 2.1×10^{-3} and 4.8×10^{-2}, respectively.

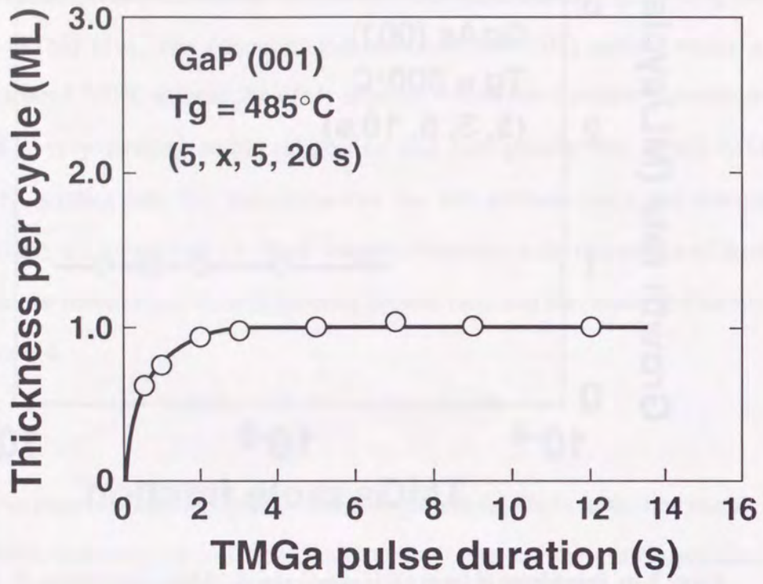

Figure 3-12. Dependence of GaP (001) growth rate on TMGa pulse duration.

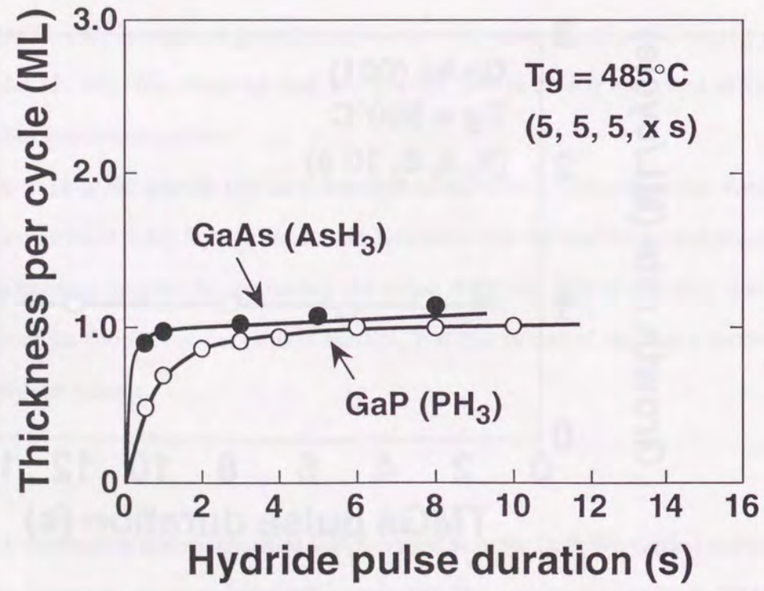

Figure 3-13. Growth rates of PJE-grown GaP and GaAs as a function of hydrides pulse duration.

GaAs growth. To suppress the Ga droplet formation, we lowered the growth temperature to 485°C. Growth was carried out on unintentionally-doped, n-type GaP (001) substrates.

Figure 3-12 shows the dependence of the growth thickness per cycle (growth rate) on TMGa pulse duration. Growth was self-limited to 1 ML/cycle at this growth temperature. The mole fraction of TMGa was 2.1×10^{-3}, and that of PH_3 was 9.6×10^{-2}. The surface morphology was specular for the samples grown with pulse durations shorter than 9 s, while it was a little rough at the duration of 12 s.

As shown in Fig. 3-13, we also observed saturated monolayer growth when PH_3 pulse duration was varied. To investigate the growth kinetics of PJE, we compared the rate of saturation in GaP with that of the GaAs under the same growth conditions: the TMGa mole fraction and the duration were kept at 2.1×10^{-3} and 5 s; the mole fractions of PH_3 and AsH_3 were both 4.8×10^{-2}. It takes longer to reach 1 ML with the corresponding hydride duration in GaP than in GaAs. At 485°C, the pyrolysis of PH_3 is heterogeneous [18]. The decomposition of PH_3 proceeds catalytically only on the GaP surface. Therefore, the result in Fig. 3-13 implies that the rate of surface chemical reaction between Ga (or Ga-containing alkyls), which is adsorbed on the surface, and PH_3 is slower. This surface reaction consists of several steps, such as PH_3 cracking or Ga-P bond formation. However, the rate-limiting step, which causes the difference between the AsH_3 and PH_3 durations needed to reach the saturated growth rate, is not clear at present.

3.3.1.4 InAs

We obtained the preliminary results of InAs growth using the horizontal reactor. As described in Section 3.3.1.1, for InP, we observed the self-limiting growth at a temperature of as low as 350°C. With the similar growth conditions employed in InP growth, we tried to grow InAs by flowing AsH_3 instead of PH_3. Undoped n-type InAs (001) was used as the substrate.

Figure 3-14 shows the growth rate dependence on the TMIn pulse duration. Significantly, the growth rate of InAs was clearly self-limited at about 0.7 to 0.8 ML/cycle, unlike the result of InP where the rate was saturated at 0.5 ML/cycle. Note that all the growth

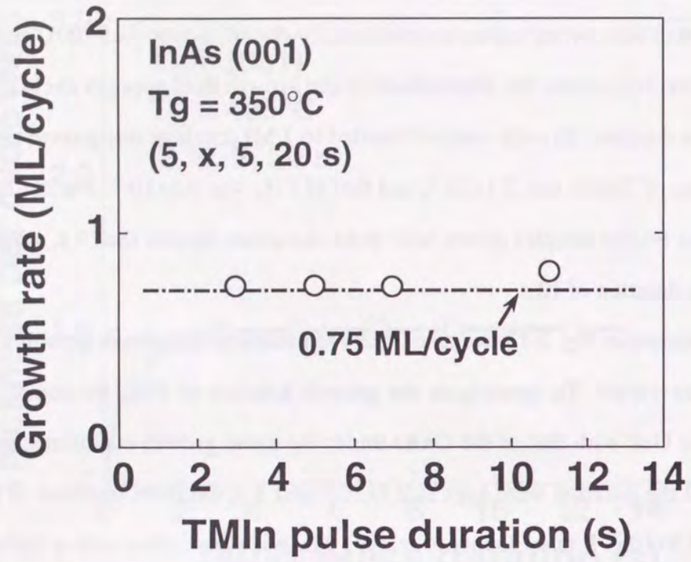

Figure 3-14. Growth rate dependence of InAs (001) on TMIn pulse duration. The growth pressure was 15 Torr. The mole fraction of TMIn and AsH_3 was $1.2x10^{-4}$ and $4.8x10^{-2}$, respectively. Note that the purge time by H_2 is 5 s.

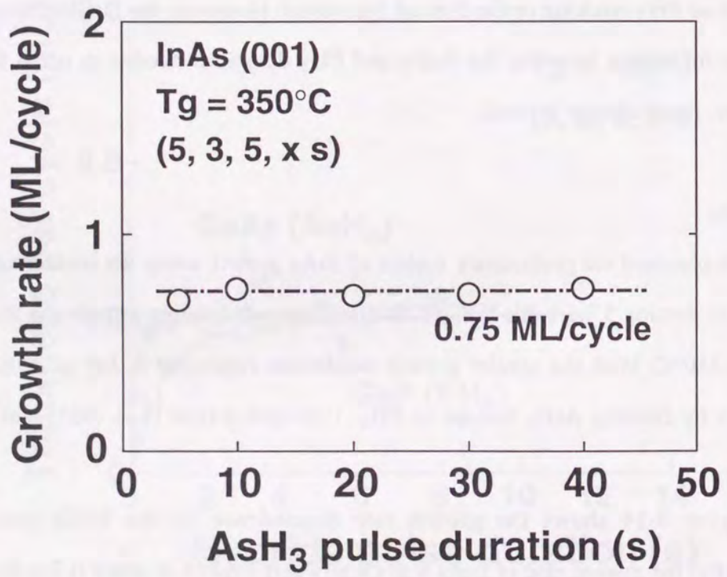

Figure 3-15. Growth rate variation of InAs (001) on AsH_3 pulse duration. The mole fractions of sources were the same as those in fig. 3-14.

conditions, *i.e.*, growth temperature, pressure, mole fractions of TMIn and hydrides and the gas sequence, were the same as those used in Fig. 3-4.

We studied how the AsH_3 pulse duration affects the self-limited value of InAs. Results are shown in Fig. 3-15. Although there is small amount of scatter among the data, the growth rate was not affected by the AsH_3 exposure time and was self-limited at about 0.7 to 0.8 ML/cycle.

Here, we briefly comment on the growth mechanism. As discussed in the PJE of InP (Section 3.3.1.1), this fractional self-limiting growth rate of InAs is caused neither by the slow decomposition rate of AsH_3 nor the steric hindrance of the adsorbed methylindium, $(CH_3)_xIn$ (x=1, 2, or 3) [11]. Later, we will clarify that this is strongly related to the surface As stoichiometry or the surface reconstruction of InAs (001). Due to the desorption of surface As atoms during the H_2 purge duration, we observed the decrease in the growth rate. To make the growth rate self-limited at 1 ML/cycle, we have to shorten the H_2 purge time after supplying AsH_3. An explanation of this phenomena is given later in Chapter 6.

3.3.2 Some problems in horizontal reactor

As described above, we basically observed the self-limiting growth for InP, GaP, GaAs, and InAs in the horizontal reactor, using the trimethyl alkyls (TMGa, TMIn) and hydrides (AsH_3, PH_3) as precursors. However, there are some problems in using the horizontal reactor. The major problems are summarized as follows:

(1) Narrow "ALE window". The growth conditions for self-limiting growth are restricted. For example, droplets appeared on the growth surface when we grew GaAs (001) with long TMGa pulse durations. Figure 3-16 shows the surface morphologies of GaAs epilayers grown with the TMGa pulse duration of 3 s and 9 s at 500°C. With increasing the TMGa pulse duration, the density of the droplets increased dramatically. There is a hot runway on the graphite susceptor at the upstream of the substrates. Since the supplied gases are heated before reaching the substrates, we can hardly avoid the excess deposition of Ga on the surface. Thus, there is a limitation to the suppression of the gas-phase decomposition of group-III precursors in the horizontal configuration.

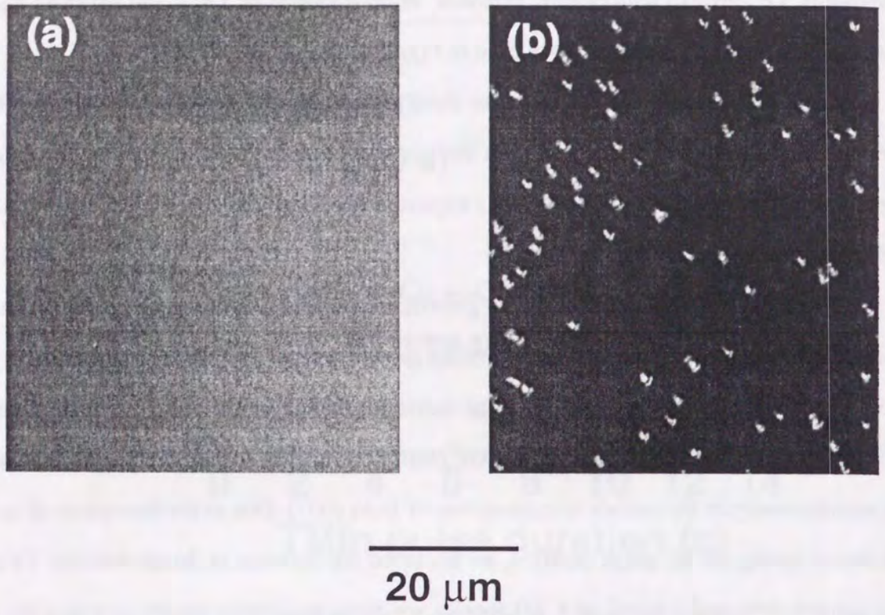

Figure 3-16. Nomarski micrographs of PJE-grown GaAs layers for TMGa duration of (a) 3 s and (b) 9 s.

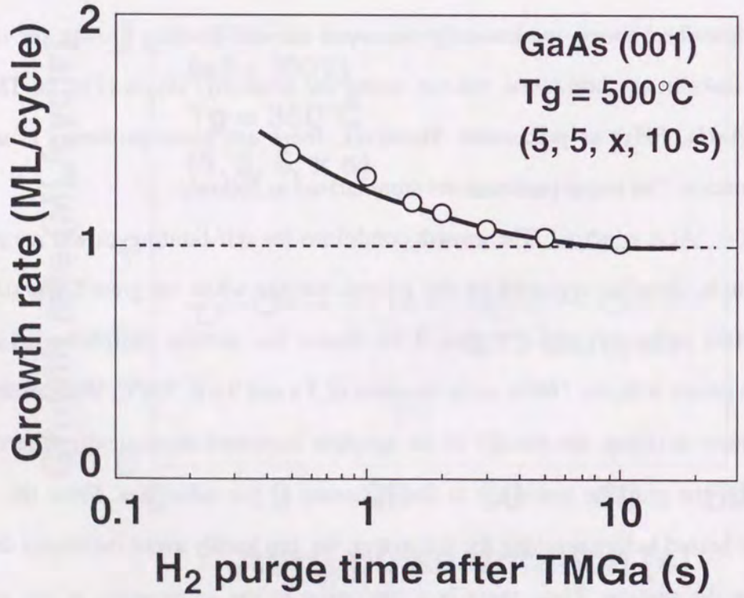

Figure 3-17. Variation of GaAs growth rate as a function of H_2 purge time after TMGa. Note that the horizontal-type reactor was used.

(2) Difficulty in fast purging of reactants. Figure 3-17 shows the dependence of the GaAs (001) growth rate, obtained in the horizontal-type reactor at 500°C, on the H_2 purge time after TMGa supply. We observed the excess growth rate of more than 1 ML/cycle for purge times of under 5 s. This undesired growth behavior might be due to the gas-phase mixing reaction, or MOVPE-mode growth, between TMGa and AsH_3. In spite of the careful reactor design, it is difficult to eliminate the vortices perfectly near the substrates at the growth temperatures, probably caused by the buoyancy effect from the horizontal hot susceptor. As a result, it takes longer H_2 purge time than that calculated from the flow rate and the reactor volume to purge out the reaction gases from the reactor. The slow gas exchange also becomes a barrier, for example, in attaining the growth rate of 1 ML/cycle for InAs (001) [19]. The InAs growth rate will be less than 1 ML/cycle. This is not related to the gas-phase mixing but to the desorption of surface As atoms. We have to realize fast gas switching with H_2 from AsH_3 to TMIn. Shortening the pulse duration of H_2 purge is crucial for realizing the ideal monolayer growth of InAs.

3.3.3 Results in chimney reactor

Using the reactor of the chimney configuration seen in Fig. 2-12 (b), the above-mentioned problems are relaxed. The advantages of this reactor are as follows: (1) since there is no hot zone upstream of the substrates, the residence time at the hot zone for the group-III precursors becomes much smaller in this reactor. This leads to the minimum gas-phase decomposition of the precursors in the boundary layer; (2) the gas flow direction coincides with the direction of buoyancy caused by the heated susceptor. Therefore, the recirculation of wasted gas might be eliminated and the purging of the reactants could be accomplished in a shorter time. Here, we will report the results of GaAs (001) and InAs (001) growth.

3.3.3.1 GaAs

We could dramatically expand a range of growth temperatures in which the self-limiting growth of GaAs (001) occurred [2]. GaAs growth was done using TMGa and AsH_3.

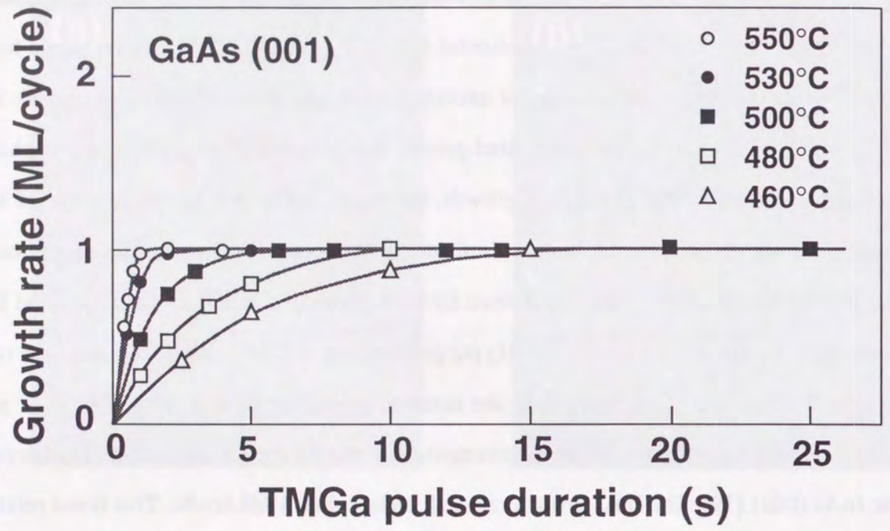

Figure 3-18. Dependence of GaAs growth rate as a function of TMGa pulse duration from 460 to 550°C.

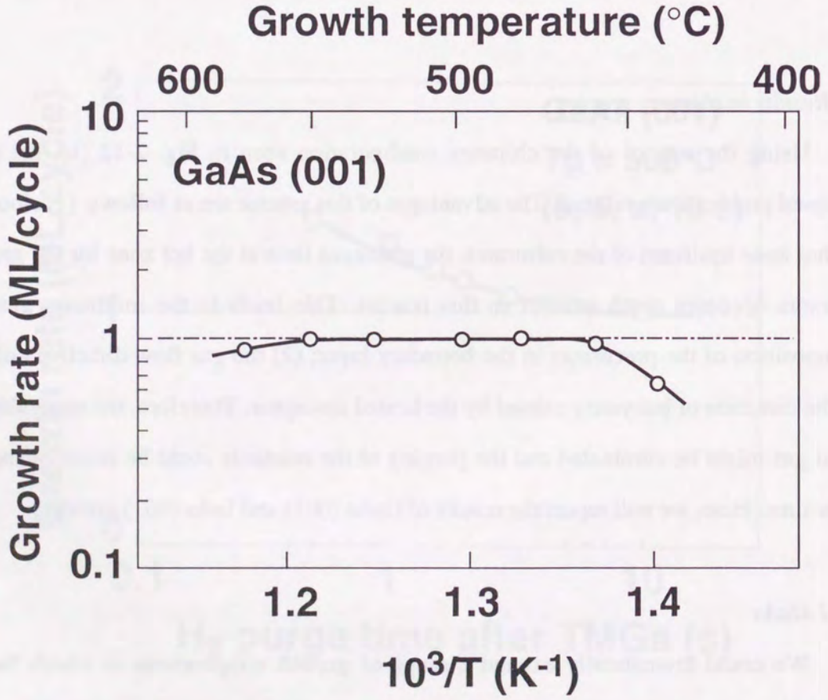

Figure 3-19. GaAs growth rate as a function of reciprocal growth temperatures.

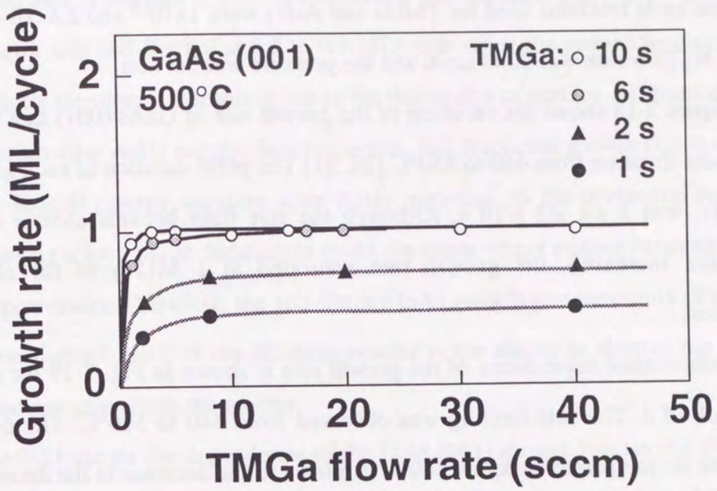

Figure 3-20. GaAs growth rate as a function of TMGa flow rate under different pulse durations.

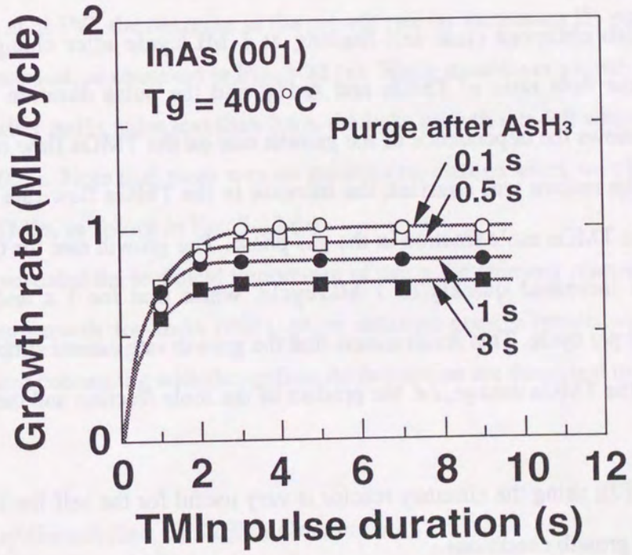

Figure 3-21. Dependence of InAs (001) growth rate on TMIn pulse time. AsH_3 pulse was 10 s and H_2 purge after TMIn was 0.5 s.

The typical mole fractions used for TMGa and AsH_3 were $1x10^{-3}$ and $2.4x10^{-2}$, respectively. The total H_2 flow rate was 2000 sccm and the pressure was 20 Torr.

Figure 3-18 shows the variation of the growth rate of GaAs (001) as a function of the TMGa pulse duration from 460 to 550°C [20, 21].The pulse duration of each gas, H_2/ TMGa/ H_2/ AsH_3, was 3 s/x s/3 s/10 s. Although the rise time became shorter as the growth temperature increased, the growth rate saturated at 1 ML/cycle for all the growth temperatures.

Temperature dependence of the growth rate is shown in Fig. 3-19 for a TMGa pulse duration of 15 s. The self-limiting was observed from 440 to 560°C. The decrease in the growth rate for temperatures below 440°C is related to the decrease in the decomposition rate of methylgallium, $(CH_3)_xGa$ (x=1, 2, or 3), on the growth surface. In contrast, the decrease in growth rate at higher growth temperatures above 560°C is probably attributed to the desorption of the methylgallium or surface As atoms. The range of growth temperatures where we observed self-limiting growth is the widest among those obtained by the ALE techniques [22, 23].

We also observed clear self-limiting at 1 ML/cycle after changing other growth parameters: the flow rates of TMGa and AsH_3, and the pulse duration of AsH_3 [20, 24]. Figure 3-20 shows the dependence of the growth rate on the TMGa flow rate. Since the total flow rate in the reactor was constant, the increase in the TMGa flow rate corresponds to an increase in the TMGa mole fraction in the gas phase. The growth rate for the TMGa pulse of 6 s and 10 s increased quickly to 1 ML/cycle, while that for 1 s and 2 s saturated at submonolayer per cycle. This result means that the growth rate cannot simply be described as a function of the TMGa dosage, *i.e.* the product of the mole fraction and the pulse duration of TMGa.

Thus, PJE using the chimney reactor is very useful for the self-limiting growth over a wide range of growth conditions.

3.3.3.2 InAs

As described in Section 3.3.1.4, we observed that the InAs (001) growth rate in the horizontal reactor was self-limited at 0.7 to 0.8 ML/cycle when the growth temperature was 350°C. We briefly mentioned that this is due to the desorption of surface As atoms during the H_2 purge duration after AsH_3 supply. In other words, this fractional growth rate is caused by the relatively long H_2 purge duration after AsH_3 injection. In the horizontal reactor, we cannot avoid using a long purge duration to avoid the vapor-phase mixing between group-III and group-V precursors. Therefore, the self-limited InAs growth rate inevitably falls below 1 ML/cycle. One distinct merit of the chimney reactor is the ability to shorten the exchange time of the reactant gases from the reactor.

Figure 3-21 shows the dependence of the InAs (001) growth rate on the TMIn pulse length at 400°C in the chimney reactor [19]. The H_2 purge time after AsH_3 ranged from 0.1 to 3 s. Although the growth was self-limiting, the saturated growth rate was smaller for longer H_2 purges. To achieve monolayer growth of InAs at 400°C, the H_2 purge must be shortened to less than 0.1 s.

Figure 3-22 clearly indicates the effect of As desorption from the outermost surface of InAs (001). Even at 365°C, the decrease in the growth rate by increasing H_2 purge time after AsH_3 was also observed, as observed in Fig. 3-22 (a). While monolayer growth was achieved using H_2 purges after AsH_3 pulse less than 0.5 s, the InAs growth rate fell when the H_2 purge was longer than 0.5 s. Note that there was no growth rate change when we changed the H_2 purge time after TMIn, as shown in Fig. 3-22 (b).

Thus, we revealed the technical importance of using the chimney reactor to realize the ideal self-limiting growth for InAs (001). More detailed growth results and the surface reaction mechanism concerning with the surface As desorption are described in Chapter 6.

3.4 Dependence of Growth Rate on Surface Orientations

The surface chemical reactions which occur at the gas/solid interface are very important in PJE. Therefore, the structures (bonding geometry) and the chemical properties of

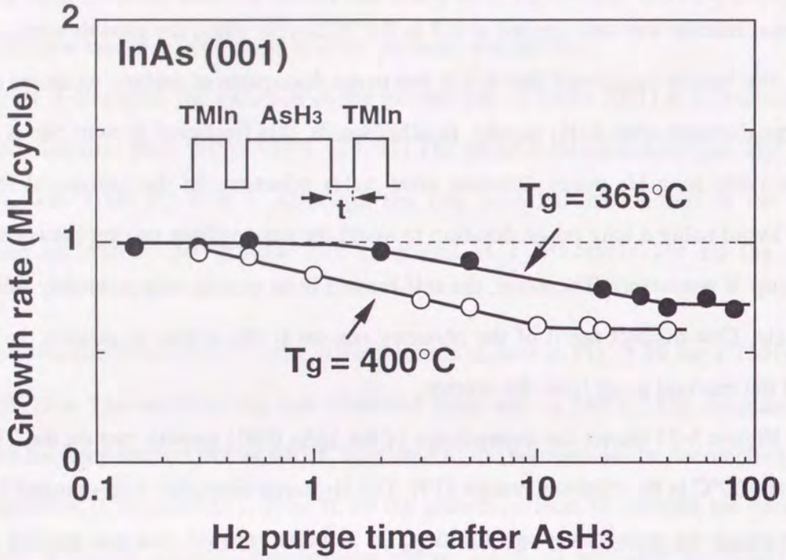

Figure 3-22(a). Variation in InAs growth rate as a function of H_2 purge time after AsH_3.

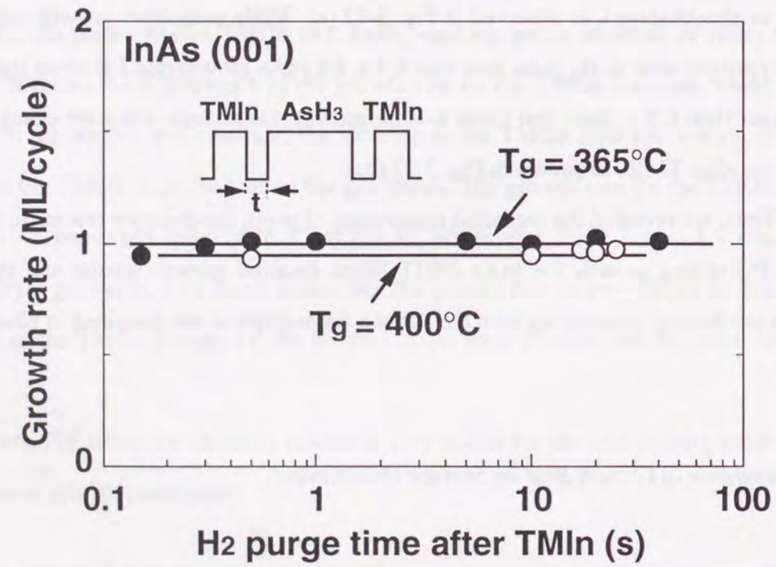

Figure 3-22(b). Variation in InAs growth rate as a function of H_2 purge time after TMIn.

the substrates' surfaces will strongly affect the surface reactions, such as morphologies, doping behavior, and the growth rate, as has been reported for other growth techniques [25-29]. The crystallographic orientation dependence of the PJE growth rate provides us with not only information about the growth mechanism, but also helpful hints for fabricating some novel device structures on non-planar substrates [30]. In this section, we describe some preliminary results of the PJE growth studies on the substrates with various orientations.

3.4.1 GaAs

In Fig. 3-23, we compare the dependence of the GaAs growth rate as a function of TMGa pulse duration for substrates of several crystallographic orientations: (001), (011), (111)A, and (111)B. The vertical axis of the figure is normalized with a monolayer per cycle because the monolayer thickness differs among orientations. The ideal monolayer thickness, d, has a relationship with lattice constant a_o, as described in Eq. (3-3). The growth was carried out at 500°C under a pressure of 20 Torr. The mole fraction of TMGa and AsH_3 was $1x10^{-3}$ and $1.25x10^{-2}$. The gas sequence, H_2/ TMGa/ H_2/ AsH_3, was 0.5 s/ x s/ 0.5 s/ 5 s. We found several novel features in this figure.

(1) The growth rate tends to saturate with increasing TMGa pulse duration, and the saturated value differs among the substrates of different orientations.

(2) The saturated growth rate is less than 1 ML/cycle for (011), (111)A, and (111)B GaAs.

(3) The self-limiting growth rate on GaAs (001) is about 1.25 ML/cycle.

In spite of the saturated growth rate at fractional monolayers, we achieved self-limiting growth on (011), (111)A, and (111)B surfaces. There have been few reports so far of the successful self-limiting growth of GaAs on substrates with these crystallographic orientations [31, 32]. Our results clearly indicate the superiority of PJE in obtaining the self-limiting growth on substrates with various orientations.

A perfect understanding of the growth behaviors shown in Fig. 3-23 is difficult. However, we have some important results which indicate the influence of surface As atoms on the growth kinetics. Figure 3-24 shows the growth rate dependence of GaAs (011) on the TMGa pulse duration at three different growth temperatures. Since the injected AsH_3 mole

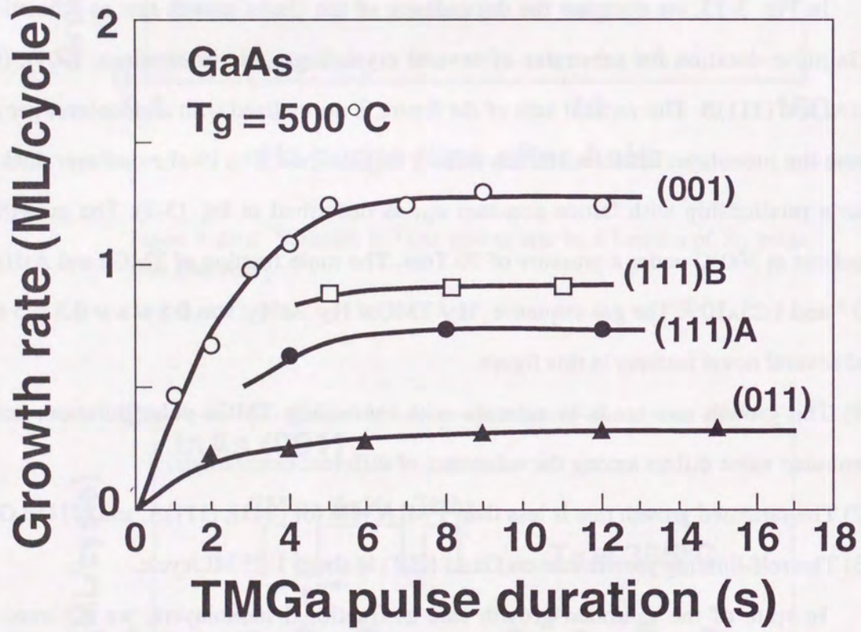

Figure 3-23. GaAs growth rate on several surface orientations as a function of TMGa pulse duration.

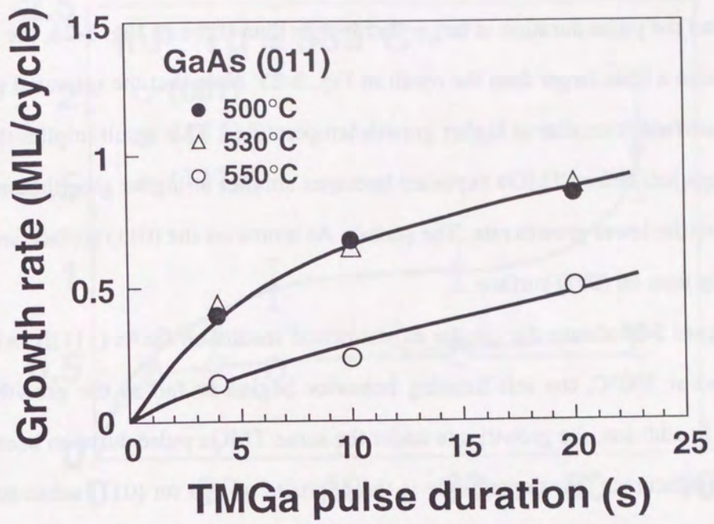

Figure 3-24. Growth rate dependence of GaAs (011) on TMGa pulse duration at different temperatures. The mole fraction of TMGa and AsH_3 was $1x10^{-3}$ and $2.4x10^{-2}$, respectively. The gas sequence was 3/ x/ 3/ 10 s.

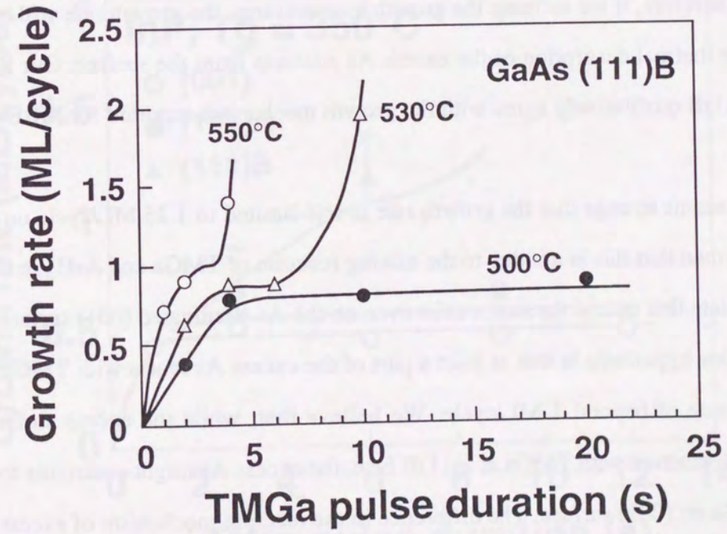

Figure 3-25. Growth rate dependence of GaAs (111)B on TMGa duration at different temperatures. The mole fractions and gas sequence are identical with those in fig. 3-24.

fraction and the pulse duration is larger and longer than those in Fig. 3-23, the growth rate at 500°C is also a little larger than the result in Fig. 3-23. Note that the saturated growth rate on the (011) surface is smaller at higher growth temperatures. This result implies that the surface As coverage just before TMGa exposure becomes smaller at higher growth temperatures and this leads to the lower growth rate. The surface As atoms on the (011) surface seems to desorb more easily than on (001) surface.

Figure 3-25 shows the similar experimental results on GaAs (111)B. Although being self-limited at 500°C, the self-limiting behavior begins to fail as the growth temperature increases. In addition, the growth rate under the same TMGa pulse duration becomes larger at higher temperatures. This dependence is the opposite of that on (011) substrate. It has been reported that excessively adsorbed As atoms forming a trimer structure exist on As-rich (111)B surface [33]. These surface As atoms deactivate the surface reactivity and suppress the incorporation of Ga into sublattice sites on the (111)B surface, leading to a decrease in the growth rate [34, 35]. We speculate that excess As atoms exist on the AsH_3-exposed (111)B GaAs surface also under our PJE environment, and this leads to the suppressed reaction with TMGa. Therefore, if we increase the growth temperatures, the growth rate will become larger due to the thermal desorption of the excess As adatoms from the surface. Our PJE results on GaAs (111)B qualitatively agree with the growth mechanism reported for MBE and MOVPE [34, 35].

It seems strange that the growth rate is self-limited to 1.25 ML/cycle on (001) GaAs. We confirmed that this is not due to the mixing reaction of TMGa and AsH_3 in the gas phase. We speculate that excess As atoms exist even on the As-terminated (001) surface, as reported [36-39]. Our hypothesis is that at least a part of the excess As reacts with TMGa and leads to a growth rate of beyond 1 ML/cycle. We believe that, while the excess surface As atoms prevent the reaction with TMGa at (111)B face, the excess As might contribute to the reaction with TMGa on (001) surface. The difference in the reaction mechanism of excess As between (001) and (111)B surface will be very important but little is known at present.

Thus, it is rather complicated to systematically explain GaAs growth on the substrates with several kinds of crystallographic orientations. However, we would like to point out that

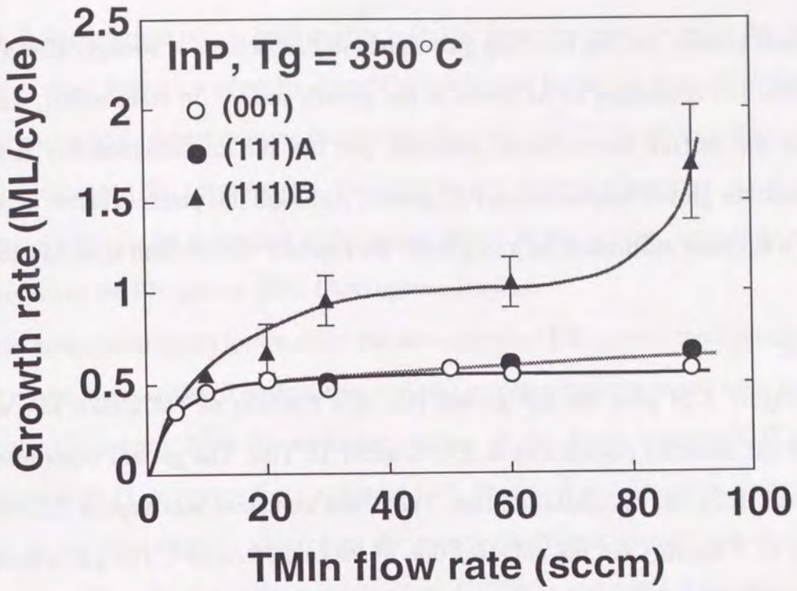

Figure 3-26. Crystallographic orientation of InP growth rate as a function of TMIn flow rate.

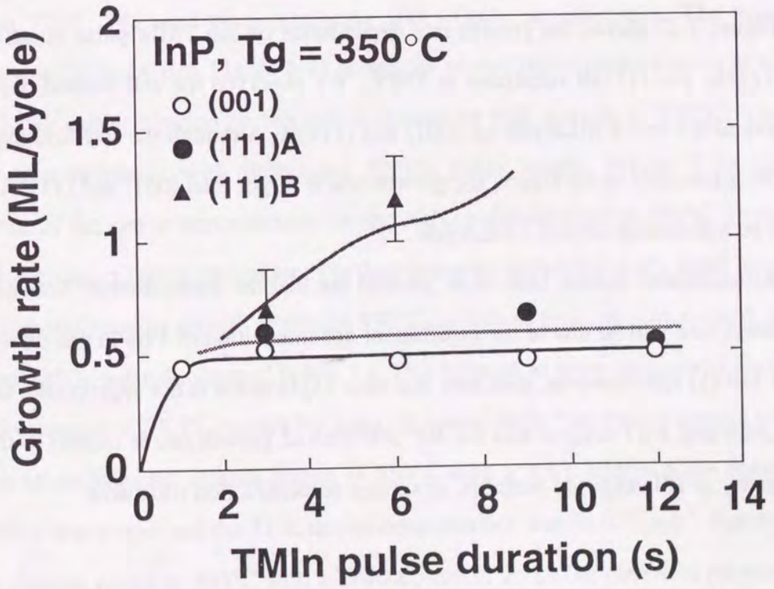

Figure 3-27. Crystallographic orientation of InP growth rate as a function of TMIn pulse duration.

the growth kinetics and the resulting growth rate in PJE process is strongly affected by the adsorption and desorption of As atoms at the growth surface. In other words, we have to consider the surface reconstructed structure and the surface stoichiometry in order to understand the growth mechanism in PJE growth. Although this problem seems to be crucial in PJE, it has been overlooked for a long time. We consider this problem again in Chapter 6.

3.4.2 InP

Figure 3-26 plots the InP growth rate as a function of TMIn flow rate when we changed the substrate orientations at 350°C under 15 Torr. The growth experiments were performed using the horizontal reactor. The TMIn container was kept at 27.1°C (vapor pressure of 3 mmHg) and the mole fraction of PH_3 was $9.6x10^{-2}$. The gas sequence, H_2/ TMIn/ H_2/ PH_3, was 5/ 3/ 5/ 20 s. Similar to the results for GaAs, we observed different self-limiting behaviors for different orientations: (001), (111)A, and (111)B. While the self-limiting growth rate is around 0.5 to 0.6 ML/cycle for (001) and (111)A, the growth rate tends to saturate at 1 ML/cycle on (111)B.

Figure 3-27 shows the growth rate dependence on the TMIn pulse duration for InP (001), (111)A, and (111)B substrates at 350°C. We observed the self-limited deposition of InP at around 0.5 to 0.6 ML/cycle on (001) and (111)A. Although the self-limiting behavior on (111)B is not clear in the figure, the growth rate is larger than (001) and (111)A and there seems to be a plateau at around 1 ML/cycle.

As mentioned before, Usui *et al.* pointed out that the submonolayer limitation of InP (001) growth rate will be due to the insufficient decomposition of PH_3 in gas phase [9]. The result on InP (111)B, however, indicates that their explanation is not appropriate. Our results in Figs. 3-26 and 3-27 suggest that the InP self-limited growth rate is related to the surface stoichiometry of PH_3 exposed-surfaces, or surface reconstruction structures.

3.5 Electrical and Optical Properties of PJE-Grown Layers

It is necessary to obtain high quality epitaxial layers in order to apply the layers to practical devices. For unintentionally-doped GaAs epitaxial layers, we have investigated the electrical and optical properties using the conventional (van der Pauw) Hall measurement and photoluminescence (PL) spectroscopy. For other binary materials, however, we don't have systematic studies on the properties of the grown layers. In this section, we briefly describe the properties of the PJE-grown (001) GaAs epitaxial layers.

GaAs epitaxial layers grown under the non-optimized PJE growth conditions normally showed p-type conductivity. The dominant residual acceptor impurity atoms were identified as carbon (C) judging from the emission energy of the donor-acceptor (D^0-A^0) pair recombination in PL spectrum from epilayers [40]. Electrical and optical properties of the epitaxial layers were strongly affected by the growth conditions; growth temperatures, the mole fractions (flow rates), and the pulse durations for TMGa and AsH_3. It has been clarified that a shorter TMGa pulse duration and sufficient AsH_3 supply are necessary to grow higher purity GaAs epitaxial layers [21, 40].

Carrier concentrations of the epitaxial layers were evaluated by the van der Pauw method at 77 K. We used semi-insulating (001) GaAs as substrates. The typical film thickness was 0.5 to 1.0 μm. Figure 3-28 shows the carrier (hole) concentration as a function of the TMGa pulse duration in the gas sequence of PJE growth at 550°C. The carrier concentration increases with increasing TMGa pulse length. Figure 3-29 shows the dependence of the carrier concentration on the AsH_3 pulse duration at 550°C. In contrast to Fig. 3-28, the carrier concentration tends to decrease with increasing AsH_3 pulse length.

High-temperature growth at around 550°C enables us to attain 1 monolayer saturation for a short TMGa pulse duration of below 1 s. This helps us to grow high-purity GaAs layers. Fig. 3-30 compares 4.2 K PL spectra for epitaxial layers under two typical growth conditions. Spectrum (a) is from the sample grown at 550°C with a 0.8 s TMGa pulse duration. The conductivity was n-type and the 77 K carrier concentration was $3x10^{14}$ cm^{-3}. Spectrum (b) is from the sample grown at 500°C with a TMGa pulse of 20 s. The electrical property was p-type with a hole density of $3x10^{18}$ cm^{-3}. Although spectrum (b) shows a broad luminescence around 830 nm due to (D^0-C^0) pair recombination, spectrum (a) exhibits sharp emissions due

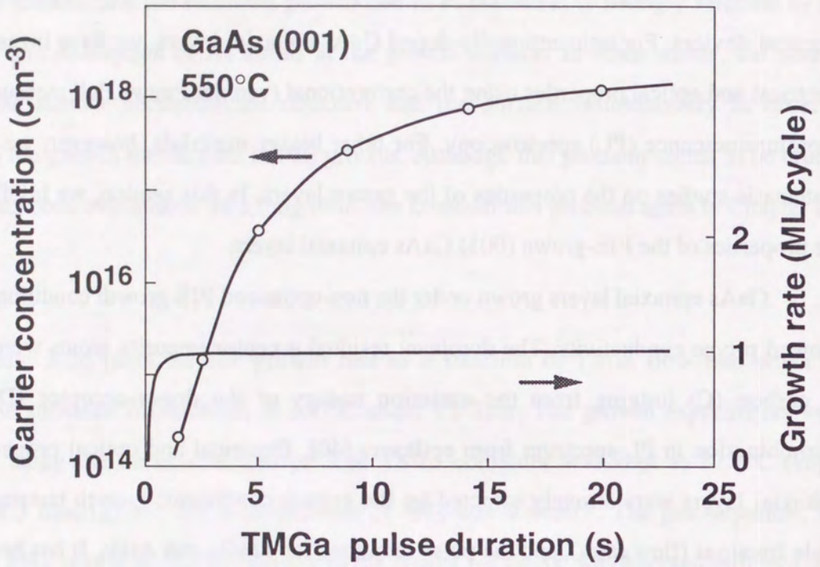

Figure 3-28. Variation of carrier concentration with TMGa pulse duration.

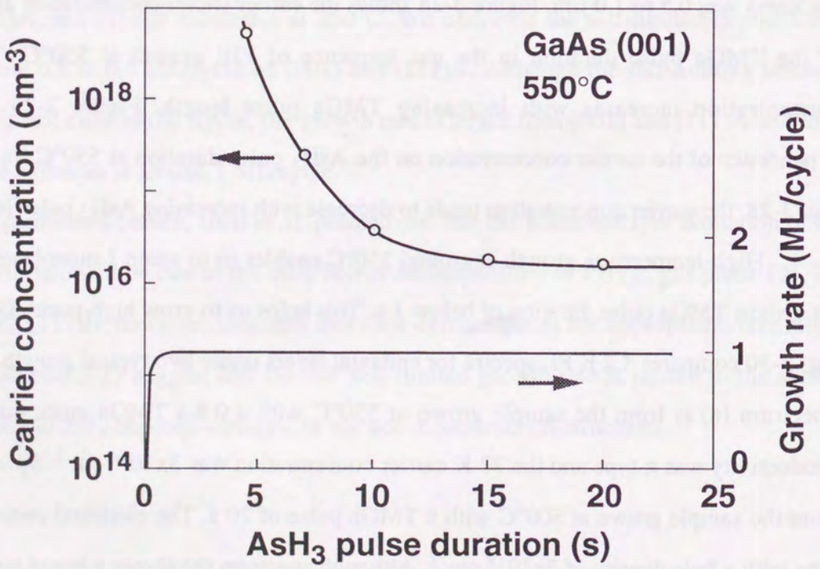

Figure 3-29. Variation of carrier concentration with AsH_3 pulse duration.

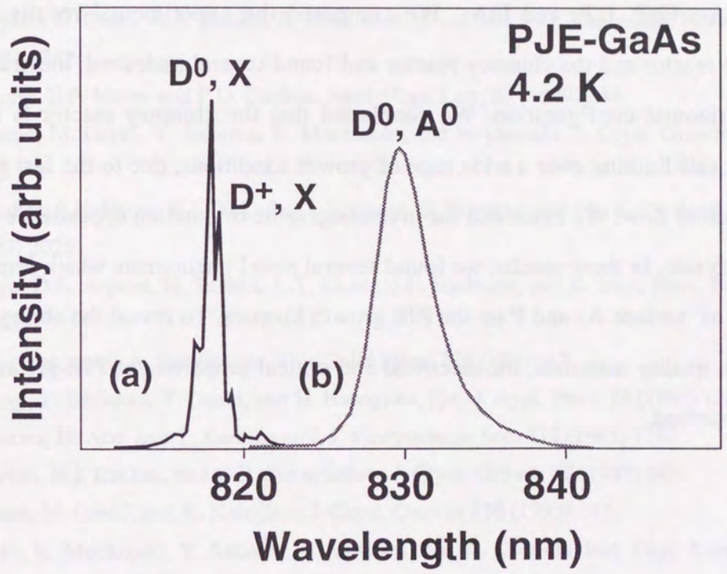

Figure 3-30. PL spectra from PJE-GaAs layers; (a) 550°C, TMGa pulse of 0.8 s, and (b) 500°C, TMGa pulse of 20 s.

to free and bound exciton peaks which reflect the high purity of the grown layer. Thus, PJE provides us with device-quality highly pure epitaxial GaAs layers if we choose the appropriate growth conditions.

3.6 Summary

We have shown the self-limiting growth results for several III-V binary compounds; (001) GaAs, GaP, InP, and InAs. We compared the experimental results between the horizontal reactor and the chimney reactor and found several undesired, inevitable problems in the horizontal configuration. We concluded that the chimney reactor is beneficial in achieving self-limiting over a wide rage of growth conditions, due to the fast gas switching with a laminar flow. We examined the crystallographic orientation dependence of GaAs and InP growth rate. In these results, we found several novel phenomena which imply the strong influence of surface As and P on the PJE growth kinetics. To reveal the ability in obtaining the device quality materials, the electrical and optical properties of PJE-grown GaAs were briefly described.

REFERENCES (Chap. 3)

[1] M. Ozeki, K. Mochizuki, N. Ohtsuka, and K. Kodama, J. Vac. Sci. Technol. **B5** (1987) 1184.

[2] M. Ozeki, K. Mochizuki, N. Ohtsuka, and K. Kodama, Appl. Phys. Lett. **53** (1988) 1509.

[3] Y. Sakuma, K. Kodama, and M. Ozeki, Jpn. J. Appl. Phys. **27** (1988) L2189.

[4] Y. Sakuma, K. Kodama, and M. Ozeki, Appl. Phys. Lett. **56** (1990) 827.

[5] M.G. Jacko and S.J.W. Price, Can. J. Chem. **42** (1964) 1198.

[6] N.N. Travkin, P.K. Skachkov, I.G. Tonoyan, and B.I. Kozyrkin, J. Gen. Chem. **48** (1978) 2428.

[7] C.A. Larsen and G.B. Stringfellow, J. Cryst. Growth **75** (1986) 247.

[8] F. Houzay, M. Bensoussan, and F. Barthe, Surf. Sci. **168** (1986) 347.

[9] A. Usui, H. Sunakawa, and Y. Kato, "Oyou Butsuri" (in Japanese) **59** (1990) 41.

[10] D.E. Aspnes, E. Colas, A.A. Studna, R. Bhat, M.A. Koza, and V.G. Keramidas, Phys. Rev. Lett. **61** (1988) 2782.

[11] W.G. Jeong, E.P. Menu, and P.D. Dapkus, Appl. Phys. Lett. **55** (1989) 244.

[12] K. Kodama, M. Ozeki, Y. Sakuma, K. Mochizuki, and N. Ohtsuka, J. Cryst. Growth **99** (1990) 535.

[13] D.W. Kisker, P.H. Fuoss, K.L. Tokuda, G. Renaudo, S. Brennan, and J.L. Kahn, Appl. Phys. Lett. **56** (1990) 2025.

[14] I. Kamiya, D.E. Aspnes, H. Tanaka, L.T. Florez, J.P. Harbison, and R. Bhat, Phys. Rev. Lett. **68** (1992) 627.

[15] J.R. Creighton and B.A. Bansenauer, Thin Solid Films **225** (1993) 17.

[16] B.X. Yang, Y. Ishikawa, T. Ozeki, and H. Hasegawa, Jpn. J. Appl. Phys. **35** (1996) 1267.

[17] J. Nishizawa, H. Abe, and T. Kurabayashi, J. Electrochem. Soc. **132** (1985) 1197.

[18] C.A. Larsen, N.I. Buchan, and G.B. Stringfellow, J. Cryst. Growth **85** (1987) 148.

[19] Y. Sakuma, M. Ozeki, and K. Nakajima, J. Cryst. Growth **130** (1993) 147.

[20] M. Ozeki, K. Mochizuki, Y. Sakuma, N. Ohtsuka, and K. Kodama, Inst. Phys. Conf. Ser. **106** (1990) 31.

[21] M. Ozeki, N. Ohtsuka, Y. Sakuma, and K. Kodama, J. Cryst. Growth **107** (1991) 102.

[22] J. Nishizawa, T. Kurabayashi, H. Abe, and N. Sakurai, J. Electrochem. Soc. **134** (1987) 945.

[23] S.P. DenBaars, P.D. Dapkus, J.S. Osinski, M. Zandian, C.A. Beyler, and K.M. Dzurko, Inst. Phys. Conf. Ser. **96** (1989) 89.

[24] M. Ozeki, K. Mochizuki, N. Ohtsuka, and K. Kodama, Thin Solid Films **174** (1989) 63.

[25] W.I. Wang, J. Vac. Sci. Technol. **B1** (1983) 630.

[26] W.I. Wang, Appl. Phys. Lett. **47** (1985) 826.

[27] D.H. Reep and S.K. Ghandhi, J. Cryst. Growth **61** (1983) 449.

[28] D.H. Reep and S.K. Ghandhi, J. Electrochem. Soc. **130** (1983) 675.

[29] T.F. Kuech and E. Veuhoff, J. Cryst. Growth **68** (1984) 148.

[30] H. Isshiki, Y. Aoyagi, T. Sugano, S. Iwai, and T. Meguro, Appl. Phys. Lett. **63** (1993) 1528.

[31] A. Usui and H. Sunakawa, Jpn. J. Appl. Phys. **25** (1986) L212.
[32] J. Nishizawa, T. Kurabayashi, H. Abe, and N. Sakurai, J. Vac. Sci. Technol. **A5** (1987) 1572.
[33] D.K. Biegelsen, R.D. Bringans, J.E. Northrup, and L.-E. Swartz, Phys. Rev. Lett. **65** (1990) 452.
[34] M.Y. Yen and T.W. Haas, Appl. Phys. Lett. **56** (1990) 2533.
[35] S. Ando, S.S. Chang, and T. Fukui, J. Cryst. Growth **115** (1991) 69.
[36] P.K. Larsen, J.H. Neave, J.F. van der Veen, P.J. Dobson, and B.A. Joyce, Phys. Rev. **B27** (1983) 4966.
[37] M. Sauvage-Simkin, R. Pinchaux, J. Massies, P. Claverie, N. Jedrecy, J. Bonnet, and I.K. Robinson, Phys. Rev. Lett. **62** (1988) 563.
[38] D.K. Biegelsen, R.D. Bringans, J.E. Northrup, and E.-L. Swartz, Phys. Rev. **B41** (1990) 5701.
[39] I. Kamiya, H. Tanaka, D.E. Aspnes, L.T. Florez, E. Colas, J.P. Harbison, and R. Bhat, Appl. Phys. Lett. **60** (1992) 1238.
[40] K. Mochizuki, M. Ozeki, K. Kodama, and N. Ohtsuka, J. Cryst. Growth **93** (1988) 557.

CHAPTER 4
Self-Limiting Growth Mechanism

4.1 Preliminaries

Understanding the growth mechanism of PJE is very important from both a scientific and technical point of view. Clarifying the growth mechanism and having an atomistic image of the crystal growth process is useful for improving the conventional growth technology and for providing a clue to help us exploit some new growth technology.

In this chapter, we describe the growth mechanism of PJE that has been revealed to date. We focus on the "self-limiting" deposition mechanism of gallium (Ga) and indium (In) from TMGa and TMIn. Since arsenic (As) and phosphorous (P) elements have a high vapor pressure at the growth temperature, it is usually considered that the deposition of group-V elements is automatically limited to 1 monolayer on the growth surface. Therefore, the self-limiting deposition of group-III elements is a key to revealing the self-limiting growth mechanism of PJE. Since the surface chemical reactions play an important role in PJE, we have to identify the chemical nature of the adsorbed species on the substrate surface, especially the Ga- or In-containing species. It is well known that X-ray photoelectron spectroscopy (XPS) has a big advantage in the quantitative analysis of surface elements below monolayer coverage. To study the PJE-grown surface *in situ*, we formed a new setup having both a growth chamber and an analytical chamber with XPS. Results show that the adsorbed group-III molecules such as TMGa and TMIn are thermally decomposed into atomic Ga and In on the substrate surfaces under typical PJE growth conditions. Based on these observations, we propose a "selective adsorption model" of trimethyl sources as a new model explaining the self-limiting growth mechanism. Using this model, we can reasonably explain the GaAs growth kinetics in PJE. Moreover, we describe some other experimental results supporting our selective adsorption model.

4.2 In-Situ Study of Surface Adsorbates by XPS

4.2.1 Apparatus

Figure 4-1 shows our apparatus used for the *in-situ* study of the adsorbates on the growth surface during PJE. This apparatus consists of two stainless steel chambers. One is the vertical growth chamber and the other is the analytical chamber equipped with XPS (JEOL JPS-90SX). The two chambers were separated by a gate valve. The substrate can be transferred between these chambers using a magnetic transfer rod. In the growth chamber, the source gases were supplied downward to the substrate surface. The growth chamber can be evacuated with either a conventional rotary pump or a turbomolecular pump. The growth was carried out under the conventional PJE growth conditions using the rotary pump. We had to carry out XPS analysis under the UHV condition (less than 10^{-7} Torr). Therefore, prior to the transportation of the grown substrate to the XPS chamber, the growth chamber was evacuated with the turbomolecular pump after stopping the source supply. The analyzer of the XPS was a hemispherical type and the excitation line used was Mg K_α (1254 eV) or Al K_α (1487 eV).

4.2.2 Experiment

Epitaxial layers for *in situ* XPS measurements were grown in the growth chamber. We tried to conduct the XPS measurements on the growth surface of (001)-oriented GaAs, InP, and GaP. The source gases were TMGa, TMIn, AsH_3 and PH_3. We employed growth conditions that allowed the growth of each material to proceed in a self-limiting manner. Details of growth conditions are described in a later section. We used the substrates of n-type conductivity to minimize the energy shift of the core level emission of photoelectrons due to charging up of the substrates. After growth by PJE, the substrate was cooled down and transferred to the XPS chamber after evacuating the growth chamber by the turbomolecular pump. It took about 12 min to start the XPS measurements after growth. We prepared and examined two kinds of surfaces after different gas procedures. One was the surface exposed to AsH_3 or PH_3 at the end of PJE growth and cooled down in these hydrides' environments. The

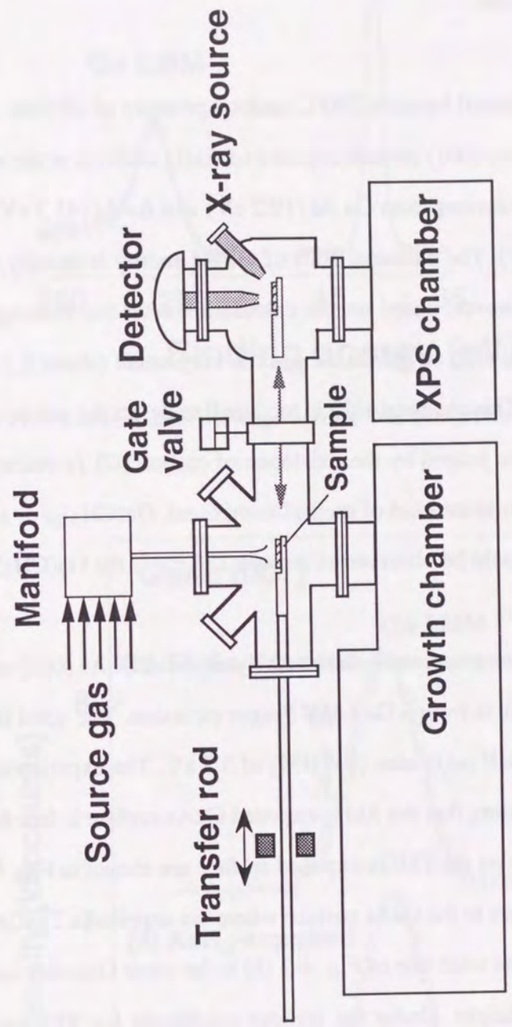

Figure 4-1. Schematics of PJE and XPS combined system.

other was the surface exposed to TMGa or TMIn flow at the end of PJE and cooled down in H_2 environment.

4.2.3 Results and implications

4.2.3.1 GaAs

We grew GaAs epitaxial layers at 500°C under a pressure of 20 Torr. Figure 4-2 shows the XPS spectra of the GaAs (001) surface exposed to AsH_3 ambient at the end [1]. The three peaks are the core level emissions from Ga *3d* (19.2 eV) and As *3d* (41.3 eV), and a Ga *LMM* Auger emission (282.3 eV). The chemical shift of Ga *3d* energy is usually used to study the chemical bond states. However, based on the calculation after the Pauling method [2], we estimated that the chemical shift of the Ga *3d* peak is very small (about 0.1 eV) between the atomic Ga and $Ga(CH_3)_3$. This chemical shift is too small to detect the nature of the adsorbates. Therefore, in this study, we judged by the existence of carbon (C) *1s* emission to determine whether the Ga adsorbate is some kind of methyl compound, $Ga(CH_3)_n$, or atomic Ga. In this case, the C *1s* emission should be observed at around 285 eV if the $Ga(CH_3)_n$ is adsorbed on the TMGa-exposed surface.

The results of XPS measurements on the AsH_3-exposed GaAs (001) surface are shown in Fig. 4-3 (a) [3]. The peak is from a Ga *LMM* Auger emission. The solid line is a Gaussian curve with a full width at half maximum (FWHM) of 3.5 eV. The experimental result fits the Gaussian curve well, indicating that the AsH_3-exposed GaAs surface is free from C caused by methyl radicals. The results on the TMGa-exposed surface are shown in Fig. 4-3 (b). Here, the TMGa-exposed surface refers to the GaAs surface where we supplied a TMGa pulse at the end of the growth procedure. The solid line of Fig. 4-3 (b) is the same Gaussian curve as in Fig. 4-3 (a) except for the peak height. Under the present conditions for XPS measurements, we expect that the adsorption of a monolayer $Ga(CH_3)_n$ will result in C *1s* emission at around 285 eV with an intensity of 2 kilocounts. This was estimated from the intensity of the Ga *3d* peak for the AlAs sample with monolayer Ga adsorption on the top, considering the difference in photoionized cross-sections of Ga *3d* and C *1s* and also the dependence of XPS sensitivity on electron kinetic energy. The experimental results show that there is no evidence indicating the

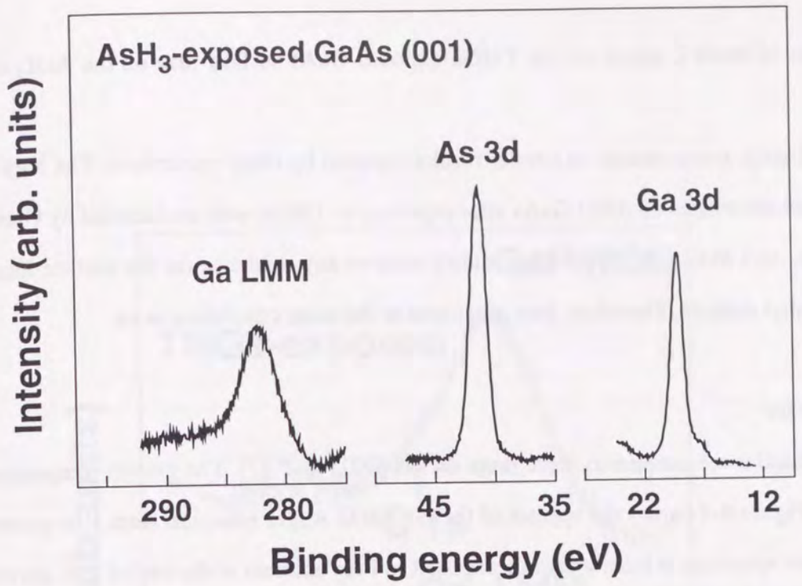

Figure 4-2. Core level emissions and Auger spectra from PJE-grown GaAs (001) at 500°C.

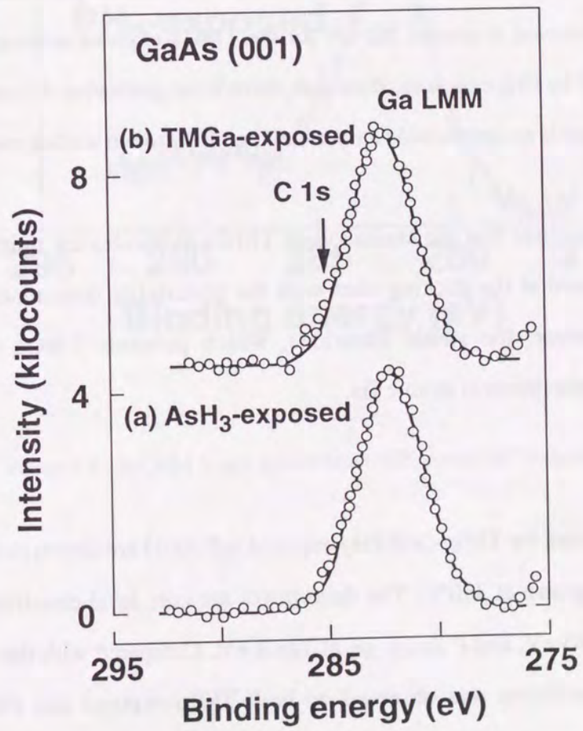

Figure 4-3. Ga LMM Auger spectra from AsH_3 and TMGa-exposed GaAs surfaces.

existence of more C atoms on the TMGa-exposed GaAs surface than on the AsH_3-exposed one.

Lastly, we comment on similar results reported by other researchers. The XPS studies of surface adsorbates on (001) GaAs after exposing to TMGa were reexamined by Ohno *et al.*, Yu *et al.*, and Maa *et al.* [4-6]. They didn't observe any evidence for the surface terminated with methyl radicals. Therefore, they also came to the same conclusion as us.

4.2.3.2 GaP

Similar measurements were done on the (001) GaP [7]. The growth temperature was 485°C. Figure 4-4 shows the spectra of the Ga *LMM* Auger emission from PJE-grown GaP. The lower spectrum is from a sample exposed to PH_3 ambient at the end of PJE growth. The upper spectrum is from a sample exposed to a TMGa pulse at the end. Both spectra were taken after growing 16.4-nm-thick GaP epilayers by 60 cycles of gas pulses. As explained above, if TMGa-related radicals are the stable adsorbates on (001) GaP, the photoemission from C *1s* levels should be observed at around 285 eV for the TMGa-exposed surface and its intensity should be decreased by PH_3 exposure. However, there is no qualitative difference between the two spectra, and there is no appreciable amount of C on the growth surface even after exposure to TMGa.

Thus, we conclude that the chemisorbed TMGa molecules are quickly desorbed, or thermally decomposed at the sticking sites with the probability determined by the growth temperature. Therefore, the stable adsorbate, which prevents TMGa from exceeding monolayer-limited adsorption, is atomic Ga.

4.2.3.3 InP

The XPS spectra for TMIn- and PH_3-exposed InP (001) are shown in Fig. 4-5 [3]. The InP epilayers were grown at 350°C. The three peaks are core level emissions of In $3d_{5/3}$ at 444.4 eV, C *1s* at 285 eV, and P $2p_{1/2,\ 3/2}$ at 128.8 eV. Compared with the GaAs results in Fig. 4-3, the C *1s* emission was observed on both TMIn-exposed and PH_3-exposed InP surfaces. Detailed spectra around the C 1*s* are shown in Fig. 4-6. The bottom trace in the figure

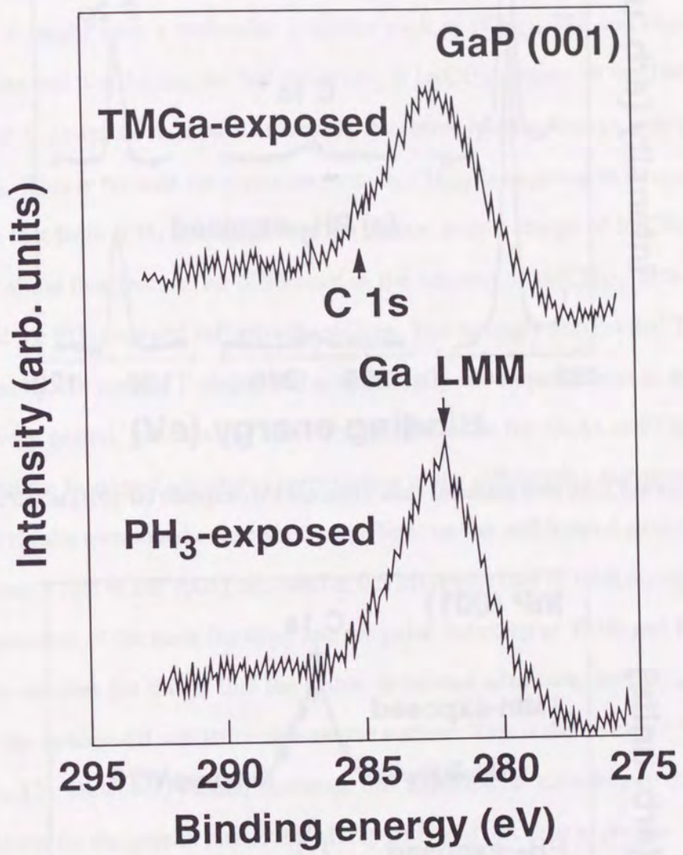

Figure 4-4. Ga LMM Auger spectra from PJE-grown GaP surfaces.

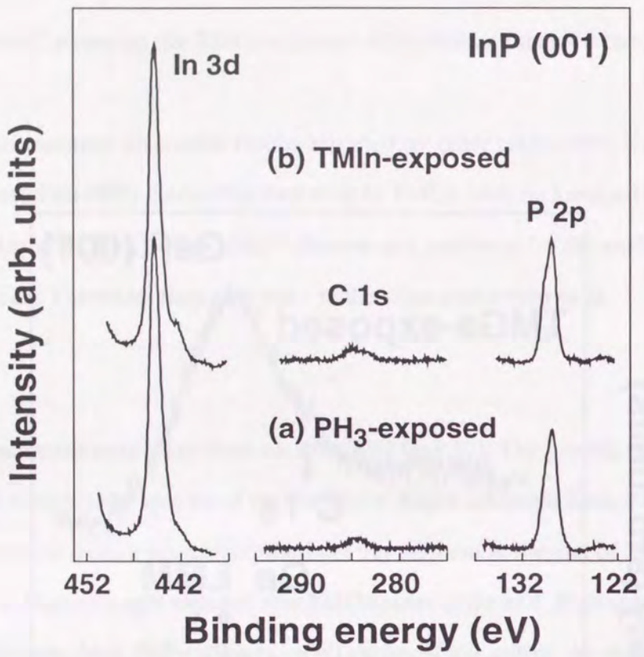

Figure 4-5. Core level emissions from TMIn and PH_3-exposed InP (001) at 350°C.

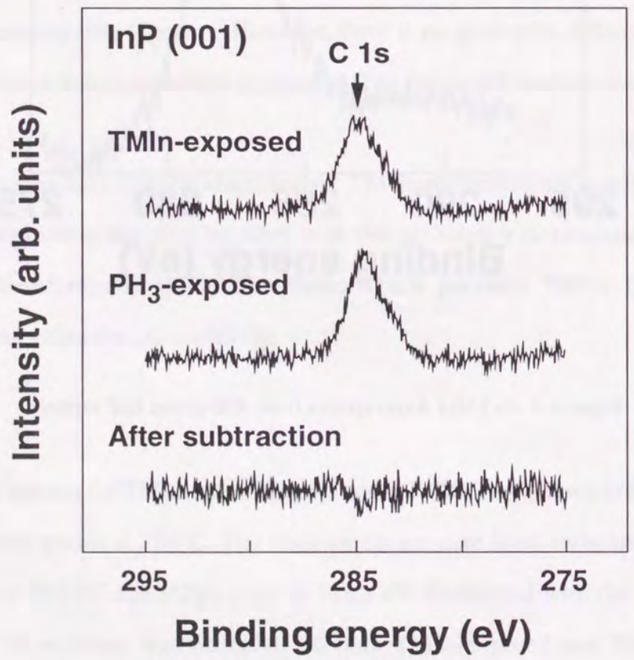

Figure 4-6. C 1s emission from TMIn and PH_3 exposed InP, and difference spectrum.

is the difference between the upper two spectra. It does not have any structure except for a small dip at around 285 eV, which is due to the difference in the amount of some adsorbed hydrocarbons between the two surfaces. The emission at 285 eV seems to originate from the adsorbed hydrocarbon remaining in the vacuum chamber, as was also reported for the GaAs surface [8]. It might have a molecular structure such as $(CH_2)_n$ [9], and might be adsorbed during cooling and transferring the InP substrates. If $In(CH_3)_n$ exists on the TMIn-exposed InP surface, their C *1s* emission should emerge at the lower binding energy side of the emission from $(CH_2)_n$. This is because the emission from $In(CH_3)_n$ is expected to have a lower binding energy than that from $(CH_2)_n$, considering the carbon atom's charge of $In(CH_3)_n$ and $(CH_2)_n$. Our results show that there is no difference in the amount of $In(CH_3)_n$ between the TMIn-exposed and the PH_3-exposed InP growth surfaces. This strongly implies that TMIn precursors are adsorbed by the surface P atoms and are thermally decomposed into In atoms during the TMIn delivery period, just like the behavior of TMGa on the GaAs and GaP surfaces. We conclude that the In-related adsorbates participating in the self-limiting InP growth is atomic In.

The results mentioned above shed some light on the self-limited growth mechanism of InP. The growth rate of InP (001) saturated at 0.5 ML/cycle (not at 1 ML/cycle as in GaAs and GaP), independent of the mole fractions and the pulse durations of TMIn and PH_3 [10]. One of the possible reasons for this is that the stable In-related adsorbate, $In(CH_3)_n$, is too large to occupy all the column-III sublattice sites on the surface. This is the so-called "steric hindrance effect" [11, 12]. However, we can eliminate this assumption according to the present result. The real reason for the growth rate of 0.5 ML/cycle is still not clear at present, but we speculate that the InP (001) may be reconstructed so that the growth surface has minimum energy when the surface column-III (or V) sublattice sites are half-occupied.

4.3 Mechanism of Self-Limiting Growth

4.3.1 Selective adsorption model

In this section we discuss the self-limiting growth mechanism of PJE. We consider the case of GaAs, but a similar explanation can be basically applied to other binary III-V compounds.

Based on the surface analysis using XPS, we concluded that the adsorbed TMGa molecules are decomposed into atomic Ga on the surface and that the excessively adsorbed TMGa will be quickly desorbed from the surface after stopping the TMGa supply. To explain the self-limiting GaAs growth, we have to consider that the TMGa molecules are preferentially adsorbed and decomposed on the surface As atoms until the surface coverage by Ga reaches 1 monolayer (full coverage).

Figure 4-7 shows a growth model explaining the self-limiting deposition of Ga on the As-terminated GaAs surface during TMGa exposure time. We call this model a "selective adsorption model". In this model, we assume the dynamical equilibrium of Ga-containing species between the gas phase and the growth surface. Actually, during the TMGa delivery period, TMGa molecules are quickly repeating the adsorption and desorption many times at the surface lattice sites [13]. Self-limited Ga deposition can be attained as a consequence of the competition among the adsorption, decomposition, and desorption kinetics of TMGa at the surface Ga and As sites. Here, we assume that the average residence time (or lifetime) of TMGa on surface Ga atoms is short enough such that we can neglect the decomposition probability at the sites. In other words, TMGa molecules sticking on the surface Ga atoms quickly reevaporate without decomposition. Therefore, we consider the decomposition probability to be finite only at the As atoms because of the longer residence time of TMGa. This is effectively the same as allowing TMGa to be selectively adsorbed and decomposed by the surface As atoms. The Ga participating in the growth comes from the TMGa which is adsorbed by the surface As atoms. Ga deposition stops after all the surface As atoms are covered with Ga adatoms. This consideration is basically the same as the well-known "Rideal-Eley" reaction mechanism [14].

We think that the large difference in the TMGa residence time between on the Ga and As atoms is crucial for understanding the self-limiting mechanism. A plausible explanation for the residence time difference between the two sites is given as follows. Generally, the charge

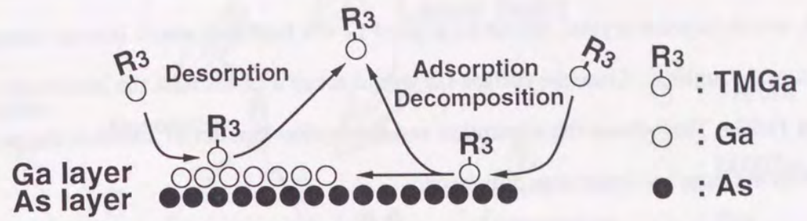

Figure 4-7. Selective adsorption model. TMGa is assumed to be selectively adsorbed and therefore decomposed on As-terminated surface.

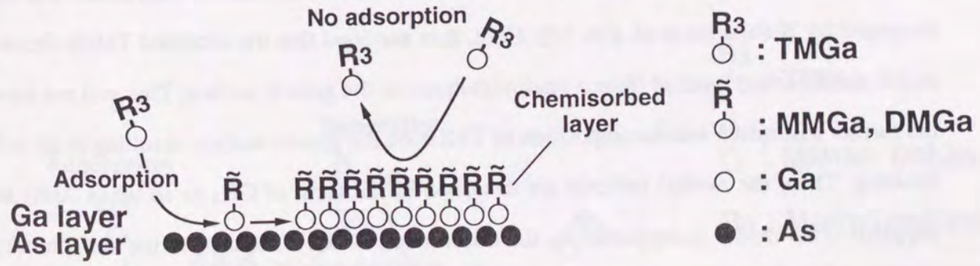

Figure 4-8. Radical inhibition model. The adsorption of Ga-species over monolayer-coverage is restricted by the stable chemisorbed layer such as monomethylgallium (MMGa) or dimethylgallium (DMGa).

transfer between adsorbates and surface atoms seems to be important in chemisorption. TMGa is classified as a Lewis acid or electron acceptor, while AsH_3 is as a Lewis base or electron donor [15]. Judging from the electronegativity of the constituents, a surface As atom on (001) GaAs, which is polar crystal, would be a good Lewis base and would interact strongly with TMGa in the ambient. Since the surface Ga would act as a Lewis acid, the lattice site might not accept TMGa. This affects the adsorption and desorption kinetics of TMGa at the surface and results in the large residence time difference.

4.3.2 Comparison with other models

In this section, we briefly describe other models that have been proposed for explaining the self-limiting growth of GaAs ALE, and compare with our selective adsorption model. As described in Chapter 1, there are several methods to realize the self-limited growth of GaAs. Researchers proposed their own growth models based on their experimental results. However, to date, none of these models consistently explain all the ALE data published so far. There is still controversy about the real picture of the self-limiting mechanism.

4.3.2.1 Radical inhibition (site blocking) model

Figure 4-8 shows the radical (or adsorbate) inhibition mechanism. This model was first proposed by Nishizawa *et al.* [16, 17]. Here, it is assumed that the adsorbed TMGa forms a stable chemisorbed layer of (mono-)methylgallium on the growth surface. This will not allow the further adsorption and decomposition of TMGa on the growth surface, resulting in the self-limiting. Then, the methyl radicals are desorbed in the form of CH_4 or so when AsH_3 are supplied. This model is supported by the observation of alkyl radicals on the surface using quadropole mass spectroscopy (QMS) combined with temperature programmed desorption (TPD) [18].

4.3.2.2 Selective decomposition model

The selective decomposition model was proposed by Doi *et al.* to explain the self-limited deposition of Ga [19]. Actually, this model was used to explain the Ar^+ laser-beam

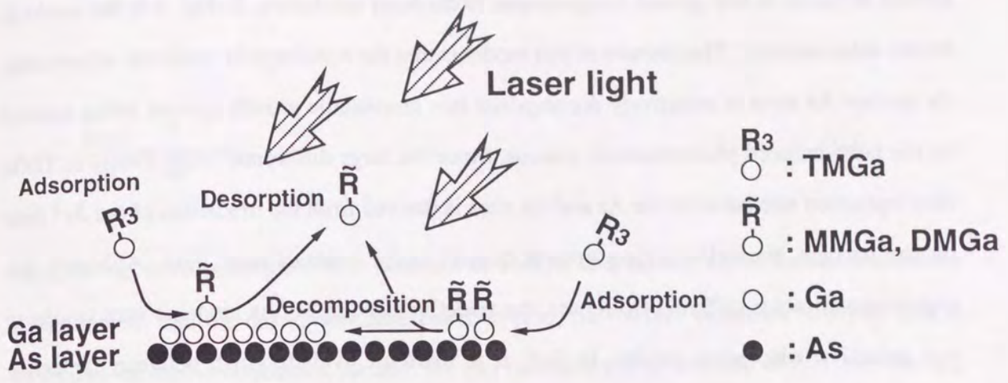

Figure 4-9. Selective decomposition model. TMGa decomposition rate into Ga is much enhanced on As-terminated surface rather than on Ga-terminated surface due to laser irradiation.

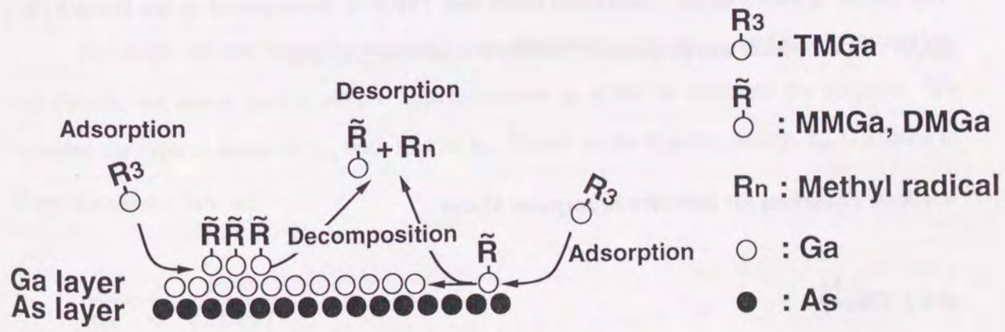

Figure 4-10. Flux balance model. Incoming TMGa is decomposed even on Ga-terminated surface, but is balanced by desorption of decomposed Ga-alkyls.

assisted ALE using TMGa (or TEGa) and AsH_3 as sources. They observed the self-limiting growth of GaAs at low growth temperatures under laser irradiation. In Fig. 4-9, the model is shown schematically. The essence of this model is that the metalorganic molecule adsorbed on the surface As atom is selectively decomposed into nonvolatile growth species, being assisted by the laser-induced photochemical process. Since the large difference in the TMGa or TEGa decomposition rate between the As and Ga sites is derived from the irradiation of the Ar^+ laser on the surface, the self-limiting growth doesn't occur without laser light. Although this experimental fact is different from ours, the selective decomposition model is very similar to our selective adsorption model. In fact, it is difficult to distinguish between "selective decomposition" and our proposed "selective adsorption".

4.3.2.3 Flux balance model

The flux balance model, shown in Fig. 4-10, was proposed by Yu *et al.* It requires a balance to be kept between desorbing Ga-alkyl species and adsorbing Ga alkyls during the TMGa exposure [20, 21]. TMGa may be still adsorbed and decomposed even on the Ga-rich surface, *i.e.* the incoming flux of Ga-alkyl species is balanced by the desorbing Ga-alkyl species. The desorbing Ga species need not to be the same molecule which is dosed. This balance of adsorbing and desorbing Ga alkyls prevents deposition of more than 1 ML of Ga. This model is based on the overlooked result that TMGa is decomposed on the Ga-rich (001) GaAs surface which was prepared in the UHV condition [22, 23].

4.4 Rate Equations for Selective Adsorption Model

4.4.1 Theory

Assuming the selective adsorption model, we can express the self-limited Ga deposition process during a TMGa exposure period to the As-terminated (001) GaAs using simple rate equations described below. The surface coverage of adsorbed TMGa, n_{TMGa}, and the coverage of atomic Ga on the surface for a unit area, n_{Ga}, can be written as:

$$\frac{dn_{TMGa}}{dt} = \frac{1}{\tau_{ad}}(1 - n_{TMGa} - n_{Ga}) - (\frac{1}{\tau_{dc}} + \frac{1}{\tau_{rs}})n_{TMGa} \quad (4\text{-}1)$$

and

$$\frac{dn_{Ga}}{dt} = \frac{1}{\tau_{dc}} n_{TMGa} \quad (4\text{-}2)$$

Here, the τ_{ad} is the adsorption time constant of TMGa, and τ_{dc} and τ_{rs} are the decomposition time constant and the desorption time constant (*i.e.*, the surface residence time) of TMGa molecules on the As-terminated surface. We can calculate the growth rate of PJE from the n_{Ga} (ML/cycle) value at the end of the TMGa pulse. From Eqs. (4-1) and (4-2), n_{TMGa} are generally given by:

$$n_{TMGa}(t) = A_1 \exp \lambda_1 t + A_2 \exp \lambda_2 t + A_3 \quad (4\text{-}3)$$

where A_1, A_2 and A_3 are the coefficients and $\lambda_{1,2}$ are given by

$$\lambda_{1,2} = \frac{1}{2}\left\{-\left(\frac{1}{\tau_{ad}} + \frac{1}{\tau_{dc}} + \frac{1}{\tau_{rs}}\right) \pm \sqrt{\left(\frac{1}{\tau_{ad}} + \frac{1}{\tau_{dc}} + \frac{1}{\tau_{rs}}\right)^2 - \frac{4}{\tau_{ad} \cdot \tau_{dc}}}\right\} \quad (4\text{-}4)$$

Although we can solve the accurate time dependence of n_{TMGa} and n_{Ga} by numerical calculation, we adopt here a simple approximation in order to estimate the solution. We compare the typical value of τ_{ad} with that of τ_{rs}. Based on the kinetic theory, τ_{ad} is related to Hertz-Knudsen's law as:

$$\frac{1}{\tau_{ad}} = \frac{1}{n_s} \cdot \frac{p_{TMGa}}{\sqrt{2\pi MkT}} \quad (4\text{-}5)$$

where n_s is the total density of surface sites (n_s=6.26x10^{14} cm^{-2} at (001) GaAs), k is the Boltzmann constant, and p_{TMGa} and M are the partial pressure and the mass (M=114.8) of TMGa molecule, respectively. Equation (4-5) refers to how many times TMGa molecules strike

per a specific surface lattice site per second under a given p_{MGa} and temperature T. With our GaAs growth conditions employed in the chimney reactor, the p_{TMGa} (Torr) is determined by the H_2 flow rate through the TMGa bubbler, f_{TMGa} (sccm), as:

$$p_{TMGa} = 5.25 \times 10^{-4} f_{TMGa} \tag{4-6}$$

Therefore, if f_{TMGa} is 30 (sccm), then τ_{ad} becomes about 3.5×10^{-4} (s) at 500°C from Eq. (4-5).

On the other hand, τ_{rs} is given by the Arrhenius form as:

$$\frac{1}{\tau_{rs}} = \nu \exp\left(-\frac{E_{ds}}{RT}\right) \tag{4-7}$$

where the ν is the preexponential factor and E_{ds} is the activation energy for TMGa desorption from the As-terminated GaAs (001) surface, and R is the molar gas constant (1.987×10^{-3} kcal/(mol•K)). Using the Arrhenius parameters of $\nu = 10^8$ (s^{-1}) and E_{ds}=19-28 (kcal/mol) as reported by McCaulley *et al.* [24], τ_{rs} is calculated to be 2.4×10^{-3}-8.4×10^{-1} (s) at 500°C. The E_{rs} and τ_{rs} vary according to the surface coverage of TMGa [22, 24].

Anyway, from our growth conditions, the relationship of $\tau_{ad} << \tau_{rs}$ (or $1/\tau_{ad} >> 1/\tau_{rs}$) is obtained. In order to see easily the growth rate dependence on the growth parameters, we treat here the extreme approximation that the desorption of TMGa is negligible. Although we cannot neglect the TMGa desorption process in the actual growth situation, this approximation is almost good under the condition of $\tau_{ad} << \tau_{rs}$. This is because the surface As sites are always fully covered with TMGa molecules. Therefore, Eq. (4-4) becomes

$$\lambda_1 = -\frac{1}{\tau_{dc}}, \quad \lambda_2 = -\frac{1}{\tau_{ad}} \tag{4-8}$$

We have to solve $n_{TMGa}(t)$ and $n_{Ga}(t)$ under the critical conditions of

$$n_{TMGa}(t=0) = 0, \quad n_{Ga}(t=0) = 0 \tag{4-9}$$

and

$$n_{TMGa}(t \to \infty) = 0, \quad n_{Ga}(t \to \infty) = 1 \tag{4-10}$$

The condition of Eq. (4-9) means that no TMGa molecules and Ga atoms exist on the initial As-terminated surface. The condition of Eq. (4-10) means that the Ga coverage reaches 1 ML after a long TMGa pulse, and that at the same time the TMGa molecules are no longer adsorbed on the Ga-terminated GaAs surface. These are reasonable assumptions in the selective adsorption model. Finally, we obtain the solutions:

$$n_{TMGa}(t) = \frac{\tau_{dc}}{\tau_{dc} - \tau_{ad}} \left\{ \exp\left(-\frac{t}{\tau_{dc}}\right) - \exp\left(-\frac{t}{\tau_{ad}}\right) \right\} \tag{4-11}$$

and

$$n_{Ga}(t) = \frac{\tau_{ad}}{\tau_{dc} - \tau_{ad}} \exp\left(-\frac{t}{\tau_{ad}}\right) - \frac{\tau_{dc}}{\tau_{dc} - \tau_{ad}} \exp\left(-\frac{t}{\tau_{dc}}\right) + 1 \tag{4-12}$$

4.4.2 Simulation of growth kinetics

4.4.2.1 Dependence on TMGa pulse duration

Now, we try to simulate the GaAs growth kinetics in PJE. As mentioned above, each lattice site is occupied by TMGa for an average time of $\tau_{ad} = 3.5 \times 10^{-4}$ (s) when a TMGa pulse is supplied on the As-terminated surface. If all these TMGa are decomposed and incorporated into the crystal lattice sites, the growth rate might reach 1 ML/cycle at around the time of τ_{ad}. This is inconsistent with the experimental results shown in Figs. 3-11 and 3-18. This discrepancy implies that each TMGa does not always result in the decomposition into Ga, probably because the decomposition time constant is longer than the adsorption time constant, *i.e.*, $\tau_{dc} >> \tau_{ad}$. Under this condition, Eq. (4-12) becomes:

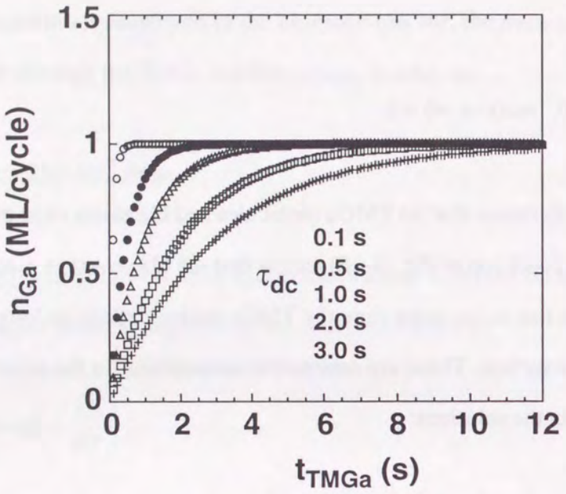

Figure 4-11. Simulated result of PJE-GaAs growth rate (n_{Ga}) versus TMGa pulse time (t_{TMGa}) after eq. (4-13). TMGa decomposition time constant, τ_{dc}, was varied.

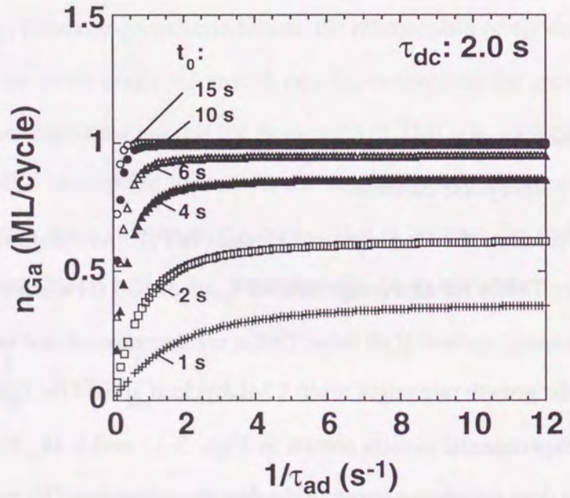

Figure 4-12. Simulated result of PJE-GaAs growth rate (n_{Ga}) versus TMGa flow rate (f_{TMGa}) after eq. (4-15). Note that the $1/\tau_{ad}$ is proportional to f_{TMGa}.

$$n_{Ga}(t) = 1 - \exp\left(-\frac{t}{\tau_{dc}}\right) \tag{4-13}$$

Figure 4-11 shows n_{Ga} versus t given by Eq. (4-13). This is in good agreement with the dependence of the GaAs growth rate on the TMGa pulse duration shown in Figs. 3-11 and 3-18.

In addition, if we measure the growth rate variation on the growth temperatures under a specific TMGa pulse duration, t_0, where the growth rate is less than 1 ML/cycle, we can determine the rate constant of TMGa decomposition into Ga atoms on the surface, k_{dc}, according to the following relationship.

$$\ln n_{Ga}(T)\big|_{t=t_0} = \frac{t_0}{\tau_{dc}(T)} \propto k_{dc}(T) \tag{4-14}$$

Since k_{dc} is expressed as an Arrhenius form, we can determine the activation energy, E_{dc}, of TMGa decomposition into Ga atoms on the As-terminated GaAs (001) surface. In our growth conditions, we obtained E_{dc}=42 kcal/mol [25, 26]. This value is lower than those measured by Jacko and Price (59.5 kcal/mol) and by DenBaars *et al.* (58-62 kcal/mol) in the gas phase [27, 28]. The difference is considered to be the catalytic effect on TMGa decomposition occurring at the As-terminated GaAs surface.

4.4.2.2 Dependence on TMGa flow rate

One of the distinct features of GaAs growth kinetics in PJE is that the growth rate is saturated at submonolayers with increasing TMGa flow rate under a short TMGa pulse duration. This behavior is shown in Fig. 3-20. Some researchers have ascribed this behavior to the "steric hindrance effect" of TMGa adsorbed on the surface [12]. However, we can explain the dependency using the selective adsorption model instead. For a constant TMGa pulse duration of t_0, n_{Ga} is given as:

$$n_{Ga}(t=t_0)=\frac{\tau_{ad}}{\tau_{dc}-\tau_{ad}}\exp\left(-\frac{t_0}{\tau_{ad}}\right)-\frac{\tau_{dc}}{\tau_{dc}-\tau_{ad}}\exp\left(-\frac{t_0}{\tau_{dc}}\right)+1 \qquad (4\text{-}15)$$

Note that τ_{ad} is a function of f_{TMGa}, $\tau_{ad}=C/f_{TMGa}$, where C is a coefficient.

Within the region of small f_{TMGa}, Eq. (4-15) is rewritten as:

$$n_{Ga}(f_{TMGa})=1-\exp\left(-\frac{t_0}{\tau_{ad}}\right)=1-\exp(-t_0\cdot C\cdot f_{TMGa}) \qquad (4\text{-}16)$$

due to the relationship of $\tau_{ad} >> \tau_{dc}$.

Increasing f_{TMGa}, τ_{ad} becomes smaller. In the region where $\tau_{ad} << \tau_{dc}$, n_{Ga} is given by:

$$n_{Ga}(f_{TMGa})=1-\exp\left(-\frac{t_0}{\tau_{dc}}\right)=const. \qquad (4\text{-}17)$$

Based on the above-mentioned arguments, we can draw the growth rate dependence on the TMGa flow rate, f_{TMGa}, as shown in Fig. 4-12. This behavior is consistent with the experimental results shown in Fig. 3-20.

Thus, using the simple rate equations assuming the selective adsorption model, we could reasonably explain the growth kinetics of GaAs growth.

4.5 Evidences of Selective Adsorption Model

In this section, we describe some experimental results supporting the justice of our selective adsorption model. We have already reported that the surface stable adsorbate on the As-terminated GaAs surface is bare Ga from XPS analysis. However, there still exists an ambiguity in that the TMGa-exposed surface might change, from a chemical point of view, during the period of cooling and transportation to the XPS chamber. The following results clearly eliminate this ambiguity.

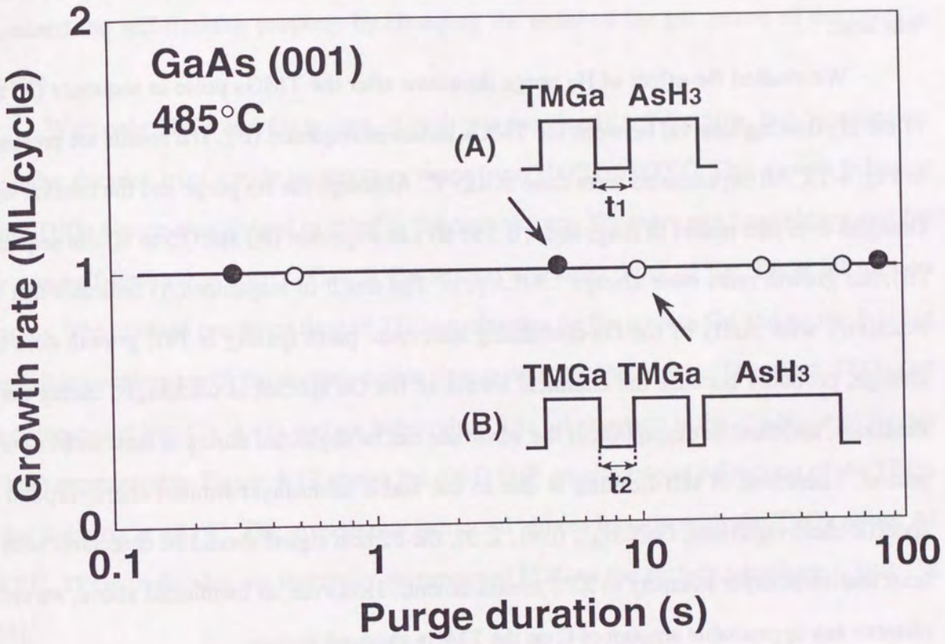

Figure 4-13. GaAs growth rate with two different gas sequences. Each TMGa pulse has a 4 s duration and a mole fraction of $1x10^{-3}$, sufficient for monolayer growth. AsH_3 was supplied with a mole fraction of $2.4x10^{-2}$ and the duration of 5 s in (A) and of 10 s in (B). H_2 purge is 0.5 s except for t1 and t2.

4.5.1 Growth by consecutive supply of TMGa

To investigate the dynamics of change in the chemical state of the TMGa-exposed (001) GaAs surface, we studied the GaAs growth rate with the two kinds of gas introduction procedures [29]. In sequence (A), TMGa and AsH_3 were alternately introduced to the substrate. In contrast, in sequence (B), another TMGa pulse, which has the same mole fraction and pulse duration as sequence (A), was consecutively supplied after forming a perfect, self-limited TMGa-exposed surface by the first TMGa pulse. Then, a sufficient amount of AsH_3 was sent.

We studied the effect of H_2 purge durations after the TMGa pulse in sequence (A) and of the H_2 flowing interval between the TMGa pulses in sequence (B). The results are presented in Fig. 4-13. All experiments were done at 485°C. Although the H_2 purge and the interval were changed over two orders of magnitude, 0.3 to 80 s in sequence (A) and 0.5 to 60 s in sequence (B), the growth rates were always 1 ML/cycle. The result of sequence (A) indicates that the reactivity with AsH_3 of the Ga-containing adsorbate participating in PJE growth does not change, probably because the chemical nature of the Ga species is unchanged during purge durations, and that the desorption of the adsorbate can be neglected during at least an 80 s purge period. Therefore, if self-limiting is due to the stable monolayer-limited chemisorption of specific methylgallium, $Ga(CH_3)_n$ (n=1, 2, 3), the carbon signal should be detectable with at least one-monolayer intensity in XPS measurements. However, as mentioned above, we didn't observe any appreciable amount of C on the TMGa-exposed surface.

So, we can conclude that the surface adsorbate, which prevents the monolayer-exceeding adsorption and decomposition of TMGa, must be atomic Ga. The result of sequence (B) is good proof that the chemical condition and self-limiting of the TMGa-exposed GaAs surface do not change after the first TMGa pulse is stopped. This is contrary to the results by Chiu where the self-limiting growth is possible only while a metastable monomethylgallium overlayer, which is fully decomposed to Ga in several seconds, exists on the surface [30]. In our case, a reasonable interpretation is that a full-coverage, monolayer Ga plane has already formed during the first TMGa exposure, so a metallic Ga plane causes the self-limiting.

In addition, Maa *et al.* also examined by similar experiments using XPS measurements and came to the same conclusions as us [31].

4.5.2 Growth by sequential supply of TEGa and TMGa

Next, we confirmed the selective adsorption model using a sequential supply of TEGa and TMGa. Here, we describe the results on (001) GaP. To check the selective adsorption of TMGa, we grew GaP by PJE at 485°C using alternate flows of TEGa, TMGa, and PH_3. We examined the self-limiting property by changing the order of the gas pulses of the two Ga sources.

With only TEGa as a Ga source, growth was not clearly self-limiting, but depended on the pulse duration over a wide temperature range from 300°C to 600°C. This growth behavior using TEGa source is explained in detail in the next chapter. There are two possible reasons for the non-self-limiting property. One is the weaker site selectivity of the TEGa adsorption process. The average residence time of TEGa molecules on the surface Ga and on the P is not negligible compared with the decomposition time constant at the surface. Therefore, TEGa can be decomposed into Ga at any surface lattice sites. The other reason is the gas-phase pyrolysis at high temperatures. Figure 4-14 shows the (001) GaP growth rate as a function of the TEGa pulse duration at 485°C. The growth rate increased almost linearly with the TEGa pulse. At 485°C, TEGa molecules are thermally decomposed [32], so the surface adsorbate is bare Ga [33].

Anyway, we are interested in whether growth is self-limiting when the substrate, which has a submonolayer coverage of surface Ga, is exposed to a flow containing a sufficient amount of TMGa. Table 4-1 lists the growth rates obtained for two different gas pulse sequences at 485°C, with both TEGa and TMGa as Ga sources. In sequence (A), TEGa, TMGa, then PH_3 were sent in order. In sequence (B), on the other hand, the order was TMGa, TEGa, then PH_3. Each reactant in the gas cycle was separated by 3-second H_2 pulses. The mole fraction and the pulse duration of TMGa were kept at 2.1×10^{-3} and 5 s, sufficient to obtain a saturated monolayer growth of (001) GaP. TEGa was supplied with a mole fraction of 3.2×10^{-5}, and the duration was varied to change the amount (coverage) of the surface Ga fed

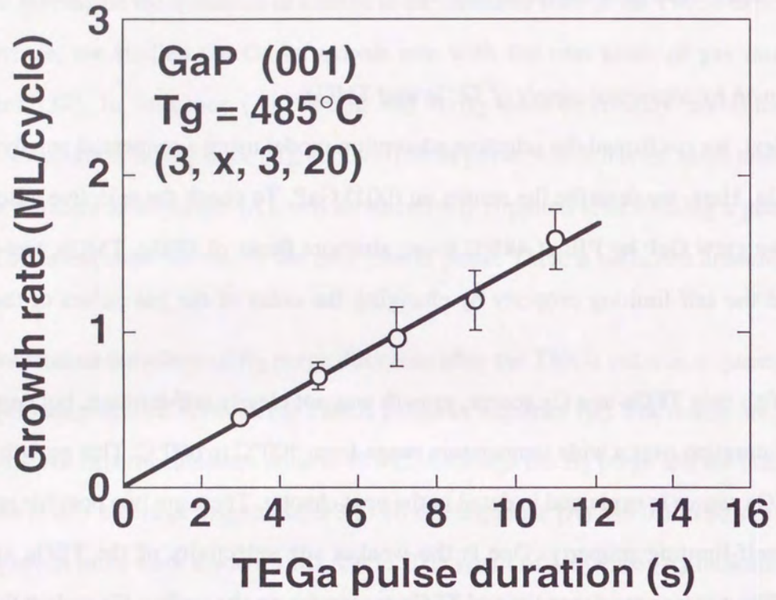

Figure 4-14. GaP growth rate at 485°C using TEGa and PH_3 as a function of TEGa pulse duration. Growth was at 15 Torr. The mole fraction of TEGa and PH_3 was $3.2x10^{-5}$ and $9.6x10^{-2}$, respectively.

Table 4-1: Comparison of GaP growth rates for two different gas sequence at 485°C.

TEG condition		Growth rate (ML/cycle)	
		Sequence (A)	Sequence (B)
Duration (s)	Feed rate (ML/cycle)	TEG→TMG→PH_3	TMG→TEG→PH_3
3	0.4	1	1.4
5	0.7	1	1.7
7	0.94	1	1.94

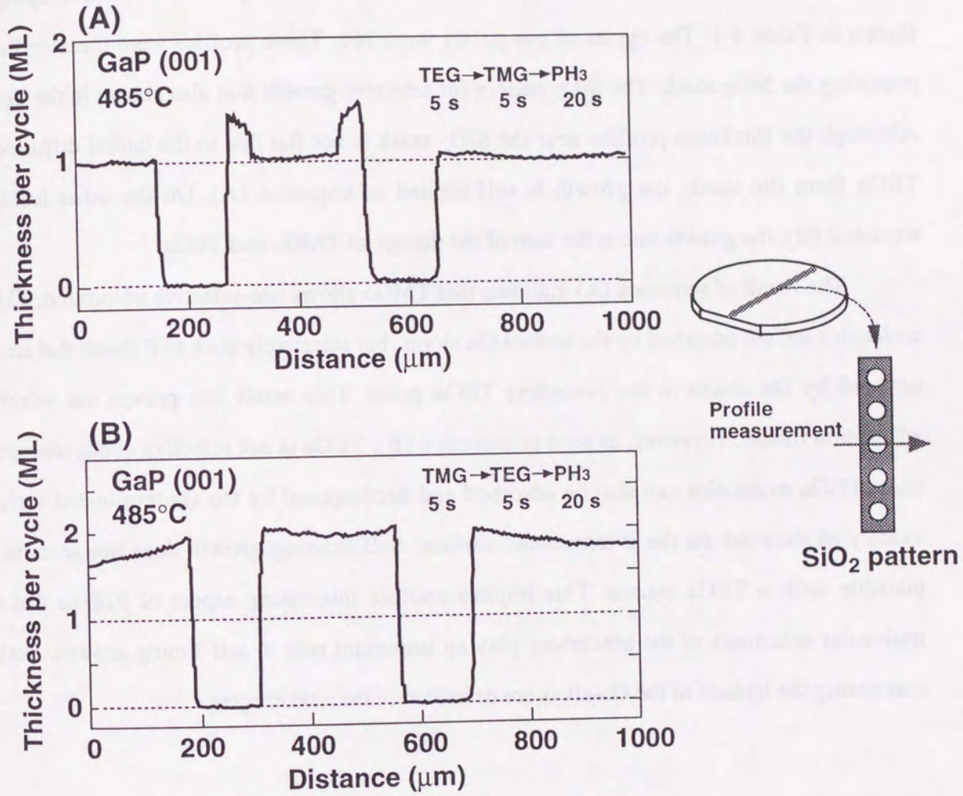

Figure 4-15. Thickness profiles of GaP grown with two different gas sequences in table 4-1.

during the pulse (see Fig. 4-14). The PH_3 exposure time was 20 s with a mole fraction of $9.6x10^{-2}$. We found that the growth rate was significantly changed by reversing the order of TEGa and TMGa pulses. Growth was self-limited in sequence (A), even when the TEGa pulse duration was varied. In sequence (B), the growth rate was almost the sum of the rates for TMGa and TEGa.

In Fig. 4-15, we showed the typical row data of thickness profiles of the GaP epilayers shown in Table 4-1. The cycles of gas pulses were 366. These profiles were measured after removing the SiO_2 mask. The SiO_2 pattern for selective growth was also shown in the figure. Although the thickness profiles near the SiO_2 mask is not flat due to the lateral diffusion of TEGa from the mask, the growth is self-limited in sequence (A). On the other hand, in sequence (B), the growth rate is the sum of the dosage of TMGa and TEGa.

The result of sequence (A) indicates that TMGa allows site-selective adsorption; TMGa molecules are not adsorbed by the surface Ga atoms, but selectively stick to P atoms that are not covered by Ga atoms in the preceding TEGa pulse. This result just proves our selective adsorption model. However, as seen in sequence (B), TEGa is not selective about adsorption sites. TEGa molecules can also be adsorbed and decomposed by the Ga-terminated surface, exactly as they are on the P-terminated surface. Self-limiting growth does not seem to be possible with a TEGa source. This implies another interesting aspect of PJE in that the molecular structures of the precursors play an important role in self-liming growth. Details concerning the ligands of the Ga-alkys are described in the next chapter.

4.6 Summary

We have explained the self-limiting growth mechanism which is a specific feature of PJE. By examining the TMGa-exposed (or TMIn-exposed) growth surface *in-situ* using XPS, we identified that the surface adsorbates causing the self-limiting are atomic Ga (or In). Considering the experimental fact that TMGa (or TMIn) quickly decomposes into Ga (or In) at the surface, we proposed a selective-adsorption model to explain the self-limiting growth

process. With the rate equations based on the selective adsorption model, we showed that we can reasonably describe the growth kinetics during GaAs PJE.

Finally, we reported two kinds of growth experiments which strongly justify the selective adsorption model. One is growth using consecutive TMGa supply, and the other is the use of TMGa and TEGa consecutive supply. We found that the results on these growth experiments can be well explained by the selective adsorption model.

REFERENCES (Chap. 4)

[1] K. Kodama, M. Ozeki, K. Mochizuki, and N. Ohtsuka, Appl. Phys. Lett. **54** (1989) 656.

[2] L. Pauling, *The Nature of The Chemical Bond*, 3rd ed. (Cornell University Press, Ithaca, New York, 1960).

[3] K. Kodama, M. Ozeki, Y. Sakuma, K. Mochizuki, and N. Ohtsuka, J. Cryst. Growth **99** (1990) 535.

[4] H. Ohno, H. Ishii, K. Matsuzaki, and H. Hasegawa, Appl. Phys. Lett. **54** (1989) 1124.

[5] M.L. Yu, U. Memmert, and T.F. Kuech, Appl. Phys. Lett. **55** (1989) 1011.

[6] B.Y. Maa and P.D. Dapkus, J. Electron. Mater. **19** (1990) 289.

[7] Y. Sakuma, K. Kodama, and M. Ozeki, Appl. Phys. Lett. **56** (1990) 827.

[8] Y. Mizokawa, H. Iwasaki, R. Nishitani, and S. Nakamura, J. Electron Spectrosc. Related Phenomena **14** (1987) 129.

[9] C.D. Wagner, W.M. Riggs, L.E. Davis, J.F. Moulder, and G.E. Muilenberg, *Handbook of X-ray Photoelectron Spectroscopy* (Perkin-Elmer, 1979).

[10] Y. Sakuma, K. Kodama, and M. Ozeki, Jpn. J. Appl. Phys. **27** (1988) L2189.

[11] D.E. Aspnes, E. Colas, A.A. Studna, R. Bhat, M.A. Koza, and V.G. Keramidas, Phys. Rev. Lett. **61** (1988) 2782.

[12] W.G. Jeong, E.P. Menu, and P.D. Dapkus, Appl. Phys. Lett. **55** (1989) 244.

[13] D.E. Aspnes, R. Bhat, E. Colas, V.G. Keramidas, M.A. Koza, and A.A. Studna, J. Vac. Sci. Technol. **A7** (1989) 711.

[14] S.J. Thompson and G. Webb, *Heterogeneous Catalysis* (John Wiley & Sons, New York 1968).

[15] D.J. Schlyer and M.A. Ring, J. Electrochem. Soc. **124** (1977) 569.

[16] J. Nishizawa, H. Abe, and T. Kurabayashi, J. Electrochem. Soc. **132** (1985) 1197.

[17] J. Nishizawa, T. Kurabayashi, H. Abe, and N. Sakurai, J. Electrochem. Soc. **134** (1987) 945.

[18] J. Nishizawa, T. Kurabayashi, H. Abe, and A. Nozoe, Surf. Sci. **185** (1987) 249.

[19] A. Doi, S. Iwai, T. Meguro, and S. Namba, Jpn. J. Appl. Phys. **27** (1988) 795.

[20] M.L. Yu, U. Memmert, N.I. Buchan, and T.F. Kuech, Mater. Res. Soc. Symp. Proc. **204** (1991) 37.

[21] M.L. Yu, N.I. Buchan, R. Souda, and T.F. Kuech, Mater. Res. Soc. Symp. Proc. **224** (1991) 3.

[22] J.R. Creighton, Surf. Sci. **234** (1990) 287.

[23] J.R. Creighton, K.R. Lykke, V.A. Shamamian, and B.D. Kay, Appl. Phys. Lett. **57** (1990) 279.

[24] J.A. MacCaulley, R.J. Shul, and V.M. Donnelly, J. Vac. Sci. Technol. **A9** (1991) 2872.

[25] M. Ozeki, K. Mochizuki, N. Ohtsuka, and K. Kodama, Appl. Phys. Lett. **53** (1988) 1509.

[26] M. Ozeki, N. Ohtsuka, Y. Sakuma, and K. Kodama, J. Cryst. Growth **107** (1991) 102.

[27] M.G. Jacko and S.J.W. Price, Can. J. Chem. **41** (1963) 1560.

[28] S.P. DenBaars, B.Y. Maa, P.D. Dapkus, A. Danner, and H.C. Lee, J. Cryst. Growth **77** (1986) 188.

[29] Y. Sakuma, M. Ozeki, N. Ohtsuka, and K. Kodama, J. Appl. Phys. **68** (1990) 5660.

[30] T.H. Chiu, Appl. Phys. Lett. **55** (1989) 1244.

[31] B.Y. Maa and P.D. Dapkus, J. Cryst. Growth **105** (1990) 213.

[32] P.W. Lee, T.R. Omstead, D.R. Mckenna, and K.F. Jensen, J. Cryst. Growth **85** (1987) 165.

[33] H. Ohno, S. Ohtsuka, H. Ishii, Y. Matsubara, and H. Hasegawa, Appl. Phys. Lett. **54** (1989) 2000.

CHAPTER 5
Role of Group-III Precursors

5.1 Preliminaries

In the previous chapter, we explained the self-limiting growth mechanism of GaAs using TMGa as a Ga precursor. However, so far, we have tried using alternative Ga precursors for the GaAs growth in the PJE reactor. Our motivation is to expand the so-called "ALE window" in the growth temperatures and to find the appropriate precursors providing the epitaxial layers of high purity, while still maintaining the self-limiting. Few researchers seem to recognize that the Ga precursors play a significant role in achieving self-limiting. From a technological point of view, we have not found any novel precursors showing self-limited Ga deposition, which are superior to TMGa. Through these studies, however, we obtained much important knowledge about the surface chemistry and the self-limiting mechanism.

In this chapter, we firstly summarize our GaAs growth experiments done in our PJE reactor by an alternate supply of AsH_3 and Ga precursors except for TMGa. The precursors we studied were $(C_2H_5)_3Ga$ (TEGa), ethyldimethylgallium or $(C_2H_5)(CH_3)_2Ga$ (EDMGa), tri-isobutylgallium or $(C_4H_9)_3Ga$ (TiBGa), and galliumtrichloride or $GaCl_3$. We explain the growth results for each Ga precursor from the viewpoint of self-limiting and the growth temperature range.

Then, we propose a method to evaluate the "site selectivity" of the Ga precursor's surface chemistry including adsorption, desorption, and decomposition between As and Ga sites at the surface. We show this "site selectivity" reflects well the degree or ability of self-limiting. By comparing experimental results using EDMGa and TEGa sources with that using TMGa, we found that the tendency towards self-limiting is weakened as methyl groups attached to a Ga atom were replaced by ethyl groups. From these results, we consider the important role of ligands of the starting Ga precursors in the self-limiting growth mechanism.

At the end of this chapter, we report some novel approaches to the self-limiting growth of GaAs. We used the combination of TEGa and TMGa as a Ga source, where TEGa and TMGa were consecutively or simultaneously supplied. We also tried the consecutive supply of TEGa and carbon tetrachloride (CCl_4). This is the first trial in which we aim to separate the self-limiting function from the Ga depositing function of the Ga precursor; both are inherent in the case of TMGa.

5.2 Chemistry of Ga Precursors

As described later, the self-limiting is strongly affected by the starting molecules of Ga. Few researchers seem to notice this important fact [1]. The fundamental physical and chemical properties of each precursor are summarized in Table 2-3. However, at present, we cannot directly estimate the each precursor's self-limiting ability from this data. So far, the choice of source molecules has been quite simple. Only compounds used for other growth techniques such as MOVPE, GSMBE, and chloride (hydride) VPE were tried as PJE sources. However, it is evident that some restrictions are imposed on the ALE or PJE process due to the limited kinds of sources. We have to emphasize a strong need to develop new sources suitable for ALE or PJE.

In this section, we provide a general description of the chemistry of Ga organometals to help the understanding of our experiments. Figure 5-1 shows the bonding and configurations of some Ga precursors. We also show the molecular structures of AsH_3 and PH_3. Consideration of the molecular structure is important because it is related to the thermal stability, *i.e.*, the kinetics of pyrolysis of the molecules. In general, the molecular structure can be understood from the valence bond theory of hybridized covalent bonding [2], or the valence-shell, electron-pair repulsion (VSEPR) model [3]. The incomplete electron shell of Ga atoms contains one *p (4p)* and two *s* $(4s^2)$ electrons. The three covalent bonds are formed with a hybridized sp^2 bonding configuration. Thus, a planar, trigonal molecule is formed with the three ligands separated by angles of 120°. An important point is that an unfilled *p* orbital remains after the

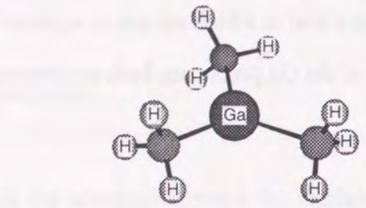

(a) TMGa

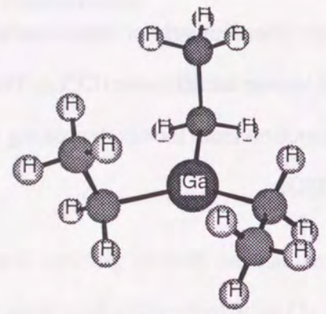

(b) TEGa

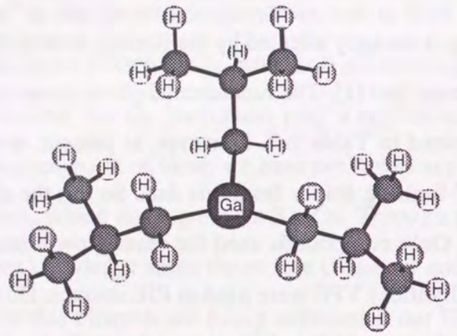

(c) TiBGa

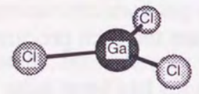

(d) $GaCl_3$

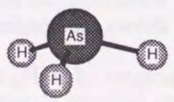

(e) AsH_3

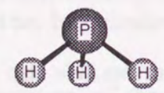

(f) PH_3

Figure 5-1. Molecular structures of some Ga precursors. AsH_3 and PH_3 are also shown.

three covalent bonds are formed. This unfilled *p* orbital lies perpendicular to the plane of the molecules and makes them electron acceptors, or Lewis acids.

The basic properties of organometals can be explained by considering the chemical bond between the metals and carbon. The "strength of the metal-C bond" and its "degree of polarity" are key factors to understanding some chemical and physical properties of metalorganic compounds, as described below.

(1) Thermal stability: the bonding energy of the metal-C bond is important because it determines the stability of the molecule against decomposition by free-radical homolysis. In general, the metal-C bond strength depends both on the nature of the metals, especially on their electronegativity, and the size and configuration of the radicals. For example, for a specific radical, the metal-C bond strength decreases in the order of Al > Ga > In. This is because the eletronegativities of these metals decrease in this order. On the other hand, the thermal stability for the compounds of a particular metal element depends largely on the nature of the attached organic groups, and in a number of cases the stability may be greatly enhanced by the substitution of more electronegative units (including halogen) [4]. It is decreased as the number of carbons bonded to the central carbon is increased. The weakening of the C-metal bond is attributed to the delocalization of the free-radical electronic charge [4].

(2) Vapor pressure: the vapor pressure varies rather systematically with the alkyl group. In principle, the vapor pressures are higher for the lighter molecules. Of course, the intermolecular interactions in the liquid phase also affect the vapor pressures, which makes quantitative predictions impossible. Generally, higher order, more branched molecules have weaker interactions, which enhances the vapor pressure. However, for the usual Ga alkyls we used, the effect of intermolecular interaction might be small. Therefore, the vapor pressures of the Ga alkyls decrease as their masses increase.

5.3 GaAs Growth using Several Ga Precursors

5.3.1 TEGa

TEGa is one of the most widely used Ga precursors in the MOVPE and GSMBE. It provides lower growth temperatures and epilayers with a lower carbon contamination than TMGa, due to the specific decomposition via the β-hydride elimination pathway [5, 6]. Therefore, we expected the use of this source for PJE.

5.3.1.1 Growth results

Figure 5-2 shows the growth rate of GaAs (001) as a function of the TEGa pulse duration in a gas cycle of alternate TEGa and AsH_3 source supply. Although the growth temperature was varied from 350°C to 480°C, no self-limiting was observed. The growth rate seems to increase linearly with TEGa pulse duration. The surface morphology was mirror-like at a growth rate of below 1 ML/cycle. However, it became rougher when increasing the growth rate above 1 ML/cycle. This is probably due to agglomerates of the excess Ga atoms (or Ga droplets) on the surface.

Figure 5-3 shows the typical growth rate dependence on the TEGa flow rate at 450°C, under several fixed TEGa pulse durations t_{TEGa}. Note that the growth rate tends to be saturated by increasing the TEGa flow rates when the pulse duration is short. However, for a longer TEGa exposure time of 0.8 s, the saturated value exceeded 1 ML/cycle, indicating there was no self-limiting growth using TEGa source.

5.3.1.2 Growth model using TEGa source

PJE requires that the deposition of Ga atoms is self-limited. To confirm that it is, some researchers have discussed the dependence of the growth rate on the total amount of group-III molecules supplied within a gas cycle [7, 8]. They define the amount of supplied molecules as the product of the flow rate and the pulse duration of group-III sources. We state here, however, that the growth rate dependence on the flow rate of the source differs from that on the pulse duration of the source when growth is conducted using an alternate group-III and group-V source gas supply. We can see this situation from Figs. 5-2 and 5-3. As shown in Fig. 5-3, when the pulse duration of TEGa is fixed, the Ga deposition rate per cycle saturates if the flow

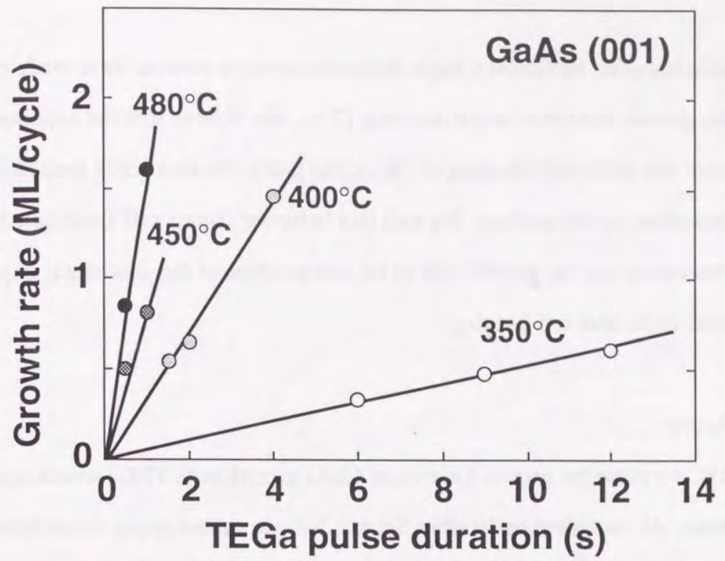

Figure 5-2. Growth rate of GaAs (001) as a function of TEGa pulse duration in an alternative supply of TEGa and AsH_3. The mole fraction of TEGa was $1.4x10^{-4}$ for 480°C and 450°C, and $3.3x10^{-4}$ for 400°C and 350°C. AsH_3 mole fraction was $2.4x10^{-2}$. Growth pressure was 20 Torr. The gas sequence was (0.3, x, 0.3, 10 s).

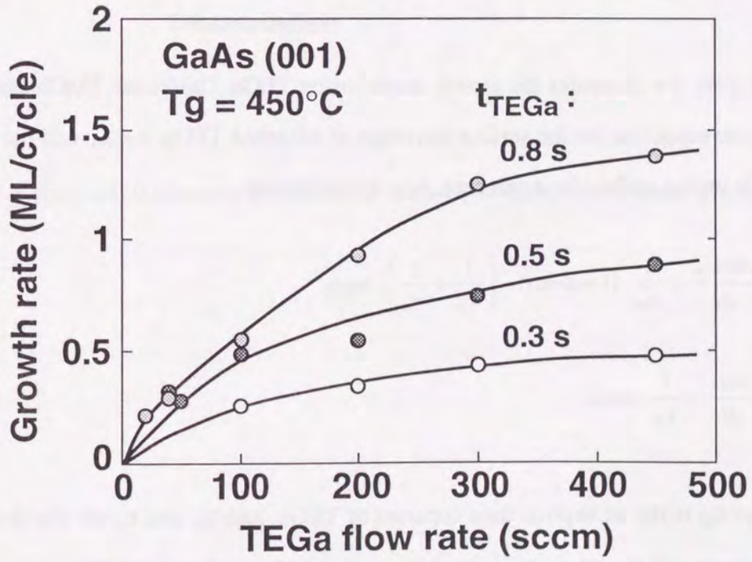

Figure 5-3. Growth rate of GaAs (001) as a function of TEGa flow rate in an alternative supply of TEGa and AsH_3. TEGa bath was maintained at 11°C (vapor pressure of 2.5 Torr). AsH_3 mole fraction was $2.4x10^{-2}$. Growth pressure was 20 Torr. The gas sequence was (0.3, t_{TEGa}, 0.3, 10 s).

rate of TEGa becomes sufficiently high. Some researchers seem to have made the mistake of judging this growth behavior as self-limiting [7-9]. We believe that the saturated behavior in Fig. 5-3 is not due to the self-limiting of TEGa, but just to the kinetically limited decomposition of TEGa adsorbed on the surface. We call this behavior "quasi self-limiting", hereafter. It is therefore necessary for the growth rate to be independent of the source gas exposure time in order to confirm the true self-limiting.

5.3.1.3 Theory

Next, we show the growth kinetics of GaAs growth with TEGa source using the simple rate equations. As described in detail in Section 5.4, we cannot apply the selective adsorption model to TEGa. Instead, we adopt the following two assumptions:

(1) No site selectivity: TEGa molecules are adsorbed and decomposed at both surface Ga and As atoms with the same probability.

(2) Inhibition of multiple adsorption: TEGa molecules are not adsorbed on the chemisorbed layer of TEGa itself.

Figure 5-4 illustrates the growth model using TEGa. Unlike the TMGa case in Section 4.4, the rate equations for the surface coverage of adsorbed TEGa, n_{TEGa}, and the coverage of atomic Ga on the surface for a unit area, n_{Ga}, are written as:

$$\frac{dn_{TEGa}}{dt} = \frac{1}{\tau_{ad}} \cdot (1 - n_{TEGa}) - \left(\frac{1}{\tau_{dc}} + \frac{1}{\tau_{rs}} \right) \cdot n_{TEGa} \qquad (5\text{-}1)$$

$$\frac{dn_{Ga}}{dt} = \frac{1}{\tau_{dc}} \cdot n_{TEGa} \qquad (5\text{-}2)$$

where the τ_{ad} is the adsorption time constant of TEGa, and τ_{dc} and τ_{rs} are the decomposition time constant and the desorption time constant (residence time) of TEGa molecules on the surface. We don't distinguish the value of each time constant between Ga and As sites, and we justify this assumption in Section 5.4. We solve the equations under the condition of:

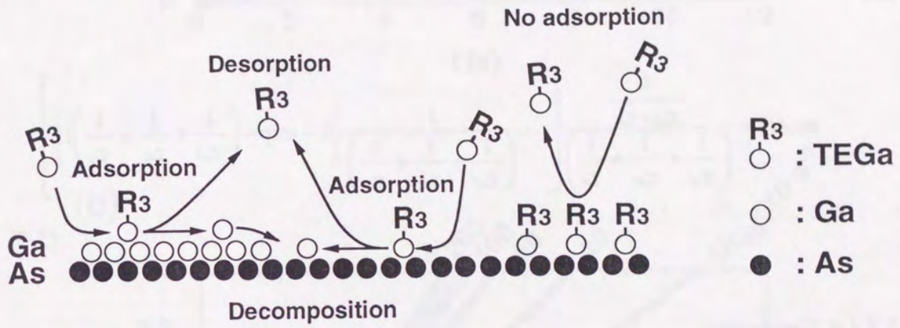

Figure 5-4. Assumed Ga deposition process during TEGa exposure on As-terminated GaAs surface.

$$n_{TEGa}(t=0)=0,\ \ n_{Ga}(t=0)=0 \tag{5-3}$$

because no TEGa and Ga exist on the initial As-terminated GaAs surface. The solutions are given as:

$$n_{TEGa}(t)=\frac{\frac{1}{\tau_{ad}}}{\left(\frac{1}{\tau_{ad}}+\frac{1}{\tau_{dc}}+\frac{1}{\tau_{rs}}\right)}\left\{1-\exp-\left(\frac{1}{\tau_{ad}}+\frac{1}{\tau_{dc}}+\frac{1}{\tau_{rs}}\right)t\right\} \tag{5-4}$$

and

$$n_{Ga}(t)=\frac{\frac{1}{\tau_{ad}\cdot\tau_{dc}}}{\left(\frac{1}{\tau_{ad}}+\frac{1}{\tau_{dc}}+\frac{1}{\tau_{rs}}\right)}\left[t-\frac{1}{\left(\frac{1}{\tau_{ad}}+\frac{1}{\tau_{dc}}+\frac{1}{\tau_{rs}}\right)}\left\{1-\exp-\left(\frac{1}{\tau_{ad}}+\frac{1}{\tau_{dc}}+\frac{1}{\tau_{rs}}\right)t\right\}\right] \tag{5-5}$$

5.3.1.4 Simulation

The GaAs growth rate is related to the n_{Ga} (ML/cycle) given by Eq. (5-5) if the reaction with AsH_3 completes. Figure 5-5 plots the n_{Ga} versus TEGa pulse duration of *t*. With increasing *t*, n_{Ga} increases almost linearly. This is in good agreement with the result in Fig. 5-2. Note that the slope of the n_{Ga} versus *t* curve becomes steeper with the decreasing τ_{dc}, which corresponds to the increase in the growth temperatures (Fig. 5-5 (a)). This is also in good agreement with the result of Fig. 5-2. On the other hand, the n_{Ga} versus *t* curve is not affected so much by τ_{ad} at the large $1/\tau_{ad}$ ($\propto f_{TEGa}$) regions (Fig. 5-5 (b)). Thus, the growth rate is determined by the TEGa decomposition rate on the surface.

Figure 5-6 shows the dependence of n_{Ga} on f_{TEGa} ($\propto 1/\tau_{ad}$) for various TEGa pulse durations. The growth rate tends to saturate with the increasing TEGa flow rate. Note that the saturation level is beyond 1 ML/cycle when *t* is long. These simulated results agree well with our experimental results of "quasi self-limiting" behavior in Fig. 5-3.

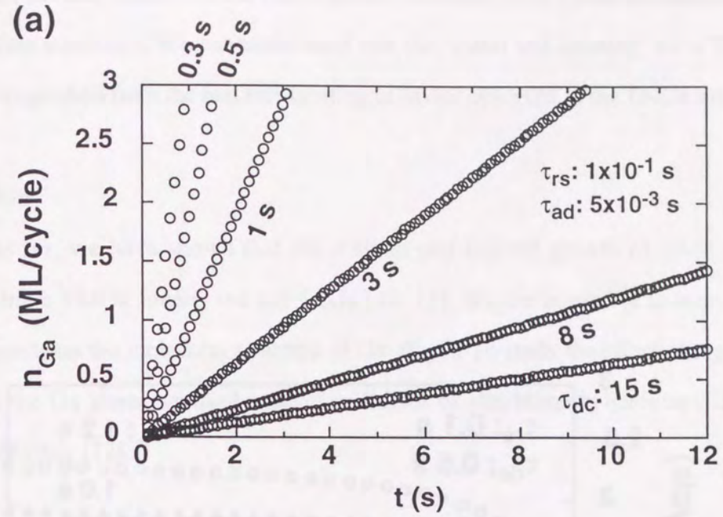

Figure 5-5. Simulated results of GaAs growth rate (n_{Ga}) versus TEGa pulse duration (t). Decomposition time constant, τ_{dc}, was changed in (a) and TEGa feed rate, $1/\tau_{ad}$, was changed in (b).

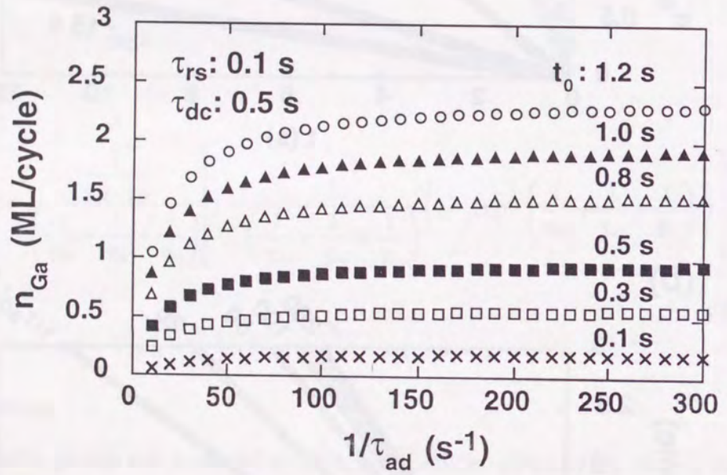

Figure 5-6. Simulated results of GaAs growth rate (n_{Ga}) versus TEGa flow rate (f_{TEGa}). Note that the flow rate is proportional to $1/\tau_{ad}$.

Thus, several features in the GaAs growth kinetics using TEGa are simulated well by the simple rate equations. We can understand that the "quasi self-limiting" for a TEGa source must be distinguished from the real self-limiting behavior observed in the TMGa source.

5.3.2 EDMGa

Thus far, we have shown that the distinct self-limited growth of GaAs and GaP is possible using a TMGa source, but not TEGa [10, 11]. We are interested in how self-limited growth depends on the molecular structure of Ga-alkyls. To study the effect of organic groups attached to the Ga atom, we used a novel precursor of ethyldimethylgallium (EDMGa) and tested self-limiting [12].

5.3.2.1 NMR study for synthesis

The source material was specially synthesized at Morton International, Ltd. (now CVD Ltd.) at our request, and this is the first report of GaAs growth using EDMGa. We measured proton nuclear magnetic resonance (^{1}H-NMR) and ^{13}C-NMR spectra to confirm EDMGa synthesis. The reagent was dissolved in $CDCl_3$ together with tetramethylsilane (TMSi) to mark the origin of the chemical shift. Figure 5-7 shows NMR data for the product. We observed two singlets (H-1, H-2), a triplet (H-4), and a quartet (H-3) peak in ^{1}H-NMR spectrum (Fig. 5-7(a)). In the ^{13}C-NMR spectrum (Fig. 5-7(b)), four peaks were detected (C-1~C-4) and the integrated intensity ratio of C-1, C-2, and C-3 was 1:2:1. Ideal EDMGa has three kinds of H and C atoms distinguished by their chemical configuration. ^{1}H-NMR should show three peaks; one is a singlet due to methyl groups, and the other two peaks split into three and four signals with the same energy interval caused by the interaction between CH_2 and CH_3 in the ethyl group. The ^{13}C-NMR spectrum should show three different peaks with an intensity ratio of 1:2:1. The results in Fig. 5-7 are consistent with an expected NMR spectra of EDMGa, although there is an extra ^{1}H peak and a ^{13}C peak (C-4) probably from some organic impurity. Moreover, we measured the NMR spectra of TMGa and TEGa, and found that the spectra in the figure are not a simple superposition of those for TMGa and TEGa. Thus, we confirmed that the chemical substance is true EDMGa and not a mixture of TMGa and TEGa.

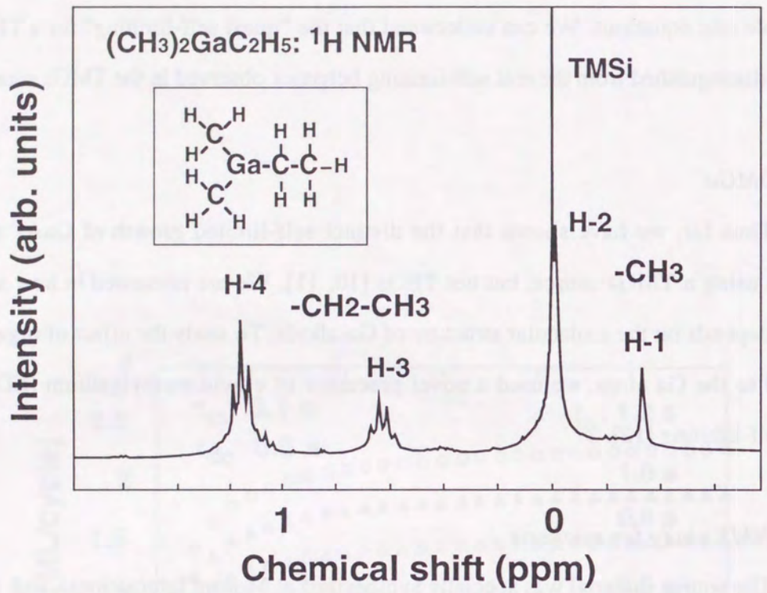

Figure 5-7(a). ^{1}H-NMR spectrum of EDMGa in $CDCl_3$.

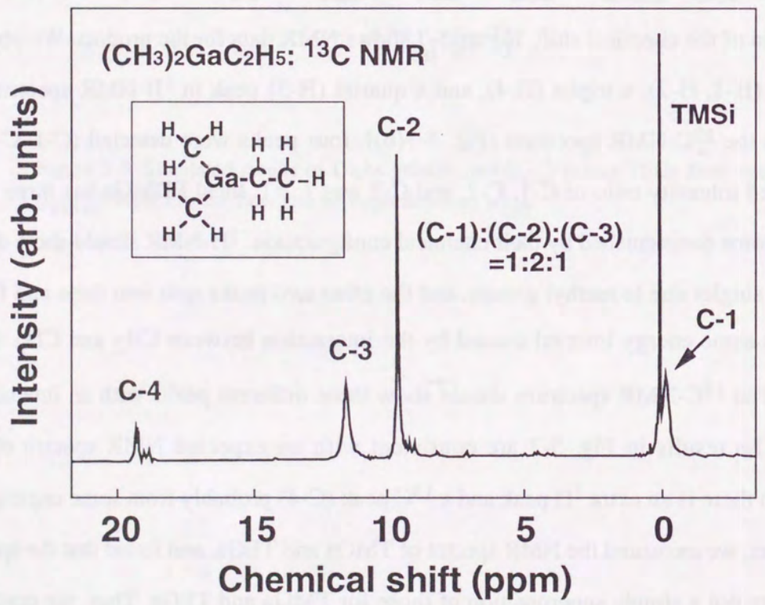

Figure 5-7(b). ^{13}C-NMR spectrum of EDMGa in $CDCl_3$.

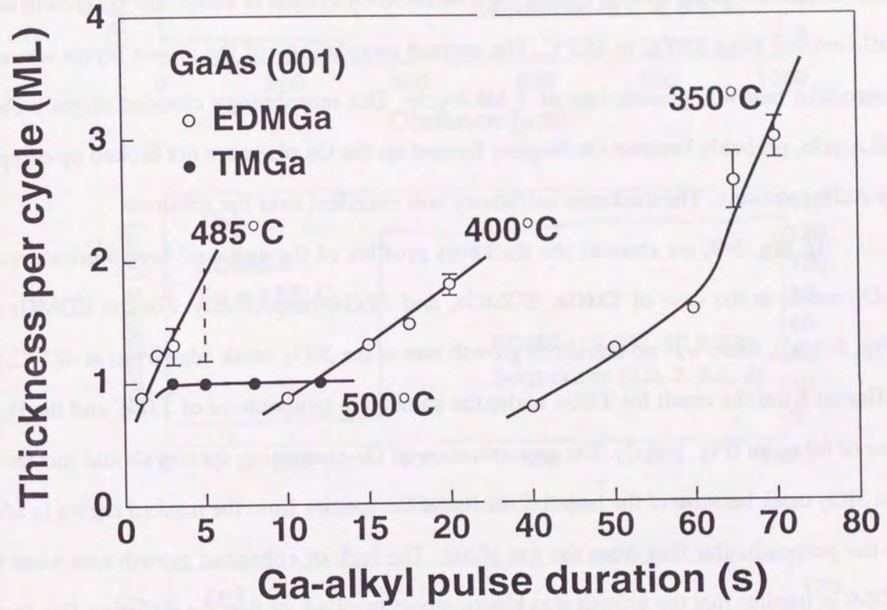

Figure 5-8. Growth rate dependence on EDMGa pulse durations. The gas sequence, H_2/ EDMGa/ H_2/ AsH_3, was 5/ x/ 5/ 10 s. AsH_3 mole fraction was 4.8×10^{-2}. EDMGa was fed by passing 40 sccm H_2 through container kept at 3°C.

5.3.2.2 Growth results

Figure 5-8 shows the growth thickness of GaAs (001) per PJE cycle as a function of the EDMGa pulse duration, for temperatures between 350°C and 485°C. Also shown is similar data for TMGa at 500°C for comparison. Growth occurred even at 350°C when using EDMGa, although growth was scarcely observed using TMGa, indicating that EDMGa has a lower thermal stability than TMGa. Unlike the TMGa-AsH_3 system at about 500°C, growth was not self-limiting from 350°C to 485°C. The surface morphology of the grown layers was always mirrorlike below a growth rate of 1 ML/cycle. The morphology clouded slightly above 1 ML/cycle, probably because Ga droplets formed on the Ga plane are not broken up completely by AsH_3 exposure. The thickness uniformity was excellent over the substrate.

In Fig. 5-9, we showed the thickness profiles of the epitaxial layers grown near the SiO_2 mask, in the case of TMGa, EDMGa, and TEGa, respectively. For the EDMGa result (Fig. 5-9(b)), there was no enhanced growth rate at the SiO_2 mask edge even at 485°C, being different from the result for TEGa under the same bath temperature of 3.0°C and the H_2 flow rate of 40 sccm (Fig. 5-9(c)). The concentration of Ga-containing species should increase near the SiO_2 mask because of the lateral diffusion of the species from the masked region in addition to the perpendicular flux from the gas phase. The lack of enhanced growth rate when using EDMGa implies that the growth was kinetically-controlled, or that the diffusion flux from the SiO_2 mask region is negligible, probably due to the fast reevaporation of EDMGa from the surface because of its vapor pressure being higher than that of TEGa.

Figure 5-10 shows the dependence of the growth rate on the H_2 flow rate through the EDMGa bubbler. The pulse duration of EDMGa was fixed at 2 s. The growth rate increases rapidly up to about 1 ML/cycle, then gradually increases with a linear slope. To obtain further evidence that EDMGa in the cylinder is not a mixture of TMGa and TEGa, we compared the GaAs growth rate when using EDMGa with that obtained by simultaneously introducing TMGa and TEGa. If EDMGa is only a mixture of TMGa and TEGa, the growth rate by EDMGa should be equal to that by the TMGa and TEGa mixture when the temperature of the thermostatic baths and the H_2 feed rate for both TMGa and TEGa are regulated to be the same

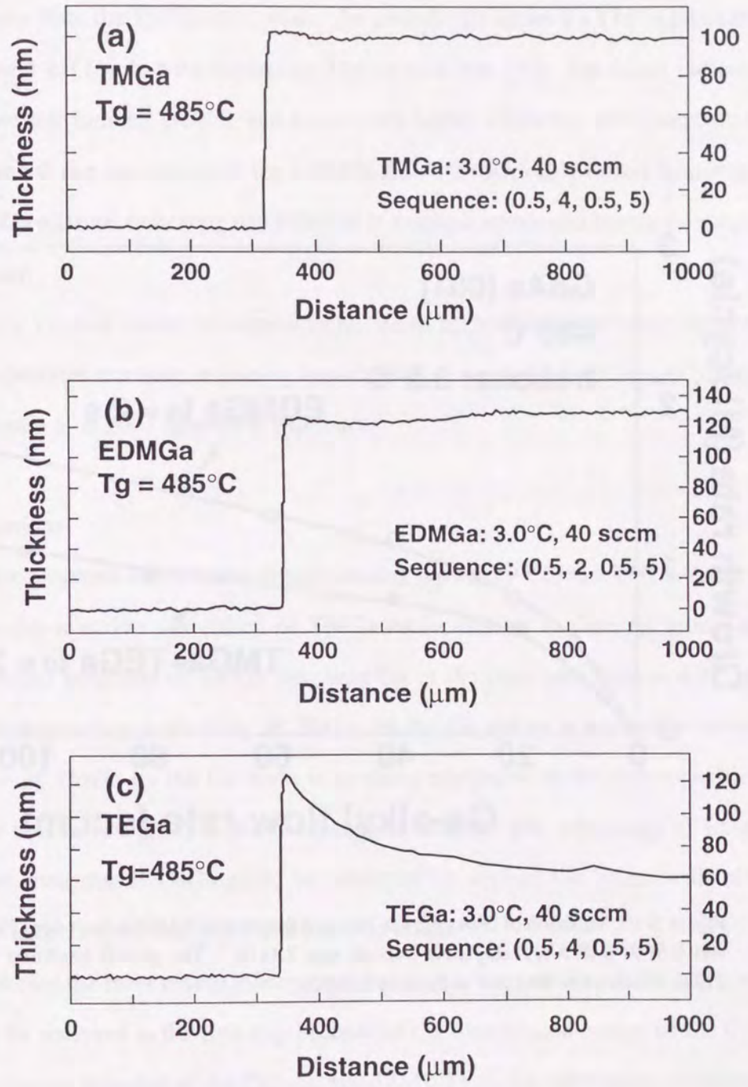

Figure 5-9. Comparison of thickness profiles of GaAs epilayers among three kinds of Ga precursors.

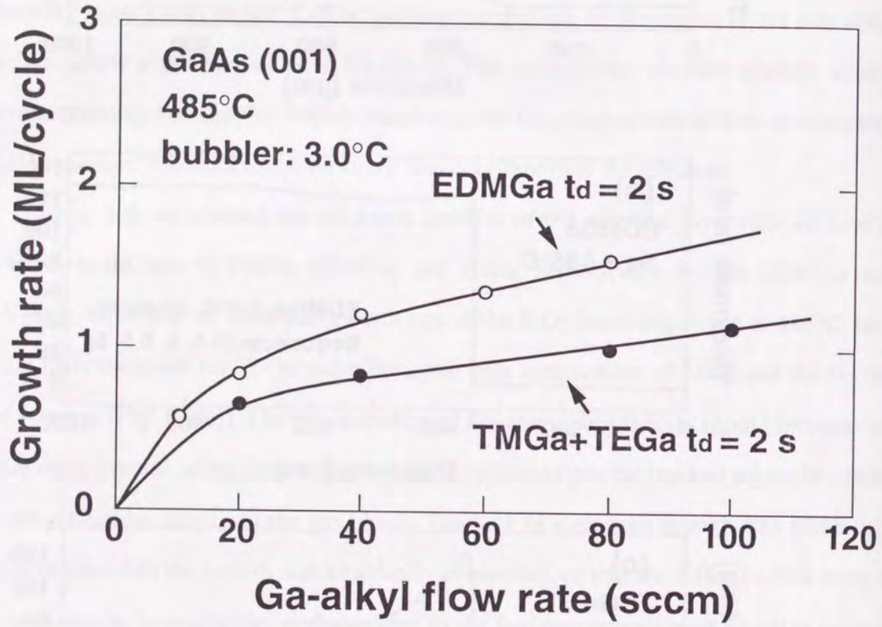

Figure 5-10. Variation of GaAs growth rate as a function of EDMGa flow rate. The gas sequence was 0.5/ 2/ 0.5/ 5 s. AsH_3 mole fraction was 2.4×10^{-2}. The growth condition for TMGa and TEGa mixture was the same as those of EDMGa.

as those of EDMGa. The growth rate results are also shown in the figure. Although the TEGa/TMGa flux ratio is only about 2×10^{-2} in this condition, the growth rate gradually increases with the increasing TMGa and TEGa flow rate, and does not seem to saturate. This result is different from the TMGa case, where the growth rate under 2 s TMGa pulse duration saturates below 1 ML/cycle with increasing TMGa flow rate [13]. The result indicates that TEGa shows no self-limiting growth, and has a much higher efficiency of Ga deposition than TMGa. The growth rate variation with the EDMGa flow rate obviously differs from that of the TMGa and TEGa mixture, indicating that EDMGa is a unique compound having its own surface reaction pathway.

Recently Yu *et al.* traced our experimental results mentioned above using the numerical simulation of chemical reactions, assuming hypothetical compounds, $Ga(CH_3)_m(C_2H_5)_{3-m}$ [1]. Their conclusion was in good agreement with ours.

5.3.2.3 Implications

We have proposed that completely self-limiting growth by PJE in a TMGa-AsH_3 system is due to the site-selective adsorption of TMGa molecules on surface As atoms and the subsequent perfect pyrolysis of TMGa into bare Ga at the sites (see Section 4.3). In other words, the decomposition probability of TMGa on the Ga atoms is negligible because the residence time of TMGa on the Ga atom is so short compared to the decomposition time constant. The results in Figs. 5-8 and 5-10 suggest that the site selectivity of EDMGa is somewhat low such that EDMGa could be adsorbed by surface Ga atoms with sufficient residence time to decompose and generate excess Ga atoms.

Considering the most reasonable thermal decomposition pathway of EDMGa, an ethyl radical would be removed in the first step because of the dissociation energy of the C_2H_5-Ga bond, which is lower than that of the CH_3-Ga bond [14]. Thus, the same kinds of intermediate radicals, such as dimethylgallium, $Ga(CH_3)_2$, or monomethylgallium, $GaCH_3$, would be produced from EDMGa and TMGa. The fact that growth limitation occurred with TMGa, not by EDMGa, implies:

(1) Self-limiting does not seem to originate from the above radicals, $Ga(CH_3)_2$ or $GaCH_3$.

(2) Under the conditions for achieving self-limiting growth, TMGa molecules are adsorbed on the (001) GaAs without decomposition in the first step.

(3) Three CH_3 groups attached to a Ga play an important role in the site selectivity and the self-limiting.

5.3.3 TiBGa

5.3.3.1 Background

TiBGa has been used in the conventional MOVPE process [15]. It is reported that the fairly large growth rate was obtained even at a lower temperature range than the case using TEGa and TMGa, due to the lower thermal stability of TiBGa. Also, as TiBGa is liquid at room temperature and has an appropriate vapor pressure (1.5 Torr at 54°C), it is convenient for growth. Therefore, we did the PJE growth experiments with expectation of the self-limiting growth behavior at lower growth temperatures.

5.3.3.2 Growth results

Figure 5-11 shows the relationship between the TiBGa pulse duration and the GaAs growth thickness per cycle. The duration of each gas pulse was as follows: H_2 purge for 3 s, a variable TiBGa pulse duration, H_2 purge for 3 s, and AsH_3 exposure for 10 s. At the growth temperature of 400°C, the growth rate increased monotonously with the TiBGa pulse duration. This might be due to the gas-phase pyrolysis of TiBGa in the boundary layer near the substrate surface. By further lowering the growth temperature to 300°C, the growth rate tended to saturate at 1 ML/cycle within the narrow range of TiBGa exposure time. However, the growth rate increased again thereafter. We believe that this observation of the narrow plateau at 1 ML/cycle is not due to the self-limiting of TiBGa, but is rather related to the AsH_3 supply conditions [16]. Thus, we should conclude that the self-limiting ability is very weak for TiBGa.

5.3.4 $GaCl_3$

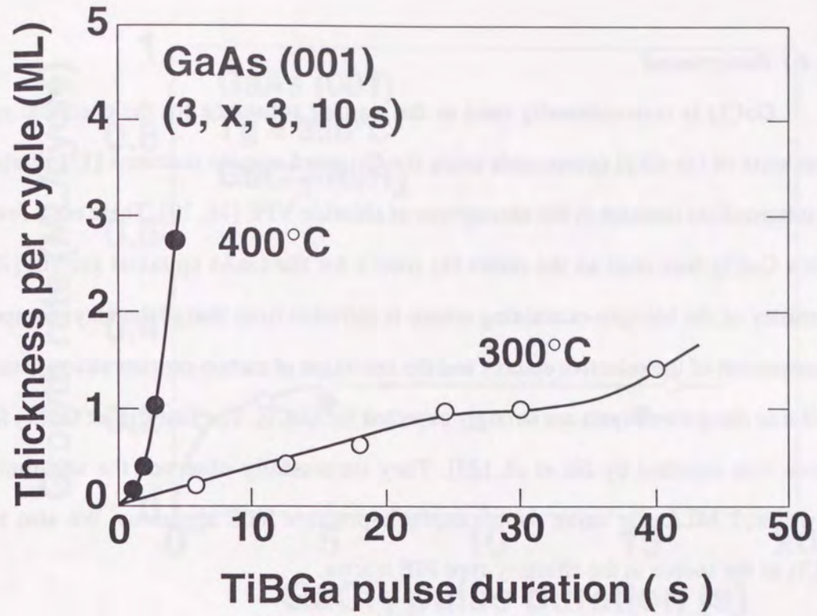

Figure 5-11. GaAs growth rate dependence on TiBGa pulse duration.

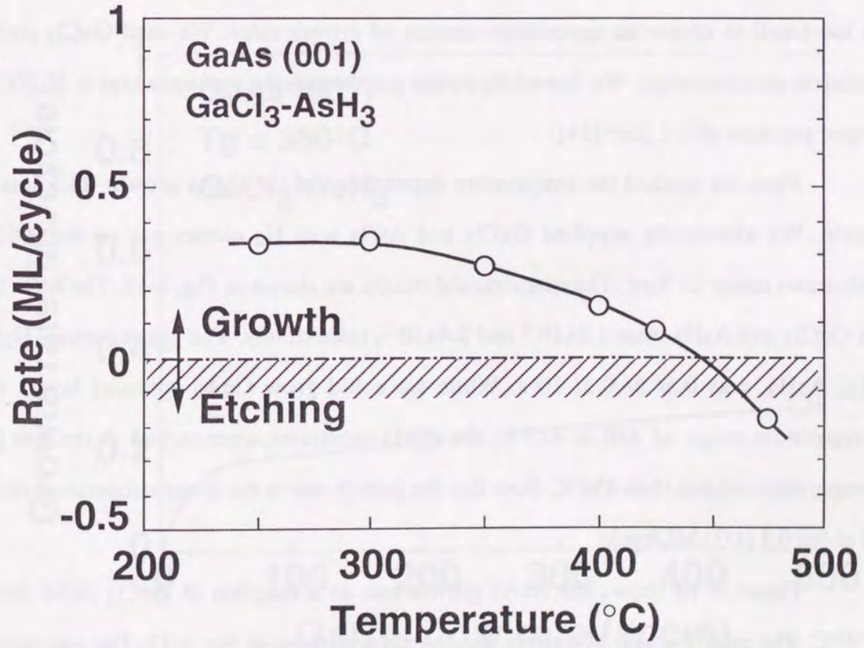

Figure 5-12. Temperature dependence of GaAs growth (etch) rate with $GaCl_3$.

5.3.4.1 Background

$GaCl_3$ is conventionally used as the starting substance for the chemical synthesis of some sorts of Ga-alkyl compounds using the Grignard reagent reactions [17]. It also exists as the intermediate reactant in the atmosphere of chloride VPE [18, 19]. There are a few reports in which $GaCl_3$ was used as the direct Ga source for the GaAs epitaxial growth [20-22]. The chemistry of the halogen-containing source is different from that of the alkyl compounds. The improvement of the selective epitaxy and the inhibition of carbon contamination from the source itself into the grown layers are strongly expected for $GaCl_3$. The first trial of $GaCl_3$ for the ALE source was reported by Jin *et al.* [23]. They successfully observed the self-limiting GaAs growth at 1 ML/cycle using the atmospheric-pressure VPE apparatus. We also tried to use $GaCl_3$ as the source in the chimney-type PJE reactor.

5.3.4.2 Growth results

$GaCl_3$ is solid (white crystalline substance) at room temperature and its vapor pressure is too small to obtain an appreciable amount of growth rates. We used $GaCl_3$ packed in a stainless steel container. We flowed H_2 carrier gas through the container kept at 50.0°C under a vapor pressure of 1.2 Torr [24].

First, we studied the temperature dependence of the GaAs growth thickness per gas cycle. We alternately supplied $GaCl_3$ and AsH_3 with H_2 carrier gas on the (001) GaAs substrates under 15 Torr. The experimental results are shown in Fig. 5-12. The mole fractions of $GaCl_3$ and AsH_3 were 1.2×10^{-4} and 2.4×10^{-2}, respectively. The gas sequence, H_2/ $GaCl_3$/ H_2/ AsH_3, was 0.5/ 5/ 0.5/ 10 s. While we could grow GaAs epitaxial layers at a low temperature range of 250 to 425°C, the (001) substrates were etched in the gas phase at temperatures higher than 450°C. Note that the growth rate at the lower temperature range stays at about 0.3 (1/3) ML/cycle.

Figure 5-13 shows the GaAs growth rate as a function of $GaCl_3$ pulse duration at 350°C. The mole fraction of sources was the same as those in Fig. 5-12. The gas sequence for open circles was 0.5/ x/ 0.5/ 20 s. Although we observed clear self-limiting growth, the growth rate saturated at about 0.3 ML/cycle. In the same figure, we plotted the results under different

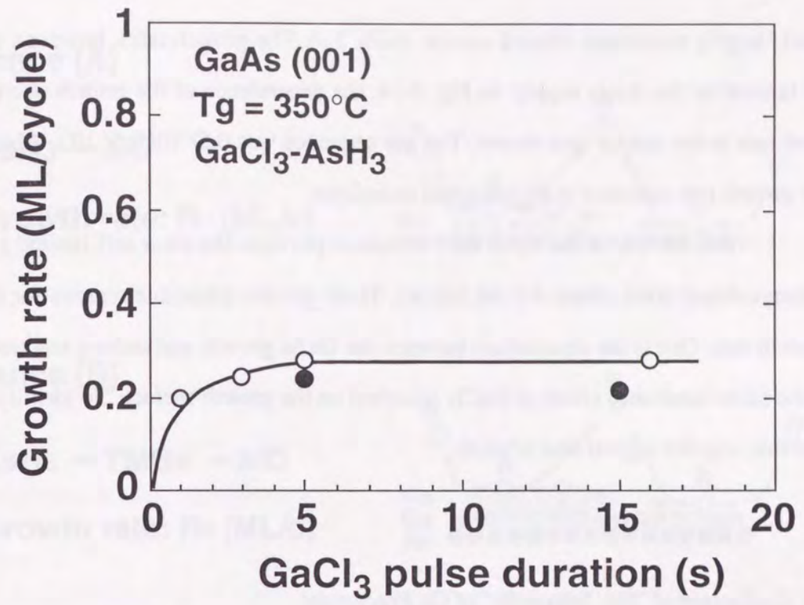

Figure 5-13. Dependence of GaAs growth rate on $GaCl_3$ pulse duration.

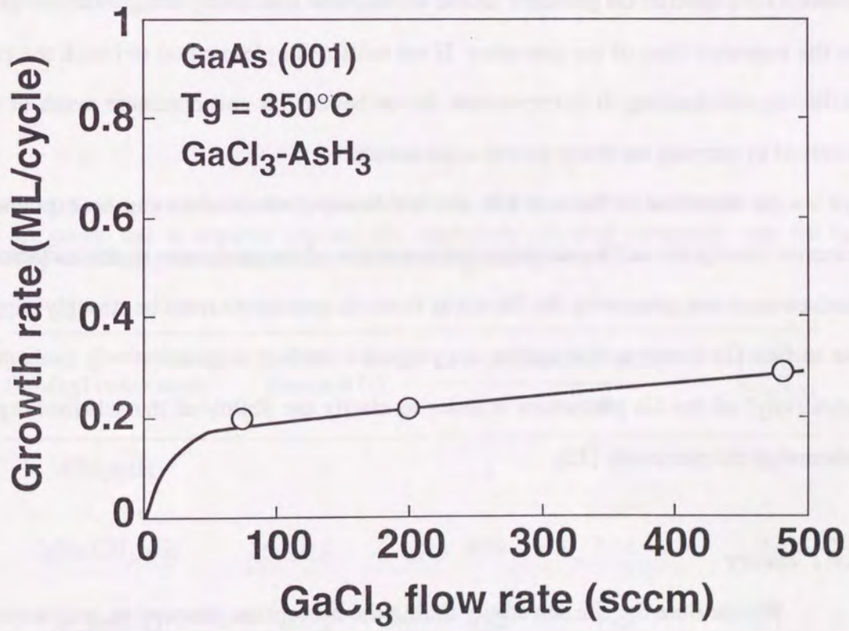

Figure 5-14. Dependence of GaAs growth rate on $GaCl_3$ flow rate.

AsH_3 supply conditions (closed circles; AsH_3 5 s). The growth rates, however, don't seem to be limited by the AsH_3 supply. In Fig. 5-14, the dependence of the growth rate on the $GaCl_3$ flow rate in the reactor was shown. The gas sequence was 0.5/ 10/ 0.5/ 10 s. Also in this case, the growth rate saturated at the fractional monolayer.

Thus, the use of $GaCl_3$ as the PJE source provides the clear self-limited growth rate at submonolayer level (about 0.3 ML/cycle). There are two plausible reasons for the fractional growth rate. One is the equilibrium between the GaAs growth and etching reactions. The other is the steric hindrance effect of $GaCl_3$ adsorbed on the growth surface. To identify which is the real one requires a great deal of work.

5.4 Evaluation of "Site Selectivity" of Ga Precursors

So far, there has been no way to judge whether the self-limiting GaAs growth can be attained for a specific Ga precursor unless we examine elaborately the growth rate dependence on the exposure time of the precursor. If we have a simple method to check the precursor's ability in self-limiting, it is convenient for us because it can eliminate much of the effort involved in carrying out many growth experiments.

As described in Section 4.3, the self-limiting mechanism can be explained by the selective adsorption and the resultant decomposition of the precursors on the surface As atoms. Surface reactions generating the Ga atoms from the precursors must be strongly suppressed at the surface Ga atoms. In this section, we propose a method to quantitatively evaluate the "site selectivity" of the Ga precursors in order to clarify the ability of the self-limiting property inherent in the precursors [12].

5.4.1 Theory

We measure the site selectivity during the adsorption, desorption, and decomposition processes of the metalorganic (MO) molecules by comparing the growth rates under two specific gas sequences. Figure 5-15 illustrates the two kinds of sequences. We assume that MO

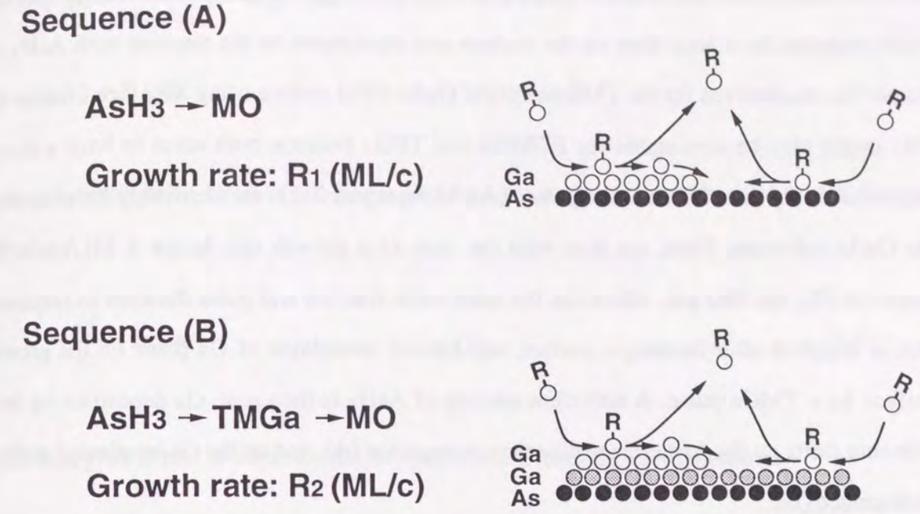

Figure 5-15. Illustration of two different gas sequences to evaluate site selectivity of Ga precursors. Closed circles show As atoms and open circles are Ga atoms produced by thermal decomposition of MO molecules. Shaded circles in (B) sequence represent Ga atoms by TMGa after AsH_3. R shows some ligands such as methyls and ethyls.

Table 5-1: Comparison of site selectivity among TMGa, EDMGa, and TEGa at 485°C. R_1 and R_2 are the growth rate in sequence (A) and (B), respectively. Ga-alkyl compounds were fed by bubbling 40 sccm H_2 through containers kept at 3°C. H_2 purging took 0.5 s.

Ga-alkyl compounds	Duration (s)	Growth rate (ML/cycle)		k_{Ga}/k_{As}
		R_1	R_2	
$(CH_3)_3Ga$	4	1	1	0
$C_2H_5(CH_3)_2Ga$	2	0.58	1.31	0.45
$(C_2H_5)_3Ga$	3	0.64	1.64	1

molecules repeat adsorption and desorption many times at the surface, and that the Ga species, which remains for a long time on the surface and contributes to the reaction with AsH_3, is atomic Ga, as observed for the TMGa-exposed GaAs (001) surface using XPS (see Chapter 4). This might also be reasonable for EDMGa and TEGa because both seem to have a lower thermal stability than TMGa. In sequence (A), MO gas and AsH_3 are alternately introduced to the GaAs substrate. Here, we deal with the case of a growth rate below 1 ML/cycle. In sequence (B), the MO gas, which has the same mole fraction and pulse duration as sequence (A), is supplied after forming a perfect, self-limited monolayer of Ga plane on the growth surface by a TMGa pulse. A sufficient amount of AsH_3 is then sent. Ga deposition by MO exposure starts on the As-terminated surface in sequence (A), and on the Ga-terminated surface in sequence (B).

We define the Ga generation rates on each surface As and Ga atom as k_{As} and k_{Ga}. Strictly speaking, both Ga generation rates are determined by the rate of adsorption, desorption, and decomposition of individual MO molecules at surface lattice sites. However, we cannot clarify the surface process that discriminates the Ga generation rate between the two sites. The absolute value of k_{As} and k_{Ga} should depend on growth conditions such as the MO's partial pressure in the reactor, physical or chemical properties of molecules, or the substrate temperature. Hence, we cannot compare the values among different kinds of MO molecules. We therefore used "k_{Ga}/k_{As}" as the scale of site selectivity.

Assuming that Ga atoms are arranged two-dimensionally on the As-terminated (001) GaAs surface due to the fast surface diffusion of Ga atoms on the Ga growth plane, the rate equation for the number of Ga atoms per unit area, N, is

$$\frac{dN}{dt} = \frac{dn_{Ga}}{dt} = k_{As} \cdot (n_s - n_{Ga}) + k_{Ga} \cdot n_{Ga} \tag{5-6}$$

where n_s is the surface lattice density ($6.26 \times 10^{14} cm^{-2}$) and n_{Ga} the surface Ga density. By solving Eq. (5-6), the growth rate in sequence (A), R_1 (ML/cycle), is

$$R_1 = \frac{k_{As}}{k_{As} - k_{Ga}} \left\{ 1 - \exp -(k_{As} - k_{Ga}) \cdot t_d \right\}, \quad (k_{Ga} \neq k_{As})$$
$$= k_{As} \cdot t_d, \qquad (k_{Ga} = k_{As}) \tag{5-7}$$

where t_d is the pulse duration of MO gas supplied. Contrary to this, N in sequence (B) is given by

$$\frac{dN}{dt} = k_{Ga} \cdot n_s \tag{5-8}$$

The total growth rate in sequence (B), R_2 (ML/cycle), from Eq. (5-8), becomes

$$R_2 = 1 + k_{Ga} \cdot t_d \tag{5-9}$$

From Eqs. (5-7) and (5-9), we can determine k_{As} and k_{Ga}, and compare the self-limiting property among the different Ga-alkys by k_{Ga}/k_{As}.

5.4.2 Comparison of TMGa, EDMGa, and TEGa

We evaluated the site selectivity of TMGa, EDMGa, and TEGa, according to the above-mentioned method [12]. Table 5-1 lists the growth rates for the two gas sequences and the values of k_{Ga}/k_{As} for TMGa, EDMGa, and TEGa at 485°C. The pulse duration and the mole fraction of the TMGa pulse in sequence (B) are 4 s and 1.0×10^{-3}, enough to make a complete monolayer Ga plane by self-limiting deposition. A systematic change appears to occur in the site selectivity among the three Ga-alkyls as methyl groups in the TMGa are replaced by ethyl groups. For TMGa, k_{Ga}/k_{As} is zero under our growth conditions. We could not observe any detectable amount of excess Ga deposition on the Ga-terminated surface when another TMGa pulse impinged to the substrate. This shows that TMGa is selectively adsorbed and pyrolized on the surface As atoms, resulting in complete self-limiting growth. However, for TEGa, k_{Ga}/k_{As} is very close to unity, indicating almost no difference in the TEGa surface chemistry for the two lattice sites. Therefore, the growth process is not self-limiting with TEGa. The Ga generation

rate ratio of 0.45 for EDMGa lies between those of TMGa and TEGa. EDMGa molecules hinder its adsorption and decomposition by surface Ga atoms slightly, but growth does not self-limit Ga deposition due to the imperfect site selectivity. This explains the growth rate variation when using EDMGa shown in Figs. 5-8 and 5-10. As seen from Table 5-1, the self-limiting mechanism inherent in PJE is strongly affected by the kinds of Ga-alkyls used and, apparently, the three methyl groups are crucial to achieving complete growth limitation. Once all methyl groups are replaced by ethyl groups like TEGa, the chemistry becomes almost the same as at Ga and As sites.

5.5 Elucidation for Role of Ligands in Self-Limiting Mechanism

In this section, first we refer to the two growth models in which the interactions of the gas-phase source molecules with the surface are taken into consideration. Then, based on these models, we try to explain the important role of ligands of the starting Ga precursors in the self-limiting mechanism.

5.5.1 Crystal growth via Lewis acid and Lewis base reaction

We can regard the GaAs growth process as Lewis acid-base reactions at the interface between gas phase and the surface [25]. In Fig. 5-16, we showed the electron configurations of ^{31}Ga and ^{33}As. Since there are three valence electrons ($4s^24p$) in N shell of Ga atom, an sp^2 hybridized orbital is formed when it reacts with three alkyl radicals. Therefore, a Ga precursor has an empty orbital around a Ga atom and acts as an electron acceptor (Lewis acid). For As, there are five valence electrons ($4s^24p^3$) in the N shell. So sp^3 hybridization occurs on reacting with three H atoms, giving a tetragonal bonding configuration. As a result, AsH_3 molecule has a lone pair around an As atom, acting as an electron donor (Lewis base).

On the other hand, the chemical (covalent) bonds of GaAs are sp^3 hybridized in the bulk crystal. At the surface, however, the dangling bonds should be formed. The energy levels of these dangling bonds can be estimated from the energies of the s-like and p-like atomic levels

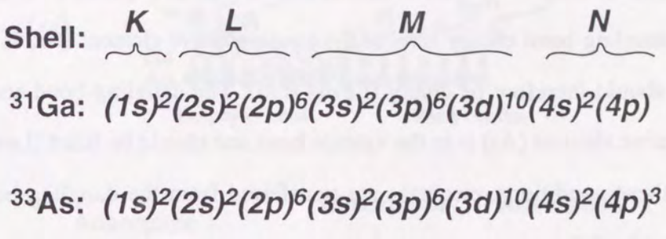

Figure 5-16. Electron configurations of ^{31}Ga and ^{33}As.

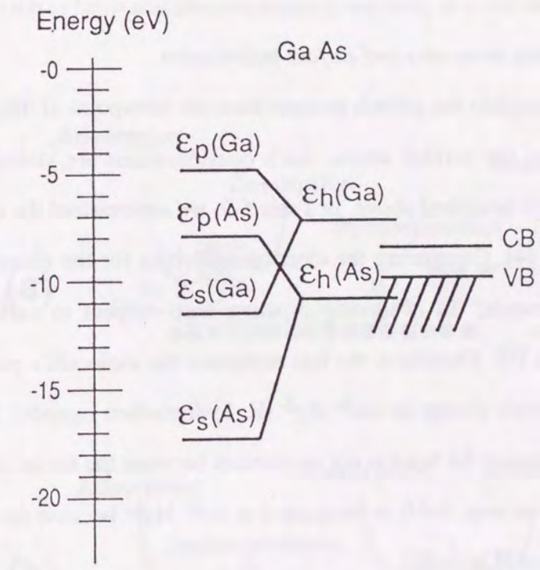

Figure 5-17. Energy levels ε_h of sp^3 dangling bonds states of GaAs. The energy is derived from that of s and p orbitals, ε_s and ε_p, respectively. The Ga dangling bond energy is above the conduction band minimum and the As dangling-bond energy is below the valence-band maximum.

from which they are derived. These energies can be compared with the conduction-band minimum and the valence-band maximum of the bulk GaAs. Figure 5-17 is taken from Pashley [26]. The dangling-bond energy level of the electropositive element (Ga) is in the conduction band, and should therefore be empty (Lewis acid). The dangling-bond energy level for the electronegative element (As) is in the valence band and should be filled (Lewis base). In order to realize these conditions, electrons are transferred from the dangling bonds of Ga to the dangling bonds of As.

Figure 5-18 (a) illustrates the reaction between the gas-phase Ga precursors and the (001) GaAs growth surface. Since the Ga precursors are electron acceptors, the attractive force will act at the surface As atoms. In contrast, the force will be repulsive at the surface Ga atoms and Ga precursors scarcely react there. In a similar way, the gas-phase AsH_3 will tend to react with surface Ga atoms, and not with surface As (Fig. 5-18 (b)).

5.5.2 Crystal growth via molecular and surface polarization

We can also explain the growth process from the viewpoint of the polarization of both source molecules and the surface atoms. Such considerations are strongly related with the Lewis acid-base model described above. In Table 5-2, we summarized the electronegativities of the typical elements [4]. Comparing the electronegativities for the elements included in the metalorganic compounds, Ga is usually positive with respect to carbon atoms or some hydrocarbon radicals [4]. Therefore, we can designate the molecule's polarity by indicating fractions of an electronic charge as $Ga^{\delta+}$-$R_3^{\delta-}$ (R: hydrocarbon ligands). This means that the electron cloud constituting the bond is not equidistant between the nuclei, but is shifted toward the C atom. In the same way, AsH_3 is designated as $As^{\delta-}$-$H_3^{\delta+}$ because the electronegativity of As is larger than that of H atom [4].

Since GaAs is a polar crystal and has some ionic characteristics, polarization will occur between the two constituent atoms. The polarization of the surface Ga and As atoms is easily estimated from Table 5-2. We can express the polarity as $Ga^{\delta+}$-$As^{\delta-}$ because As has a larger electronegativity than Ga.

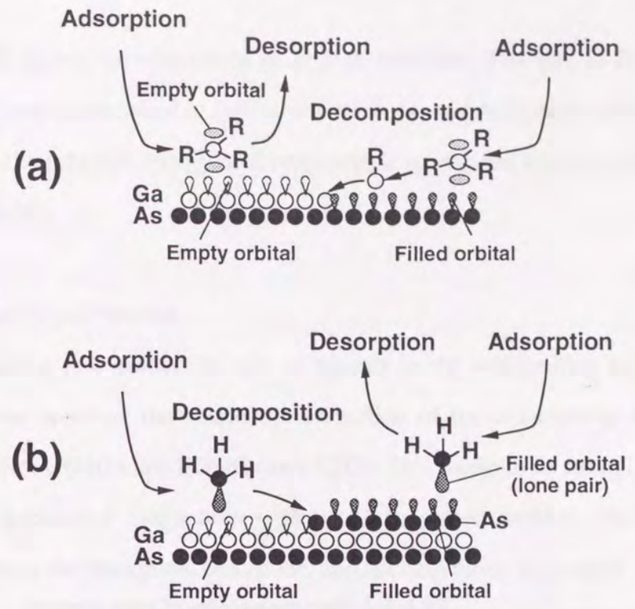

Figure 5-18. GaAs growth model via Lewis acid-base reaction at gas/solid interface. Note that TMGa acts as Lewis acid (electron acceptor) and AsH_3 as Lewis base (electron donor).

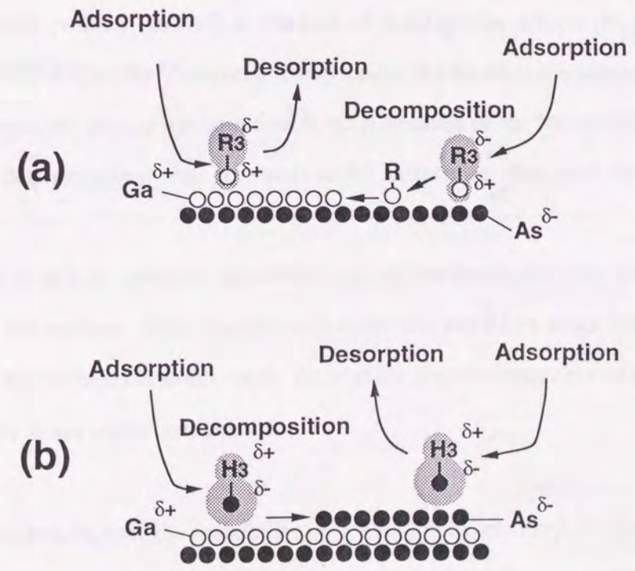

Figure 5-19. GaAs growth model via polarization of molecules and surface. Note that attractive force is operative between TMGa and As surface and between AsH_3 and Ga surface.

Table 5-2: Electronegativities of some elements.

	Mulliken	Pauling	Sanderson	Haissinsky
Cl	3.1	3.0	4.9	
C	2.7	2.5	3.7	
H	2.1	2.1	3.5	
As		2.0	3.9	2.0(III)/ 2.2(V)
Al		1.5	1.9	
Ga				1.6
In				1.6

Figure 5-19 shows the schematics of growth reactions. Just like in Fig. 5-18, it is expected that the Ga precursors tend to approach surface As, and AsH_3 approach surface Ga in order to minimize the potential energy of dipoles which are formed by adsorbing the source molecules at the surface.

5.5.3 Role of ligands in self-limiting

It is interesting to consider the role of ligands in the self-limiting mechanism. As previously seen, we observed the systematic extinction of the self-limiting degree as the molecule changes from TMGa into EDMGa and TEGa. This seems to be strongly related with the change of the precursors' interactions with the GaAs growth surface, that is to say, the mutual balance among the adsorption, desorption, and decomposition is changed.

By replacing the methyl groups in TMGa with ethyl groups, the degree of polarity for the corresponding carbon-Ga bond is weakened due to the lower electronegativity of the ethyl radical [4]. Therefore, we speculate about the effect of the molecular structure of starting materials on the site selectivity as follows.

(1) The molecular polarity, as well as the size of the ligands, affects the chemical and physical properties of Ga-alkyl compounds. Especially, the thermal decomposition rates are enhanced by replacing the methyl ligand with ethyl because of the lower thermal stability. Therefore, the decomposition time constants at the surface are shortened for EDMGa and TEGa.

(2) The polarity affects the potential (activation) energy for desorption with which Ga alkyls are trapped at the surface. Ethyl ligands will make the repulsive force between the Ga precursors and the surface Ga atoms weak. As a result, the residence time of the precursors at the surface Ga atoms might be increased.

Due to these two factors, the probability of generating excess Ga from the precursors at the surface Ga atoms is increased. We think that the systematic difference in the self-limiting behavior among TMGa, EDMGa, and TEGa occurs from the competition between the decomposition and desorption steps at surface lattice sites; the average residence times of

EDMGa and TEGa on surface Ga are not negligible compared with their decomposition time constants, while the residence time of TMGa on the Ga is short enough to neglect the decomposition probability. The three methyl groups in TMGa will make a large difference in the lifetimes between the surface Ga and As atoms, leading to perfect self-limiting.

We can apply this consideration into the growth results of TiBGa and $GaCl_3$. The electronegativity of the ligands and the thermal stability of the corresponding Ga precursors lie in the order:

$$-Cl > -CH_3 > -C_2H_5 > -C_4H_9 \qquad (5\text{-}10)$$

Therefore, the self-limiting behavior of the $GaCl_3$ source and the non-self-limiting of TiBGa are reasonable.

5.6 Novel Approaches to Self-Limiting

5.6.1 TMGa plus TEGa

We tried a new approach to using the combination of TMGa and TEGa as the Ga source for the growth of GaAs in PJE. We studied two kinds of gas introduction modes. One is the consecutive supply of TEGa and TMGa. The other is the simultaneous supply of TEGa and TMGa. Both experiments were done in order to develop a novel method to obtain self-limiting growth.

5.6.1.1 TEGa, TMGa consecutive supply

The Ga deposition on the As-terminated GaAs (001) surface by the TEGa and TMGa consecutive supply shows interesting behavior. Figure 5-20 shows the GaAs growth rates at 500°C under two different gas sequences: TEGa→AsH_3 and TEGa→TMGa→AsH_3. Here, the TEGa (kept at 11°C) flow rate was changed to vary the amount of deposited Ga on the surface, while TMGa (kept at 3°C) pulse duration was fixed at 8 s and its flow rate at 30 sccm. The

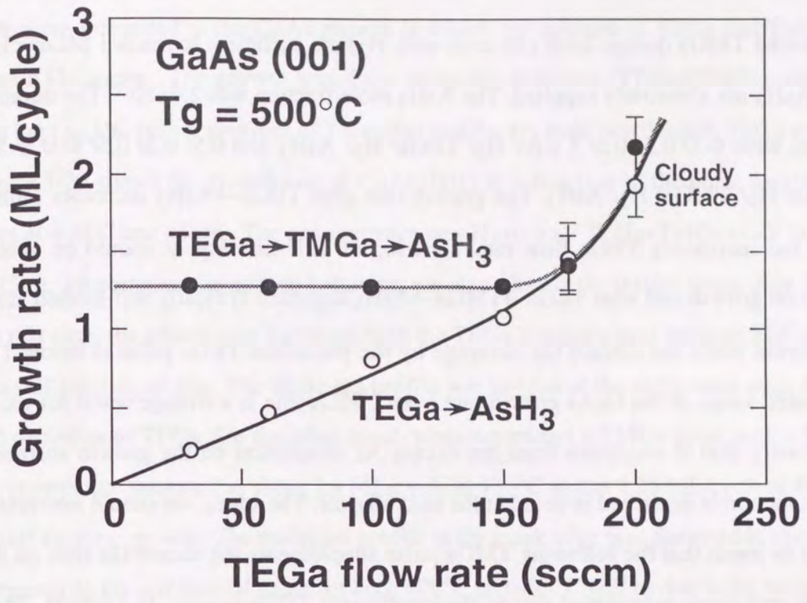

Figure 5-20. Variation of GaAs growth rate in two gas sequences; TEGa→AsH_3 and TEGa→TMGa→AsH_3. TEGa flow rate was changed while the conditions of TMGa and AsH_3 were fixed.

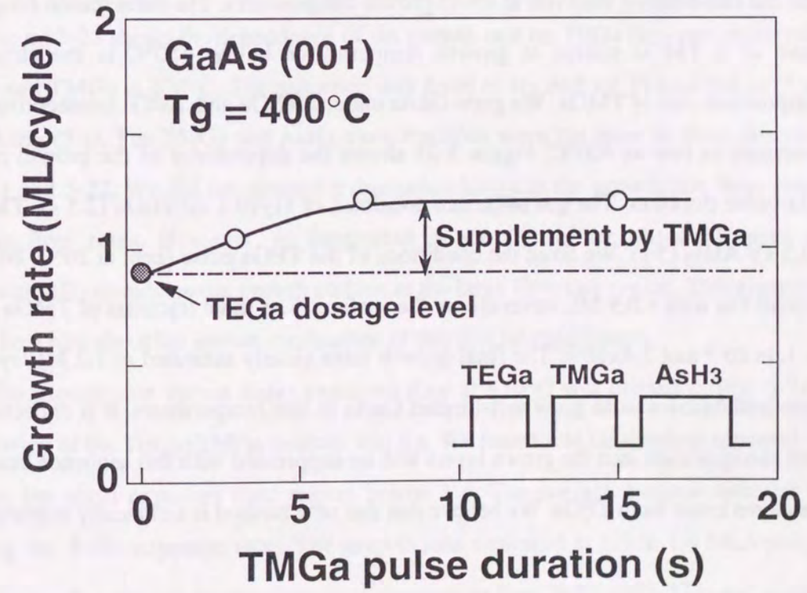

Figure 5-21. Self-limiting GaAs growth as low as 400°C using supplement of Ga atoms by TMGa.

employed TMGa dosage level (30 sccm with H_2) are sufficient to reach 1 ML/cycle if TMGa and AsH_3 are alternately supplied. The AsH_3 mole fraction was $2.4x10^{-2}$. The durations of gas pulses were 0.5/ 0.5/ 0.5/ 5 s for H_2/ TEGa/ H_2/ AsH_3 and 0.5/ 0.5/ 0.5/ 8/ 0.5/ 5 s for H_2/ TEGa/ H_2/ TMGa/ H_2/ AsH_3. The growth rate after TEGa→AsH_3 increases monotonously with the increasing TEGa flow rate, showing no self-limiting. It should be noted that the resultant growth rate after TEGa→TMGa→AsH_3 sequence is clearly self-limited at around 1.2 ML/cycle when the surface Ga coverage by the precedent TEGa pulse is below 1 ML. This saturated value of the GaAs growth rate over 1 ML/cycle is a strange result for us. However, we clarify that it originates from the excess As adsorption on the growth surface, and this phenomenon is described in detail in the next chapter. Therefore, we should interpret the above result to mean that the following TMGa pulse supplements the vacant Ga sites on the surface which remained unoccupied due to the insufficient TEGa supply. In contrast, TMGa didn't seem to be adsorbed and decomposed at all by the surface Ga atoms of a full coverage once the TEGa pulse generated Ga more at than 1 ML coverage.

The ability of supplementing the surface Ga vacancy by a TMGa pulse is useful to realize the self-limiting behavior at lower growth temperatures. The main reason for preventing the use of a TMGa source at growth temperatures below 450°C is the slow thermal decomposition rate of TMGa. We grew GaAs under a TEGa and TMGa consecutive supply at temperature as low as 400°C. Figure 5-21 shows the dependence of the growth rate on the TMGa pulse duration. The gas sequence consisted of H_2 (0.3 s)/ TEGa (2.5 s)/ TMGa (x s)/ H_2 (0.3 s)/ AsH_3 (5 s). We fixed the conditions of the TEGa pulse (kept at 20°C, 80 sccm H_2) to deposit Ga with a 0.9 ML coverage on the surface. The mole fractions of TMGa and AsH_3 were $1.1x10^{-3}$ and $2.4x10^{-2}$. The final growth rates clearly saturated at 1.2 ML/cycle. Thus, this method enables us to grow self-limited GaAs at low temperatures. It is expected that the carbon incorporation into the grown layers will be suppressed with this sequence because most of Ga atoms come from TEGa. We believe that this new method is technically important.

5.6.1.2 TEGa, TMGa simultaneous supply

We were interested in the GaAs growth in which the mixture of TEGa and TMGa is supplied as a Ga source. The growth was done using the sequence (TEGa+TMGa)→AsH_3. TEGa was kept at 3°C (vapor pressure of 1 mmHg) and the H_2 flow rate through TEGa was 40 sccm. Figure 5-22 shows the growth rate of GaAs (001) as a function of the pulse duration of the mixture at 470°C and 485°C. The gas sequence was H_2 (0.5 s)/ TEGa+TMGa (x s)/ H_2 (0.5 s)/ AsH_3 (5 s). To compare the growth behavior, we also plotted the results using only TEGa source. In this case, the growth rate increased with the TEGa exposure time because TEGa does not have a self-limiting ability. The thickness profile was not flat at the SiO_2 mask edge due to the lateral diffusion of TEGa. On the other hand, when we mixed a TMGa pulse with a TEGa pulse, the growth rate saturated at about 1.4 ML/cycle at 470°C and at 1.25 ML/cycle at 485°C, showing self-limiting growth. The thickness profile at the mask edge was flattened in this case. The discrepancy in the self-limited value between 470°C and 485°C will be due to the amount of excess surface As atoms. This is described in the next chapter. Note that the growth with the TEGa and TMGa mixture was more suppressed than that of only TEGa for pulse durations of longer than 6 s at 470°C. The growth proceeds in a different manner when mixing TMGa with TEGa.

Figure 5-23 shows the dependence of the growth rate on TEGa flow rate in the mixture of TEGa and TMGa at 470°C. The sequence was fixed to H_2 (0.5 s)/ TEGa+TMGa (5 s)/ H_2 (0.5 s)/ AsH_3 (5 s). The TMGa and AsH_3 mole fractions were the same as those described in Figs. 5-21 and 5-22. We did not observe a dramatic change in the growth rate from changing the TEGa flow rates. However, as illustrated in the figure, we observed small three-dimensional (3D) islands on the growth surface at the large flow rate region. This phenomenon seems to be a hint about the growth mechanism of this special experiment.

The growth rate versus AsH_3 exposure time at 470°C was plotted in Fig. 5-24. The pulse duration of the TEGa+TMGa mixture was 8 s. We found that Ga droplets appeared on the surface at the short exposure time region below 1 s. The surface became specular while increasing the AsH_3 exposure time. The growth rate saturated at 1.3 to 1.4 ML/cycle. This result indicates that the self-limiting behavior observed in Figs. 5-22 and 5-23 is not ascribed to the lack of surface reaction with AsH_3, but due to the real self-limited deposition of Ga atoms.

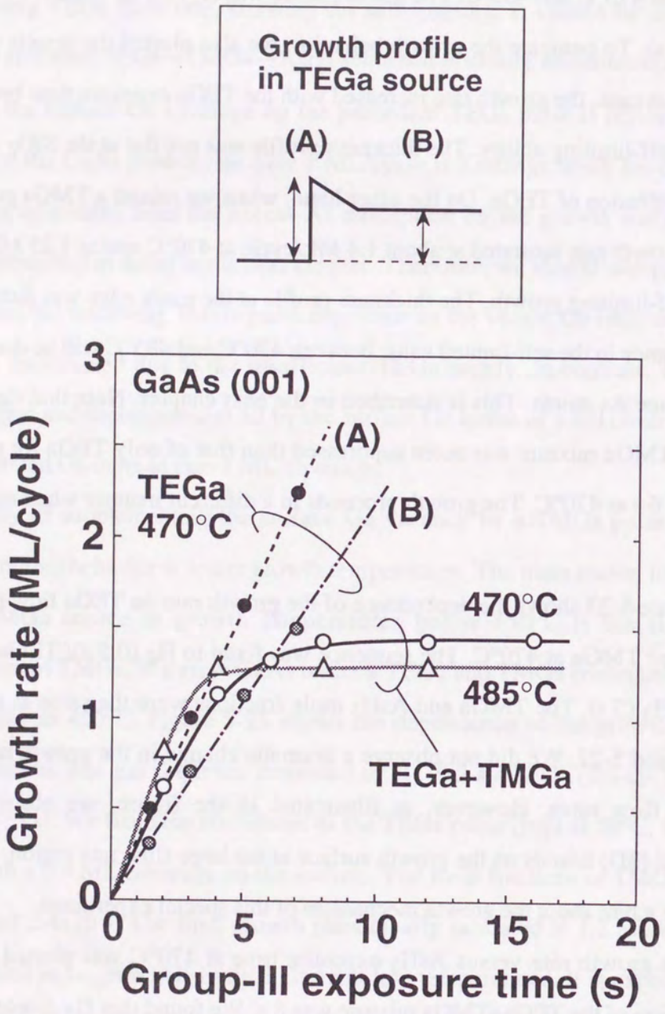

Figure 5-22. Comparison of GaAs growth rate between TEGa source and TEGa+TMGa mixture source. Typical thickness profile is illustrated.

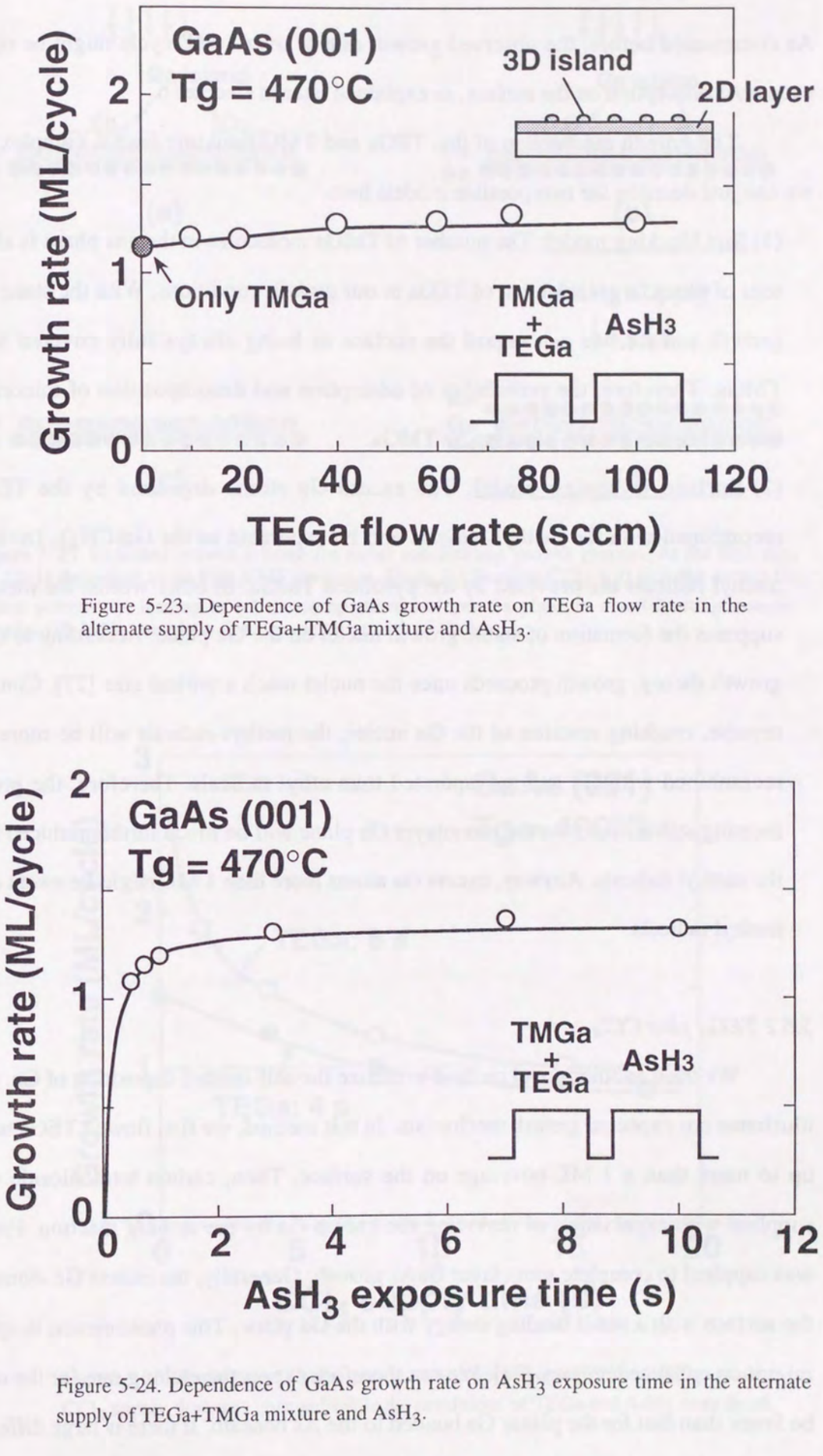

Figure 5-23. Dependence of GaAs growth rate on TEGa flow rate in the alternate supply of TEGa+TMGa mixture and AsH_3.

Figure 5-24. Dependence of GaAs growth rate on AsH_3 exposure time in the alternate supply of TEGa+TMGa mixture and AsH_3.

As commented before, the observed growth rate of over 1 ML/cycle might be related to the excess As adsorption on the surface, as explained later in Chapter 6.

The growth mechanism of this TEGa and TMGa mixture case is complex. Therefore, we can just describe the two possible models here.

(1) Site blocking model: The number of TMGa molecules in the gas phase is about several tens of times larger than that of TEGa in our growth conditions. With the static view of the growth surface, we can regard the surface as being always fully covered by adsorbed TMGa. Therefore, the probability of adsorption and decomposition of minority TEGa is lowered due to the site blocking by TMGa.

(2) Surface sweeping model: The excess Ga atoms deposited by the TEGa will be recombined with the methyl radicals and reevaporated as the $Ga(CH_3)_n$ (n=1, 2, 3). The methyl radicals are provided by the pyrolized TMGa. In other words, the methyl radicals suppress the formation of stable growth nuclei on the Ga plane. According to basic crystal growth theory, growth proceeds once the nuclei reach a critical size [27]. Considering the reverse, cracking reaction of the Ga nuclei, the methyl radicals will be more effectively recombined with Ga and reevaporated than ethyl radicals. Therefore, the probability of forming stable nuclei on the monolayer Ga plane will be much further reduced by injecting the methyl radicals. Anyway, excess Ga atoms more than 1 ML might be swept away by the methyl radicals.

5.6.2 TEGa plus CCl_4

We tried another novel method to realize the self-limited deposition of Ga. Figure 5-25 illustrates our expected growth mechanism. In this method, we first flowed TEGa to deposit Ga up to more than a 1 ML coverage on the surface. Then, carbon tetrachloride (CCl_4) was supplied with expectation of removing the excess Ga by the etching reaction. Finally, AsH_3 was supplied to complete monolayer GaAs growth. Generally, the excess Ga atoms will sit on the surface with a small binding energy with the Ga plane. This phenomenon is applied to the migration enhanced epitaxy [28]. We can therefore expect the etching rate for the excess Ga to be faster than that for the planar Ga bonded to the As beneath. If there is large difference in the

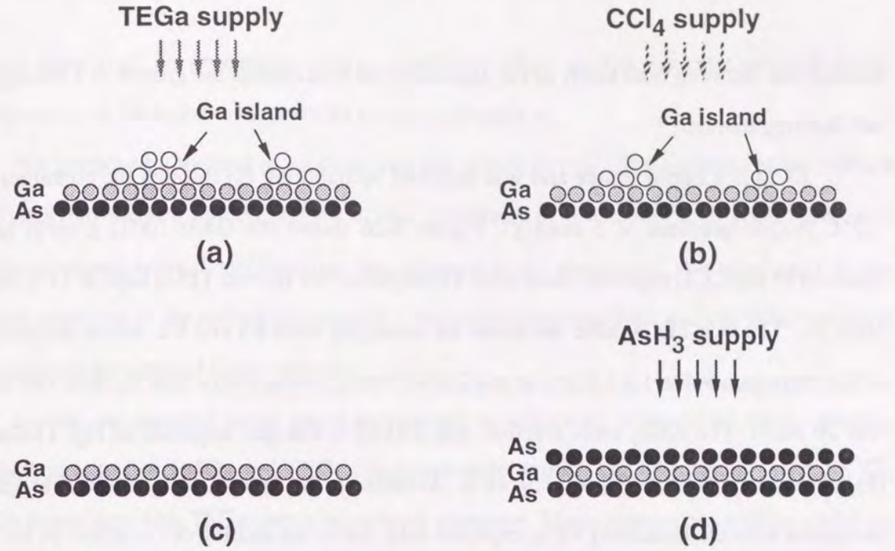

Figure 5-25. Expected growth scheme for novel self-limiting growth process. At the first step, (a) Ga is deposited more than 1 ML coverage. Then, (b) flowing CCl_4 will etch the excess Ga island selectively, leading to (c) the complete monolayer Ga plane in a self-limiting manner. Finally, (d) AsH_3 completes the monolayer growth of GaAs.

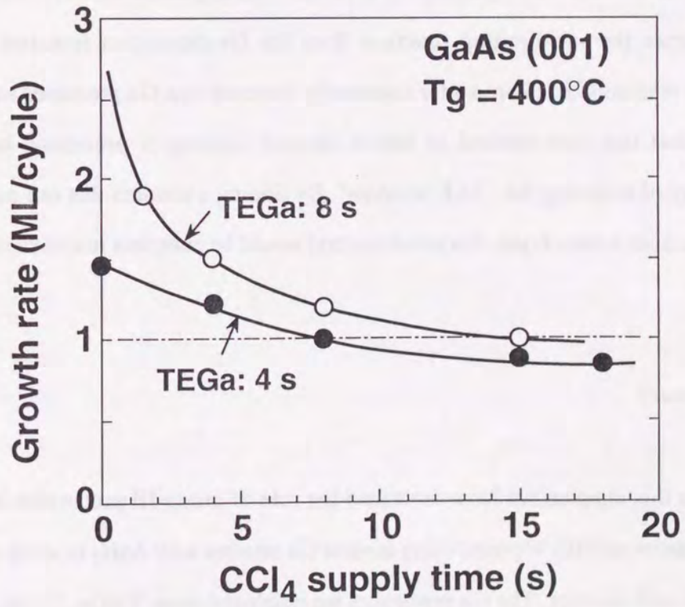

Figure 5-26. Variation of GaAs growth rate in sequence of TEGa→CCl_4→AsH_3. CCl_4 supply time was changed while the conditions of TEGa and AsH_3 were fixed.

etching rate between both kinds of Ga, we will be able to control the growth at 1 ML/cycle in a self-limiting manner.

CCl_4 is a liquid source and was supplied by bubbling H_2 through the container kept at -15°C (vapor pressure of 5 mmHg). Figure 5-26 shows the GaAs (001) growth rate as a function of the CCl_4 exposure time after TEGa pulse. We flowed TEGa kept at 11°C with 400 sccm H_2. The two TEGa pulse durations we employed were 4 s and 8 s, whose deposition rate of Ga corresponded to 1.4 ML/cycle and 2.8 ML/cycle, respectively. The H_2 flow rate for CCl_4 was 20 sccm. The AsH_3 mole fraction was $2.4x10^{-2}$. The gas sequence of H_2/ TEGa/ CCl_4/ H_2/ AsH_3 was 0.5/ 4 (8)/ x/ 0.5/ 10 s. As seen in the figure, the growth rate gradually decreased with the increasing CCl_4 exposure time due to the etching of Ga atoms on the growth surface by CCl_4. It should be noted that the slope of the decrease in the growth rate changes at around 1 ML/cycle. This implies that the etching rate of the excess Ga is faster. However, this result also suggests that the etching of the Ga plane bonded with As atoms is not perfectly prevented.

This method is still preliminary at present. An important aspect of this method is that we can separate the self-limiting function from the Ga-deposition function by adopting two different reactants. Both are so far commonly inherent in a Ga precursor such as TMGa. We believe that this new method to obtain the self-limiting is promising because it has the possibility of widening the "ALE window". By finding a reactant that can more softly etch the Ga atoms over a monolayer, this novel method would be complete in a technological sense.

5.7 Summary

In this chapter, we have described the role of group-III precursors in the self-limiting growth nature of PJE. We tried using several Ga sources with AsH_3 to study whether the GaAs growth is self-limiting. The Ga precursors we employed were TMGa, TEGa, EDMGa, TiBGa, and $GaCl_3$. Although distinct self-limiting was observed with TMGa, results indicate that the

chemical ligands of Ga precursors have a significant effect on the selective adsorption and decomposition at the surface As atoms on the growth surface.

We proposed a method to evaluate the site selectivity of Ga precursors at the surface lattice sites and showed that the degree of site selectivity of precursors is in good agreement with the tendency toward self-limiting. We discussed the precursors' site selectivity in the chemical reactions at the surface in terms of Lewis acid-base reactions and the polarization of both source molecules and GaAs crystals.

Lastly, we reported some novel approaches to achieving self-limiting GaAs growth. One method is to use TMGa and TEGa combination to deposit Ga. The other is to add CCl_4 after Ga deposition with TEGa over a monolayer coverage. These approaches will be useful for attaining self-limiting at lower growth temperatures and for obtaining highly pure epiatxial layers over a wide range of growth conditions.

REFERENCES (Chap. 5)

[1] M.L. Yu, J. Appl. Phys. **73** (1993) 716.

[2] L. Pauling, *The Nature of The Chemical Bond*, 3rd ed. (Cornell University Press, Ithaca, New York, 1960).

[3] R.J. Gillespie, *Molecular Geometry* (Van Nostrand Reinhold, London, 1972).

[4] E.G. Rochow, D.T. Hurd, and R.N. Lewis, *The Chemistry of Organometallic Compounds* (John Wiley & Sons, Inc., New York, 1957).

[5] M. Yoshida, H. Watanabe, and F. Uesugi, J. Electrochem. Soc. **132** (1985) 677.

[6] P.W. Lee, T.R. Omstead, D.R. Mckenna, and K.F. Jensen, J. Cryst. Growth **85** (1987) 165.

[7] H. Ohno, S. Ohtsuka, H. Ishii, Y. Matsubara, and H. Hasegawa, Appl. Phys. Lett. **54** (1989) 2000.

[8] W.G. Jeong, E.P. Menu, and P.D. Dapkus, Appl. Phys. Lett. **55** (1989) 244.

[9] M.A. Khan, R.A. Skogman, J.M. Van Hove, D.T. Olson, and J.N. Kuznia, Appl. Phys. Lett. **60** (1992) 1366.

[10] M. Ozeki, K. Mochizuki, N. Ohtsuka, and K. Kodama, Thin Solid Films **174** (1989) 63.

[11] Y. Sakuma, K. Kodama, and M. Ozeki, Appl. Phys. Lett. **56** (1990) 827.

[12] Y. Sakuma, M. Ozeki, N. Ohtsuka, and K. Kodama, J. Appl. Phys. **68** (1990) 5660.

[13] M. Ozeki, N. Ohtsuka, Y. Sakuma, and K. Kodama, J. Cryst. Growth **107** (1991) 102.

[14] M. Suzuki and M. Sato, J. Electrochem. Soc. **132** (1985) 1684.

[15] C. Plass, H. Heinecke, O. Kayser, H. Lüth, and P. Balk, J. Cryst. Growth **88** (1988) 455.

[16] N. Ohtsuka, private communication.

[17] A.C. Jones, A.K. Holliday, D.J. Cole-Hamilton, M.M. Ahmad, and N.D. Gerrard, J. Cryst. Growth **68** (1984) 1.

[18] D.W. Shaw, J. Electrochem. Soc. **117** (1970) 683.

[19] J. Nishizawa, H. Shimawaki, and Y. Sakuma, J. Electrochem. Soc. **133** (1986) 2567.

[20] M. Rubenstein and E. Myers, J. Electrochem. Soc. **113** (1966) 365.

[21] J. Nishizawa, H. Shimawaki, and Y. Sakuma, J. Electrochem. Soc. **135** (1988) 1813.

[22] F. Hasegawa, H. Yamaguchi, and K. Katayama, Jpn. J. Appl. Phys. **27** (1988) L1546.

[23] Y. Jin, R. Kobayashi, K. Fujii, and F. Hasegawa, Jpn. J. Appl. Phys. **29** (1990) L1350.

[24] A.W. Laubengayer and F.B. Schirmer, J. Am. Chem. Soc. **62** (1940) 1578.

[25] D.J. Schlyer and M.A. Ring, J. Electrochem. Soc. **124** (1977) 569.

[26] M.D. Pashley, Phys. Rev. **B40** (1989) 10481.

[27] J.W. Gibbs, Am. Sci. Arts. **16** (1878) 454.

[28] Y. Horikoshi, M. Kawashima, and H. Yamaguchi, Jpn. J. Appl. Phys. **27** (1988) 169.

CHAPTER 6

Influence of Adsorption and Desorption of Group-V Atoms

6.1 Preliminaries

Here, we deal with some overlooked problems concerning the kinetics of group-V atoms on the growth surface. So far, most studies of the PJE or ALE for III-V compounds have focused on the self-limited deposition of group-III atoms [1, 2]. Little attention, however, has been paid to the growth conditions which lead to the formation of the monatomic surface layer of group-V atoms. This is based on the assumption that the deposition of arsenic (As) or phosphorus (P) multilayers on the growth surface is automatically inhibited so long as a sufficient amount of AsH_3 or PH_3 is supplied to the substrates, judging from the high vapor pressure of the elemental As or P at growth temperatures [1, 3]. However, this assumption has not been verified yet. No one seems to suspect this problem concerning the excess adsorption of group-V atoms on the growth surface.

Another overlooked problem is the desorption of group-V atoms from the growth surface. In PJE, which is based on a low-pressure MOVPE, growth is halted after group-V or group-III supply by purging the source gases from the reactor with H_2 flows. Any changes in the growth surface and the growth kinetics during these halts have previously been ignored, neglecting the desorption of the volatile group-V atoms from the epitaxial layers.

In this chapter, we first report the effect of the H_2 purge duration on the growth kinetics in the PJE-grown InAs (001) in detail. Then, we show that the InAs growth rate decreased and then saturated at the submonolayer levels as we increased the post-AsH_3 H_2 purge time. The growth rate was independent of the post-TMIn H_2 purge time, however. Our results imply that As atoms are desorbed from the outermost As-terminated surface of the grown layers. We discuss the significance of this phenomena from both a technical and scientific point of view. Similar results on InP (001) are briefly covered.

Next, we discuss the results for GaAs (001). In addition to the similar decrease in the growth rate with the increasing post-AsH_3 H_2 purge time, we found another previously undiscovered result in that the GaAs growth rate becomes around 1.2 to 1.3 ML/cycle with a sufficient AsH_3 supply, maintaining the self-limiting for TMGa injection. Results suggest the existence of the adsorbed As layer of more than 1 ML on the GaAs (001) growth surface, and these excess As atoms contribute to the growth beyond 1 ML/cycle. The ideal self-limiting growth at 1 ML/cycle for the TMGa injection can be achieved by optimizing the reaction kinetics producing the surface As layer, so as to complete just at a monolayer coverage of As.

We speculate that the experimentally observed growth rate variations, caused by the adsorption and desorption of group-V atoms at the surface, are strongly related with the surface reconstruction and the surface stoichiometry, just like those observed normally on the growth surface in an ultra-high vacuum (UHV) environment. We then propose a PJE growth model including the several surface reconstruction and the phase transition among them. We try to explain our model by connecting it with the recent studies on the structures of MOVPE-grown III-V semiconductor surfaces using grazing incidence X-ray diffraction (GIXD) and reflectance difference spectroscopy (RDS).

6.2 Role of H_2 Purge in PJE Gas Sequence

Figure 6-1 shows the typical PJE gas sequence for the growth of III-V compounds. We introduce hydrides and organometals alternately to the substrates, and repeat the gas cycle many times to grow epitaxial layers. There are two H_2 purge periods (denoted by 1 and 2 in the figure) in a gas cycle to prevent the gas-phase mixing reaction between the group-III and group-V sources. It has been considered that the role of these periods is merely to flush the reactants from the reactor. That is, researchers had previously thought that the growth surface is not changed in the H_2 ambient. However, this seems to have been an oversimplified view. Since the epitaxial layer lacks the overpressure of group-V atoms during the purge periods as well as the group-III supply period, there must be some chemical and structural change in the growth

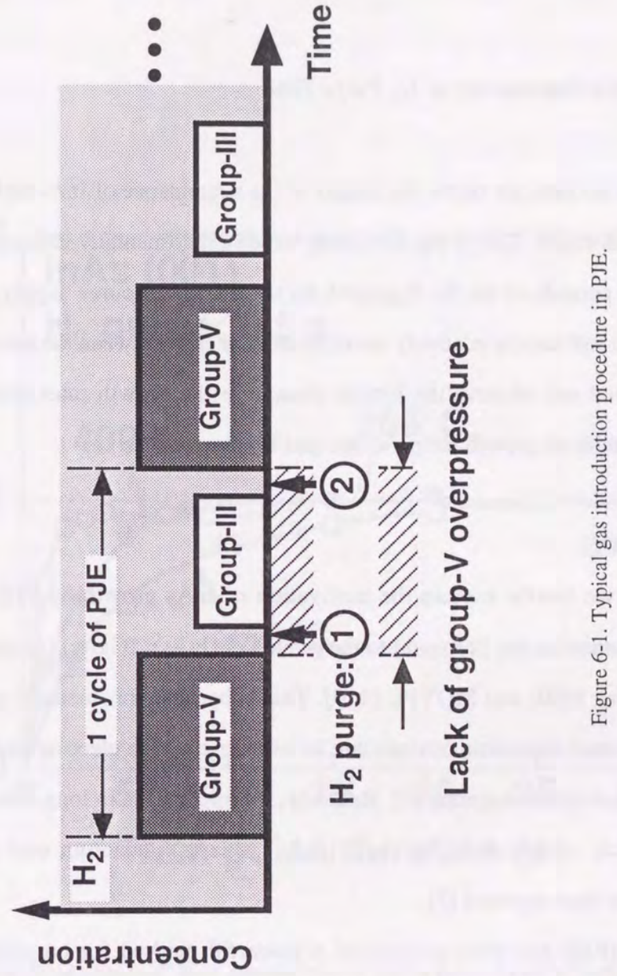

Figure 6-1. Typical gas introduction procedure in PJE.

surface. In particular, we have to restudy the role of these two H_2 purge periods independently in terms of the growth kinetics.

6.3 Growth Rate Dependence on H_2 Purge Time

In this section, we report the results of the dependence of InAs and InP growth rates on the H_2 purge duration. This is the first study which experimentally indicates the significance of the H_2 purge periods of the III-V growth by the alternate source supply. As explained later, both InAs and InP have a relatively small binding energy between the anions and cations. This helps us to find and observe the kinetic change in the growth rates under the conventional growth conditions of growth temperatures and H_2 purge times.

6.3.1 InAs (001)

First, we briefly explain the motivation of InAs growth by PJE. In the last decade, considerable attention has been paid to the growth of $(InAs)_m(GaAs)_n$ strained-layer superlattice structures using MBE and MOVPE [4, 5]. This is because this material system is suitable for high-performance electronic devices due to its inherent high electron mobility resulting from reduced random alloy scattering [6]. Recently, the application in long-wavelength optical fiber communication devices using strained $(InAs)_m(GaAs)_n$ quantum well structures grown on GaAs has also been reported [7].

ALE (PJE) has been considered a powerful method for preparing these atomically controlled short-period superlattices because we can control the growth layer-by-layer due to the self-limiting deposition mechanism [8, 9]. To tailor the desired materials using ALE (or PJE), however, several problems must be solved. One is the difference between the appropriate growth temperatures among the binary semiconductors. Self-limited GaAs can be grown at 440 to 560°C using our PJE [10]. However, few studies have been made into InAs ALE, and the temperatures for monolayer growth are restricted to less than 340°C [11, 12]. Also, as we explained in Chapter 3, the self-limiting value of the InAs growth rate by PJE was at fractional

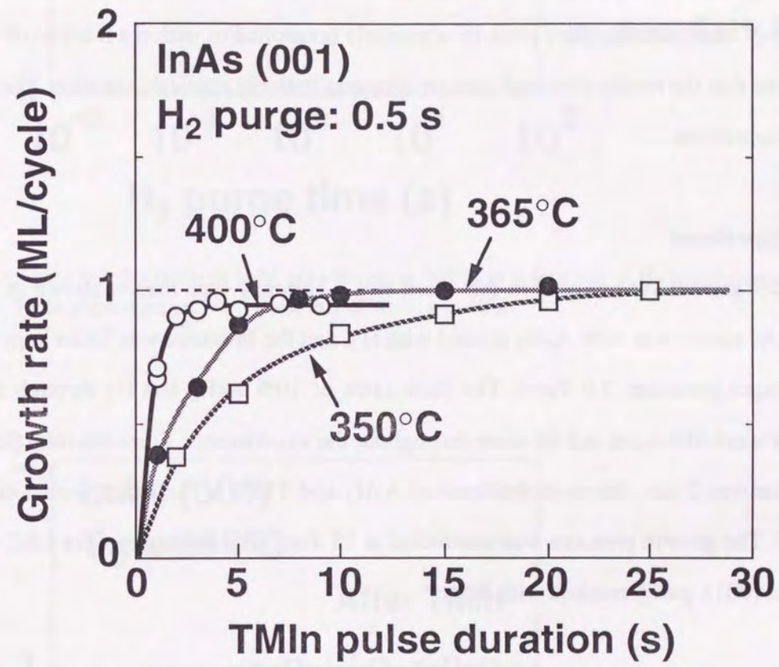

Figure 6-2. Dependence of InAs growth rate on TMIn pulse duration from 350 to 400°C. AsH_3 pulse was 10 s and H_2 purge time after both TMIn and AsH_3 was 0.5 s.

monolayer when we used the horizontal reactor. Techniques must therefore be developed to increase the range of InAs growth conditions for monolayer growth.

The purpose of this section is to clarify the major factor which limits the temperature range of InAs monolayer growth. We describe the growth of InAs (001) by PJE at temperatures up to 400°C. The successful expansion of the growth temperature range is possible due to new findings about important aspects of the purge duration in the PJE process. That is, to achieve ideal self-limited monolayer growth at high growth temperatures, the purge time after forming the group-V terminated surface must be accurately controlled to within a fraction of a second. We believe that the results obtained here are also qualitatively applicable to other materials and crystal orientations.

6.3.1.1 Experiment

Our growth system used in this work was a chimney-type reactor shown in Fig. 2-12 (b). The As source was 10% AsH_3 diluted with H_2, and the In source was TMIn kept at 27.1°C (TMIn vapor pressure: 3.0 Torr). The flow rates of 10% AsH_3 and H_2 through the TMIn container were 480 sccm and 60 sccm throughout the experiments. Since the total flow rate in the reactor was 2 slm, the mole fractions of AsH_3 and TMIn in the vapor were 2.4×10^{-2} and 5.9×10^{-5}. The growth pressure was controlled at 15 Torr. The substrates were LEC-grown n-type InAs (001), partly masked with SiO_2.

6.3.1.2 Kinetics during H_2 purge

We studied the dependence of the InAs growth rate on the TMIn exposure time, varying the growth temperature from 350°C to 400°C (Fig. 6-2) [13]. The H_2 purge time, after both TMIn and AsH_3 pulses, was 0.5 s. The growth was self-limiting and the rise time of the growth rate decreased as the temperature increased. The growth per gas cycle saturated at an InAs (001) thickness of 1 ML, that is, 0.303 nm, at 350°C and 365°C. The growth rate does not, however, strictly reach 1 ML/cycle at 400°C. We previously clarified that the self-limiting monolayer growth proceeds by the selective reaction of gas-phase group-III (group-V) molecules only with the group-V (group-III) atoms on the surface [3]. Based on the simple

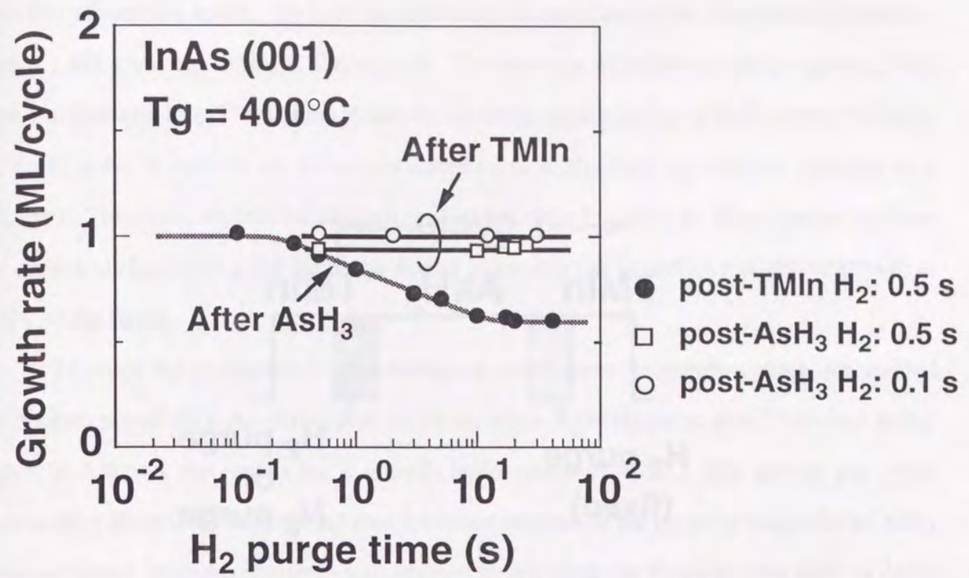

Figure 6-3. Variation of InAs growth rate at 400°C as a function of H_2 purge time. TMIn pulse duration was 5 s and that of AsH_3 was 10 s.

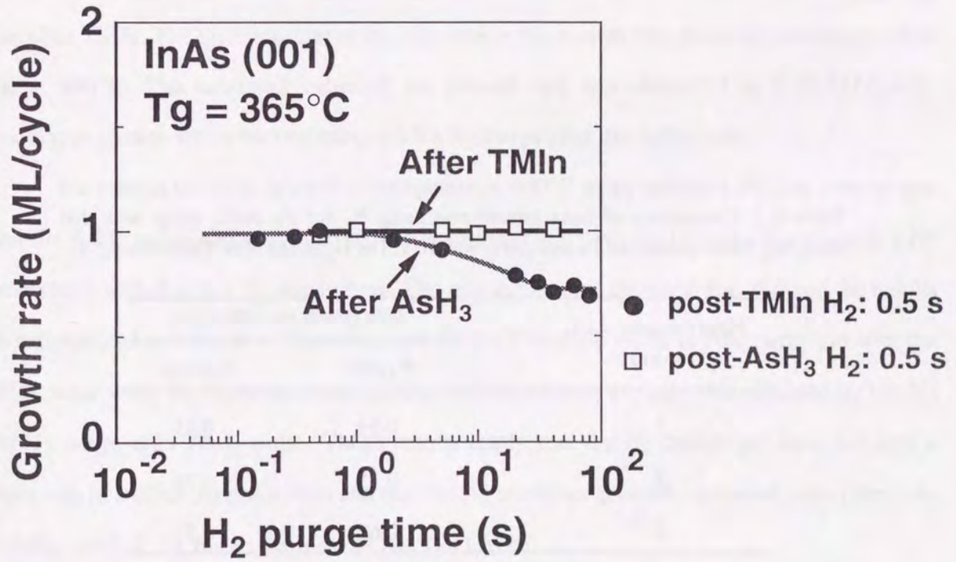

Figure 6-4. Variation of InAs growth rate at 365°C as a function of H_2 purge time. TMIn pulse duration was 20 s and that of AsH_3 was 10 s.

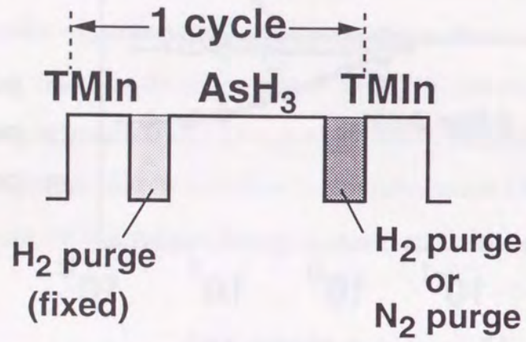

Figure 6-5. Gas sequence for growing InAs using N_2 or H_2 as a purge gas after AsH_3 exposure.

Table 6-1: Comparison of InAs growth rate using N_2 for the AsH_3 purge with that using H_2. TMIn pulse was 5 s and AsH_3 was 10 s. The H_2 purge after TMIn was 0.5 s.

Purge time after AsH_3 (seconds)	InAs growth rate (ML/cycle)	
	N_2 purge	H_2 purge
1	0.84	0.85
3	0.75	0.74
5	0.67	0.71

selective adsorption model, the In atoms gradually accumulate on the As-terminated surface with a 1 ML coverage during a TMIn pulse. The coverage of In atoms finally reaches 1 ML with a sufficiently long TMIn pulse. A similar situation applies during an AsH_3 supply period if an AsH_3 pulse is injected on an In-terminated surface: the InAs growth rate saturates at 1 ML/cycle. Therefore, we have to take into consideration the In and/or As atoms desorption from the growth surface during the H_2 purge period to explain the imperfect monolayer growth at 400°C in the figure.

To study the desorption of the constituent atoms from the growth surface, we studied the dependence of the InAs growth rate on the duration of the H_2 purge after TMIn and AsH_3. Figure 6-3 shows the results for a growth temperature of 400°C. The growth per cycle decreased to about 0.6 ML/cycle and then remained constant as the H_2 purge time after an AsH_3 pulse increased. Monolayer growth was attained by adjusting the H_2 purge time after an AsH_3 pulse to less than 0.1 s. On the contrary, the growth rate was independent of the H_2 purge time after the TMIn pulse which was varied from 0.5 to 30 s.

At 365°C, a decrease in the growth rate with the increasing H_2 purge time after AsH_3 was also observed, as shown in Fig. 6-4. Again, the rate remained independent of the H_2 purge time after TMIn. The time constant of the decrease in the growth rate, however, was longer than that at 400°C. The saturated value of the growth rate was about 0.7 to 0.75 ML/cycle. Monolayer growth was achieved using a 0.5 s H_2 purge after the AsH_3 pulse.

We conducted InAs growth experiments at 400°C using nitrogen (N_2) as a purge gas after the AsH_3 pulse, and compared the As desorption rate from the InAs (001) surface in a N_2 atmosphere with that in a H_2 atmosphere. The gas sequence is shown in Fig. 6-5 and the results are summarized in Table 6-1. The carrier gas for the TMIn and AsH_3 and the purge gas after the TMIn pulse were H_2. There was no significant difference in growth rates obtained by the N_2 and H_2 purge after AsH_3 pulse. These results imply that the H_2 carrier gas does not play a major role in surface As desorption and that the As atoms are probably desorbed not in the form of AsH_n (n=1, 2, 3), but in the form of As_x (x=1 to 4).

6.3.1.3 Surface morphologies

The surface morphologies of InAs layers grown at 350 and 365°C were always specular and smooth, independent of the H_2 purge time both after TMIn and after AsH_3. At 400°C, however, the morphology strongly depends on the growth conditions. Photographs of InAs layers, grown at 400°C and observed using a Nomarski interference microscope, are shown in Fig. 6-6. As the H_2 purge time after exposure to AsH_3 increased, the surface morphology of the layers whose growth rates were below 1 ML/cycle became rough as shown in Fig. 6-6 (a). The mechanism of this surface roughening remains unclear. When the purge time after AsH_3 is shortened, however, a mirror-like morphology was obtained (Fig. 6-6 (b)). When we changed the H_2 purge time after the TMIn pulse, however, the mirror morphology always occurred (Fig. 6-6 (c)). Both the surface morphology and the growth rate are affected by the purge time after exposure to AsH_3, and are independent of the purge time after exposure to TMIn at 400°C.

6.3.1.4 Implications

The results in Figs. 6-3 and 6-4 indicate that growth during an PJE cycle is limited by the number of surface As atoms, determined by the H_2 purge time after an AsH_3 pulse. In Fig. 6-7, the plausible models at the growth surface are shown. The outermost As atoms of InAs (001) seem to desorb after the AsH_3 supply is removed. According to the selective adsorption model, TMIn molecules can only be decomposed by the remaining As atoms, but not on the In atoms exposed by surface As desorption. The decrease in the growth rate, shown in Figs. 6-3 and 6-4, is therefore consistent with the model. Thus, InAs epilayers grown with a long H_2 purge time also have a stoichiometric composition. The In-terminated surface, however, is thermally stable and prevents the desorption of As atoms sitting beneath the top In layer. The difference in the desorption rate of As on the surface and in the bulk might be related to the number of covalent bonds with In atoms. Each As atom in the bulk has more chemical bonds with In than an As atom on the surface, so the activation energy of desorption from in the bulk is much larger. Shimawaki *et al.* studied self-limiting InAs growth with submonolayer coverages in a chloride-based ALE at temperatures above 350°C [14]. They studied the dependence of the InAs growth rate on the substrate orientation and observed that the rate was highest for (111)B, then (100), and the (111)A orientations. They attributed the result to the

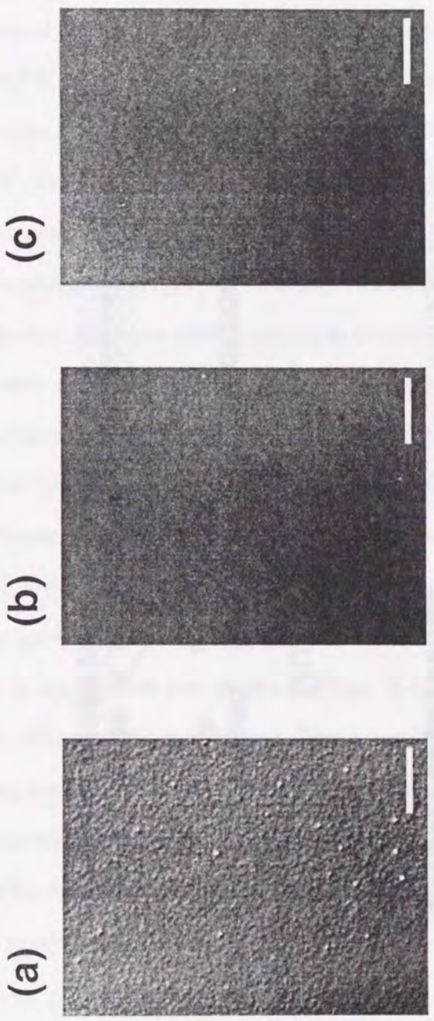

Figure 6-6. Nomarski micrographs of InAs (001) surfaces grown at 400°C. Marker represents 25 μm.

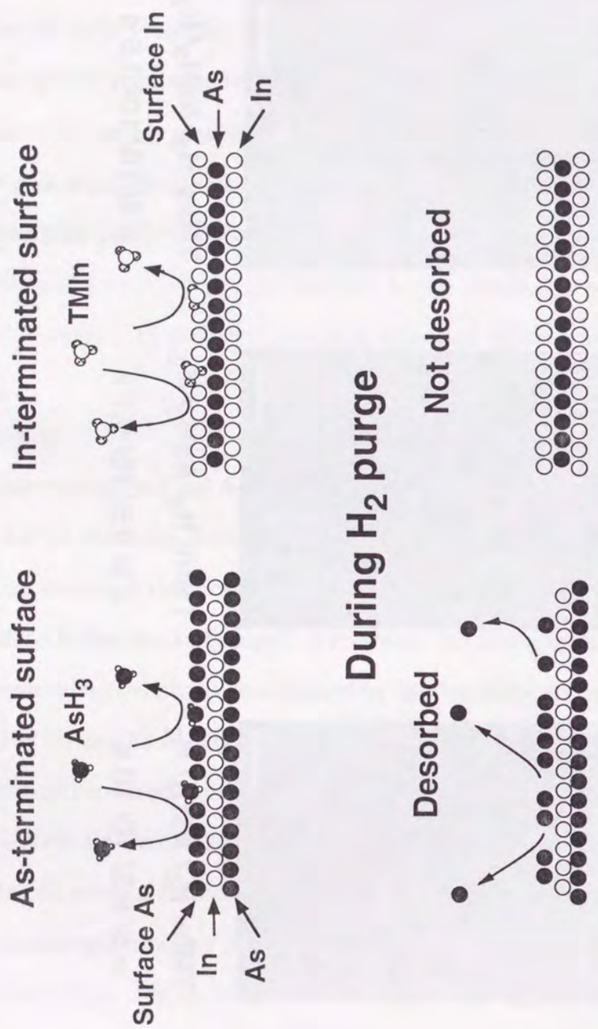

Figure 6-7. Growth model including As desorption from As-terminated surface.
The stable In-terminated surface was also shown.

adsorption stability of InCl at each growth surface. We speculate, however, that the surface As atoms are desorbed during the 24 s interruption in growth after the AsH_3 pulse in their experiments, and that the crystallographic dependence of the growth rate is determined by the stability or the number of surface As atoms.

We noticed that the growth rates saturate at about 0.6 ML/cycle at 400°C and 0.7 to 0.75 ML/cycle at 365°C, as shown in Figs. 6-3 and 6-4. It has recently been reported that the GaAs surface grown in an MOVPE environment has reconstructed surface structures like surfaces grown in UHV [15, 16]. The InAs surface grown by MBE also shows reconstructed surface structures, characterized by reflection high-energy electron diffraction (RHEED) and scanning tunneling microscopy (STM) [17-20]. We believe that the PJE-grown InAs surface also shows well-defined surface structures corresponding to the surface stoichiometry of each stage in PJE. Our results imply that the initial state of an As-terminated InAs surface, stable during the presence of sufficient AsH_3 in the gas phase and in equilibrium with the ambient AsH_3, shifts to another stable surface structure. This is consistent with the result from the MBE experiment reported by Yamaguchi and Horikoshi [19]. Our data implies that the InAs surface has stable structures with lower (but not zero) As coverage after the AsH_3 pulse. The stable surface As coverage after stopping the AsH_3 supply may be determined mainly by growth temperatures. The decrease in the growth rate shown in Figs. 6-3 and 6-4 cannot be fitted to a simple exponential function of the purge time. These results are contrary to Kobayashi's results measured using a surface photoabsorption (SPA) technique, in which the As-stabilized surface changes exponentially into an In-terminated surface when the AsH_3 supply is removed above 400°C [21]. This discrepancy might be due to the difference in the growth temperatures, but more detailed studies are required.

6.3.1.5 Achievement in monolayer growth

Figure 6-8 shows the dependence of the growth rate on the TMIn pulse length at 400°C. The H_2 purge time after AsH_3 was ranged from 0.1 to 3 s. Although the growth was self-limiting, the saturated growth rate was smaller for longer H_2 purges. Again, the growth was

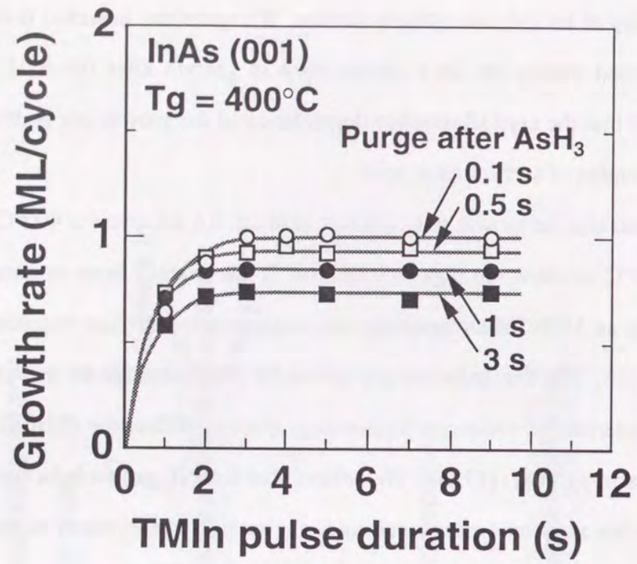

Figure 6-8. Dependence of growth rate on TMIn pulse time at 400°C. The H_2 purge time after AsH_3 was varied from 0.1 to 3 s. AsH_3 pulse was 10 s and H_2 purge time after TMIn was 0.5 s.

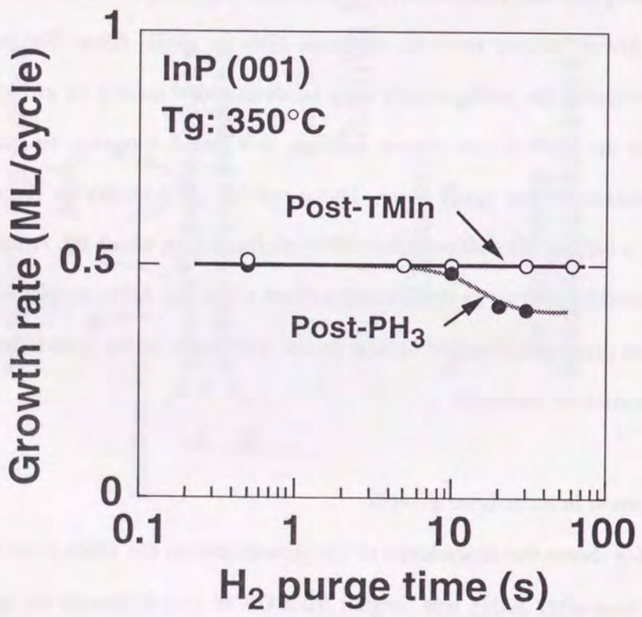

Figure 6-9. InP growth rate as a function of H_2 purge times. For the dependence of post-TMIn, the post-PH_3 H_2 purge was 0.5 s. For the dependence on post-PH_3, the post-TMIn H_2 was 0.5 s. The mole fraction of TMIn was 5.9×10^{-5} and that of PH_3 was 9.6×10^{-2}. The pulse duration of TMIn and PH_3 was 5 s and 20 s.

limited by the duration of the H_2 purge after the AsH_3 pulse. To achieve the monolayer growth of InAs at 400°C, the H_2 purge must be shortened after the AsH_3 pulse to less than 0.1 s.

The growth rate saturated above the 3 s TMIn pulse duration, indicating that it takes about that long to fully cover the surface As atoms with In atoms, produced by the surface dynamical processes including adsorption, desorption, and the decomposition of TMIn. The time needed for 1 ML/cycle is fairly long, compared with the time constant of As desorption during the H_2 purge. Surface As atoms therefore have a possibility of desorption because part of the surface As is still on the outermost layer during the 3 s TMIn pulse. If the As desorption occurred during the initial part of each TMIn exposure period, the growth rate would not reach 1 ML/cycle. The experimental results imply that the As desorption does not occur during the 3 s TMIn exposure. We speculate that the TMIn, or some kinds of methylindium, adsorbed on the As atoms has the same suppression effect on As desorption as In atoms on the surface.

6.3.2 InP (001)

6.3.2.1 Experiment

The growth experiments were carried out at 350°C in the chimney-type reactor. The mole fraction of TMIn was 5.9×10^{-5} and that of PH_3 was 9.6×10^{-2}. The TMIn pulse duration was 5 s and that of PH_3 was 20 s. The growth rate of PJE-grown InP (001) was self-limited at 0.5 ML/cycle, independent of the TMIn and PH_3 supply conditions with the typical duration of H_2 purge [22]. The results showed the same behavior as observed in the horizontal reactor described in Section 3.3.

6.3.2.2 Effect of H_2 purge

We measured the variation of InP (001) growth rates at 350°C as a function of post-PH_3 and post-TMIn H_2 purge times (Fig. 6-9). We observed similar phenomena in InP to that in InAs. The growth rate of InP decreased to about 0.4 ML/cycle, then remained constant as the post-PH_3 H_2 purge time increased. Half a monolayer of growth was attained when the post-PH_3 purge time was shorter than about 10 s. The InP growth rate was also independent of the post-TMIn H_2 purge time at 350°C. Thus, suppression of the P desorption from the PH_3-

exposed surface is important. However, we found that the distinct self-limiting growth did not occur and that the surface morphology of the InP epilayers became rough when we raised the growth temperatures to 365°C and 400°C [9]. There seems to be a factor other than surface P desorption that limits the temperature range of InP PJE.

6.3.3 Relationship between growth temperatures and congruent temperatures

The difficulties in accomplishing InP PJE at temperatures above 365°C do not seem to be merely due to the homogeneous pyrolysis of TMIn in the gas phase, differing with our previous report [22]. Clearly, self-limiting InAs growth is attained under the same TMIn flow conditions, even at 400°C [13]. Some problems must exist on the InP surface. We speculate that the difficulty is due to P desorption from the bulk thermally degrading the grown layers, since the growth temperatures are higher than the congruent evaporation temperature (363°C) of InP [23].

In Table 6-2, we show the congruent evaporation temperatures of some III-V binaries [23]. The empirical maximum growth temperatures for self-limiting growth are also shown. Note that the upper limits of growth temperatures for self-limiting growth are strongly related with the congruent temperatures. We believe that the group-V atoms are preferentially desorbed from the bulk crystal if we grow epitaxial layers above congruent temperatures and that, as a result, the growth surface becomes rough due to the agglomeration of the group-III atoms remaining on the surface. The congruent temperature of III-V compounds may be one of the keys to determine the critical temperatures for ideal PJE.

6.4 As-Related Problems at GaAs (001)

As mentioned above, we clarified, for the first time, that PJE-grown InAs and InP have a basic problem of group-V desorption from the surface. In addition to the similar As desorption at GaAs (001), we explain here the excess As adsorption problem on a GaAs (001) growth surface and its influence on the PJE growth [24].

Table 6-2: Approximate congruent sublimation temperatures (T_c) for Langmuir evaporation.

Materials	T_c (°C)
AlP	>700
GaP	670
InP	363
AlAs	~850
GaAs	650
InAs	380

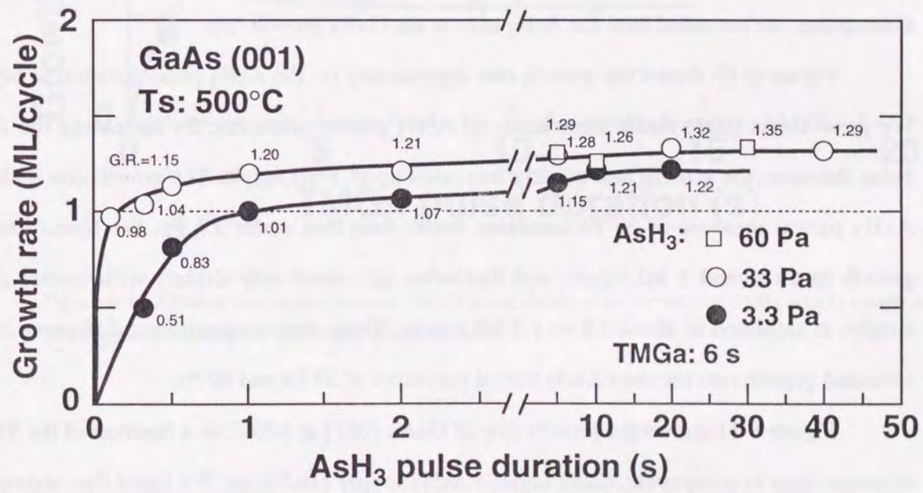

Figure 6-10. Growth rate dependence on AsH_3 pulse duration for various AsH_3 partial pressures. The H_2 purge times after TMGa and AsH_3 pulses are both 0.5 s.

6.4.1 Experiment

The experimental procedure was the same as reported in Section 2.6. The As source was 10% AsH_3 diluted with H_2. The Ga source was TMGa kept at 3.0°C (TMGa vapor pressure: 79.4 Torr). The flow rates of the H_2 through the TMGa bubbler were kept at 30 sccm throughout the experiments. The TMGa flow supply was 6.9×10^{-5} mol/min. The total flow rate in the reactor was always 2 slm and the growth pressure was kept at 2.7 kPa.

6.4.2 As adsorption

Up until now, much attention has been paid to the self-limiting deposition of Ga atoms in the ALE-grown GaAs. Self-limiting growth of GaAs was usually checked by examining the dependence of the growth rate on the TMGa dosage level and its pulse duration in a gas cycle. This is because As adsorption on the Ga-terminated GaAs growth surface has been assumed to stop automatically at just 1 ML if the AsH_3 partial-pressure in the reactor and its exposure time is sufficient, due to the high vapor pressure of As atoms. To confirm the validity of this assumption, we restudied how the AsH_3 affects the GaAs growth rate.

Figure 6-10 shows the growth rate dependence on the AsH_3 pulse duration at 500°C. We grew GaAs (001) under three kinds of AsH_3 partial pressures. By increasing the AsH_3 pulse duration, the growth rate quickly increases up to 1 ML/cycle. The growth rate under an AsH_3 partial pressure of 33 Pa increases faster than that under 3.3 Pa. We found that the growth rate reached 1 ML/cycle, and thereafter increased only slightly with further AsH_3 supply. It saturated at about 1.2 to 1.3 ML/cycle. There was no significant difference in the saturated growth rate between AsH_3 partial pressures of 33 Pa and 60 Pa.

Figure 6-11 shows the growth rate of GaAs (001) at 500°C as a function of the TMGa exposure time in a gas cycle, under various AsH_3 supply conditions. We found that, although it is still self-limiting, the saturated value of the growth rate varies according to the amount of AsH_3 supplied. The filled circles show the ideal behavior; the growth rate is self-limited to 1 ML/cycle. When the AsH_3 pulse duration decreased to 0.3 s, the growth rate was saturated at submonolayers per cycle. In this case, GaAs growth is limited by the As population on the

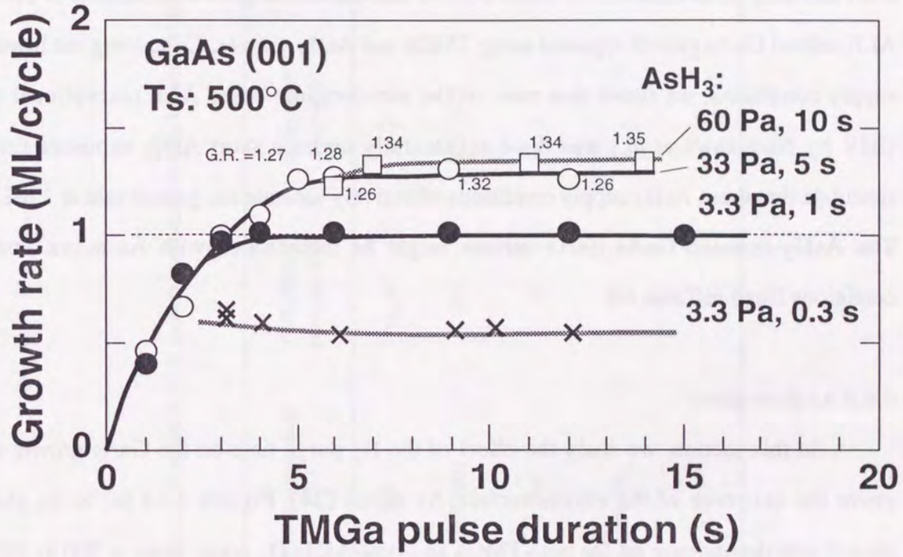

Figure 6-11. Growth rate dependence on TMGa pulse duration under various AsH_3 supply conditions. The H_2 purge times after TMGa and AsH_3 are 0.5 s.

surface because the supplied AsH_3 is not sufficient to form an As monolayer on the TMGa-exposed surface. More importantly, supplying a large amount of AsH_3 (33 and 60 Pa) increases the self-limited GaAs growth rate to about 1.2 to 1.3 ML/cycle. This result, not previously reported, suggests that As adsorption on GaAs (001) is not limited to monolayer coverage. Excess As atoms seem to be adsorbed on the GaAs (001) and react with TMGa to contribute to the GaAs growth exceeding 1 ML/cycle.

As shown in Figs. 6-10 and 6-11, the self-limited GaAs growth rate, using TMGa and AsH_3 in our pulsed-jet reactor, apparently exceeds 1 ML/cycle with the sufficient AsH_3 dosage level and long pulse duration. In Table 6-3, we summarize the growth conditions of the typical ALE-related GaAs growth reported using TMGa and AsH_3 sources. Comparing the listed AsH_3 supply conditions, we found that most of the metalorganic-based ALE (exceptional case in UHV by Nishizawa *et al.*) was done accidentally under a short AsH_3 exposure time. We speculate that these AsH_3 supply conditions effectively saturate the growth rate at 1 ML/cycle. The AsH_3-exposed GaAs (001) surface might be unsaturated with As atoms under the conditions listed in Table 6-3.

6.4.3 As desorption

In this section, we study the effect of the H_2 purge time on the GaAs growth rate, to prove the existence of the excess surface As atoms [24]. Figures 6-12 (a) to (c) show the growth rate dependence on the post-TMGa and post-AsH_3 H_2 purge times at 500 to 580°C. In these experiments, AsH_3 was supplied for 5 s at a partial pressure of 33 Pa. The empty and filled circles in Fig. 6-12 (a) represent data for a 6 s TMGa pulse duration at 500°C. The growth rate was 1.28 ML/cycle for the shortest 0.5 s H_2 purge times after both AsH_3 and TMGa supply. As shown in the figure, the growth rate remains at around 1.21 to 1.28 ML/cycle, independent of the post-TMGa H_2 purge time. The surface morphology was always very smooth even if the post-TMGa H_2 purge time was varied. In contrast, the growth rate decreases with increasing post-AsH_3 H_2 purge times and saturates at 1 ML/cycle. Surface morphology was specular for the samples grown with a short post-AsH_3 H_2 purge time. However, with the increasing post-AsH_3 H_2 purge time, roughness (not Ga droplet) also increased. We can

Table 6-3: Summary of reported ALE growth conditions for GaAs using TMGa and AsH_3 as sources.

Type of system and growth pressure	Growth temperature (°C)	AsH_3 partial pressure (Pa)	AsH_3 exposure time (s)	Self-limiting value (ML/cycle)	Reference
MLE (UHV)	500	$7x10^{-3}$	20	0.78-0.81	[54]
Vertical MOVPE (30 Torr)	550-600	400	0.15-0.42	1	[55]
Vertical MOVPE (10 Torr)	500	14	2	1	[56]
Vertical MOVPE (70 Torr)	490-500	28	1	1	[57]
Horizontal MOVPE (9 Torr)	530-570	12	2	1	[58]

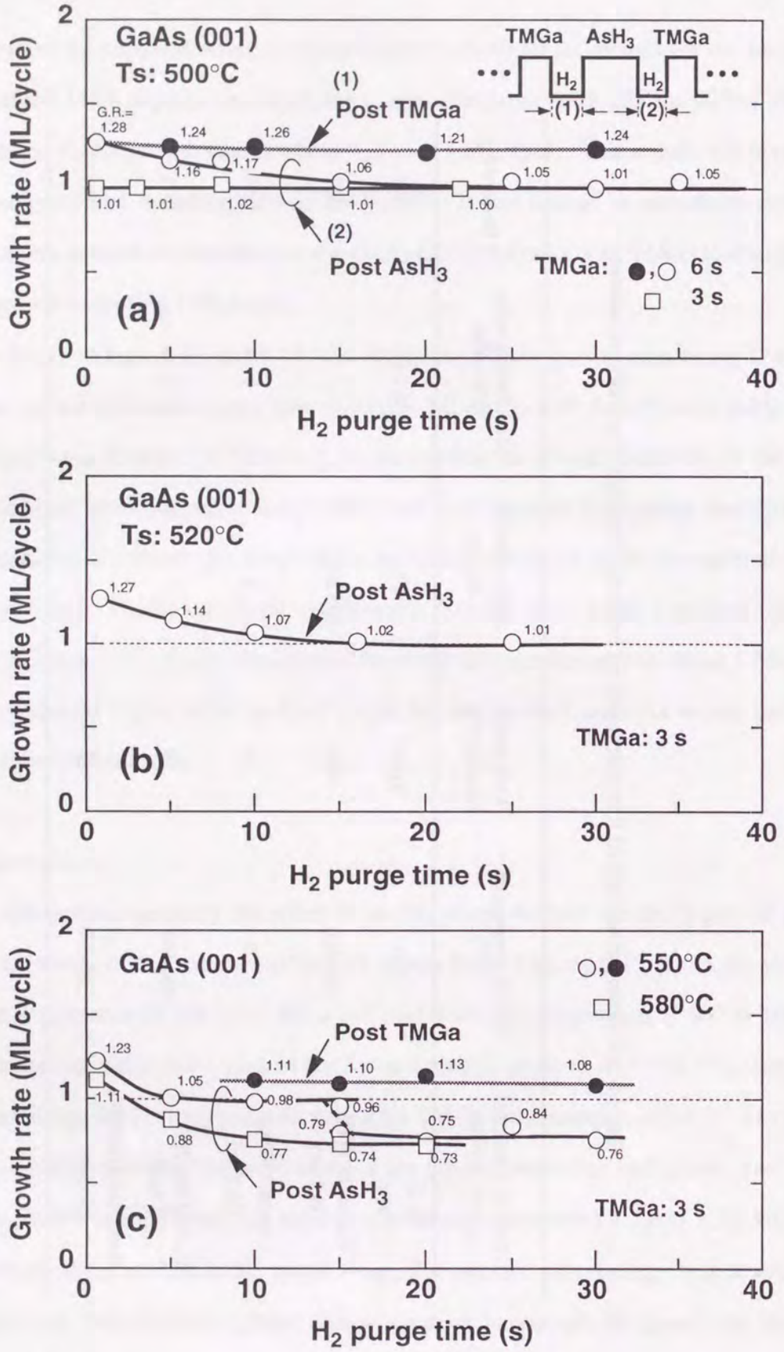

Figure 6-12. Growth rate variations for post-TMGa and post-AsH_3 H_2 purge times (a) at 500°C, (b) at 520°C, and (c) at 550 and 580°C. AsH_3 was supplied for 5 s with a partial pressure of 33 Pa. The H_2 purge time after AsH_3 was 0.5 s for the post-TMGa H_2 change, and after TMGa it was 0.5 s for the post-AsH_3 H_2 change.

explain these growth rate results as follows. When plenty of AsH_3 is supplied on the GaAs (001), more than 1 ML-As atoms are adsorbed. Although the total number of adsorbed As atoms during and just after the AsH_3 exposure is not clear, at least some of the As reacts with TMGa to form a GaAs layer in excess of 1 ML/cycle. Some of the adsorbed As atoms can be desorbed during the post-AsH_3 H_2 purge period. However, the As layer of the monolayer coverage remains stable at 500°C. The TMGa-exposed GaAs (001) surface is not affected by the post-TMGa H_2 purge time in terms of the growth rate. Therefore, the decrease in the growth rate is due to the desorption of the excessively adsorbed surface As atoms. In other words, the As atoms beneath the surface Ga layer are not desorbed.

Note that when the TMGa exposure time was 3 s, we could not observe any decrease in the growth rate, as indicated by the open squares in Fig. 6-12 (a), even if the post-AsH_3 H_2 purge time was increased. The difference in the growth rate dependence on the post-AsH_3 H_2 purge time between the TMGa pulse duration of 3 s and 6 s can eliminate the possible undesired mixing between TMGa and AsH_3 in the gas phase which produces the growth in excess of 1 ML/cycle. In the case of a 3 s TMGa injection, the growth is limited by the amount of supplied TMGa as seen in Fig. 6-11. Therefore, although the excess As atoms must exist on the AsH_3-exposed surface for about 15 s post-AsH_3 H_2 purge, the GaAs growth per cycle is limited to 1-ML thickness due to insufficient TMGa.

Figure 6-12 (b) shows the dependence of the growth rate on the post-AsH_3 H_2 purge time at 520°C. TMGa pulse duration was 3 s, which is long enough to saturate the growth rate due to the enhanced TMGa decomposition rate at 520°C. The growth rate decreases from 1.27 to 1 ML/cycle with increasing post-AsH_3 H_2 purge times, showing the similar tendency to that observed in Fig. 6-12 (a). There seems to be a stable surface structure with an As coverage of 1 ML at 500 and 520°C.

We obtained striking results by raising the growth temperatures to 550 and 580°C, as shown in Fig. 6-12 (c). At 550°C, the initial 1.23 ML/cycle growth rate decreased to about 1 ML/cycle when the post-AsH_3 H_2 purge was 5 s and leveled off at about 1 ML/cycle from 5 to 15 s. Then, the growth rate was saturated at around 0.76 ML/cycle for post-AsH_3 purges of longer than 15 s. There are apparently two stable plateaus at 550°C. The dependence on the

post-TMGa H_2 purge time is also shown in the figure. In this case, the growth rate was scarcely changed for a H_2 purges of longer than 10 s. However, the reason for the small discrepancy between the rate of 1.23 ML/cycle at 0.5 s purge, and the constant value of around 1.1 ML/cycle for the H_2 purge times of over 10 s, is not clear. Contrary to the result at 550°C, the growth rate monotonically decreased from 1.11 ML/cycle and saturated at about 0.73 ML/cycle for the change of the post-AsH_3 H_2 purge time at 580°C. In the samples grown at 550 and 580°C, the surface morphologies were specular for the samples grown under the shortest 0.5 s post-AsH_3 H_2 purge, independent of the purge time after TMGa. Increasing the purge time after AsH_3, however, the surface degraded. The morphological roughness was higher than that at 500 to 520°C. Compared with the total growth thickness (about 100 nm), the undulation was sufficiently small. Therefore, the accuracy of the thickness measurement was not worse.

As shown in Fig. 6-11, the growth was self-limited at 1 ML/cycle at 500°C when the AsH_3 was supplied under a partial pressure of 3.3 Pa for 1 s. Under this condition, we studied the dependence of the growth rate on the post-AsH_3 H_2 purge time. Results are indicated in Fig. 6-13. The results for the 2 s AsH_3 exposure are also shown. Unlike the results in Fig. 6-12 (a), the growth rate decreased from 1 ML/cycle to 0.8 ML/cycle at 40 s H_2 purge. The growth rate does not seem to reach to a steady value within the purge time studied. The surface morphology observed by a Nomarski microscope was specular for all the samples, implying a different As desorption pathway from that of Fig. 6-12 (a).

6.5 Growth Mechanism Considering Surface Reconstructions

6.5.1 Surface reconstructions of GaAs (001)

It is well known that, under a UHV condition, the growth surface of GaAs (001) has a variety of reconstructed structures and surface stoichiometry according to the growth environment [25]. Especially in conventional MBE, the (2x4) or c(2x8) reconstructed surface structure is commonly observed as the As-rich GaAs (001) using reflection high-energy electron diffraction (RHEED) or low-energy electron diffraction (LEED) [26]. The atomic

arrangement corresponding to the (2x4)/c(2x8) diffraction in a real space was proposed by Chadi as a "missing-dimer row model" with 75% coverage of the outermost As layer [27]. It was proved by Pashley *et al.* using scanning tunneling microscopy (STM) [28, 29]. In contrast, in an MOVPE environment, it was believed that there is no surface reconstruction, or if any the reconstruction is much different from that under UHV, due to the H_2 or H adsorption on the surface [30]. The lack of useful surface-sensitive analytical tools has limited the information on growth surface structures for a long time. Recently, grazing-incidence x-ray diffraction (GIXD) and optical monitoring techniques such as reflectance-difference spectroscopy (RDS) and surface photo absorption (SPA) have shown that the GaAs (001) surface is reconstructed even when being static in an MOVPE environment [31-33]. Results show that the AsH_3-exposed GaAs (001) in a MOVPE reactor normally has a c(4x4) or newly defined d(4x4) symmetry with an As coverage of more than 1 ML. The difference in the surface As coverage between MBE and MOVPE is thought to be mainly due to the As impinging rate at the surface, or, to the partial pressure of As-containing species in the growth environment [32].

6.5.2 Surface stoichiometric problem at GaAs (001) during ALE

Although the surface reconstruction and the surface As stoichiometry of GaAs (001) change significantly with growth conditions, the growth rate observed in most of ALE reports so far has been self-limited to 1 ML/cycle. Some researchers pointed out that none of the well-known reconstructed surfaces of GaAs (001) are terminated with 1 ML coverage of Ga or As [25-29]. It is then very puzzling how an ideal monolayer-limited growth is achieved. This is the so-called "surface stoichiometric problem" of ALE [24, 34, 35]. Thus, the self-limiting monolayer growth mechanism of ALE or PJE GaAs is still unsolved in terms of surface reconstruction and related surface As stoichiometry. We try to solve this problem in this section.

6.5.3 Growth model including surface reconstructions

Based on the experimental results mentioned in Section 6.4, we stress here that the As adsorption and desorption at the GaAs (001) growth surface plays a very important role in

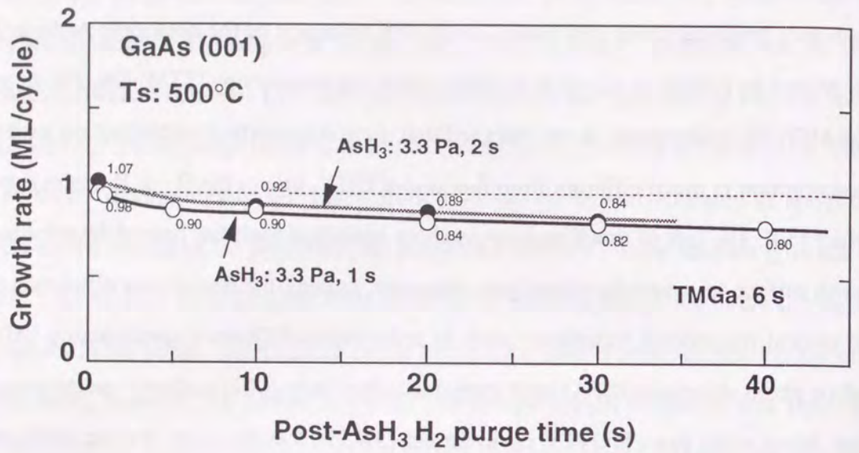

Figure 6-13. Growth rate dependence on the post-AsH_3 H_2 purge time at 500°C. The H_2 purge time after TMGa was 0.5 s. AsH_3 was supplied with 3.3 Pa for 2 s.

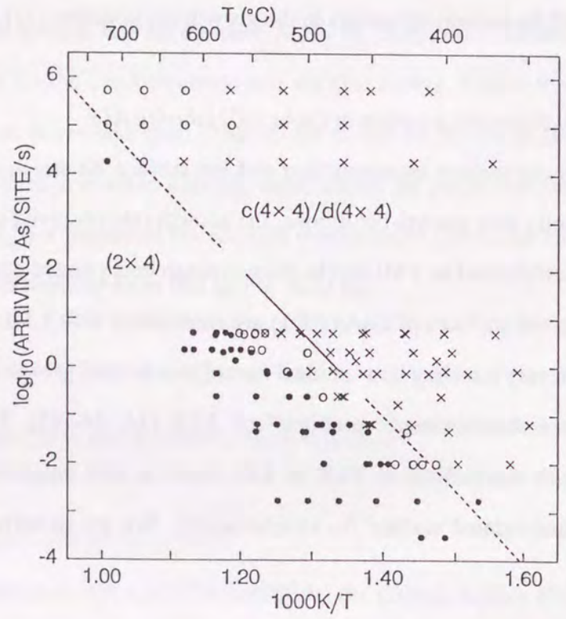

Figure 6-14. (2x4)-c(4x4)/d(4x4) phase diagram of GaAs(001) as a function of substrate temperature and incorporation rate of As atoms. Dots, crosses, and circles represent (2x4)-like, c(4x4)/d(4x4)-like, and mixed structures, respectively. The solid line shows the (2x4)/c(4x4) phase boundary by Van Hove. (see ref [32])

determining the self-limiting growth rate, being related to the reconstructed surface structure and its surface stoichiometry. We propose a new PJE growth model which explains our results and includes the effects of surface reconstruction and related surface stoichiometry. This model will help us solve the surface As stoichiometric problem at the GaAs (001) discussed in the ALE or PJE growth mechanism.

6.5.3.1 Model for As adsorption at GaAs (001)

In this section, we consider the growth mechanism which explains the practical behavior of the growth rates shown in Figs. 6-10 and 6-11, taking the surface reconstruction and surface stoichiometry of GaAs (001) into consideration. Recently, the As-rich GaAs (001) surface was extensively studied using several techniques under both UHV and low- or atmospheric-pressure environment. As well as the GIXD experiments [31], RDS and SPA studies have revealed that the GaAs (001) surface annealed under the typical AsH_3 flow rates in an MOVPE reactor produces a c(4x4)-like surface. This was determined by comparing the measured spectra of the GaAs (001) with the spectral database gathered and simultaneously related to RHEED patterns in UHV [32, 33].

Figure 6-14 is the surface phase diagram provided by Kamiya *et al.* from the RDS measurements [32]. Based on this, the AsH_3 partial pressures we employed (see Fig. 6-10) are within the regime giving a c(4x4)/d(4x4)-like reconstruction. Therefore, the GaAs (001) in our reactor must have a c(4x4)-like surface if the surface is in equilibrium at 500°C after the sufficiently long exposure to AsH_3. (Hereafter, we do not distinguish between the d(4x4) and the c(4x4), and simply use the expression c(4x4).) The determination of the surface As coverage (θ_{As}) and the atomic arrangement corresponding to the c(4x4) surface observed in UHV has been tried by several workers.

Three proposed surface structures representing c(4x4) symmetry and the respective surface As coverage are illustrated in Fig. 6-15. The common feature of the models is that the c(4x4) surface consists of the As monolayer and the additional As dimers chemisorbed along the <110> direction. From studies using angle-resolved photoemission and surface-sensitive core-level photoemission, Larsen *et al.* reported that the c(4x4) has a range of θ_{As} and the

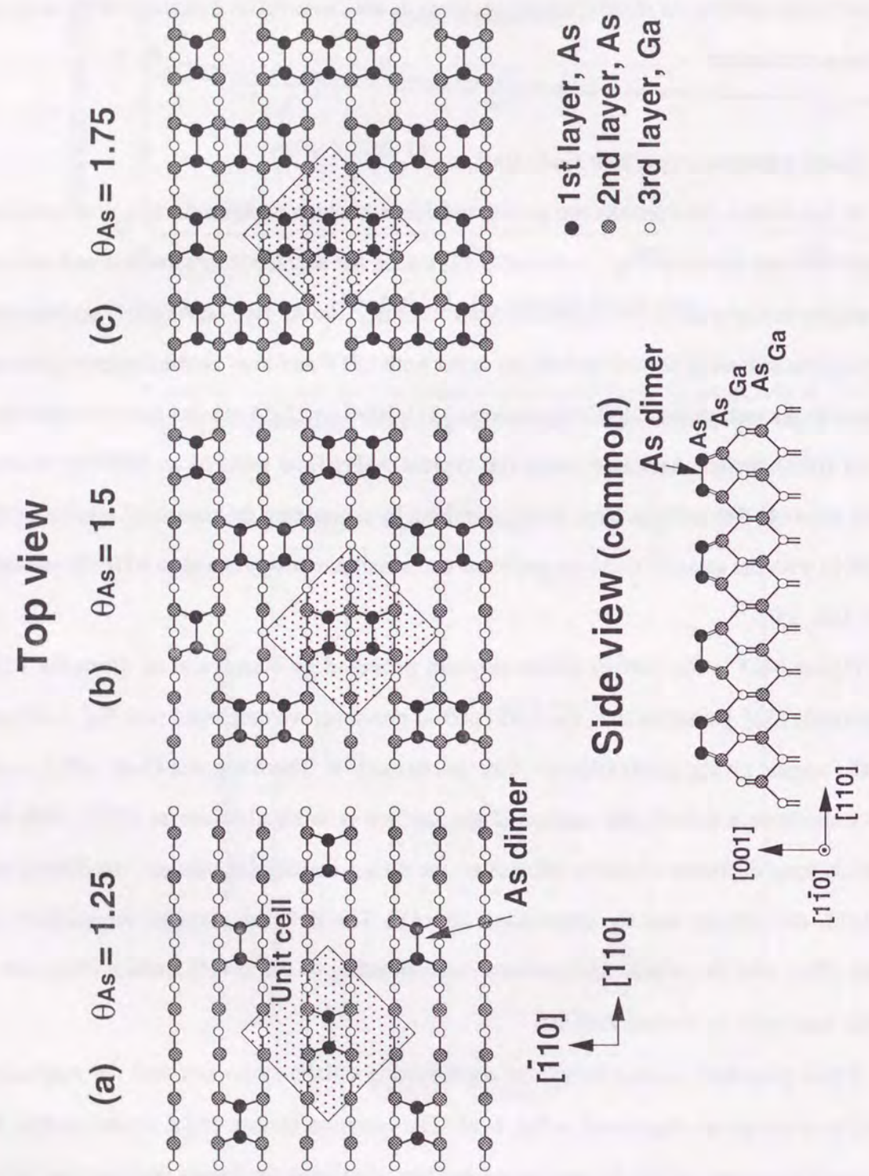

Figure 6-15. Ball and stick models for the three proposed c(4x4) surface structures. Side view is common to all three top views.

observed c(4x4) surface is a combination of both Figs. 6-15 (a) and (b) [36]. Sauvage-Simkin *et al.* also observed a variable θ_{As} in c(4x4) and reported that the actual c(4x4) is represented as a combination of Figs. 6-15 (b) and 6-15 (c) from the results of GIXD [37]. Biegelsen *et al.* studied the c(4x4) surface using STM and revealed θ_{As} was equal to 1.75 ML, as shown in Fig. 6-15 (c) [38]. Sasaoka *et al.*, however, clarified that the substrate temperatures, where the excess As adsorption occurs, lead to determining the favorable surface between the two extreme structures, as indicated in Figs. 6-15 (a) and (c) [39]. They reported that the ambiguousness of the θ_{As} and of the determination of c(4x4) among the above results originates from the way of preparing the c(4x4) surface. They measured the surface As stoichiometry of c(4x4) using a precisely calibrated quadrupole mass spectrometer in temperature programmed desorption (TPD). They concluded that the c(4x4) has a θ_{As} of about 1.28 ML, nearly equal to that in Fig. 6-15 (a), if the GaAs (001) is not cooled down below 300°C in the As flux. This As coverage agrees well with the saturated value of the growth rate in Fig. 6-10. It is reasonable, we believe, to assume that the GaAs (001) stabilized in the AsH_3 flow in our reactor has the surface like in Fig. 6-15 (a).

Looking back to Fig. 6-10, the growth rate can be divided into two regions: a fast-reaction region below 1 ML/cycle, which seems to reflect the AsH_3 (or cracked As species) reaction with a Ga-terminated surface, and a slow-reaction region over 1 ML/cycle, which seems to reflect the AsH_3 (or As species) reaction with a monolayer-adsorbed As plane to make c(4x4)-like surface. In Fig. 6-16, the plausible growth model explaining the growth rate over 1 ML/cycle is shown. Supplying AsH_3 to the initial Ga-terminated surface of Fig. 6-16 (a) quickly forms an As monolayer (Fig. 6-16 (b)). Completing the As adsorption at the monolayer coverage will produce an ideal 1 ML/cycle. Our experimental results, however, suggest that excess As adsorption continues to form a c(4x4)-like surface with a slow reaction between the AsH_3 and surface monolayer As plane (Fig. 6-16 (c)). If a sufficient amount of TMGa is supplied to the c(4x4)-like surface, the excessively adsorbed As dimers, as well as the second As monolayer, react with the impinging TMGa. The second As layer makes the 1 ML-thick GaAs, and the outermost excess As dimers also contribute to the extra growth of around 0.25 ML (Fig. 6-16 (d)). The small fluctuation in the saturated growth rates depending on the AsH_3

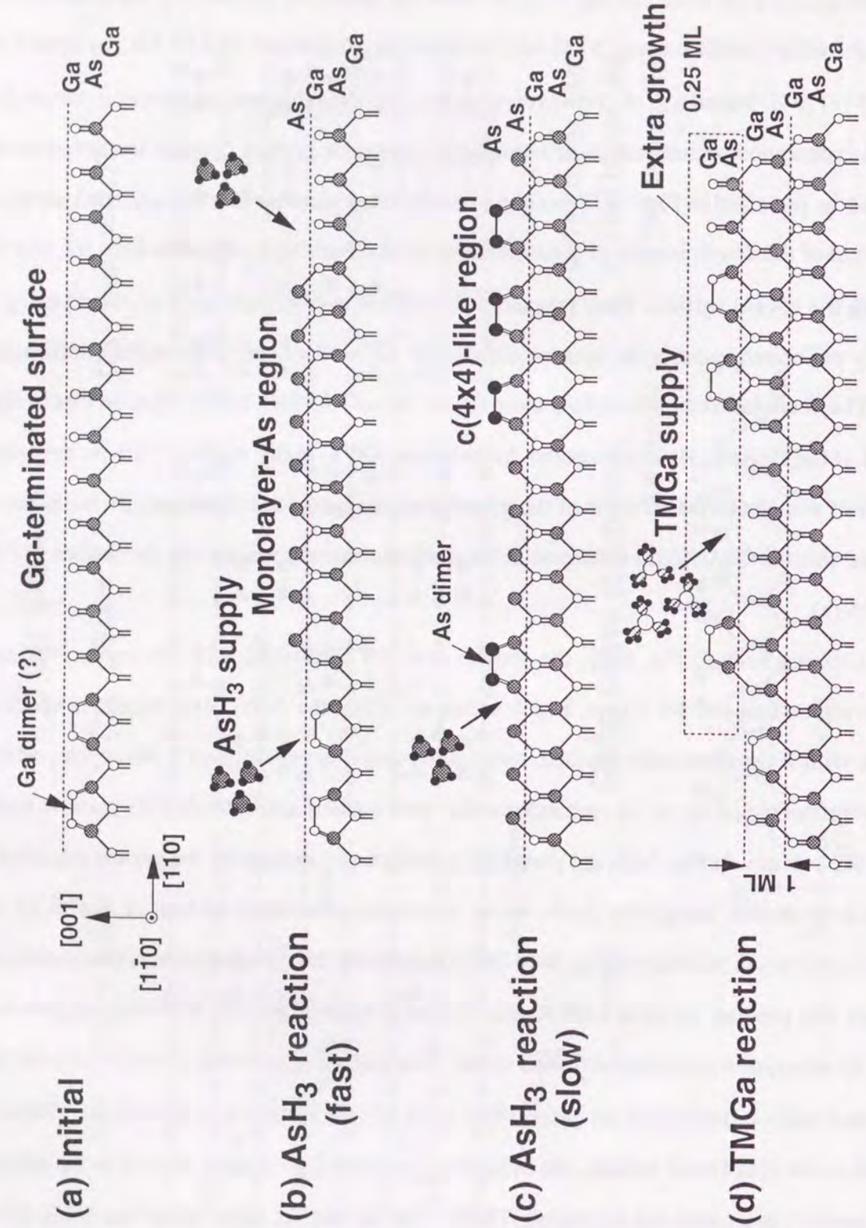

Figure 6-16. Growth model representing As adsorption in excess of 1 ML and following TMGa reaction at GaAs (001).

partial pressures (Figs. 6-10 and 6-11) is probably due to additional As adsorption on the fundamental c(4x4) surface. It might be related to the d(4x4) observed by RDS [32].

Consideration of the surface reconstruction effect on the AsH_3-exposed GaAs (001) is also valid in explaining the saturation value of the ALE growth rate in other works. The results by Nishizawa *et al.*, listed in Table 6-3, can also be explained by assuming specific reconstruction for the As-rich surface. They performed GaAs growth by MBE in UHV, under a typical AsH_3 pressure of $7x10^{-3}$ Pa at 500°C. Their AsH_3 dosage level was nearly at the boundary region of (2x4) and c(4x4), judging from the surface phase diagram of the GaAs (001) shown in Fig. 6-14 [32]. We speculate that their AsH_3-exposed surface might be (2x4)-β having a θ_{As} of 0.75 ML and/or (2x4)-γ having a θ_{As} of 1 ML. (Detailed structures will be shown later.) This will make the growth rate saturate at about 0.8 ML/cycle. Based on the mechanism shown in Fig. 6-15, we can conclude that the monolayer-limited GaAs growth is metastable. The growth rate of 1 ML/cycle is attained by controlling the kinetics of the surface reaction of the forming As layer. To achieve the self-limiting growth at 1 ML/cycle for the TMGa injection, the partial pressure and the pulse duration of AsH_3 must be optimized so that the surface As coverage becomes just 1 ML. The results from the low-pressure MOVPE reactor, listed in Table 6-3, are explained by this.

Some results are inconsistent with our model. Banse *et al.* and Uwai *et al.* reported that As atoms exceeding 1 ML at the c(4x4) surface are desorbed without reacting with TMGa or triethylgallium, resulting in the 1 ML/cycle [34, 40]. The reason for the discrepancy is not clear at this stage.

6.5.3.2 Model for As desorption from GaAs (001)

Next, we explain the growth rate dependence on the post-AsH_3 H_2 purge time. Our model assumes the transition of the surface reconstruction and the stoichiometry of As-rich GaAs (001) through the surface As desorption. The structural change in the GaAs (001) surface has been observed in both MBE and MOVPE. Kamiya *et al.* reported that the c(4x4)/d(4x4)-like GaAs (001) surface which has been stabilized in an AsH_3 flow, changes into As-rich (2x4) and Ga-rich (4x2)-like surfaces by increasing the substrate temperatures in an AsH_3-free reactor

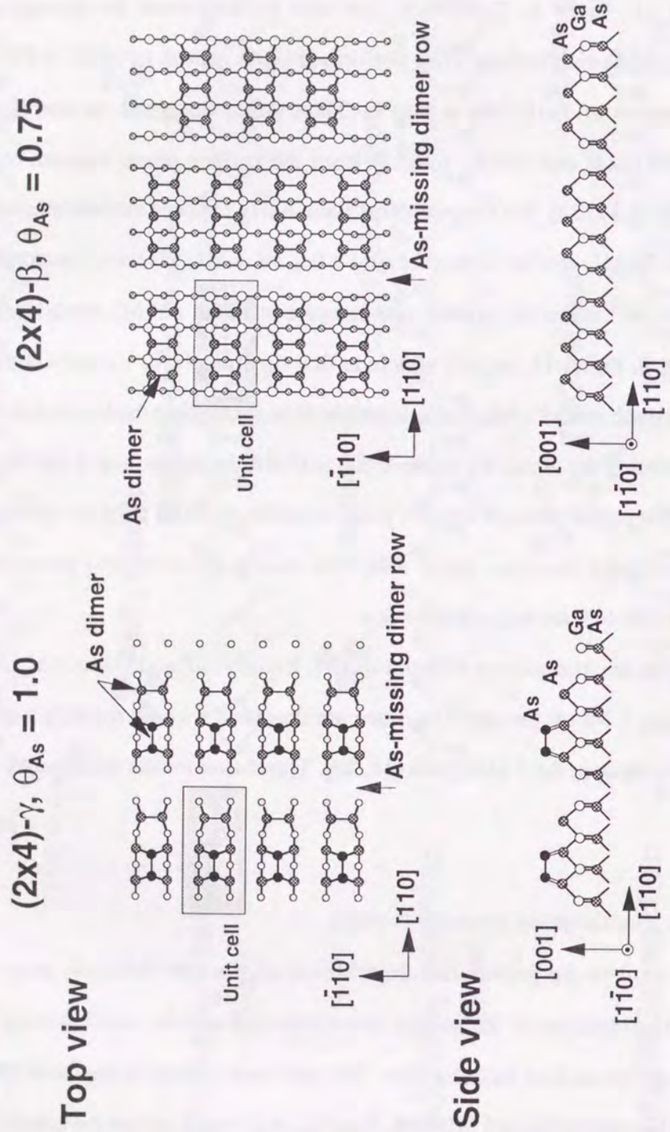

Figure 6-17. Ball and stick model for (2x4)-γ and (2x4)-β surfaces.

[32]. The temporal evolution of the reconstruction of the GaAs (001) has also been reported in several works [33, 41]. Here, we assume three major As-rich surfaces, c(4x4), (2x4)-γ, and (2x4)-β, according to the growth conditions in our reactor. The c(4x4) is illustrated in Fig. 6-15 (a), and (2x4)-γ and (2x4)-β are in Fig. 6-17. The (2x4)-γ phase was first proposed by Farrell *et al.* [42], and θ_{As} was measured by TPD to be 1 ML [39], as predicted [42]. The (2x4)-β is a well-known phase having a θ_{As} of 0.75 ML.

The expected surface phase transition is summarized in the Table 6-4. This explains the growth rate decrease by increasing the post-AsH_3 H_2 purge time. The results in Figs. 6-12 (a) and (b) are explained by assuming that the c(4x4)-like surface changes into (2x4)-γ phase after a long post-AsH_3 H_2 purge at 500-520°C. The cyclical growth is thought to be done by supplying TMGa on the (2x4)-γ As-rich surface under the long H_2 purge conditions, while on the c(4x4) surface under short H_2 purge conditions. According to the selective adsorption model of TMGa, the TMGa molecules react with only the surface As atoms [10, 43]. The growth rate, therefore, is determined by the surface As population when plenty of TMGa is supplied. The growth rate changes from about 1.25 ML/cycle to 1 ML/cycle, reflecting the θ_{As} of c(4x4) and (2x4)-γ. The growth rate variation at 550°C in Fig. 6-12 (c) shows the intermediate state involving a new phase transition. The c(4x4) surface is thought to initially change into (2x4)-γ, then begin to transit into (2x4)-β. Raising the temperature to 580°C, the plateau related to (2x4)-γ cannot be observed, and the surface structure seems to be stable at the (2x4)-β. Our observation of (2x4)-β phase at a slightly higher temperature than (2x4)-γ agrees with the RHEED and RDS results [42, 44]. The fact that the growth rate is limited at the submonolayer thickness, as shown in Fig. 6-12 (c), strongly supports the selective adsorption model. This is because the TMGa does not seem to be adsorbed on the occupied Ga sites of 0.25 ML at the (2x4)-β surface, which appeared by the surface As desorption. Because the time constant of the phase transition shortens at 580°C, growth at the 0.5 s post-AsH_3 H_2 purge occurred at the transition from c(4x4) to (2x4)-β. This might be the reason for the small growth rate of 1.11 ML/cycle.

An explanation for the result shown in Fig. 6-13 is difficult because of the lack of knowledge about the As-terminated surface structure at the shortest H_2 purge time. Although

Table 6-4: Summary of growth rate change and expected surface phase transition of GaAs (001) for various growth conditions observed by increasing the post-AsH_3 H_2 purge time.

Ts (°C)	AsH_3 condition		Growth rate (ML/cycle)	Phase transition
	Pressure (Pa)	Exposure time (s)		
500	3.3	1	0.98 -> 0.80	? -> (2x4)-β
500	33	5	1.28 -> 1.05	c(4x4) -> (2x4)-γ
520	33	5	1.27 -> 1.01	c(4x4) -> (2x4)-γ
550	33	5	1.23 -> 0.98 -> 0.76	c(4x4) -> (2x4)-γ -> (2x4)-β
580	33	5	1.11 -> 0.73	c(4x4) -> (2x4)-β

the growth temperature is the same as in Fig. 6-12 (a), the surface in Fig. 6-13 seems to change into (2x4)-β with an As coverage of 0.75 ML. The initial As-rich surface is thought to be different from the As-desorbed surface anticipated as (2x4)-γ in Fig. 6-12 (a). One possible explanation is that the initial As-rich surface in Fig. 6-13 is thermodynamically unstable because the monolayer As is attained kinetically.

As shown in Figs. 6-12 and 6-13, the surface As atoms are not desorbed perfectly from the As-rich GaAs (001) after stopping the AsH_3 pulse at 500 to 580°C, still resulting in the formation of less As-rich surfaces. However, Kobayashi *et al.* and Yamauchi *et al.* reported that the AsH_3-stabilized GaAs (001) surface changes into a Ga-terminated one when it is annealed in an AsH_3-free environment at the growth temperature [21, 33]. Our results are inconsistent with theirs. The difficulty in forming the Ga-terminated surface of (4x2) symmetry on the GaAs (001) in a MOVPE reactor was reported by Kamiya *et al.* and Uwai *et al.* [40, 45]. They observed the (2x4)-like or c(4x4)/d(4x4)-like surfaces even after purging AsH_3 with H_2, and attributed this to the small amount of residual As species desorbed from the susceptor or the reactor wall. Although our experimental observations agree with theirs, we think that the reason for the stability of the As-rich surfaces even in the AsH_3-free environment cannot be ascertained yet. If the background As pressure keeps the surface As atoms stable at GaAs (001), clear self-limiting growth of GaAs would not be obtained because of the inevitable mixing reaction between TMGa and As species. This contradicts our result in Fig. 6-11. To explain this paradox, further examination is needed.

6.5.3.3 Others

We explained the growth rate of PJE-grown GaAs (001), taking the surface reconstruction and the relevant surface As stoichiometry into consideration. Next, we briefly discuss the other binary compounds.

(1) InAs: the InAs growth rate varies from 1 to 0.75 ML/cycle at 365°C without any surface degradation, as we increase the H_2 purge time after AsH_3 (see Fig. 6-4). Additionally, as previously shown in the preliminary results using the horizontal reactor, the growth of

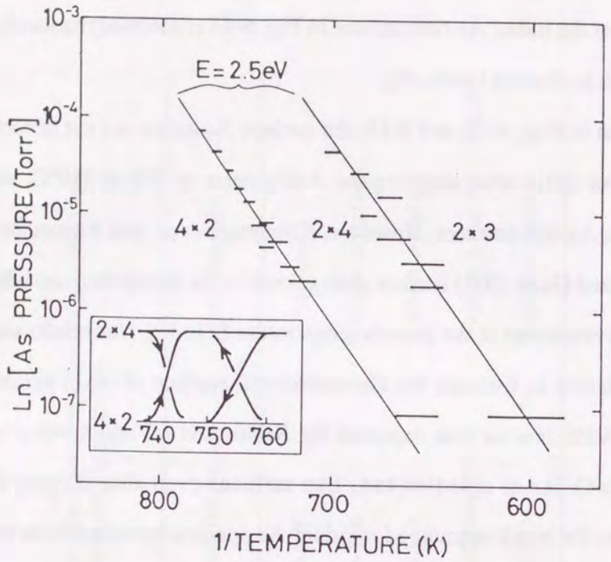

Figure 6-18. Surface phase diagram of InAs (001).

Table 6-5: Dependence of InAs surface reconstructions on substrate temperature.

Reconstruction	c(4x4)	-	2x3	-	2x4	-	4x2
Temperature (°C)		~330		~350		~540	

0.75 ML/cycle is apparently stable in our growth conditions (see Figs. 3-14 and 3-15). Figure 6-18 shows the surface phase diagram of InAs (001) reported by Moison *et al.* [18]. Table 6-5 is the data from Toyoshima *et al.* showing the relationship between reconstructions and substrate temperatures under an As_2 pressure of $6x10^{14}$ molecules cm^{-2} s^{-1} [46]. From Toyoshima's data, the c(4x4) phase will barely be able to exist at 365°C. The AsH_3 partial pressure in our InAs growth condition is about 0.36 Torr. Therefore, PJE-grown InAs surface will display (2x3) structure under the presence of AsH_3, judging from the Moison's data. If the AsH_3 flow is stopped, the phase of InAs (001) will shift to (2x4) from (2x3). Recent RHEED and STM studies have proved that the (2x4) phase of InAs (001) corresponds to a missing dimer row structure where θ_{As}=0.75 ML [20, 47]. Our results of 0.75 ML/cycle are probably related with the As coverage of the (2x4) reconstructed surface. If the As coverage of the (2x3) InAs (001) surface is 1 ML, we can explain well the observed growth rate change from 1 ML/cycle to 0.75 ML/cycle using the phase transition from (2x3) to (2x4). Further explanation is needed to clarify this assumption.

(2) InP: the PJE-grown InP (001) behaved differently from GaAs and InAs. The stable saturation value was 0.5 ML/cycle. We believe that the saturated growth rate is related to the specific surface reconstruction and its surface stoichiometry as seen in the GaAs (001). However, there has been no systematic study on the surface structures and their atomic arrangements on InP (001). Stanley *et al.* reported that the MBE-grown InP (001) exhibits P-rich (2x4) pattern [48]. Kurpas *et al.* revealed the existence of P-stabilized (2x4) on the MOVPE-grown InP (001) at 600°C using reflectance anisotropy spectroscopy (RAS), which is almost the same method as RDS [49]. If the (2x4) diffraction corresponds to the (2x4)-α phase having a surface P coverage of 0.5 ML (an analogy of the GaAs (001) surface), our experimental result of InP PJE will be reasonably explained by the surface reconstruction model. However, we have to wait further surface studies on InP in order to clearly explain our PJE results in terms of surface structures.

Very recently, Yang *et al.* reported that the P-stabilized InP (001) surface, prepared by GSMBE, revealed the (2x4) reconstruction [50]. They also studied the atomic arrangement of the InP surface using STM and clarified that the stable (2x4) cell is actually (2x4)-α phase, which has a surface P coverage of 0.5 ML at around 360°C. This result strongly supports the above-mentioned growth model of PJE-grown InP.

6.6 Explanation for Orientation Dependence of Growth Rate

Finally, we comment on the dependence of the GaAs growth rate on the crystallographic orientations in PJE from the viewpoint of surface As adsorption and desorption. As described in Section 3.4.1, the GaAs growth rate under a fixed growth condition depends on the surface orientation of the substrates (Fig. 3-23). We also showed the dependence of the GaAs growth rate on the growth temperatures for some orientations. We noticed that the crystallographic orientation dependence is strongly related to the thermal stability of As atoms adsorbed on the growth surface.

Here, we consider the H_2 purge time dependence on the growth rate. Figure 6-19 shows the variation of the GaAs (111)A growth rate as a function of the post-AsH_3 and post-TMGa H_2 purge times. The growth temperature was 500°C. The mole fraction of AsH_3 and TMGa was 1.25×10^{-2} and 1×10^{-3}, respectively. The gas sequence, H_2/TMGa/ H_2/ AsH_3, was 0.5 (or x)/ 8/ y (or 0.5)/5 s. Although the growth rate didn't change by varying the post-TMGa H_2 purge time, the rate decreased drastically with the increasing post-AsH_3 purge time.

We observed a similar dependence on the GaAs (011) substrate at 500°C. Results are shown in Fig. 6-20. In this case, the TMGa pulse duration was 9 s. The growth temperature dependence described in Section 3.4.1 also supports the similarity of the growth behavior between the (111)A and (011) faces.

Conversely, we observed the growth rate increases by increasing H_2 purge time on AsH_3-exposed GaAs (111)B (Fig. 6-21). The growth condition, the mole fraction, and the gas

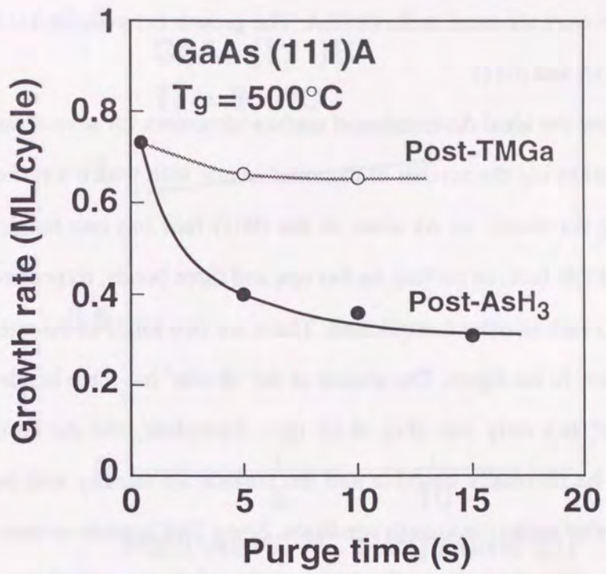

Figure 6-19. Variation of growth rate on GaAs (111)A as a function of post-AsH_3 and post-TMGa H_2 purge time.

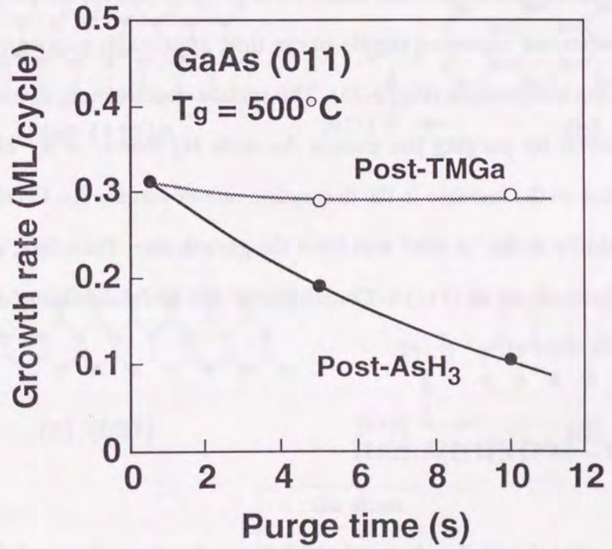

Figure 6-20. Variation of growth rate on GaAs (011) as a function of post-AsH_3 and post-TMGa H_2 purge time.

pulse sequence were the same as for (111)A. The growth behavior on (111)B was the opposite to that on (111)A and (011).

We show the ideal As-terminated surface structures for several surface orientations in Fig. 6-22. Considering the number of chemical bonds with which a surface As atom sticks to the underlying Ga atoms, an As atom on the (001) face has two bonds (Fig. 6-22 (c)). On (111)A and (111)B face, an surface As has one and three bonds, respectively (Fig 6-22 (a) and (d)). The (011) face is more complicated. There are two kinds of As sites as denoted by "A-site" and "B-site" in the figure. The arsenic of the "B-site" has three bonds with Ga, and the As of the "A-site" has only one (Fig. 6-22 (b)). Therefore, the As atom on the (111)A is considered to be thermally unstable and the surface As density will be smallest when the substrate is heated under the growth condition. Since TMGa tends to react selectively with the surface As according to the "selective adsorption model", the growth rate on (111)A becomes small. Our observation in Fig. 6-19 reflects this speculation. On the other hand, the As on (111)B is very stable. Or rather, the excessively adsorbed As atoms form trimer structures on the (111)B surface and this tends to inhibit the surface reaction with TMGa, leading to suppressed Ga incorporation into the lattice sites [51-53]. Indeed, we observed the increase in growth rates when we increased the H_2 purge time after AsH_3 exposure (Fig. 6-21) and we raised the growth temperature (Fig. 3-25). The surface deactivation, caused by the As trimers, might be relieved by purging the excess As with H_2 flows, or by elevating the growth temperatures due to the increase in the desorption rate of surface As. On the (011) face, the As sticking probability at the "A-site" will limit the growth rate. Therefore, the characteristics of (011) are similar to those of (111)A. Consequently, the thermal stability of the surface As can be written in the order of:

$$(111)B > (001) > (111)A, (011) \qquad (6\text{-}1)$$

This is closely related with the observed crystallographic dependence of the GaAs growth rate in PJE. Thus, the As adsorption and desorption process at the growth surface play an important role in the mechanism of PJE growth on different orientation substrates.

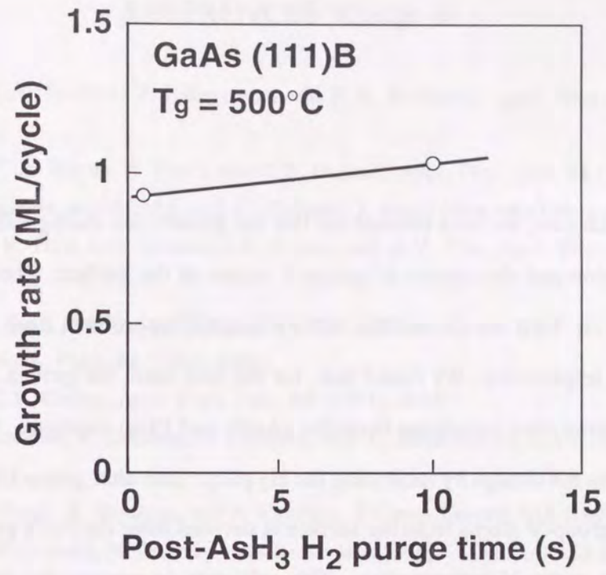

Figure 6-21. Variation of growth rate on GaAs (111)B as a function of post-AsH_3 H_2 purge time.

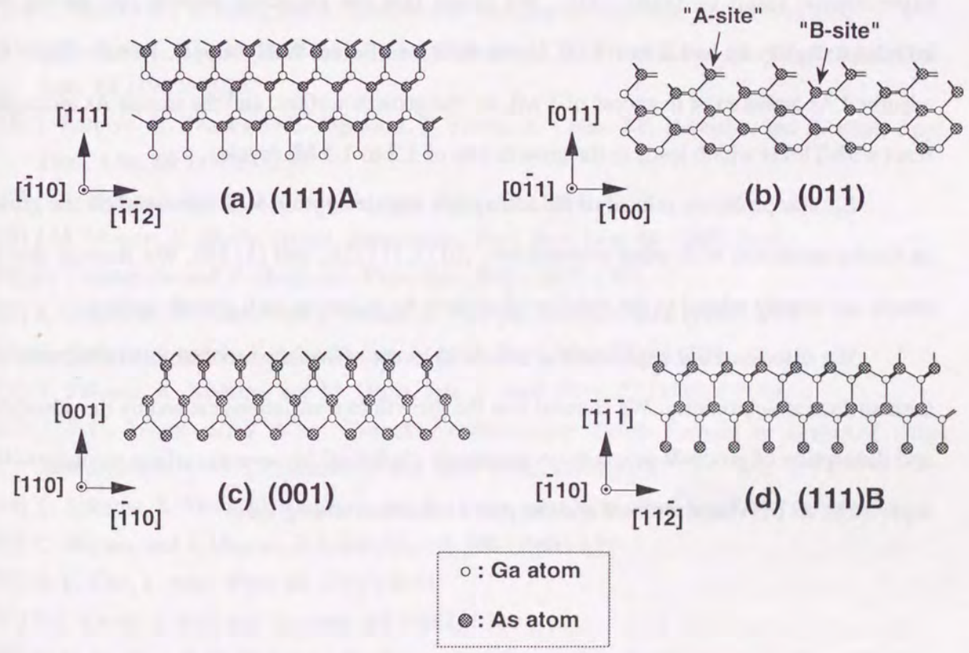

Figure 6-22. Schematics of ideal As-terminated GaAs surfaces, neglecting reconstruction (side view).

6.7 Summary

In this chapter, we have pointed out that the growth rate during PJE is strongly affected by the adsorption and desorption of group-V atoms at the surface. These things have been overlooked so far. First we showed the As or P desorption problem from InAs, GaAs and InP (001) surface, respectively. We found that, for the first time, the growth rate decreases when the H_2 purge time after supplying hydrides (AsH_3 and PH_3) increases. On the contrary, the growth rate does not change by increasing the H_2 purge time after group-III metalorganics. This desorption of group-V atoms from the surface is derived from the PJE's gas sequence having a period without group-V overpressures. The only way to prevent the desorption of surface group-V atoms is to shorten the H_2 purge time period. This technique is also useful for maintaining the specular surface morphologies. Next, we described another important experimental result on GaAs (001). We found that the saturated growth rate during PJE increases slightly up to 1.2 to 1.3 ML/cycle with a sufficient AsH_3 supply. Results imply that adsorbed As atoms exist in excess of 1 ML on the growth surface, and the excess As atoms also react with TMGa which leads to the growth rate of 1.2 to 1.3 ML/cycle.

Similar problems related to As adsorption and desorption were observed on the growth on GaAs substrates with other orientations: (011), (111)A, and (111)B. We showed that the results are closely related to the stability of surface As atoms on each growth surface.

We discussed our experimental results in terms of surface reconstructed structures and their surface stoichiometry. We showed that the growth rate variations caused by the adsorption and desorption of group-V atoms are consistently explained by several surface reconstructions reported in an UHV environment and the phase transition among them.

REFERENCES (Chap. 6)

[1] S.M. Bedair, M.A. Tischler, T. Katsuyama, and N.A. El-Marsy, Appl. Phys. Lett. **47** (1985) 51.

[2] S.P. DenBaars, C.A. Beyler, A. Hariz, and P.D. Dapkus, Appl. Phys. Lett. **51** (1987) 1530.

[3] Y. Sakuma, M. Ozeki, N. Ohtsuka, and K. Kodama, J. Appl. Phys. **68** (1990) 5660.

[4] M.C. Tamargo, R. Hull, L.H. Greene, J.R. Hayes, and A.Y. Cho, Appl. Phys. Lett. **46** (1985) 569.

[5] T. Fukui and H. Sato, Jpn. J. Appl. Phys. **23** (1984) L521.

[6] T. Yao, Jpn. J. Appl. Phys. **22** (1983) L680.

[7] E.J. Roan and K.Y. Cheng, Appl. Phys. Lett. **59** (1991) 2688.

[8] M. Ozeki, K. Kodama, Y. Sakuma, N. Ohtsuka, and T. Takanohashi, J. Vac. Sci. Technol. **B8** (1990) 741.

[9] Y. Sakuma, M. Ozeki, K. Kodama, and N. Ohtsuka, J. Cryst. Growth **115** (1991) 324.

[10] M. Ozeki, K. Mochizuki, N. Ohtsuka, and K. Kodama, Appl. Phys. Lett. **53** (1988) 1509.

[11] H. Ohno, S. Ohtsuka, A. Ohuchi, T. Matsubara, and H. Hasegawa, J. Cryst. Growth **93** (1988) 342.

[12] W.G. Jeong, E.P. Menu, and P.D. Dapkus, Appl. Phys. Lett. **55** (1989) 244.

[13] Y. Sakuma, M. Ozeki, and K. Nakajima, J. Cryst. Growth **130** (1993) 147.

[14] H. Shimawaki, Y. Kato, and A. Usui, Mater. Res. Soc. Symp. Proc. **160** (1990) 395.

[15] D.W. Kisker, P.H. Fuoss, K.L. Tokuda, G. Renaudo, S. Brennan, and J.L. Khan, Appl. Phys. Lett. **56** (1990) 2025.

[16] I. Kamiya, H. Tanaka, D.E. Aspnes, L.T. Florez, E. Colas, J.P. Harbison, and R. Bhat, Appl. Phys. Lett. **60** (1992) 1238.

[17] B.R. Hancock and H. Kröemer, J. Appl. Phys. **55** (1984) 4239.

[18] J.M. Moison, C. Guille, and M. Bensoussan, Phys. Rev. Lett. **58** (1987) 2555.

[19] H. Yamaguchi and Y. Horikoshi, Phys. Rev. **B45** (1992) 1511.

[20] S. Ohkouchi, N. Ikoma, and I. Tanaka, J. Vac. Sci. Technol. **B12** (1994) 2033.

[21] N. Kobayashi and Y. Kobayashi, Jpn. J. Appl. Phys. **30** (1991) L1699.

[22] Y. Sakuma, K. Kodama, and M. Ozeki, Jpn. J. Appl. Phys. **27** (1988) L2189.

[23] C.E.C. Wood, *III-V Alloy Growth by Molecular Beam Epitaxy in GaInAsP Alloy Semiconductors*, ed. T.P. Peasall (Wiley, New York, 1982) p. 91.

[24] Y. Sakuma, S. Muto, K. Nakajima, and N. Yokoyama, Appl. Surf. Sci. **82/83** (1994) 239.

[25] C. Deparis and J. Massies, J. Cryst. Growth **108** (1991) 157.

[26] A.Y. Cho, J. Appl. Phys. **42** (1971) 2074.

[27] D.J. Chadi, J. Vac. Sci. Technol. **A5** (1987) 834.

[28] M.D. Pashley, K.W. Haberern, W. Friday, J.M. Woodall, and P.D. Kirchner, Phys. Rev. Lett. **60** (1988) 2176.

[29] M.D. Pashley, K.W. Haberern, and J.M. Woodall, J. Vac. Sci. Technol. **B6** (1988) 1468.

[30] Y. Horikoshi, H. Yamaguchi, F. Briones, and M. Kawashima, J. Cryst. Growth **105** (1990) 326.

[31] F.J. Lamelas, P.H. Fuoss, P. Imperatori, D.W. Kisker, G.B. Stephenson, and S. Brennan, Appl. Phys. Lett. **60** (1992) 2610.

[32] I. Kamiya, D.E. Aspnes, H. Tanaka, L.T. Florez, J.P. Harbison, and R. Bhat, Phys. Rev. Lett. **68** (1992) 627.

[33] Y. Yamauchi, K. Uwai, and N. Kobayashi, Jpn. J. Appl. Phys. **32** (1993) 3363.

[34] B.A. Banse and J.R. Creighton, Appl. Phys. Lett. **60** (1992) 856.

[35] J.R. Creighton and B.A. Bansenauer, Thin Solid Films **225** (1993) 17.

[36] P.K. Larsen, J.H. Neave, J.F. van der Veen, P.J. Dobson, and B.A. Joyce, Phys. Rev. **B27** (1983) 4966.

[37] M. Sauvage-Simkin, R. Pinchaux, J. Massies, P. Calverie, N. Jedrecy, J. Bonnet, and I.K. Robinson, Phys. Rev. Lett. **62** (1989) 563.

[38] D.K. Biegelsen, R.D. Bringans, J.E. Northrup, and L.-E. Swartz, Phys. Rev. **B41** (1990) 5701.

[39] C. Sasaoka, Y. Kato, and A. Usui, Surf. Sci. **265** (1992) L239.

[40] K. Uwai, H. Saito, Y. Yamauchi, and N. Kobayashi, Jpn. J. Appl. Phys. **32** (1993) 5479.

[41] H. Yamaguchi and Y. Horikoshi, Phys. Rev. **B44** (1991) 5897.

[42] H.H. Farrell and C.J. Palmstrøm, J. Vac. Sci. Technol. **B8** (1990) 903.

[43] Y. Sakuma, K. Kodama, and M. Ozeki, Appl. Phys. Lett. **56** (1990) 827.

[44] I. Kamiya, D.E. Aspnes, L.T. Florez, and J.P. Harbison, Phys. Rev. **B46** (1992) 15894.

[45] I. Kamiya, D.E. Aspnes, H. Tanaka, L.T. Florez, E. Colas, J.P. Harbison, and R. Bhat, Appl. Surf. Sci. **60/61** (1992) 534.

[46] H. Toyoshima, T. Shitara, P.N. Fawcett, J. Zhang, J.H. Neave, and B.A. Joyce, J. Appl. Phys. **73** (1993) 2333.

[47] H. Yamaguchi and Y. Horikoshi, Phys. Rev. **B48** (1993) 2807.

[48] C.R. Stanley, R.F.C. Farrow, and P.W. Sullivan, *The Technology and Physics of Molecular Beam Epitaxy,* ed. E.H.C. Parker (Plenum Press, New York and London, 1985) Chap. 9.

[49] P. Kurpas, J. Jönsson, W. Richter, D. Gutsche, M. Pristovsek, and M. Zorn, J. Cryst. Growth **145** (1994) 36.

[50] B.X. Yang, Y. Ishikawa, T. Ozeki, and H. Hasegawa, Jpn. J. Appl. Phys. **35** (1996) 1267.

[51] D.K. Biegelsen, R.D. Bringans, J.E. Northrup, and L.-E. Swartz, Phys. Rev. Lett. **65** (1990) 452.

[52] M.Y. Yen and T.W. Haas, Appl. Phys. Lett. **56** (1990) 2533.

[53] S. Ando, S.S. Chang, and T. Fukui, J. Cryst. Growth **115** (1991) 69.

[54] J. Nishizawa, H. Abe, and T. Kurabayashi, J. Electrochem. Soc. **132** (1985) 1197.

[55] P.C. Colter, S.A. Hussien, A. Dip, M.U. Erdogan, W.M. Duncan, and S.M. Bedair, Appl. Phys. Lett. **59** (1991) 1440.

[56] Y. Kawakyu, H. Ishikawa, M. Sasaki, and M. Mashita, Jpn. J. Appl. Phys. **28** (1989) L1439.

[57] H. Yokoyama, M. Shinohara, and N. Inoue, Appl. Phys. Lett. **59** (1991) 2148.

[58] H. Issiki, Y. Aoyagi, T. Sugano, S. Iwai, and T. Meguro, Appl. Phys. Lett. **63** (1993) 1528.

CHAPTER 7
Heteroepitaxy

7.1 Preliminaries

In this chapter, we describe the heteroepitaxy of III-V compounds using PJE. Thus far, we have reported the successful self-limited homoepitaxial growth of III-V binary compounds. However, the ability or a technique to prepare high quality heterointerfaces is highly needed for making some today's practical device structures.

First, we describe the heteroepitaxy of PJE between binary compounds, where the thickness of the epitaxial layer is beyond the so-called "critical thickness". We systematically studied how the self-limiting behavior is affected by the lattice mismatch (or the strain) and by the difference in surface free energy between the substrates and epitaxial layers.

Next, we report the heteroepitaxy of ternary materials such as InGaP and InGaAs. In growing these materials by PJE mode, we faced some significant phenomena relevant to surface segregation of indium (In) atoms and the phase separation between In and gallium (Ga) compounds. To address these problems, we studied the sequences of source gas injection and the effect of growth temperatures. Compositional latching was another novel finding. We found that the ternary composition of InGaAs automatically tends to be lattice-matched to InP (001) substrates during PJE growth. The strain energy due to the lattice mismatch seems to be minimized by the compositional latching phenomena. Through these studies, we indicate that the thermodynamics strongly govern the surface reaction process during PJE.

Then, we describe the results of fabricating several kinds of strained-layer superlattices: InGaAs/GaAs, GaAs/GaP and InAs/InP. We show the results of structural characterization using X-ray diffraction (XRD). Optical properties by photoluminescence (PL) are also shown for the strained superlattices.

Finally, we comment on the technical points to which we have to pay attention in making atomically abrupt heterointerfaces using PJE. We cite the InAs/InP system as an

example, and discuss the appropriate gas switching procedure for making a superlattice with a high structural quality.

7.2 Binary Materials

In this section, the heteroepitaxy of binary compounds is reported. Our interest is in whether the self-limiting nature of PJE is still preserved for the heteroepitaxial systems. Generally, there exist some drawbacks at the heterointerfaces which lead to the collapse of layer-by-layer growth. The surface strain or dislocations due to lattice mismatch and the difference in surface free energy between substrates and epilayers might cause the three-dimensional (3D) growth. We discuss how these factors affect the self-limiting growth manner in PJE.

7.2.1 Growth results

7.2.1.1 GaAs on InAs

We studied the GaAs growth on InAs (001) substrates. The mole fractions of TMGa and AsH_3 were 2.1×10^{-3} and 4.8×10^{-2}. We repeated the gas introduction cycle 177 times. The thickness is 50 nm if the GaAs growth proceeds with a growth rate of 1 ML/cycle. We checked whether the growth is self-limiting or not by changing the TMGa pulse duration in a gas cycle. The growth temperature was 470°C and the pressure was 15 Torr. As shown in Fig. 7-1, we found that the growth was clearly self-limiting at about 1.1 to 1.2 ML/cycle (1 ML corresponds to 0.283 nm), independent of the TMGa exposure time. The surface morphology is fairly smooth from observation using a Nomarski microscope.

7.2.1.2 GaAs on InP

In Fig. 7-2, we show the results of GaAs growth on InP (001) at 485°C. Unlike the growth on InAs substrates shown in Fig. 7-1, the GaAs growth on InP (001) didn't show clear self-limiting. It seems that the growth tends to be saturated at around 1 ML/cycle below the

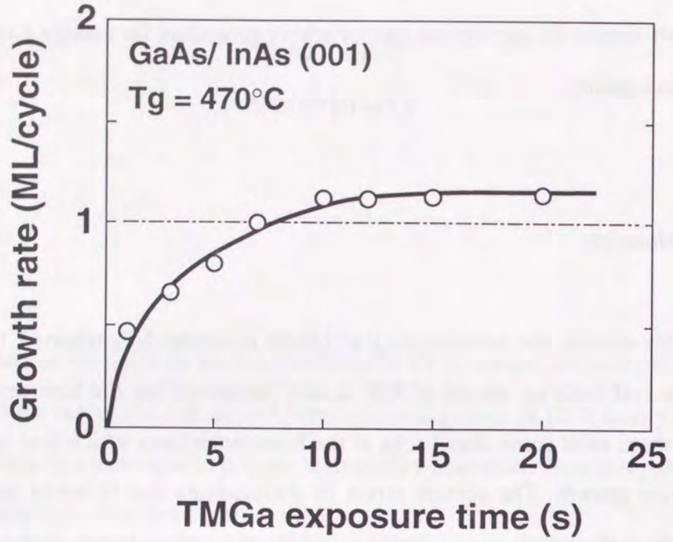

Figure 7-1. Dependence of GaAs growth rate on InAs (001) substrate as a function of TMGa pulse duration. The gas sequence of AsH_3/ H_2/ TMGa/ H_2 was 10/ 1/ x/ 1 s.

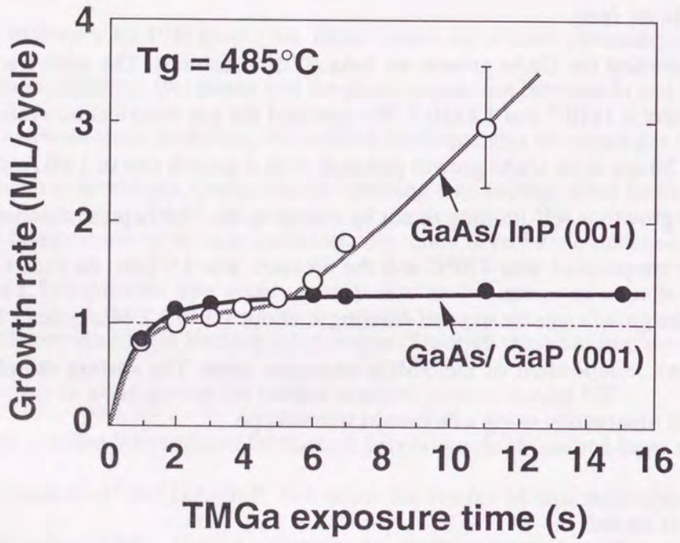

Figure 7-2. Dependence of GaAs growth rate on InP (001) and GaP (001) substrates as a function of TMGa pulse duration. The gas sequence of AsH_3/ H_2/ TMGa/ H_2 was 10/ 3/ x/ 3 s.

TMGa exposure time of 5 s. However, the growth rate drastically increased after 6 s of TMGa. The surface morphology of GaAs epitaxial layers grown on InP also depended on the TMGa pulse duration. Figure 7-3 shows Nomarski micrographs of the GaAs grown layers on InP substrates. While the surface displayed specular characteristics with a TMGa pulse of 3 s (Fig. 7-3 (a)), the surface morphology became rough under a 6 s TMGa pulse (Fig. 7-3 (b)). These results imply that the growth mode changes from two dimensional (2D) to 3D with increasing the TMGa pulse duration.

7.2.1.3 GaAs on GaP

The results on GaP (001) substrates are also shown in Fig. 7-2. Actually, GaP and InP substrates were set side-by-side on the same susceptor. For GaP (001) substrates, we observed self-limited growth over a whole range of TMGa exposure times. The saturation value reached 1.2 ML/cycle, probably resulting from the excess As adsorbed on the growth surface, as described in the previous chapter. The surface morphology of GaAs layers was always smooth, as shown in Fig. 7-4. These results are different from the results on InP substrates. Thus, the growth behavior and the surface morphology of heteroepitaxial growth of GaAs are evidently changed by the substrate materials.

7.2.1.4 GaAs on InGaP

Next, we tried GaAs growth by PJE on $In_{0.48}Ga_{0.52}P$ epilayers as the $In_{0.48}Ga_{0.52}P$ layers were prepared on the GaAs (001) substrates by chloride VPE, and the thickness of the alloy was about 3 μm. The thickness measurements of PJE-grown GaAs were made after removing a part of the GaAs top layers by selective wet chemical etching using 1 NH_4OH: 20 H_2O_2 solution. As shown in Fig. 7-5, we observed the GaAs growth self-limited at 1.2 ML/cycle. The surface morphology was always mirror-like.

7.2.1.5 GaP on GaAs

We also studied the heteroepitaxy of GaP on the GaAs (001) substrates. Growth was conducted at a temperature of 485°C and a pressure of 15 Torr. The repeated gas cycle was

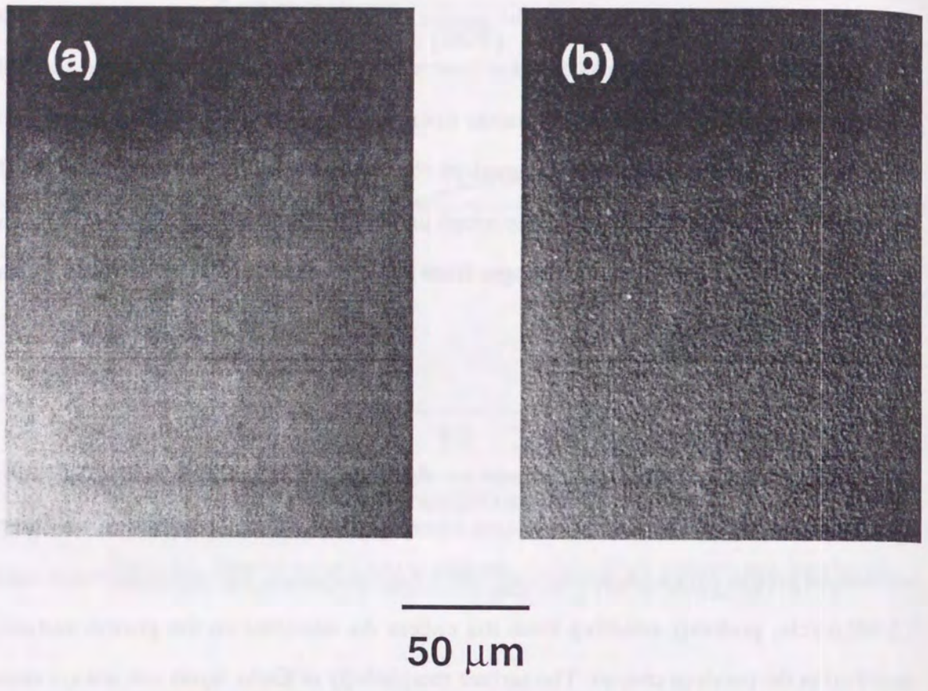

Figure 7-3. Surface morphologies of GaAs epitaxial layers grown on InP (001); (a) TMGa duration of 3 s, and (b) TMGa duration of 6 s.

Figure 7-4. Surface morphology of GaAs epitaxial layers grown on GaP (001).

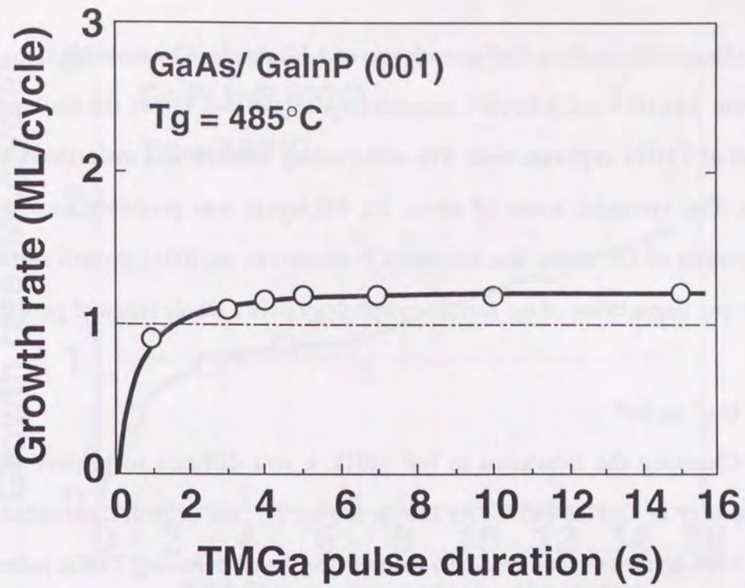

Figure 7-5. Dependence of GaAs growth rate on $Ga_{0.52}In_{0.48}P$ (001) as a function of TMGa pulse duration. The gas sequence of AsH_3/ H_2/ TMGa/ H_2 was 10/ 3/ x/ 3 s.

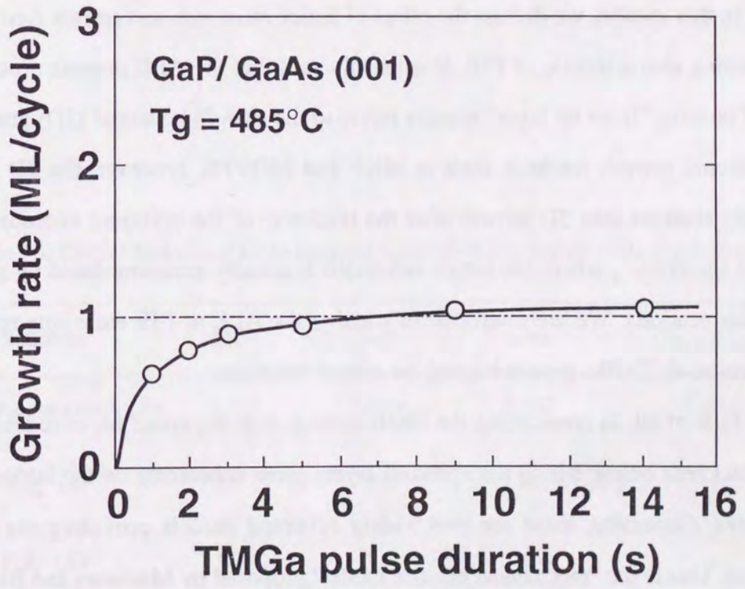

Figure 7-6. Dependence of GaP growth rate on GaAs (001) as a function of TMGa pulse duration. The gas sequence of PH_3/ H_2/ TMGa/ H_2 was 10/ 3/ x/ 3 s.

184, leading to 50 nm for a GaP growth rate of 1 ML/cycle. The mole fractions of TMGa and PH_3 were 2.1×10^{-3} and 9.6×10^{-2}, respectively. Figure 7-6 shows the GaP growth rate as a function of TMGa exposure time. The self-limiting manner was maintained for this hetero-system. The saturated value of about 1.1 ML/cycle was probably caused by the extra incorporation of Ga atoms due to excess P adsorption on (001) growth surface. We didn't observe any degradation of the surface morphology over a whole range of growth conditions.

7.2.1.6 GaP on InP

Changing the substrates to InP (001), it was difficult to achieve the self-limited heteroepitaxy of GaP at 485°C. As shown in Fig. 7-7, the growth rate tended to saturate at around 1 ML/cycle and then gradually increased with the increasing TMGa pulse duration. The surface morphology became rougher for longer TMGa exposure times. This growth behavior is similar to the GaAs on InP (001) described previously.

7.2.2 Effect of lattice mismatch and surface free energy

In this section, we discuss the effect of lattice mismatch and surface free energy on the self-limiting characteristic of PJE. It is usually said that the ALE process proceeds layer by layer. The term "layer by layer" usually refers to the two-dimensional (2D) growth mode. In conventional growth methods such as MBE and MOVPE, however, the 2D growth mode generally changes into 3D growth after the thickness of the epilayers exceeds the so-called "critical thickness", where the lattice mismatch is usually accommodated by generating the misfit dislocations. We are interested in whether the ALE or PJE technique really helps the continuation of 2D-like growth beyond the critical thickness.

First of all, in considering the heteroepitaxy, it is important for us to know the critical layer thickness below which the epitaxial layers grow coherently on the lattice-mismatched substrates. Generally, there are two widely accepted models providing the critical layer thickness. One is the "mechanical balance model" proposed by Matthews and Blakeslee [1, 2], and the other is the "energy balance model" by People and Bean [3]. If the strain-free lattice parameters of the epitaxial layer and the substrate are given as a_o and a_s, the lattice mismatch, f,

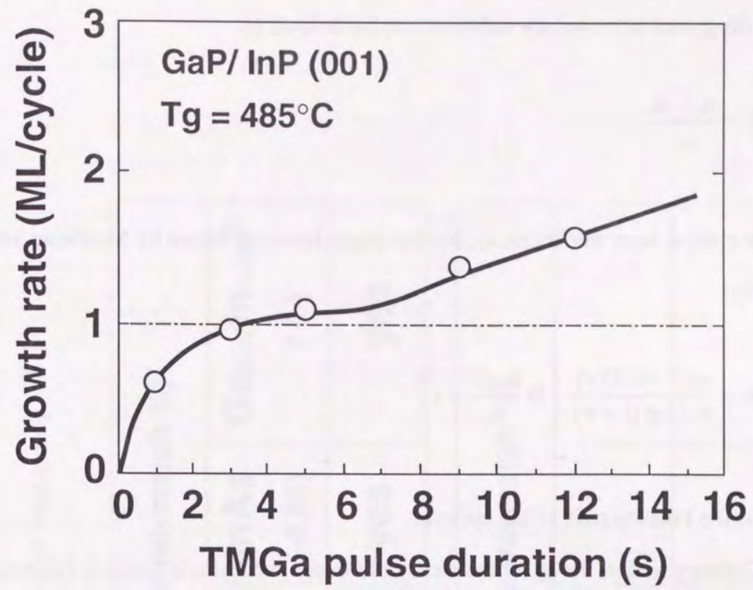

Figure 7-7. Dependence of GaP growth rate on InP (001) as a function of TMGa pulse duration. The gas sequence of PH_3/ H_2/ TMGa/ H_2 was 10/ 3/ x/ 3 s.

Table 7-1: Critical thickness of GaAs epitaxial layers grown on several kinds of substrates.

Substrate	GaP	InP	InAs	$Ga_{0.52}In_{0.48}P$
Lattice parameter (Å)	5.451	5.869	6.058	5.652
M.B. (Å)	13	14	0	∞
P.B. (Å)	31	32	0	∞

between the grown layer and the substrate can be defined as:

$$f = \frac{a_o - a_s}{a_s} \tag{7-1}$$

Then, the critical layer thickness, h_c, for the single heterostructure by Matthews and Blakeslee is given by:

$$h_c = \frac{a_o(1-0.25\nu)}{4\sqrt{2}\pi f(1+\nu)} \cdot \left(\ln \frac{h_c\sqrt{2}}{a_o} + 1 \right) \tag{7-2}$$

where ν is the Poisson ratio of the epilayer.

Contrary to this, the h_c by the theory of People and Bean is given as follows:

$$h_c = \frac{a_o(1-\nu)}{32\sqrt{2}\pi f^2(1+\nu)} \ln \frac{h_c\sqrt{2}}{a_o} \tag{7-3}$$

In Table 7-1, we have summarized the critical thicknesses of GaAs epitaxial layers on some kinds of substrates, calculated using the Matthews and Blakeslee (M.B.) model and the People and Bean (P.B.) model. We can see that the thicknesses of the grown layers shown in the previous section are far beyond the calculated critical thicknesses. Therefore, we have to recognize that the lattice mismatch will be almost accommodated by misfit dislocations in our experiments.

We have summarized our heteroepitaxy growth experiments in Table 7-2. We cannot find any significant relationship between the self-limiting growth and the degrees of lattice mismatch. Results imply that only InP substrates are not suitable for the self-limited heteroepitaxy of GaAs and GaP.

Next, we consider the effect of surface free energy. According to the basic theory of thin-film growth, the growth behavior of the overlayers is strongly influenced by the difference between the surface free energy of overlayers, γ_o, and that of the substrates, γ_s [4]. If $\gamma_o < \gamma_s$, the overlayers grow two-dimensionally on the substrates. On the other hand, if $\gamma_o > \gamma_s$,

Table 7-2: Summary of PIE growth results on GaAs and GaP heteroepitaxy.

Epilayer	Substrates (lattice-mismatch %)					
	GaAs (0)	GaP (+3.71)	InP (-3.68)	InAs (-6.69)	$Ga_{0.52}In_{0.48}P$ (0)	
GaAs	yes	yes	no	yes	yes	
Self-limiting	yes	yes	no	yes	yes	

Epilayer	Substrates (lattice-mismatch %)				
	GaAs (-3.58)	GaP (0)	InP (-7.12)		
GaP	yes	yes	no		
Self-limiting	yes	yes	no		

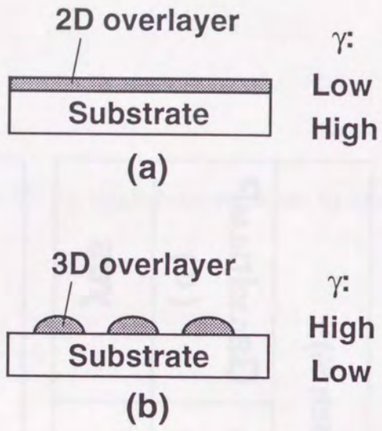

Figure 7-8. Schematic diagram showing: (a) two-dimensional growth mode and (b) three-dimensional growth mode, determined by the difference in surface free energy between substrate and overlayer.

Table 7-3: List of calculated surface free energy of III-V compounds. The surface orientation is (001).

	(001) surface
Materials	Surface free energy (erg/cm^2)
GaAs	3176.5
GaP	3790.9
InP	3210.0
InAs	2463.1
AlAs	3948.8

materials tend to grow three-dimensionally on the substrates. These behaviors are determined so as to minimize the total surface free energy of the system after growth (Fig. 7-8).

The surface of crystalline materials is considered to have a surface free energy corresponding to the amount of work needed to cleave the solid at a boundary to form two new ideal surfaces. The surface free energy, γ, can be calculated by the following formula under the assumption that the bonding energies of only the nearest-neighbor atoms are considered (the first-order assumption) [5]:

$$\gamma = \frac{n_{(hkl)}}{Z} \cdot \frac{N_{(hkl)}}{A_o} \cdot \Delta H \qquad (7\text{-}4)$$

Here, Z is the number of nearest-neighbor atoms, $n_{(hkl)}$ is the number of nearest-neighbor atoms which would be broken when the solid is cleaved in the (hkl) plane, $N_{(hkl)}$ is the atomic density of the solid in the (hkl) plane, A_o is the Avogadro constant (6.02×10^{23}), and ΔH is the latent sublimation heat.

In Table 7-3, we have summarized the calculated surface free energy of some III-V compounds. The surface orientation is (001) for all materials. As seen in the table, we cannot explain whether the system is self-limiting or not in terms of the surface free energy of the substrates and the epitaxial layers.

Thus, we cannot find any accurate factors to explain the self-limiting growth for heteroepitaxial systems. Our results simply imply that the InP (001) substrate surface is different from others. Because the Ga atoms from TMGa will be accumulated at a part of the surface in an early stage of the growth process, the InP (001) surface will continuously provide the activated sites of adsorption and decomposition for the incident TMGa (Fig. 7-9). To reveal the mechanism, we need to study the nature of the InP (001) surface and the initial stage of nucleation in detail from a more atomistic point of view.

7.3 Ternary Systems

In this section, we report our efforts to grow some ternary compounds using PJE. The growth of ternary materials is inevitably needed to make some practical device structures. So far, however, few studies have been reported the growth of ternary compounds using ALE. This seems to be mainly due to the discrepancy in the appropriate growth temperatures for the self-limited growth between binary materials. We also faced these growth temperature problems in our PJE method. From the viewpoint of growth kinetics, we have verified that the self-limiting growth in PJE can be explained by a simple selective adsorption model for the homoepitaxial growth of binary III-V materials [6, 7]. However, for ternary compounds, surface reaction kinetics seem to be more complicated due to the surface strain induced by lattice mismatch with the substrate underneath, and to the exchange reactions between atoms on the surface and subsurface layers. In particular, we found other specific problems related to the phase separation and compositional latching in our ternary studies [8].

7.3.1 InGaP on GaAs

$In_xGa_{1-x}P$ is an important material because it can be lattice-matched to GaAs with the composition of $In_{0.49}Ga_{0.51}P$ and has a direct transition of about 1.92 eV at the Γ point of the energy band. Recently, $In_xGa_{1-x}P$ has been commonly used instead of $Al_xGa_{1-x}As$ because high purity epitaxial layers can be easily prepared in MOVPE. Here, we discuss the specific phenomenon, that is, the phase separation of epitaxial layers, which we found in the growth of $In_xGa_{1-x}P$ by PJE.

7.3.1.1 Growth schemes

Table 7-4 summarizes the typical PJE growth conditions for binary compounds. The Ga-based materials, GaAs and GaP, exhibit self-limiting at around 485 to 500°C. On the other hand, the In-based materials, InAs and InP, show self-limiting at much lower temperatures of around 350°C. Therefore, we have to search for an appropriate method for growing $In_xGa_{1-x}P$ alloy. We tried the following two kinds of approaches:

(1) A way to grow both InP and GaP at 485°C, using TMIn, TMGa and PH_3. The gas

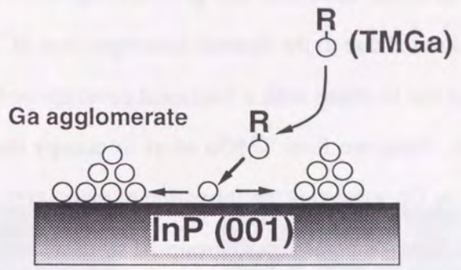

Figure 7-9. Speculated illustration of TMGa exposure period during early stage of GaAs growth on InP (001).

Table 7-4: Typical PJE growth conditions for binary compounds.

Orientation : (001)

Materials	Saturation Value (ML)	Growth Temp. (°C)	Source Materials
InP	0.5	350 °C	TMIn + PH_3
InAs	1	350°C	TMIn + AsH_3
GaP	1	485 °C	TMGa + PH_3
GaAs	1	500 °C	TMGa + AsH_3
AlAs	2	500 °C	TMAl + AsH_3

sequence is TMIn → TMGa → PH_3. The H_2 purge pulses are inserted after each reactant. The GaP growth is self-limited at this growth temperature [7]. Conversely, the growth of InP is not self-limited due to the thermal decomposition of TMIn in the boundary layer [9]. We first deposit the In atoms with a fractional coverage on the GaAs (001) substrate by the TMIn injection. Next, we flow TMGa so as to occupy the unoccupied surface group-III sublattice sites by Ga, expecting the formation of monolayer of an In and Ga metal plane in a self-limiting manner. Then the mixed group-III surface layer reacts with PH_3.

(2) A way to grow GaP and InP at 350°C, using TEGa, TMIn and PH_3. The gas sequence is TEGa → (PH_3) → TMIn → PH_3. We cannot obtain self-limiting GaP growth using TEGa, while the InP is self-limited at 0.5 ML/cycle with TMIn source. Therefore, the GaP growth must be controlled by regulating the TEGa flow rate and the length of the TEGa pulse.

7.3.1.2 Phase separation and effect of growth temperature

In accordance with Scheme (1), we grew $In_xGa_{1-x}P$ on GaAs (001). We chose a mole fraction and pulse duration of TMGa corresponding to a monolayer growth of GaP. The TMIn flow rate was changed in order to control the In content of $In_xGa_{1-x}P$ alloy. Figure 7-10 shows a typical scanning electron microscope (SEM) image of the growth surface. We observed the white-imaged clusters or islands on the growth surface with a smooth texture, and could not obtain any mirror-like morphology (Fig. 7-10 (a)). The coverage of the islands increased and the islands became elongated as the TMIn flow rate increased (Fig. 7-10 (b)).

To study the local compositions of the grown layers, we analyzed the surface using microprobe Auger analysis, or scanning Auger electron microscope (SAM). The Auger spectra are shown in Fig. 7-11. The spectrum of Fig. 7-11 (a) is from the smooth texture of 2D growth mode, and the spectrum of Fig. 7-11 (b) is from the surface island. Results indicate that the composition of surface islands is In-rich, while the texture is Ga-rich. Thus, most of the indium atoms supplied on the surface do not seem to incorporate into the surface lattice sites. In other words, the $In_xGa_{1-x}P$ alloy showed immisibility or phase separation into In-rich and Ga-

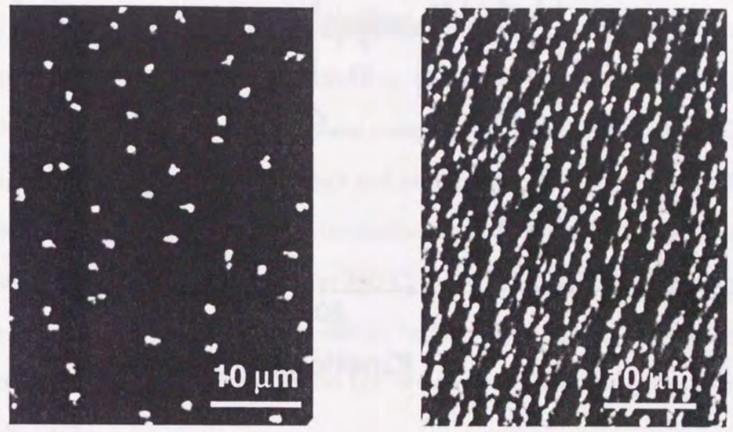

Figure 7-10. SEM image of InGaP layers grown at 485°C; (a) small TMIn flow rate and (b) large flow rate.

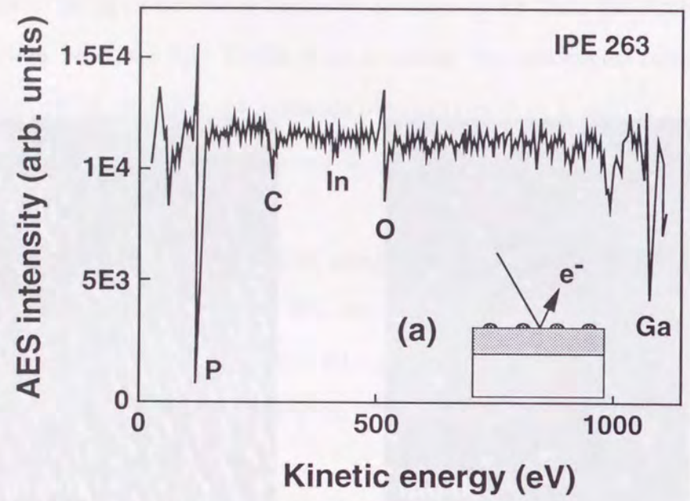

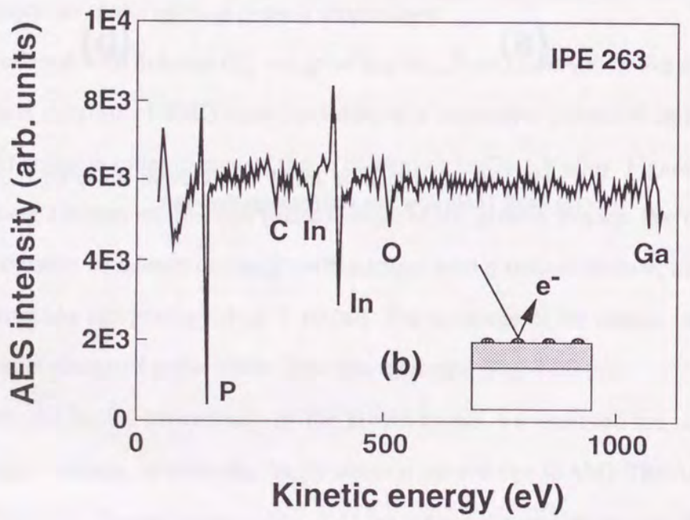

Figure 7-11. Auger spectra of PJE-grown InGaP surfaces measured at: (a) two-dimensional texture and at (b) surface islands.

rich compositions.

We quantitatively studied the local composition of the Ga-rich textures of $In_xGa_{1-x}P$ layers using Raman scattering measurements. The light source was Ar^+ laser with a wavelength of 488 nm. The Raman measurement was conducted under backscattering arrangement. The composition was determined by the frequency of the longitudinal optical (LO) phonon of $In_xGa_{1-x}P$ using data obtained by Inoshita *et al.* [10]. Figure 7-12 shows the composition at a 2D layer of $In_xGa_{1-x}P$ versus the TMIn flow rate during the gas sequence. Although the surface morphology became rougher with the increasing TMIn flow rate due to the increase in the density of In-rich surface islands, the chemical composition of the 2D layer remained constant at $In_{0.18}Ga_{0.82}P$. This is an interesting result and implies that the composition of the Ga-rich, two-dimensional $In_xGa_{1-x}P$ layer might be determined mainly by the thermodynamics.

Lowering the growth temperature to 350°C, we found that the $In_xGa_{1-x}P$ grown layers had a more specular surface than those at 485°C. Figure 7-13 compares the $In_xGa_{1-x}P$ surface morphologies grown under Schemes (1) and (2). We could not observe any surface islands on the surface at 350°C.

Figure 7-14 shows the variation of the composition of $In_xGa_{1-x}P$ as a function of the TEGa pulse duration under the gas sequence of Scheme (2). The gas introduction cycle was 177. PH_3 was inserted between TEGa and the TMIn pulse in this case. The growth thickness was also shown in the figure. The TMIn and PH_3 pulses were sent to deposit InP with 0.5 ML/cycle. The composition of the epitaxial layers was calculated by the $In_xGa_{1-x}P$ LO phonon frequency in Raman measurements. We found that we can control the Ga content by changing the TEGa pulse duration, clearly indicating no self-limiting for Ga deposition with TEGa. This implies that the immisibility problem is not severe at 350°C.

Figure 7-15 shows the dependence of the $In_xGa_{1-x}P$ growth thickness on the TMIn pulse duration in Scheme (2). The TEGa pulse and the flow rate was fixed to deposit Ga at 0.5 ML/cycle on the surface. The PH_3 gas was inserted between the TEGa and TMIn in Mode #A. The TEGa and TMIn were supplied sequentially in Mode #B. Results show that In deposition was almost self-limited at 0.5 ML/cycle in Mode #A, and the experimental growth rate was almost the expected value, shown as a broken line. However, in the Mode #B, the In

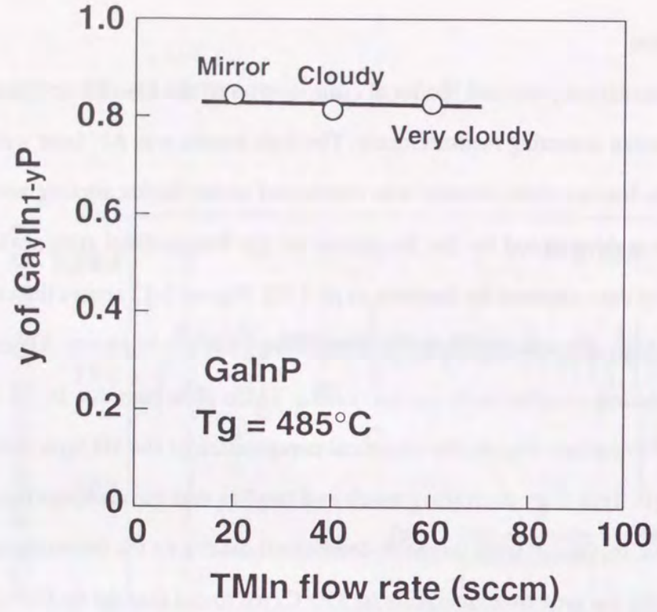

Figure 7-12. Variation of composition of two-dimensional GaInP layer versus TMIn flow rate. The composition was determined from the LO phonon frequency. TMIn and TMGa was kept at 13.5°C and 3.0°C. The flow rates of TMGa and 20% PH_3 were 40 sccm and 240 sccm. The sequence of H_2/ TMIn/ H_2/ TMGa/ H_2/ PH_3 was 5/ 3/ 3/ 5/ 5/ 10 s.

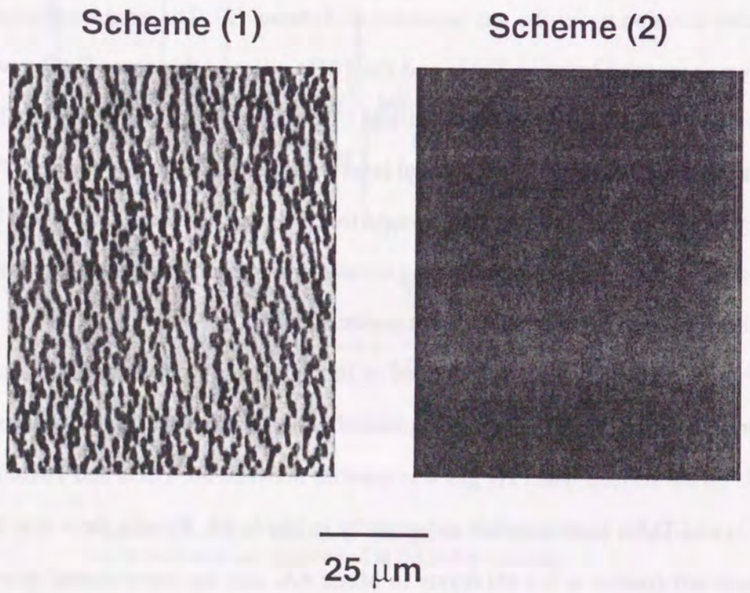

Figure 7-13. Nomarski micrographs of InGaP surface morphologies grown under Scheme (1) and (2).

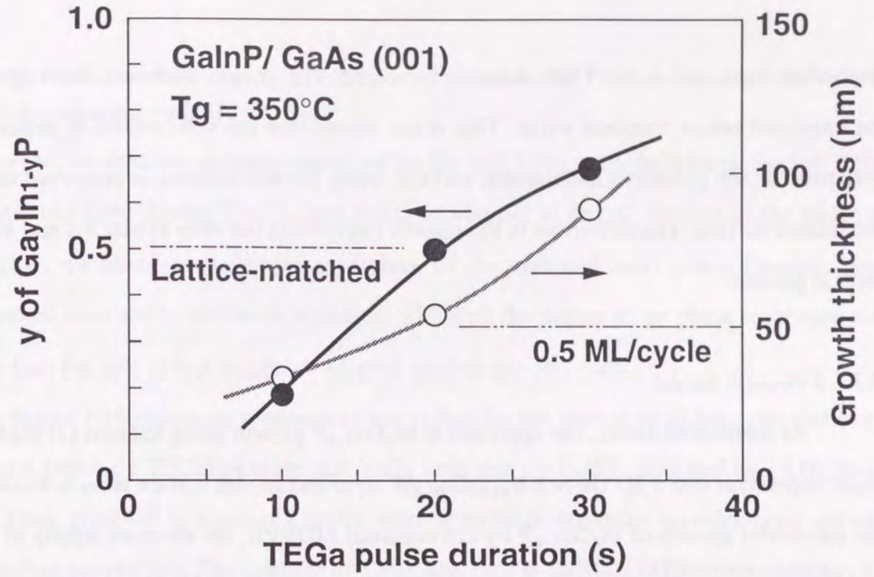

Figure 7-14. Variation of InGaP composition and the growth rate as a function of TEGa pulse duration under the sequence of scheme (2). The TMIn and TEGa was kept at 27.1°C and 0.0°C and the flow rates were 60 sccm and 40 sccm, respectively. The flow rate of 20% PH_3 was 480 sccm. Gas sequence of InP growth: H_2/ TMIn/ H_2/ PH_3 was 5/ 3/ 5/ 20 s and that of GaP: H_2/ TEGa/ H_2/ PH_3 was 5/ 20/ 5/ 20 s.

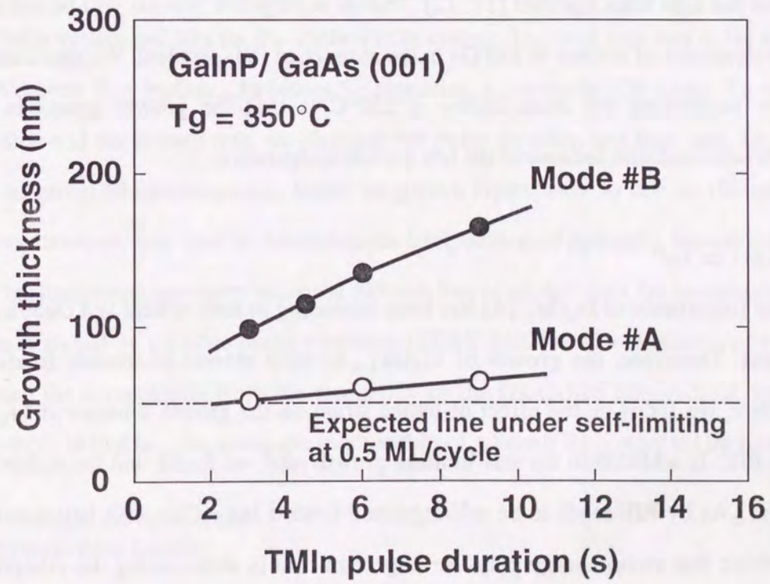

Figure 7-15. Dependence of InGaP growth thickness on TMIn flow rate in the Scheme (2). The source gas conditions were the same as those in fig. 7-14. The sequence of Mode #A; (H_2/ TMIn/ H_2/ PH_3)(H_2/ TEGa/ H_2/ PH_3) was (5/ x/ 5/ 20 s)(5/ 20/ 5/ 20 s). The sequence of Mode #B: H_2/ TEGa/ H_2/ TMIn/ H_2/ PH_3 was 5/ 20/ 3/ x/ 5/ 20 s.

deposition increased as the TMIn duration increased. The growth thickness didn't agree with the expected lattice-matched value. This result shows that the self-limited In deposition is collapsed on the partially Ga-deposited surface, while the self-limiting is preserved on the P-terminated surface. The difference in the growth mechanism between Modes #A and #B is not clear at present.

7.3.1.3 Growth model

As mentioned above, our approach to $In_xGa_{1-x}P$ growth using Scheme (1) leads to the phase separation into a 2D Ga-rich $In_{0.18}Ga_{0.82}P$ layer and In-rich surface islands. Considering the successful growth of $In_xGa_{1-x}P$ by conventional MOVPE, the alternate supply of In, Ga, and P atoms in our PJE causes the immisibility of In and Ga at 485°C. When the Ga atoms are supplied in the form of TMGa to the GaAs (001) substrate after the TMIn injection, most of the surface In atoms previously deposited will be clustered and then segregated at the surface. As a result, the surface is almost covered with Ga atoms two dimensionally. The surface segregation of In atoms has also been reported [11, 12]. This In segregation process will be controlled by the thermodynamics of surface In and Ga in the absence of PH_3 ambient. We speculate that the reason for neglecting the immisibility at 350°C is that the growth proceeds under a nonequilibrium condition because of the low growth temperature.

7.3.2 InGaAs on InP

The importance of $In_xGa_{1-x}As$ has been increasing in both optical and electrical device applications. Therefore, the growth of $In_xGa_{1-x}As$ with atomic dimension is also highly needed. Here, we focus on the effect of lattice strain on the growth kinetics of $In_xGa_{1-x}As$ grown by PJE. In addition to the self-limiting growth rate, we found that the composition of thin $In_xGa_{1-x}As$ by PJE tends to be self-regulated toward $In_{0.53}Ga_{0.47}As$ lattice-matched to InP. We think that strain energy plays an important role in determining the composition of $In_xGa_{1-x}As$ grown by PJE. Thus far, there are only a few reports about the strain effect on kinetics in growth from the vapor phase [13, 14]. PJE appears to be useful in the study of detailed surface reaction kinetics such as the strain effect.

7.3.2.1 Gas sequence and experimental

First, we tried the alternate supply of In, Ga and As to grow InGaAs on the InP (001) substrate, using the TMIn, TMGa, and AsH_3 as sources at 485°C. Similar to the result of $In_xGa_{1-x}P$, we observed the phase separation of the epitaxial layer into a Ga-rich, two-dimensional layer and In-rich surface islands. Although the degree of the phase separation was weaker than the case of $In_xGa_{1-x}P$, we adopted another gas sequence.

Figure 7-16 shows the sequence of gas pulses for the growth of $In_xGa_{1-x}As$ epilayers. TMIn and TMGa (or TEGa) mixtures and AsH_3 were sent cyclically, separated by 3 s H_2 purge flows. Thus, group-III and group-V atoms were alternately deposited layer-by-layer without any vapor-phase reaction. The cylinder of TMIn was kept at 13.5°C (TMIn vapor pressure: 1.0 mmHg) in the experiments for the TMIn-TMGa system and 5.5°C (TMIn vapor pressure: 0.5 mmHg) for TMIn-TEGa. The cylinders of TMGa and TEGa were kept at 3.0°C (TMGa vapor pressure: 79.4 mmHg) and 11.0°C (TEGa vapor pressure: 2.5 mmHg). The flow rate of 10% AsH_3 was fixed at 480 sccm throughout experiments, and its pulse duration was 10 s for the TMIn-TMGa system and 20 s for the TMIn-TEGa system. The total flow rate in the reactor was 2 slm. We grew thin $In_xGa_{1-x}As$ layers by repeating a gas cycle 170 times. To change the composition and the growth rate, we changed the pulse duration and flow rate, *i.e.*, the mole fraction of group-III metalorganics. Since the grown layers were as thin as 100 nm at most, Raman spectroscopy was used to determine the composition of epilayers. Measurements were made in backscattering geometry using the 488-nm line of an Ar^+ laser for excitation. Scattered light was analyzed by a double monochromator (SPEX 1403) with a resolution of 1 cm^{-1}. We determined the composition from the frequency of the GaAs-like longitudinal optical (LO) phonon, ω_{LO}, in $In_xGa_{1-x}As$, using the relationship of x versus ω_{LO} reported by Inoshita [10].

7.3.2.2 Composition latching

(a) TMIn-TMGa system

We studied the growth of $In_xGa_{1-x}As$ using TMIn and TMGa as group-III sources [8].

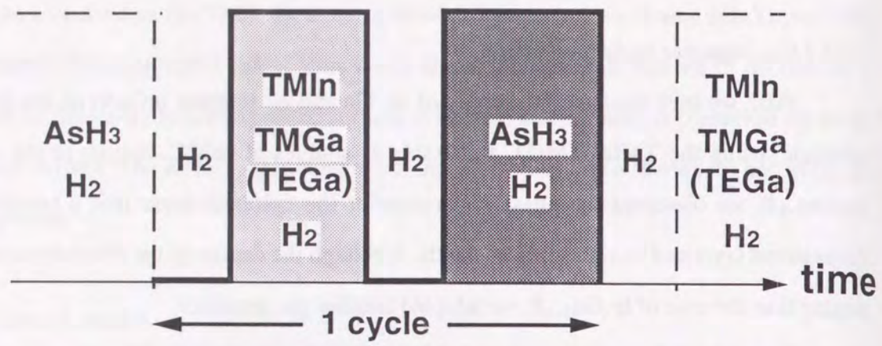

Figure 7-16. Sequence of source gas pulses for $In_xGa_{1-x}As$ growth.

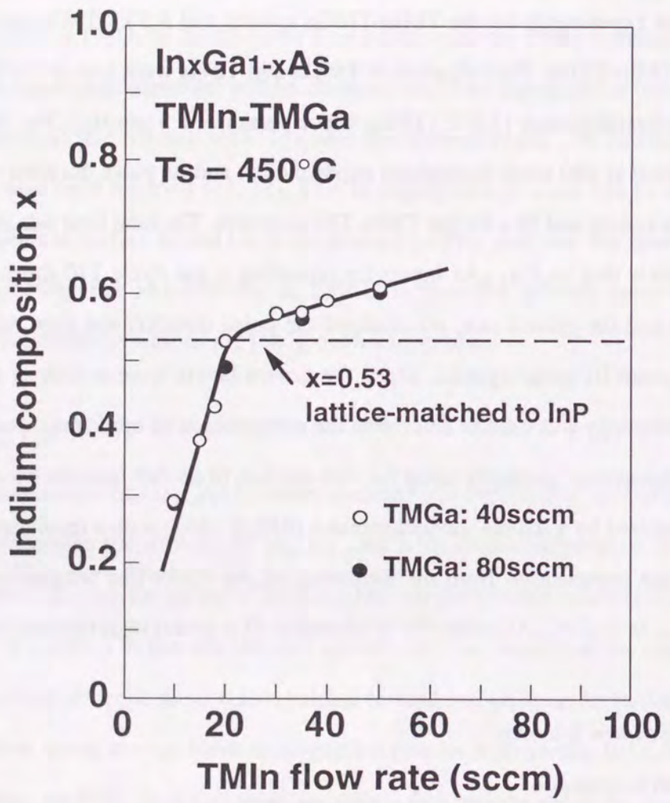

Figure 7-17. Dependence of In composition of $In_xGa_{1-x}As$ on TMIn flow rate. The TMGa flow rate was 40 sccm for open circles, and 80 sccm for solid circles.

The growth temperature and pressure were 450°C and $2.0x10^3$ Pa. Figure 7-17 shows the dependence of the In composition of the epitaxial layers on the TMIn flow rate. Here, the metalorganics and AsH_3 pulse durations are fixed at 2 s and 10 s. As the TMIn concentration in the vapor increased, the rate of increase of In composition in the solid was significantly reduced after the flow rate reached a value corresponding to x=0.53, that is, a lattice-matched composition. Since the growth thickness of the samples at around x=0.53 was almost same as the critical thickness calculated by Matthews and Blakeslee's force balance model [1], the lattice mismatch with InP substrates will be mostly accommodated by elastic strain. The residual elastic strain in the epilayers can be considered to shift the frequency of the GaAs-like LO phonon, ω_{LO}, and the composition dependence on TMIn may fluctuate. If we assume lattice mismatch to be perfectly accommodated by elastic strain, ε, the relationship between ε and the frequency shift $\Delta\omega_{LO}$ is given by

$$\frac{\Delta\omega_{LO}}{\omega_{LO}} = \frac{1}{3}\left(\frac{S_{11}+2S_{12}}{S_{11}+S_{12}}\cdot\tilde{K}_H - \frac{S_{11}-2S_{12}}{S_{11}+S_{12}}\cdot\tilde{K}_S\right)\cdot\varepsilon, \qquad (7\text{-}5)$$

where S_{11} and S_{12} are the elastic compliance constants and $\tilde{K}_H$ and $\tilde{K}_S$ the hydrostatic and shear phonon deformation potentials [15]. Data provided by Inoshita [10] shows ω_{LO} to be approximately proportional to x beyond 0.3 as

$$\omega_{LO}(cm^{-1}) = 39.8x + 251.4. \qquad (7\text{-}6)$$

From Eqs. (7-5) and (7-6), we learn the error in the composition, Δx, is proportional to the elastic strain. Therefore, the bending dependence shown in Fig. 7-17 cannot be explained just by the frequency shift by strain. The composition tends to be controlled automatically by the composition-latching effect toward $In_{0.53}Ga_{0.47}As$, lattice-matched to InP, on the compressive side.

Figure 7-18 shows the growth rate of $In_xGa_{1-x}As$ grown by PJE as a function of the TMIn flow rate. Here, the growth rate was plotted by dividing the growth thickness per cycle by half a lattice parameter of InP. Note that the latching observed in Fig. 7-17 occurs at growth

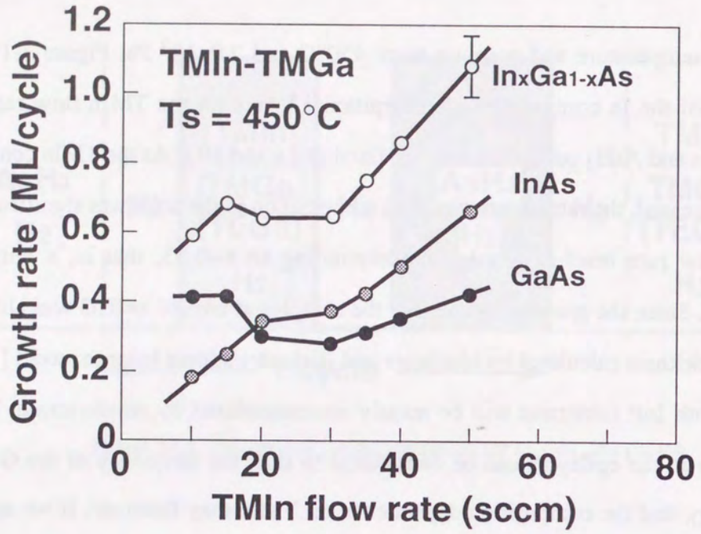

Figure 7-18. $In_xGa_{1-x}As$ growth rate as a function of TMIn flow rate. TMGa flow rate was 40 sccm. InAs and GaAs growth rate were calculated from x value. The group-III pulse duration was 2 s.

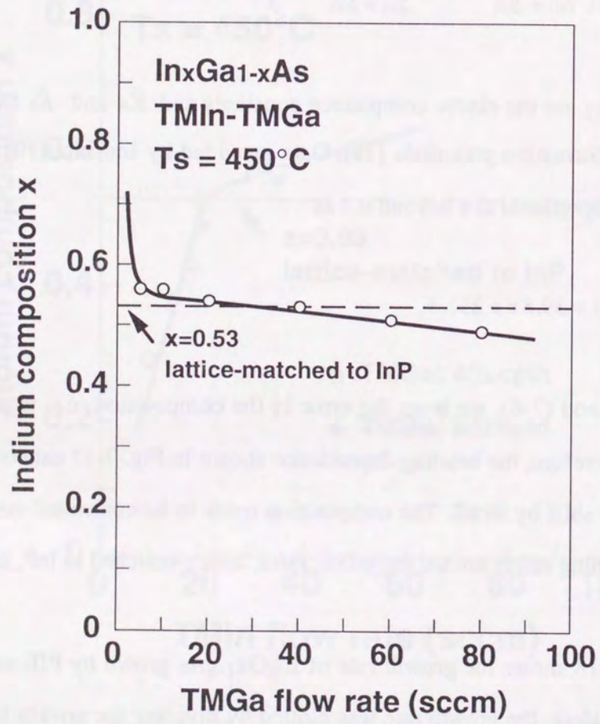

Figure 7-19. Dependence of In composition of $In_xGa_{1-x}As$ on TMGa flow rate under a TMIn flow rate of 20 sccm. The group-III pulse duration was 2 s.

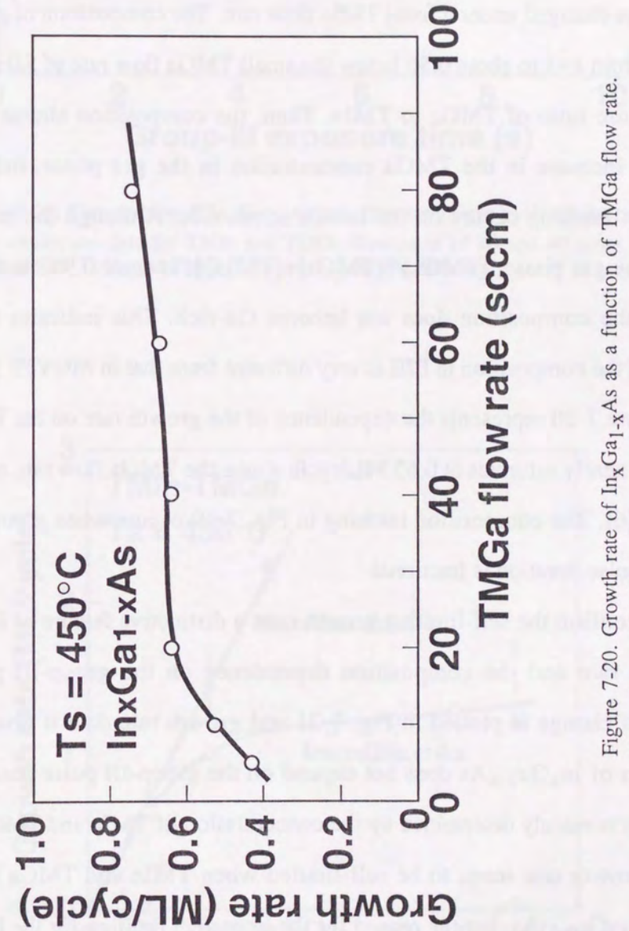

Figure 7-20. Growth rate of $In_xGa_{1-x}As$ as a function of TMGa flow rate. TMIn flow rate is 20 sccm.

rates below 1 ML/cycle. The $In_xGa_{1-x}As$ growth rate was distributed into InAs and GaAs components, the results also being shown in the figure. The InAs growth rate in $In_xGa_{1-x}As$ increases with the TMIn flow rate. The GaAs growth rate does not remain constant despite the fixed TMGa flow rate. This implies that the Ga incorporation rate into epilayers is affected by the In atom concentration on the growth surface or by surface lattice strain.

Figure 7-19 shows the variation of the In composition of epilayers when the TMGa flow rate was changed under a fixed TMIn flow rate. The composition of grown layers changed drastically from x=1 to about 0.56 below the small TMGa flow rate of 5.0 sccm due to the large vapor pressure ratio of TMGa to TMIn. Then, the composition almost saturated at x=0.53 despite the increase in the TMGa concentration in the gas phase, indicating that a clear composition latching occurs on the tensile stress side. Although the mole fraction ratio of TMGa in the gas phase, [TMGa]/{[TMGa]+[TMIn]}, is from 0.952 to 0.996 in the data for Fig. 7-19, the composition does not become Ga-rich. This indicates that the mechanism determining the composition in PJE is very different from that in MOVPE [16].

Figure 7-20 represents the dependence of the growth rate on the TMGa flow rate. The growth rate nearly saturates at 0.65 ML/cycle above the TMGa flow rate of 20 sccm, as seen in GaAs PJE [6]. The composition latching in Fig. 7-19 occurs when group-III metal coverage during the pulse duration is fractional.

To confirm the self-limiting growth rate, a distinctive feature of ideal PJE, we studied the growth rate and the composition dependence on the group-III pulse duration. The composition change is plotted in Fig. 7-21 and growth rate data is given in Fig. 7-22. The composition of $In_xGa_{1-x}As$ does not depend on the group-III pulse duration above 2 s. The composition is mainly determined by the concentration of TMIn and TMGa. As shown in Fig. 7-22, the growth rate tends to be self-limited when TMIn and TMGa flow rates are set to deposit $In_{0.53}Ga_{0.47}As$, but the reason for the imperfect limiting for the $In_{0.53}Ga_{0.47}As$ is not clear. On the other hand, the growth rate increases linearly with the exposure time for the epitaxial layers lattice-mismatched with InP substrates. The surface morphology became rougher for this case as the pulse duration increased. The result in Fig. 7-22 indicates that the self-limiting growth of $In_xGa_{1-x}As$ by PJE is very sensitive to surface conditions such as lattice

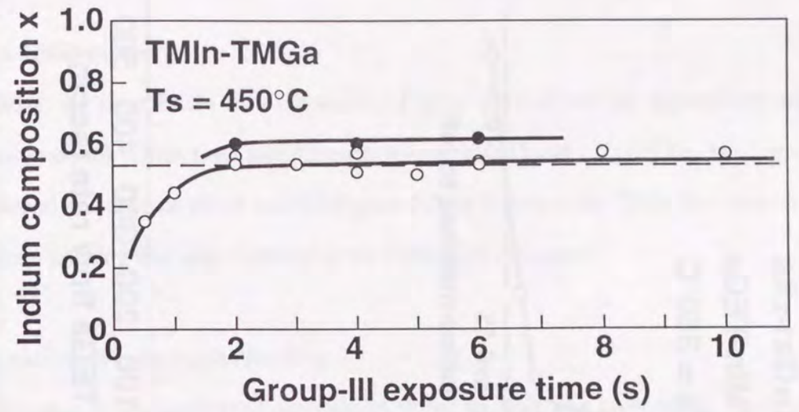

Figure 7-21. Composition of $In_xGa_{1-x}As$ as a function of group-III exposure time. Open circles are data for TMIn and TMGa flow rates of 20 and 40 sccm. Solid circles are for TMIn and TMGa flow rates of 50 and 80 sccm.

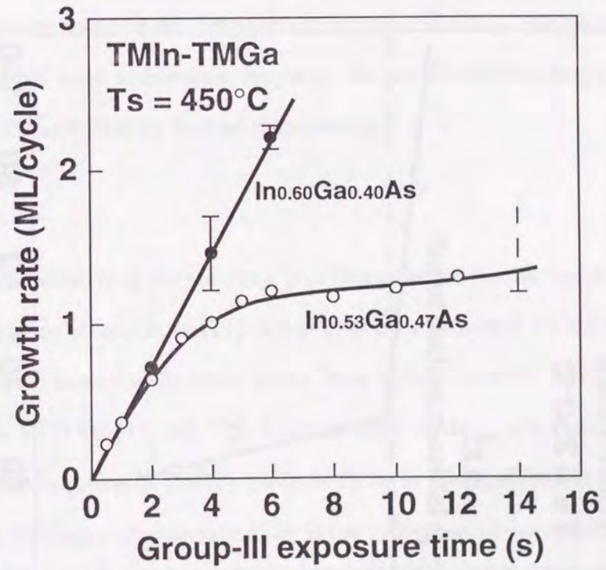

Figure 7-22. Growth rate of $In_xGa_{1-x}As$ as a function of group-III exposure time. Flow rate conditions are the same as in fig. 7-21.

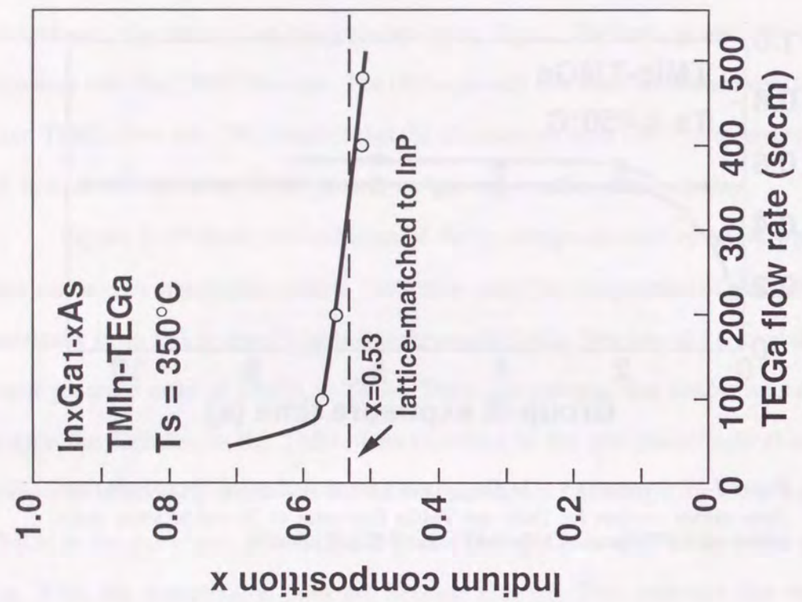

Figure 7-24. Variation of In composition as a function of TEGa flow rate. The pulse duration of TMIn and TEGa mixture was 5 s. TMIn flow rate was 30 sccm.

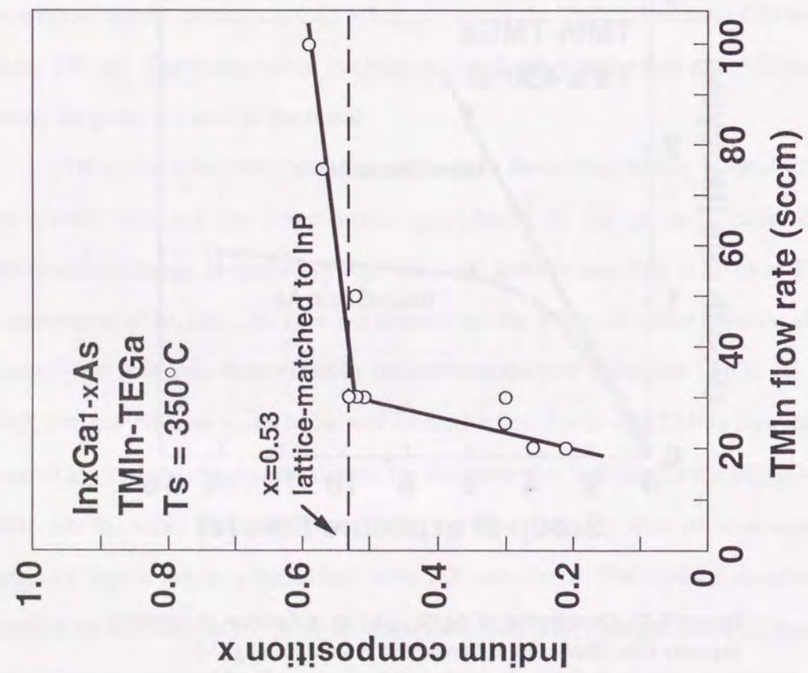

Figure 7-23. Dependence of In composition on TMIn flow rate. TEGa flow rate was 400 sccm. The group-III pulse duration was 5 s.

strain and the existence of clusters.

(b) TMIn-TEGa system

Next, we used TEGa as a Ga source. Figure 7-23 shows the dependence of the In composition on the TMIn flow rate. Growth was at 350°C and 2.7×10^3 Pa. The slope of the plot apparently changes at about x=0.53. Figure 7-24 is x versus the TEGa flow rate. Apparent composition latching was also observed in the TMIn-TEGa system.

(c) AES analysis of composition latching

We also investigated the composition of the $In_xGa_{1-x}As$ layer using Auger electron spectroscopy (AES). In this method, we don't have to pay attention to the strain effect in determining the chemical composition of epilayers. Figure 7-25 shows the dependence of the measured AES intensity ration of Ga/As and In/As on the TMIn flow rate. The samples were the same as those shown in Fig. 7-17. We clearly observed the composition latching at a TMIn flow rate of 20 sccm, in good agreement with the result in Fig. 7-17. However, it was difficult to determine the absolute value of the composition because the relative sensitive factors (RSF) of constituent elements were ambiguous. Anyway, we confirmed the composition latching phenomena using AES as well as by Raman spectroscopy

(d) Growth model

The composition-latching phenomenon was first reported for the liquid-phase epitaxial (LPE) growth of $In_xGa_{1-x}P$ on GaAs [17]. It has also been observed for the LPE growth of $In_xGa_{1-x}As$ on InP [18] as well as for other alloys. Few reports exist for vapor-phase epitaxial techniques, such as MOVPE [13, 14]. The fact that clear latching occurs in growth by PJE implies that PJE growth proceeds under situations close to thermodynamic equilibrium like LPE. We think that the degree of supersaturation in the PJE growth environment, considered to be a qualitative measure of the disparity from perfect thermodynamic equilibrium, is low because of the inherent self-limiting deposition of group-III and group-V atoms. Therefore, the growth rate is so low that the thermodynamic equilibrium conditions are more likely to be

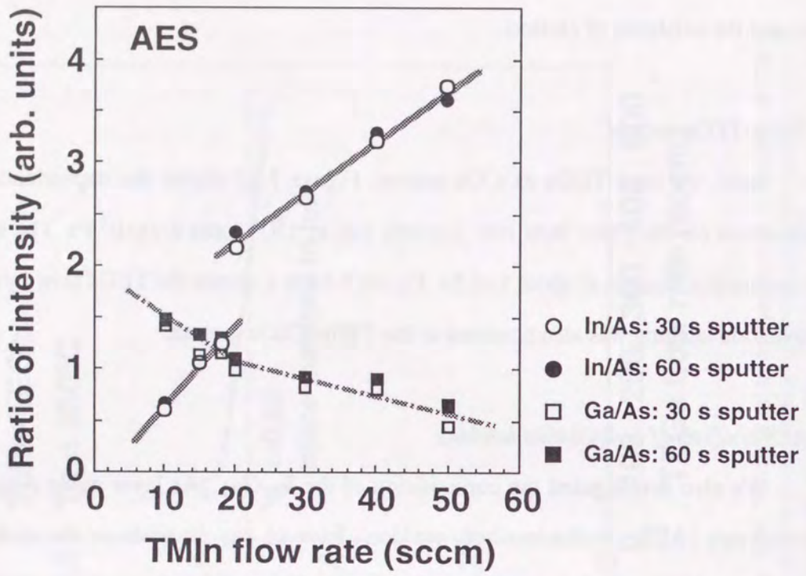

Figure 7-25. Dependence of AES intensity ratio of PJE-grown $In_xGa_{1-x}As$ on TMIn flow rate.

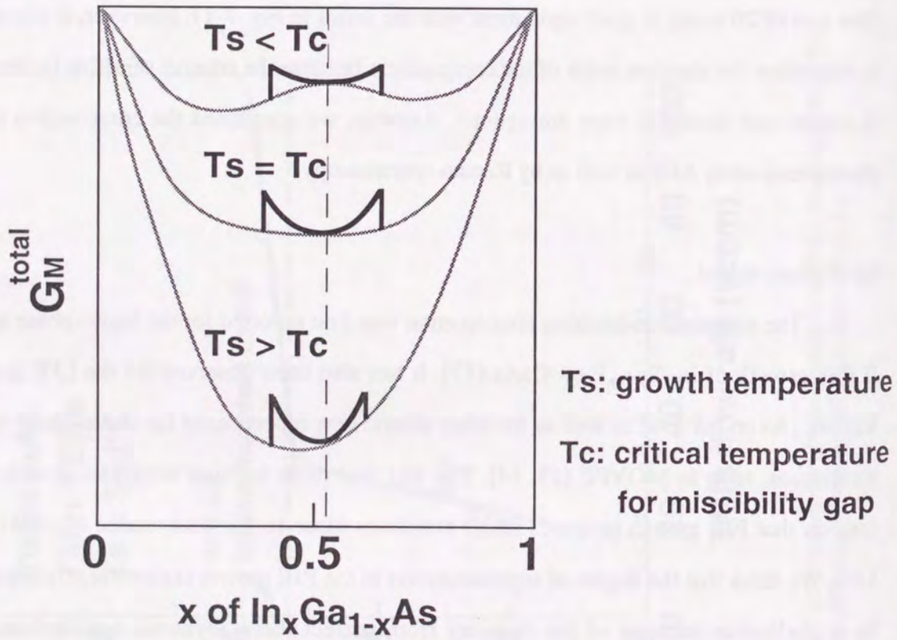

Figure 7-26. Schematics of mixing free energy for $In_xGa_{1-x}As$ in the regular solution approximation. Both stabilizing (Ts < Tc) and latching effects (Ts > Tc) can be deduced from these figure.

established at the interface. As proposed by Stringfellow [17], we believe that the strain energy of epilayers due to lattice mismatch, G_M^{st}, must be added to the excess free energy of mixing, G_M^{e}, and this strain energy perturbs solid composition toward lattice match to minimize the total free energy of the solid phase in $In_xGa_{1-x}As$ growth by PJE. The total excess free energy of epilayers, G_M^{total}, is written as,

$$G_M^{total} = G_M^{e} + G_M^{st} + G_M^{dis} \tag{7-7}$$

where G_M^{dis} is the contribution of dislocation energy due to the strain-relieving mechanism [19]. The most important factor of the strain energy can be expressed as [20]

$$G_M^{st} = \sigma\left(\frac{\Delta a}{a_s}\right)^2 \tag{7-8}$$

where a_s is a substrate lattice parameter and Δa is the difference in lattice parameter between the epilayer and substrate. σ is

$$\sigma = 2C \cdot \left\{\frac{(1+\nu)}{(1-\nu)}\right\} \cdot V_m \tag{7-9}$$

where C is the interface shear modulus of the epitaxial layer, ν the Poisson ratio, and V_m the molar volume of the layer. Although the value of G_M^{st} is about 10% of the excess free energy of mixing of unstrained layers, the strain energy has a major effect on the solid composition as calculated by Stringfellow [17]. Nahory *et al.* and Quillec *et al.* also reported that latching should be effective in the vicinity of the miscibility gap (Fig. 7-26), where the change of total free energy with composition is so small that the strain energy dominates the solid composition [21, 22]. Growth temperatures under which we found latching are in the predicted region of composition latching for $In_xGa_{1-x}As$ [22].

In PJE, growth is dominated by reactions at the gas-solid interface. For a binary compound like GaAs, Ozeki *et al.* assumed that the adsorption, desorption, and decomposition

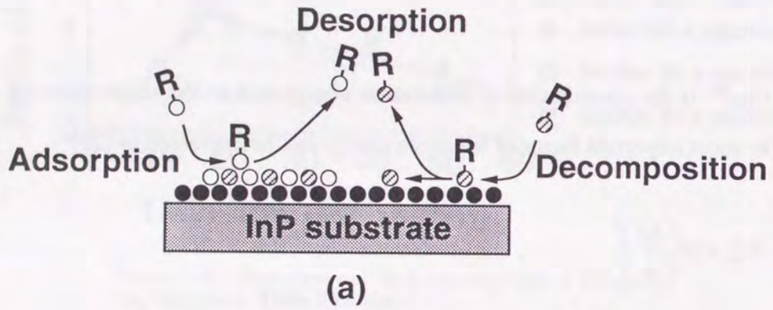

Figure 7-27. Models of compositional latching phenomenon. Closed circles are As atoms, open circles Ga atoms, and shaded circles In atoms. R- represents radicals such as methyl.

of TMGa at the surface governs the growth kinetics, and verified that self-limiting growth can be well described by simple rate equations [6]. Also in $In_xGa_{1-x}As$, growth kinetics will be mainly dominated by the adsorption, desorption, and decomposition rates of TMIn and TMGa molecules. However, unlike in the homoepitaxial system, surface lattice strain affects growth kinetics, especially in the composition determination of thin $In_xGa_{1-x}As$ layers. As shown in Figs. 7-18 and 7-20, composition latching occurs at growth rates below 1 ML/cycle. The interfacial strain energy between two-dimensional group-III metal islands with fractional coverage on the As plane and the substrate will be important.

At present, there seem to be two possible explanations for the latching phenomenon. Figure 7-27 illustrates the models. One explanation is that elastic strain energy, accumulated in the grown layer, directly affects the rates of TMIn and TMGa adsorption, desorption, and decomposition at the surface so that the lattice-matched surface layer of $In_xGa_{1-x}As$ alloy is deposited (Fig. 7-27 (a)). In the other model (Fig. 7-27 (b)), the number of In and Ga atoms produced by TMIn and TMGa pyrolysis are not changed by strain. The metal In and Ga overlayer will be rearranged lattice-matched to minimize the interfacial strain energy. Excess atoms segregated on the growth surface may form clusters on the surface, or reevaporate by recombining with the methyl-radicals. The latter case seems to be the same situation in Fig. 7-27 (a). More detailed studies are required to clarify what is the real mechanism of latching, and the relationship between self-limited growth and lattice strain requires further examination.

7.3.3 InGaAs on GaAs

7.3.3.1 Growth behavior

We studied the PJE growth of $In_xGa_{1-x}As$ on GaAs (001) substrates. Similar to the growth of $In_xGa_{1-x}As$ on InP described in the previous section, we flowed the TMGa and TMIn mixtures and AsH_3 alternately at 470°C, just as in Fig. 7-16. Bath temperatures of TMGa and TMIn were 3.0°C (79.8 mmHg) and -11.4°C (0.1 mmHg). Flow rates of H_2 through TMGa and 10% AsH_3 were 40 sccm and 480 sccm. We changed the flow rate of TMIn in the group-III pulse to change the composition of $In_xGa_{1-x}As$. The number of repeated cycles of source gas supply was 707. We measured the total growth thickness using DEKTAK and

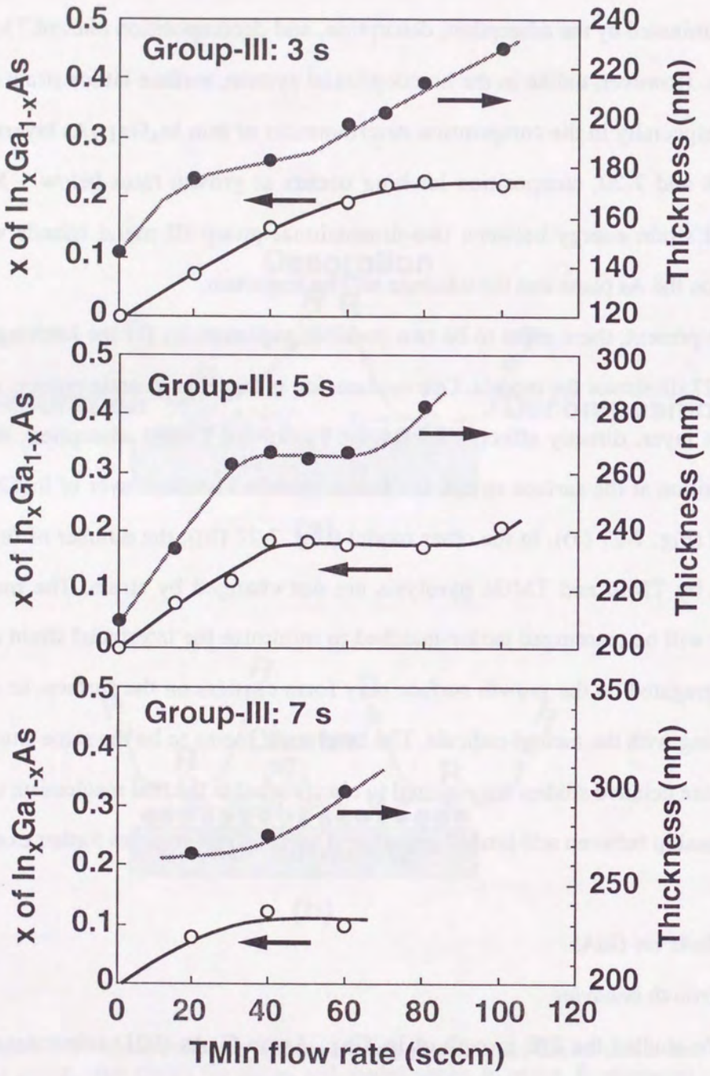

Figure 7-28. Growth thickness and the composition of $In_xGa_{1-x}As$ grown at 470°C. The group-III pulse duration was changed from 3 s to 7 s.

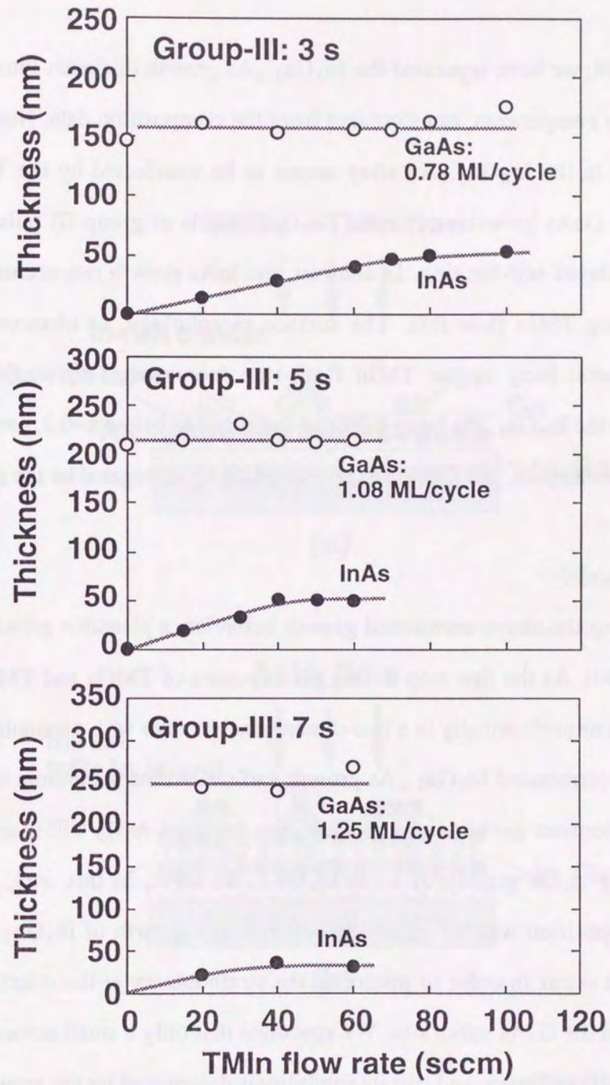

Figure 7-29. Growth thickness of GaAs and InAs in $In_xGa_{1-x}As$ shown in fig. 7-28.

evaluated the composition of $In_xGa_{1-x}As$ grown layers using X-ray diffraction. Figure 7-28 shows the experimental results for the group-III (TMGa and TMIn mixture) pulse durations of 3, 5, and 7 s.

In Fig. 7-29, we have separated the $In_xGa_{1-x}As$ growth thickness into the thicknesses of GaAs and InAs components, as calculated from the composition data. Note that the GaAs growth thickness in the $In_xGa_{1-x}As$ alloy seems to be unaffected by the TMIn flow rate. Judging from the GaAs growth rate under the three kinds of group-III pulse durations, the growth of GaAs shows self-limiting. In contrast, the InAs growth rate seems to be saturated with the increasing TMIn flow rate. The surface morphology, as observed by Nomarski microscopy, became hazy as the TMIn flow rate increased. This implies that indium incorporation into the $In_xGa_{1-x}As$ layer might be restricted to below x=0.2, probably due to the thermodynamic mechanism, and that the excess In might be segregated on the growth surface.

7.3.3.2 Growth model

Considering the above-mentioned growth behavior, a plausible growth model can be deduced (Fig. 7-30). As the first step during the exposure of TMGa and TMIn mixtures, Ga deposition will occur preferentially in a two-dimensional manner with a monolayer coverage by TMGa on the As-terminated $In_xGa_{1-x}As$ growth surface. At the same time the In atoms will remain on the outermost growth surface. Then, the supplied AsH_3 will react with the metal overlayer, leading to the growth of a 2D $In_xGa_{1-x}As$ layer. In this way, the self-limited monolayer Ga deposition will be maintained even in the growth of $In_xGa_{1-x}As$ alloy. This phenomena might occur in order to minimize the strain energy at the interface between the epitaxial layer and the GaAs substrates. We speculate that only a small amount of In atoms is incorporated into 2D epilayers, and that its solubility is determined by the growth temperatures. If the amount of deposited In is beyond the critical solubility limit, the surface In atoms will be clustered to form 2D or 3D islands. These In-rich clusters will not be broken perfectly during AsH_3 supply. Therefore, there is a possibility of forming the embedded In-rich small islands in the In-poorer $In_xGa_{1-x}As$ matrix.

The growth mechanism of the $In_xGa_{1-x}As$/GaAs (001) system is rather complicated.

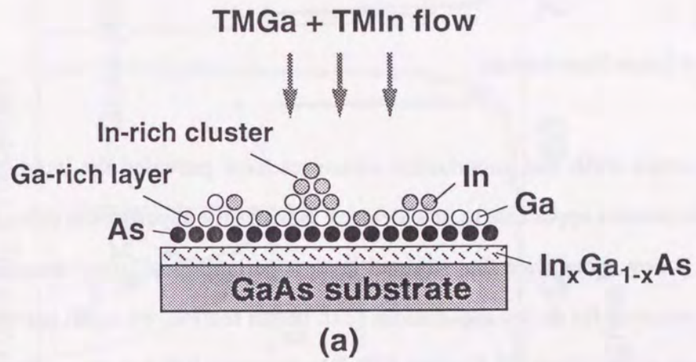

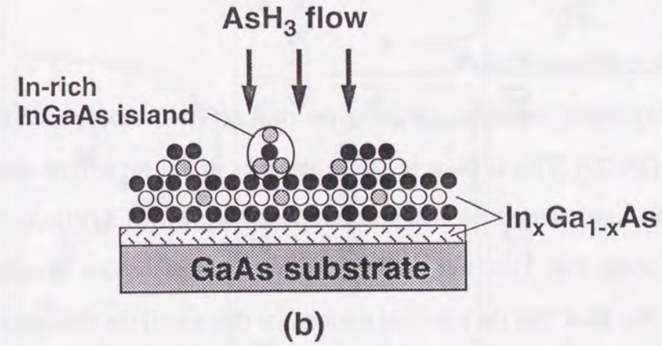

Figure 7-30. Growth model of $In_xGa_{1-x}As$ growth on GaAs (001).

Therefore, more studies are needed to understand the growth mechanism of this mismatched system in detail. Recently it has been reported, however, that the growth of this material system by PJE is useful for making high quality quantum dots [43]. It was reported that the $In_xGa_{1-x}As$ quantum dots are formed in a self-organized manner. This self-organization mechanism for quantum dots will be strongly related with the above-mentioned experimental results.

7.4 Strained-Layer Superlattices

Quantum wells and superlattice structures have provided the interesting and useful physical phenomena applicable to new devices. Besides the superlattices using lattice-matched systems, it is now recognized that strained-layer superlattices of lattice-mismatched materials have great potential for device applications [23]. In this section, we report our results of making strained-layer superlattices (SLS) using PJE. We show that PJE has an excellent controllability even when fabricating very short-period strained-layer superstructures.

7.4.1 (InGaAs)(GaAs)/GaAs

Many researchers have tried to grow (InAs)(GaAs) short-period SLS using MOVPE and MBE [24, 25]. This is because the structure is useful for several electronic and optical devices. We have carried out many experiments to grow (InAs)(GaAs) SLS on InP (001) substrates using PJE. However, to date, we have not succeeded in making good periodic structures. We think that the principal reasons for this are (i) the difference in the appropriate growth temperatures between GaAs and InAs, where the clear self-limited PJE growth occurs, (ii) the difficulty in achieving the coherent growth due to the large lattice mismatch (about 7%) between GaAs and InAs, and (iii) the occurrence of the fast exchange reactions between In and Ga at the near surface.

We grew $(In_xGa_{1-x}As)(GaAs)$ SLS on GaAs (001) at 470°C, where the In content of InGaAs is low. GaAs was deposited in a self-limiting manner. For $In_xGa_{1-x}As$ growth, we used the growth conditions described in Section 7.3.3. Figure 7-31 shows the 2θ-θ X-ray

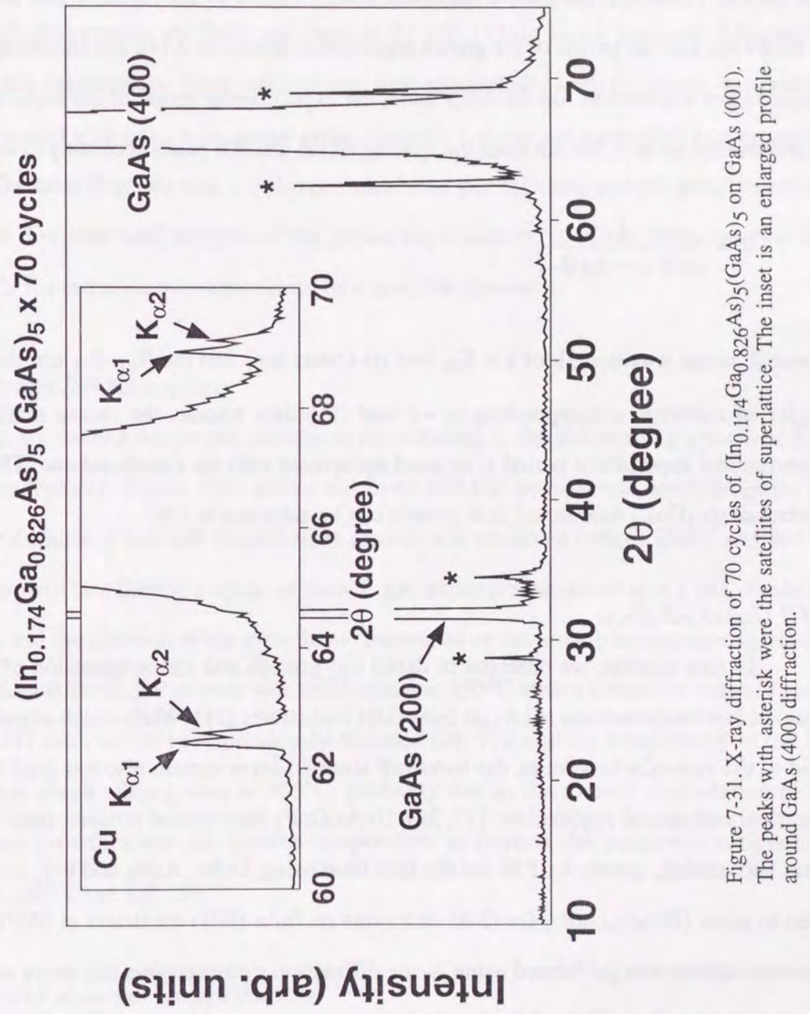

Figure 7-31. X-ray diffraction of 70 cycles of $(In_{0.174}Ga_{0.826}As)_5(GaAs)_5$ on GaAs (001). The peaks with asterisk were the satellites of superlattice. The inset is an enlarged profile around GaAs (400) diffraction.

diffraction profile for 70 cycles of $(In_{0.174}Ga_{0.826}As)_5(GaAs)_5$ SLS. We observed weak satellite peaks as indicated in the figure, indicating the formation of a superlattice structure. Since the amount of Ga deposition is self-limited to 1 ML during the $In_xGa_{1-x}As$ growth, a cycle of $In_{0.174}Ga_{0.826}As$ growth corresponds to $In_{0.211}Ga_{1.0}As_{1.211}$ (0.211 ML InAs plus 1 ML GaAs). Therefore, the growth thickness during a cycle of $In_{0.174}Ga_{0.826}As$ growth should be 0.347 nm and the period of the grown superlattice should be 3.148 nm according to a simple Vegard's law calculation. On the other hand, the experimental period of the superlattice, L, can be determined to be 3.269 nm from the spacing of the satellite peaks according to the formula:

$$L = \frac{\lambda}{\sin\theta_{+1} - \sin\theta_{-1}} \qquad (7\text{-}10)$$

where λ is the wavelength of Cu $K\alpha$ line (0.15405 nm) and the θ_{+1}, θ_{-1} are the diffraction angles of satellites corresponding to +1 and -1 orders besides the strong main peak. This experimental superlattice period is in good agreement with the calculated one. Thus, the good control of $(In_xGa_{1-x}As)(GaAs)$ SLS growth can be achieved in PJE.

7.4.2 (InAs)(InP)/InAs

In this section, we describe in detail the growth and characterization of (InAs)(InP) strained-layer superlattices (SLS) on InAs (001) substrates [26]. While much attention has been paid to the InAs/GaAs system, the InAs/InP strained-layer system also has great potential for electrical and optical applications [27, 28]. (InAs)(InP) short-period strained-layer superlattices were successfully grown by PJE for the first time using TMIn, AsH_3 and PH_3 as sources. We tried to grow $(InAs)_m(InP)_1$ (m=2-4) structures on InAs (001) substrates at 365°C. Structural characterization was performed using X-ray diffraction measurements and many satellite peaks confirming the formation of designed superstructures were detected. We clarified that self-limiting growth still exists at the InAs/InP heterointerfaces. Results indicate that, despite the 3.2% lattice mismatch, PJE forms the growth layer-by-layer from the first layer of heterointerfaces, and is a powerful method of fabricating structures with atomically controlled heterointerfaces.

7.4.2.1 Experiment

Growth experiments were done in a vertical, low-pressure MOVPE system equipped with a chimney reactor, where reactants flow up perpendicular to the substrate surface. The In source used was TMIn, while the As and P sources were 10% AsH_3 in H_2 and 20% PH_3 in H_2. The bath temperature of TMIn was kept at 27.1°C (TMIn vapor pressure: 3.0 mmHg) throughout the experiments. Each reactant was sent sequentially with H_2 carrier gas into the reactor, separated with a 0.5 s H_2 purge pulse, through a computer-controlled fast-switching manifold. The total flow rate was 2.0 slm (standard liter per minutes) and the growth pressure was 15 Torr. For structural analysis of the grown superlattices, an X-ray diffractometer was used with Cu K_α-radiation monochromized by a graphite crystal.

7.4.2.2 InAs and InP homoepitaxy

First, we studied the growth conditions contributing to the self-limiting growth of InAs and InP homoepitaxy. Figure 7-32 shows the InAs and InP growth rate dependence on the TMIn pulse duration. Clear self-limited InAs growth was observed both at 350°C and 365°C. The InAs growth rate during a cycle of source gas exposure saturated at a 1 ML thickness (0.303 nm), and the rise time of the growth rate decreased as the growth temperature increased, just as in GaAs PJE [6]. InP growth was self-limited at 350°C with a saturation value of about 0.5 ML (0.147 nm), as has been previously reported [9]. The surface morphology of the InP epilayers was rough when grown at 365°C, probably due to the thermal degradation of the layers during growth, since the growth temperature is beyond the congruent evaporation temperature (363°C) of InP [29].

7.4.2.3 InAs/InP short-period superlattices

Next, we grew (InAs)(InP) short-period strained-layer superlattices under the growth conditions where the InAs homoepitaxy is self-limited. Three types of samples, $(InAs)_2(InP)_1$, $(InAs)_3(InP)_1$ and $(InAs)_4(InP)_1$, were prepared at 365°C using PJE on InAs (001) substrates without a buffer layer. Since the InP growth thickness was expected to be 0.5 ML during one

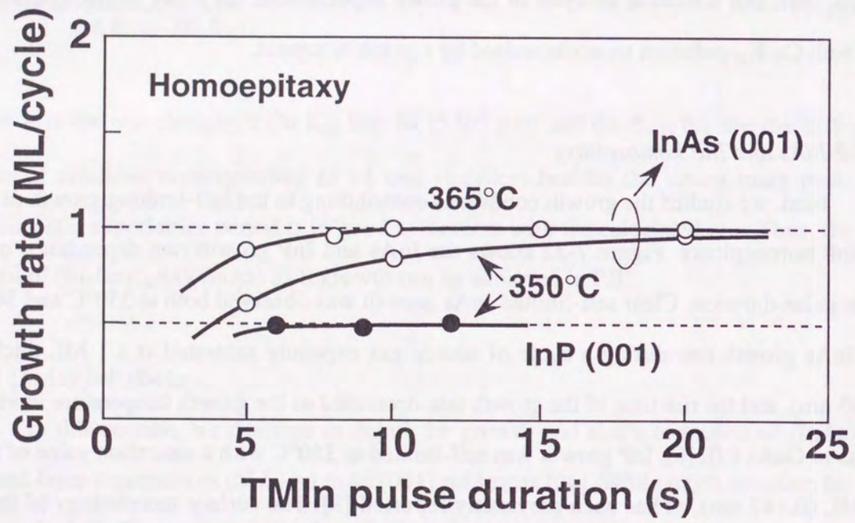

Figure 7-32. Growth rate of PJE-grown InAs and InP as a function of TMIn pulse duration. TMIn mole fraction was 5.9×10^{-5} for InAs growth and 1.2×10^{-4} for InP. AsH_3 pulse was 10 s with a mole fraction of 2.4×10^{-2}. PH_3 pulse was 20 s with a mole fraction of 9.6×10^{-2}.

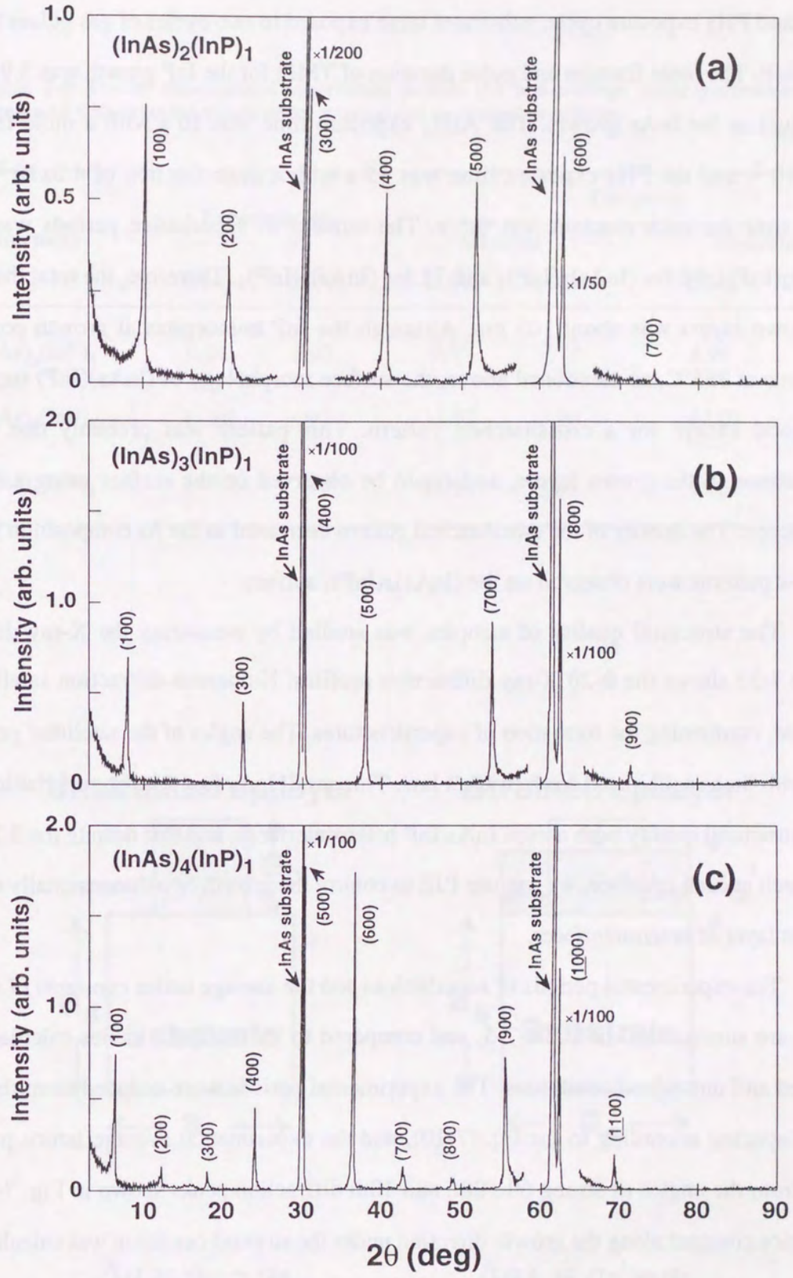

Figure 7-33. X-ray diffraction profiles for (a) $(InAs)_2(InP)_1$, (b) $(InAs)_3(InP)_1$, and (c) $(InAs)_4(InP)_1$ superlattices.

TMIn and PH_3 exposure cycle, substrates were exposed to two cycles of gas pulses to deposit 1 ML InP. The mole fraction and pulse duration of TMIn for the InP growth was $5.9x10^{-5}$ and 12 s, just as for InAs growth. The AsH_3 exposure time was 10 s with a mole fraction of $1.25x10^{-2}$, and the PH_3 exposure time was 15 s with a mole fraction of $4.0x10^{-2}$. The H_2 purge time for each reactant was 0.5 s. The number of superlattice periods was 120 for $(InAs)_2(InP)_1$, 90 for $(InAs)_3(InP)_1$ and 72 for $(InAs)_4(InP)_1$. Therefore, the total thickness of the grown layers was about 108 nm. Although the InP homoepitaxial growth posed some problems at 365°C, as mentioned above, the surface morphology of (InAs)(InP) superlattices was good except for a crosshatched pattern. This pattern was probably due to misfit dislocations in the grown layers, and could be observed on the surface using a Nomarski microscope. The density of the crosshatched pattern decreased as the As composition increased, and few patterns were observed on the $(InAs)_4(InP)_1$ surface.

The structural quality of samples was studied by measuring the X-ray diffraction. Figure 7-33 shows the θ-2θ X-ray diffraction profiles. Numerous diffraction satellites were detected, confirming the formation of superstructures. The angles of the satellites' peaks agree well with those anticipated from Bragg's law. This result indicates that the superlattices have a good structural quality with abrupt InAs/InP heterointerfaces, and that despite the 3.2% lattice mismatch at each interface, we can use PJE to control the growth two-dimensionally even from the first layer of heterointerfaces.

The experimental periods of superlattices and the average lattice constants of the grown layers are summarized in Table 7-5, and compared to the designed values calculated under strained and unstrained conditions. The experimental periods were deduced from the satellite peaks' spacing according to the Eq. (7-10), and the experimental average lattice parameters were from the angles of strong 6th, 8th, and 10th diffraction peaks shown in Fig. 7-33. Here, the lattice constant along the growth direction under the strained condition was calculated using the relationship:

$$\frac{\Delta a}{a_s} = \frac{C_{11}}{C_{11}+2C_{12}}\left(\frac{\Delta a_\perp}{a_s}\right) \qquad (7\text{-}11)$$

Table 7-5: List of experimental superlattice periods (L) and average lattice parameters (d), compared with expected values under strained and unstrained conditions.

Structures	Experimental		Designed			
			Strained		Unstrained	
	L (Å)	d (Å)	L (Å)	d (Å)	L (Å)	d (Å)
$(InAs)_2(InP)_1$	9.04	5.95	8.89	5.93	8.99	6.00
$(InAs)_3(InP)_1$	11.80	5.97	11.92	5.96	12.02	6.01
$(InAs)_4(InP)_1$	14.83	5.99	14.95	5.98	15.05	6.02

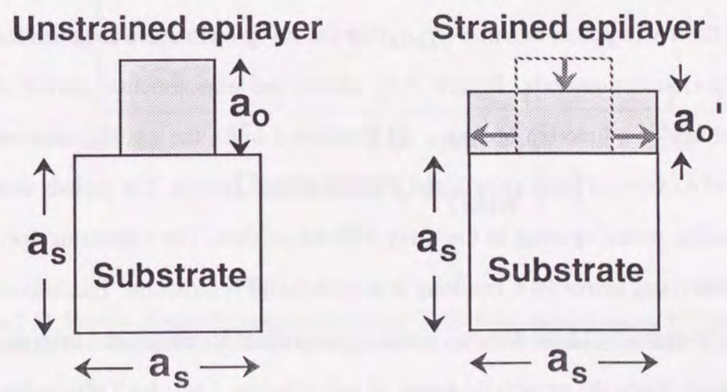

$$\Delta a = a_o - a_s \qquad \Delta a_\perp = a_o' - a_s$$

Figure 7-34. Schematics of unstrained and strained epitaxial layers on the mismatched substrate.

where a_s is the lattice parameter of the substrate, Δa is the difference in unstrained lattice parameters between epilayer, a_o, and substrate, a_s. $\Delta a_\perp$ is the difference in lattice parameters between the deformed epitaxial lattice parameter along growth direction, a_o', and a_s (see Fig. 7-34). C_{11} and C_{12} are the elastic stiffness constants for $InAs_xP_{1-x}$ epitaxial layer and these values are calculated by using the values for InP and InAs, adopting Vegard's law.

The experimental average lattice parameters are well consistent with the calculated strained values, where the tetragonal distortion [30] of the grown layers due to the lattice mismatch with InAs substrates is taken into account, rather than the expected unstrained lattice parameters. This implies that the lattice mismatch between epilayers and substrates is accommodated almost elastically. The experimental periods of superlattices are nearly consistent with those calculated for strained cases, assuming the elastic accommodation of epilayers with InAs substrates. The small difference between the experimental and expected periods may be due to the lattice distortion resulting from a 3.2% mismatch between InAs and InP. Anyway, the superlattices are well controlled by PJE.

To study the self-limiting growth during the fabrication of strained-layer superlattices, we varied the TMIn pulses duration (t_{TMIn}) for the InP growth cycle and examined the change in the superlattices periods. Figure 7-35 shows the experimental period of the grown superstructures as a function of t_{TMIn}. As illustrated inset, the gas sequence employed here consisted of 4 cycles of InAs growth and 2 cycles of InP growth. The periods were determined by the satellite peaks' spacing in the x-ray diffraction data. The superlattice period seems to saturate with t_{TMIn} above 10 s, resulting in a $(InAs)_4(InP)_1$ structure. This indicates that the In deposition reaction by TMIn decomposition at the surface is self-limited from the first layer of heteroepitaxy. Since the growth thickness of InP is below 1 ML for TMIn pulses shorter than 10 s, the period of the grown superlattices is shorter than the saturated value. The self-limiting growth obtained here allows us to fabricate the desired structures without the need of precise control of the group-III sources as would be needed in MOVPE and MBE.

Thus, we studied the growth conditions of InAs and InP PJE, and applied them to the fabrication of (InAs)(InP) short-period strained-layer superlattices. $(InAs)_m(InP)_1$ (m=2-4) structures were successfully grown by PJE on InAs (001) substrates. The structural

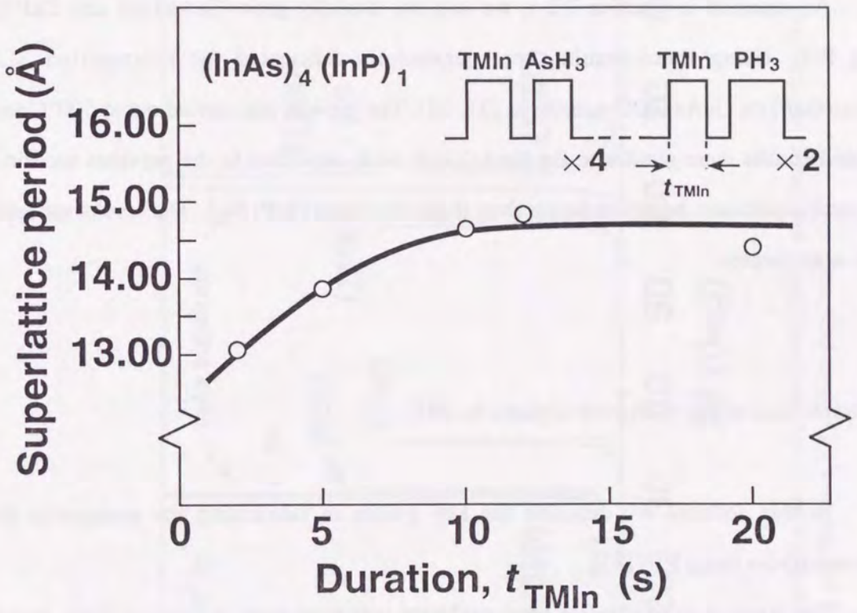

Figure 7-35. Periods of superlattices as a function of TMIn pulse duration during InP growth cycles. The periods were determined from the spacing between 4th and 6th satellite peaks.

characterization was done by measuring the X-ray diffraction and we observed many satellite peaks resulting from the superstructures. We confirmed that self-limiting growth still exists at the InAs/InP heterointerface. These results indicate that, despite the large lattice mismatch, PJE makes the growth mode layer-by-layer from the first layer of interface. Thus, PJE is a powerful method of fabricating structures having atomically controlled heterointerfaces.

7.4.3 (GaP)(GaAs)/GaAs

As reported in Section 7.2.1, we can successfully grow GaAs/GaP and GaP/GaAs using PJE. Using these results, we successfully fabricated the short-period SLS of (GaAs)(GaP) on GaAs (001) substrates [31, 32]. The growth was carried out at 500°C and the obtained results were similar to the (InAs)(InP) SLS described in the previous section. The structural results are, however, better than those for (InAs)(InP) SLS. The results are reported in the next chapter.

7.5 Fabrication of Sharp Heterointerfaces by PJE

In this section, we describe the key points in fabricating the atomically abrupt heterointerfaces using PJE [33].

The fabrication of ultrafine semiconductor structures such as quantum wells, wires and dots strongly requires an atomic-scale-controllable growth technique. PJE is one of the candidates because semiconductor materials can be prepared layer-by-layer due to the inherent self-limiting growth [5, 6]. However, the present status of PJE is not adequate for making such nanostructures. This is because our currently incomplete understanding of the PJE growth mechanism limits our ability to use it for making atomically controlled heterointerfaces [26, 31]. In PJE, which is based on low-pressure MOVPE, growth can be halted after group-V or group-III supply by purging the source gases from the reactor with H_2. Any changes in the growth surface during these halts have previously been ignored. We found, however, that, especially on the group-V-terminated surface, the stoichiometry changes dynamically during H_2

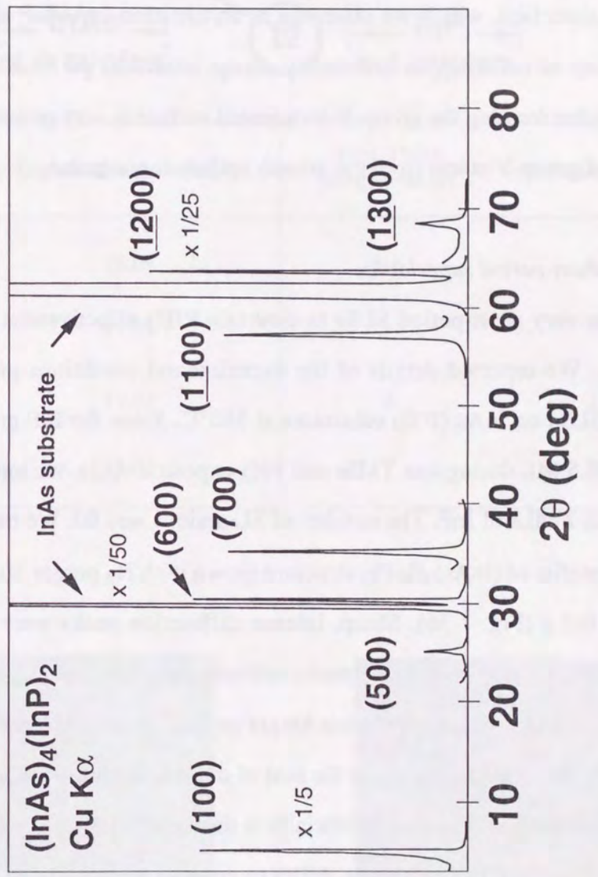

Figure 7-36. X-ray diffraction profile for $(InAs)_4(InP)_2$ superlattice. All the purge durations after TMIn, AsH_3, and PH_3 were 0.3 s. TMIn pulse was 7 s.

purging due to the preferential desorption of group-V atoms from the outermost surface. This decreases the InAs and InP growth rates during gas exposure. These results were described in Chapter 6. Here, we show that the desorption of the outermost group-V atoms causes a disparity in the designed structural parameters of InAs/InP short-period strained-layer superlattices (SLSs). Arsenic and phosphorous desorption also deteriorates the sharpness of the InAs/InP heterointerface, which we observed in an ultrathin InAs/InP single quantum well (SQW). As a way of realizing the atomically abrupt interface, we found that shortening the purge duration after forming the group-V-terminated surface is very powerful. This is because the desorption of group-V atoms from the growth surface is prevented.

7.5.1 InAs/InP short-period superlattice

We grew very short-period SLSs to ascertain PJE's effectiveness in making artificial superstructures. We reported details of the experimental conditions previously. We grew $(InAs)_4(InP)_2$ SLSs on InAs (100) substrates at 380°C. Since the InP growth thickness was expected to be 0.5 ML during one TMIn and PH_3 exposure cycle, we injected four gas pulse cycles to deposit 2 MLs of InP. The number of SL periods was 60. We measured the θ-2θ X-ray diffraction profile of $(InAs)_4(InP)_2$ structure grown with H_2 purges after TMIn, AsH_3, and PH_3 pulses of 0.3 s (Fig. 7-36). Sharp, intense diffraction peaks were observed, with the (100), (500), (700), (1100), and (1300) peaks indicating satellites, confirming the formation of superstructure. Although SLSs with much longer periods grown by other methods have been reported [34-36], this is the first time, to the best of our knowledge, that the structure with such an atomic-scale period has been made artificially in this InAs/InP system with a lattice mismatch of about 3.2%. Thus, PJE has a superior ability to grow SLS.

In Table 7-6 we have compared the structural parameters of some SLSs made with several post-AsH_3 and post-TMIn H_2 purge times on the fabrication of InAs layers. We deduced the experimental periods of the SLS from the spacing between the 5th and 7th satellite peaks. The 18.05 Å period for the SLS with the 0.3 s post-AsH_3 purge agrees well with 17.99 Å, calculated by assuming that the lattice mismatch between the epilayer and InAs substrate is relaxed by generating misfit dislocations. As the post-AsH_3 purge time increased, the SLS

Table 7-6: Structural parameters of superlattices grown under several H_2 purge conditions. For a series of changing post-AsH_3 purge, post-TMIn H_2 purge was 0.3 s. For a series of changing post-TMIn purge, post-AsH_3 H_2 purge was 0.3 s.

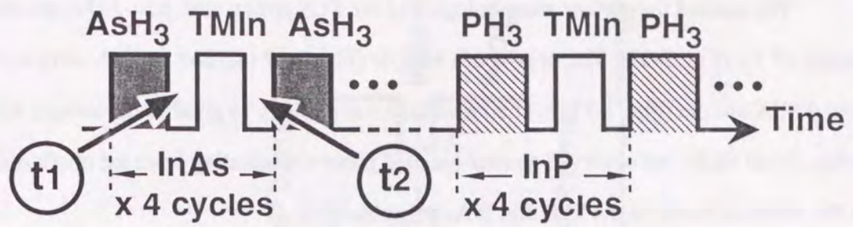

Post-AsH_3 purge time (s)	Superlattice periods (Å)	Post-TMIn purge time (s)	Superlattice periods (Å)
0.3	18.05	0.3	18.05
3	17.54	3	——
5	17.32	5	18.09
7	16.95	7	——

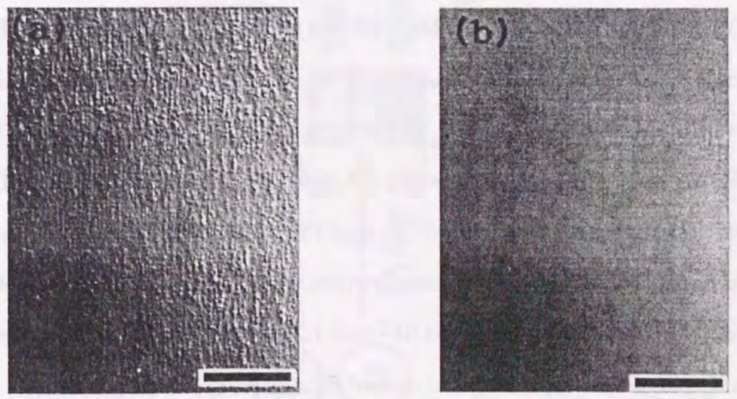

Figure 7-37. Nomarski photographs of superlattice surface morphologies. Marker represents 50 μm.

period decreased, probably due to the decreasing growth thickness of the InAs layer from As desorption. The post-TMIn purge, however, has less of an effect on periods.

We studied the surface morphologies of the SLS grown with post-AsH_3 and post-TMIn purges of 5 s (Fig. 7-37). The post-AsH_3 sample (Fig. 7-37 (a)) had a rough surface, while the post-TMIn sample (Fig. 7-37 (b)) had a surface morphology as good as the sample with a 0.3 s purge. In all SLSs, we observed a cross-hatched pattern originating from the misfit dislocations at the interface between the SLS and InAs substrate [37].

Experimental results indicate that suppressing desorption of the group-V atoms is important for fabricating SLSs with the designed structural parameters using PJE, and that the post-TMIn purge time at 380°C need not be precisely controlled.

7.5.2 InAs/InP single quantum well

To measure the abruptness of InAs/InP heterointerfaces grown by PJE, we grew ultrathin, strained InAs/InP SQWs on InP (100) substrates at 500°C and measured their PL spectra. The emission energy and its full-width at half maximum (FWHM) reflect the compositional profile at the heterointerfaces for these SQWs. In Fig. 7-38 (a) we show the gas-switching procedure in our growth process. To clear the difference in the procedures between the conventional MOVPE and ours, the gas switching procedure in MOVPE is also shown in Fig. 7-38 (b). We grew InP barriers by MOVPE and the InAs quantum well by PJE. Although the PJE windows become very narrow at 500°C, we observed self-limiting deposition of In at TMIn pulse durations of around 1 s. The source gas sequence for nominal 1-ML-thick InAs/InP SQWs was as follows: TMIn+PH_3 (24 min)/ PH_3 (10 s)/ H_2 (0.1 s)/ TMIn (1 s)/ H_2 (0.5 s)/ AsH_3 (10 s)/ H_2 (t_1)/ TMIn (1 s)/ H_2 (t_2)/ PH_3 (10 s)/ TMIn+PH_3 (12 min), where t_1 and t_2 were varied. The InP upper and lower barriers were 100 nm and 200 nm thick. The mole fractions of TMIn and AsH_3 were 2.95×10^{-5} and 1.25×10^{-2}. We changed the post-AsH_3 and post-TMIn H_2 purge times, t_1 and t_2, and studied their effect on the PL properties.

We measured the 4.2 K PL spectra from nominal 1-ML-InAs/InP SQWs, varying t_1 from 0.1 to 30 s (Fig. 7-39). We ascribed the PL of the lowest spectrum to exciton recombination because of the narrow FWHM of 8 meV and the linear dependence of its

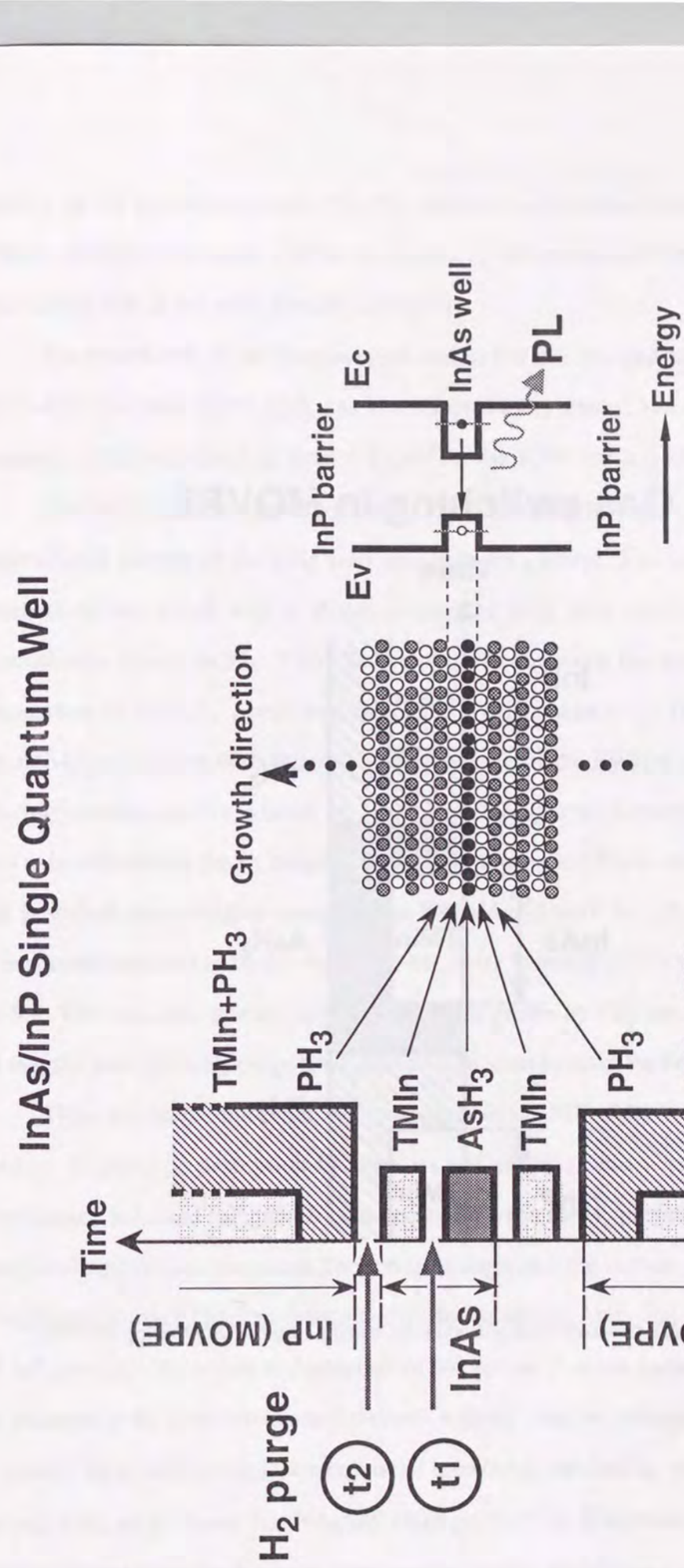

Figure 7-38(a). Gas-switching procedure for making InAs/InP SQW using PJE. SQW and its band structure was also illustrated.

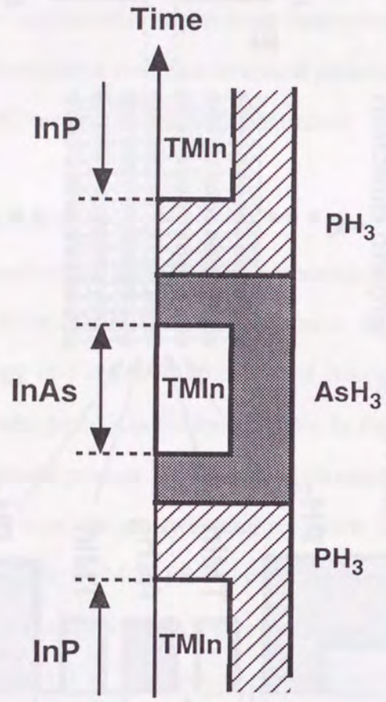

Figure 7-38(b). Gas-switching procedure for making InAs/InP SQW using MOVPE.

intensity on the excitation power. The PL emission peak shifted to higher energies and its intensity gradually decreased with the increasing t_1. An unexplained shoulder appeared on the lower energy side of the main peak for a longer t_1.

The wavelength of the emission peak and its FWHM changed as t_1 and t_2 were changed (Fig. 7-40). The peak wavelength was less affected by t_2 than t_1, and FWHM increased with increasing t_1, but was steady at about 8-9 meV for the SQW with a t_2 of 0.1 to 30 s.

Blue shifts in the emission peak caused by increasing t_1 (Fig. 7-40) may result from the compositional change of the InAs well into $InAs_xP_{1-x}$ alloys. The vacant sites made by the desorbed As are filled with P atoms during the next PH_3 exposure. This situation is schematically shown in Fig. 7-41. The relationship between the emission energy and the composition of $InAs_xP_{1-x}$ well was calculated by Schneider *et al.* [38], and our results are qualitatively consistent with theirs. The dependence of the FWHM on t_1 indicates that the InAs/InP interface quality is better for short post-AsH_3 purges. However, the quality does not seem to be affected by the H_2 purge time after forming an In adlayer, even though the emission peak is shifted toward higher energies. The FWHM of 8 meV for a 0.1 s post-AsH_3 purge is the best result reported so far for nominal 1-ML-thick InAs/InP SQWs grown by other methods [39-42]. This indicates that the InAs/InP interface grown by PJE becomes atomically abrupt and that the post-AsH_3 H_2 purge time must be kept short to make the best use of the PJE.

Thus, as pointed out in the previous chapter, the PJE of III-V compounds has a basic problem of group-V desorption because its gas sequence has a period without group-V overpressure. InAs and InP growth rates decreased when the H_2 purge time after supplying the corresponding hydrides increased. These results imply that the surface stoichiometry of group-V-terminated-surface changes dynamically after supplying AsH_3 and PH_3 supply in the InAs and InP growth. This is due to desorption of the As and P atoms from the outermost surface. The decrease in the growth rate was consistent with the selective adsorption model we proposed previously. Ideal InAs and InP homoepitaxial growth was attained by shortening the post-AsH_3 and post-PH_3 purge times. For InAs/InP short-period SLS fabrication, the experimental SLS periods differed from the designed value and the surface morphology was degraded for longer post-AsH_3 purges. From PL studies on the nominal 1-ML-thick InAs/InP

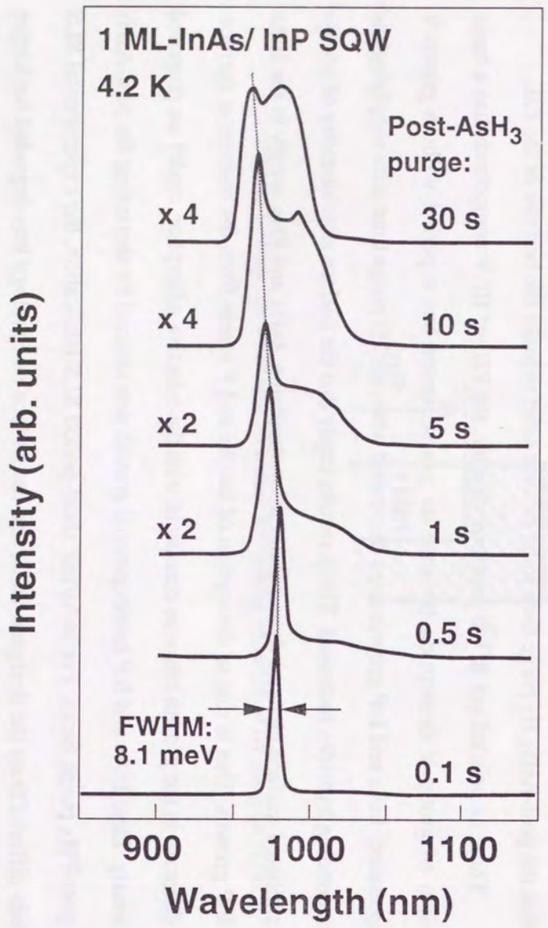

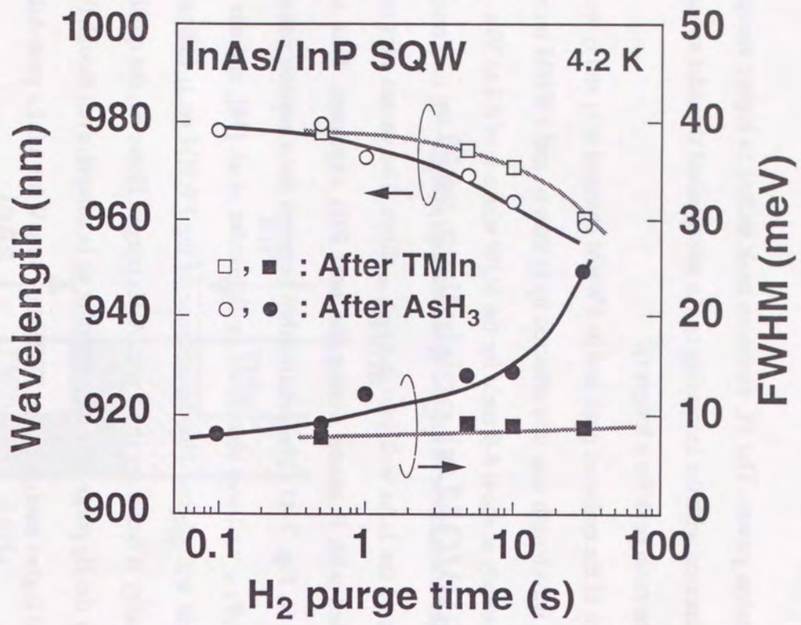

Figure 7-40. Wavelength of PL spectra and the FWHM value from the nominal 1 ML-thick InAs/InP SQW.

Figure 7-39. A series of PL spectra from the nominal 1 ML-thick InAs QW buried in InP. Post-AsH_3 H_2 purge time was changed.

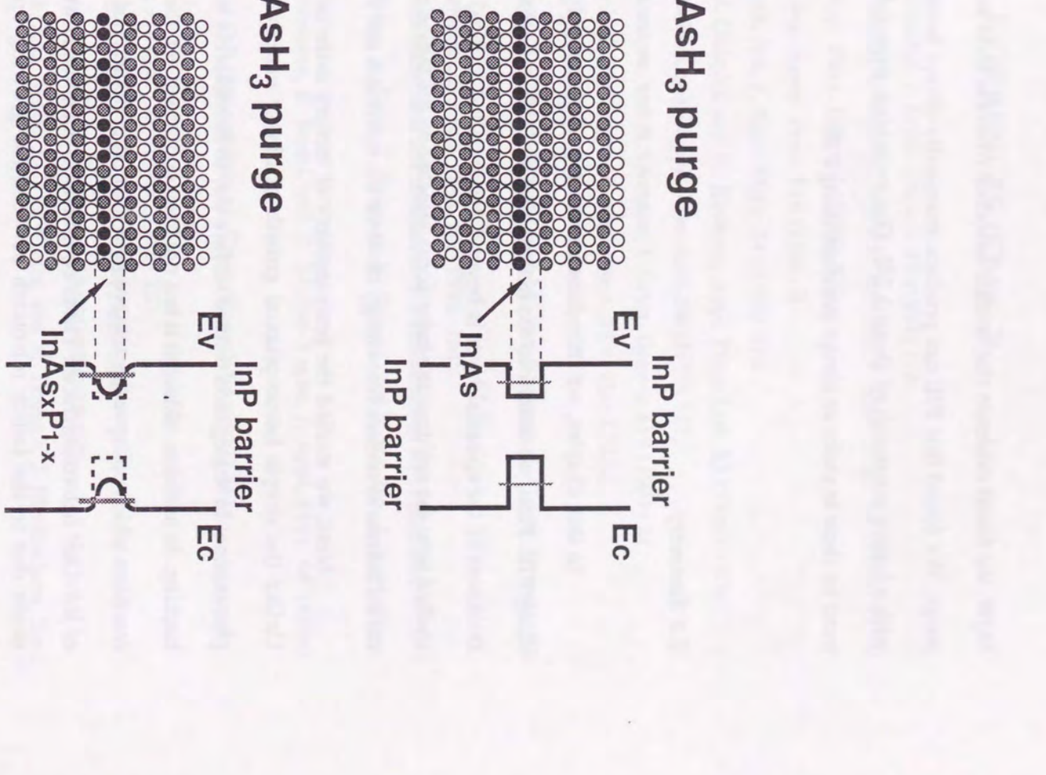

Figure 7-41. Illustrations of nominal 1 ML-thick InAs/InP SQW in the case of short and long post-AsH_3 H_2 purge time.

SQW, we found evidence that arsenic adsorbed from the InAs surface during the post-AsH_3 H_2 purge. We found that PJE can produce atomically-abrupt heterointerfaces such as InAs/InP, with a lattice mismatch of about 3.2%. Gas switching, especially from group-V to group-III, must be short to make an abrupt interface using PJE.

7.6 Summary

In this chapter, we introduced some experimental results on heteroepitaxial growth using PJE. First, we described the heteroepitaxy of PJE between binary compounds, where the thickness of the epitaxial layer is beyond the so-called "critical thickness". We systematically studied how the self-limiting behavior is affected by the lattice mismatch (or the strain) and by the difference in surface free energy between the substrates and epitaxial layers.

Next, we studied the heteroepitaxy of ternary materials such as InGaP and InGaAs. Unlike the simple homoepitaxial growth of binary materials, we observed several novel phenomena: In segregation toward surface due to immisibility of In and Ga, and compositional latching. In addition, although it has not been confirmed yet, there seem to be severe exchange reactions which collapse the achievement of short periodicity of the superlattices at InAs/GaAs or InP/GaP heterointerfaces. These complicated phenomena will be derived from the surface strain due to the lattice mismatch between the growing uppermost epitaxial layers and subsurface layers. In spite of the complicated reactions at the surfaces and heterointerfaces, we observed the successful growth of short-period superlattices in (InAs)(InP), (GaAs)(GaP), and $(In_xGa_{1-x}As)$(GaAs) systems. Thus, in some heteroepitaxial systems we showed that PJE is a powerful method to obtain the atomically controlled heterointerfaces.

Our understanding of the heteroepitaxy in PJE is still at the phenomenological stage. To systematically understand our experimental results and their growth mechanism, we have to continue further study on the basic surface reactions and surface structural change including the strain accommodation.

REFERENCES (Chap. 7)

[1] J.W. Matthews and A.E. Blakeslee, J. Cryst. Growth **27** (1974) 118.

[2] D. Morris, A.P. Roth, R.A. Masut, C. Lacelle, and J.L. Brebner, J. Appl. Phys. **64** (1988) 4135.

[3] R. People and J.C. Bean, Appl. Phys. Lett. **47** (1985) 322.

[4] L.J. Schowalter, Mat. Res. Soc. Symp. Proc. **116** (1988) 3.

[5] K. Ishibashi and S. Furukawa, Jpn. J. Appl. Phys. **24** (1985) 912.

[6] M. Ozeki, K. Mochizuki, N. Ohtsuka, and K. Kodama, Appl. Phys. Lett. **53** (1988) 1509.

[7] Y. Sakuma, K. Kodama, and M. Ozeki, Appl. Phys. Lett. **56** (1990) 827.

[8] Y. Sakuma, M. Ozeki, K. Kodama, and N. Ohtsuka, J. Cryst. Growth **114** (1991) 31.

[9] Y. Sakuma, K. Kodama, and M. Ozeki, Jpn. J. Appl. Phys. **27** (1988) L2189.

[10] T. Inoshita, J. Appl. Phys. **56** (1984) 2056.

[11] F. Houzay, J.M. Moison, C. Guille, F. Barthe, and M. van Rompay, J. Cryst. Growth **95** (1989) 35.

[12] H. Yamaguchi and Y. Horikoshi, J. Appl. Phys. **68** (1990) 1610.

[13] M.R. Leys, H. Titze, L. Samuelson, and J. Petruzzello, J. Cryst. Growth **93** (1988) 504.

[14] Y. Miura, K. Onabe, X. Zhang, Y. Nitta, S. Fukatsu, Y. Shiraki, and R. Ito, Jpn. J. Appl. Phys. **30** (1991) L664.

[15] G. Landa, R. Carles, C. Fontaine, E. Bedel, and A. Muñoz-Yagüe, J. Appl. Phys. **66** (1989) 196.

[16] C.P. Kuo, R.M. Cohen, and G.B. Stringfellow, J. Cryst. Growth **64** (1983) 461.

[17] G.B. Stringfellow, J. Appl. Phys. **43** (1972) 3455.

[18] Y. Takeda, and A. Sasaki, J. Cryst. Growth **45** (1978) 257.

[19] P.K. Bhattacharya and S. Srinivasa, J. Appl. Phys. **54** (1983) 5090.

[20] W.A. Jesser and D. Kuhlmann-Wilsdorf, Phys. Status Solidi **19** (1970) 95.

[21] R.E. Nahory, M.A. Pollack, E.D. Beebe, J.C. DeWinter, and M. Ilegems, J. Electrochem. Soc. **125** (1978) 1053.

[22] M. Quillec, H. Launois, and M.C. Joncour, J. Vac. Sci. Technol. **B1** (1983) 238.

[23] G.C. Osburn, J. Appl. Phys. **53** (1982) 1586.

[24] M.C. Tamargo, R. Hull, L.H. Greene, J.R. Hayes, and A.Y. Cho, Appl. Phys. Lett. **46** (1985) 569.

[25] T. Fukui and H. Sato, Jpn. J. Appl. Phys. **23** (1984) L521.

[26] Y. Sakuma, M. Ozeki, K. Kodama, and N. Ohtsuka, J. Cryst. Growth **115** (1991) 324.

[27] E. Yablonovitch and E.O. Kane, J. Lightwave Technol. **LT-6** (1988) 1292.

[28] R.P. Schneider, Jr. and B.W. Wessels, Appl. Phys. Lett. **57** (1990) 1998.

[29] C.E.C. Wood, *III-V Alloy Growth by Molecular Beam Epitaxy in GaInAsP Alloy Semiconductors*, ed. T.P. Peasall (Wiley, New York, 1982) p. 91.

[30] J. Hornstra and W.J. Bartels, J. Cryst. Growth **44** (1978) 513.

[31] M. Ozeki, K. Kodama, Y. Sakuma, N. Ohtsuka, and T. Takanohashi, J. Vac. Sci. Technol. **B8** (1990) 741.
[32] K. Kodama, M. Ozeki, Y. Sakuma, and N. Ohtsuka, J. Appl. Phys. **69** (1991) 6713.
[33] Y. Sakuma, M. Ozeki, O. Ueda, and T. Ashino, Advanced Materials '93, VI/ Trans. Mat. Res. Soc. Jpn. **19A** (1994) 157.
[34] R. P. Schneider, Jr., D. X. Li, and B. W. Wessels, J. Electrochem. Soc. **136** (1989) 3490.
[35] H. Q. Hou, C. W. Tu, and S. N. G. Chu, Appl. Phys. Lett. **58** (1991) 2954.
[36] C. A. Tran, R. A. Masut, P. Cova, and J. L. Brebner, Appl. Phys. Lett. **60** (1992) 589.
[37] O. Ueda, Y. Sakuma, M. Ozeki, N. Ohtsuka, K. Nakajima, in: Proceedings of Alloy Semicon. Phys. and Electronics Symp., Kyoto (1992).
[38] R.P. Schneider, Jr. and B.W. Wessels, Superlattices and Microstructures **6** (1989) 287.
[39] R. P. Schneider, Jr. and B. W. Wessels, J. Appl. Phys. **70** (1991) 405.
[40] J. F. Carlin, R. Houdré, A. Rudra, and M. Ilegems, Appl. Phys. Lett. **59** (1991) 3018.
[41] M. Hopkinson, J. P. R. David, and P. A. Claxton, Appl. Phys. Lett. **60** (1992) 841.
[42] Y. Kobayashi and N. Kobayashi, Japan. J. Appl. Phys. **31** (1992) 3988.
[43] K. Mukai, N. Ohtsuka, M. Sugawara, and S. Yamazaki, Jpn. J. Appl. Phys. **33** (1994) L1710.

CHAPTER 8
Device Applications

8.1 Preliminaries

Thus far in this thesis, we have reported the basic growth behavior for several materials and the related growth mechanism of PJE. One of the goals of developing such a new growth technique is to improve the conventional growth process for making device structures or to enable us to make novel device structures. Therefore, it is important to try to use the PJE in practical applications. Since ALE was invented by Suntola [1], an industrial application has been found in the electroluminescent panels, using the ALE of II-VI materials and dielectric films [2]. However, to date, its application in devices using III-V compounds grown by ALE has still been limited [3-5]. In this chapter, we report our attempts at applying PJE to practical device processes [6].

PJE uses a modified, low-pressure MOVPE. Therefore, it can be used in growing several III-V materials containing arsenic (As) and phosphorus (P). PJE is also expected to be suitable for mass production because MOVPE can be performed in the same reactor, by simply changing the supply sequence of the source gases. PJE still has some problems to be overcome from the viewpoint of basic growth technology. For instance, the relatively low electrical and optical quality of the grown layers compared with those prepared by MOVPE or by MBE, the slow growth rate, and the uncertain way of growing ternary or quaternary materials in a self-limiting fashion remain as unsolved problems. However, we believe it is significant to test our new growth technique in device processes. We aim to ascertain the possibility of applying PJE to device processes, or to reveal the unknown problems concerning device fabrication.

First in this chapter, we briefly summarize the growth results of PJE. Then, we describe several major sets of factors applicable to device fabrication: thickness and interface controllability, doping and low-temperature growth, and selective epitaxy. We explain each factor and show typical results. To clarify PJE's ability of growing uniform epilayers, we

compare the thickness profile of GaAs between PJE and MOVPE. As another example, we show the fabrication of GaAs/GaP superlattice structures with abrupt heterointerfaces, indicating the excellent thickness and interface controllability of PJE. In the doping section, we show the typical results of selenium (Se) doping into GaAs and beryllium (Be) doping into InGaAs, where both materials were grown by PJE. For an explanation of selective epitaxy, we compare the growth behavior of GaAs between PJE and MOVPE. In the final section of this chapter, we describe the a few practical application of PJE. One is the use of PJE to form the low resistance ohmic contact layers. We show two kinds of structures for non-alloyed contacts; (i) n^+-InAs/$In_xGa_{1-x}As$/GaAs graded-composition layer and (ii) n^+-GaAs selective regrowth layer. Another practical use of PJE is the fabrication of $In_{0.53}Ga_{0.47}As$/InP heterojunction bipolar transistors (HBT) where a p^+-doped, thin InGaAs base layer was grown by PJE, utilizing the high-concentration doping and low-temperature growth.

8.2 Summary of PJE

Table 8-1 is a summary of the PJE results for III-V binary compounds. We successfully grew five kinds of semiconductor materials in a self-limited manner, using trimethyl compounds of group-III atoms and hydrides (AsH_3 or PH_3). The large difference in the appropriate growth temperatures between Ga and In compounds is attributed to the difference in the decomposition temperatures of TMGa and TMIn. The self-limiting growth rates also differ among materials. This is closely related to the growth mechanism for the individual materials. The saturated growth rate is probably determined by the stable surface reconstruction and the surface stoichiometry of each material in the growth environment. Detailed growth conditions and the growth mechanism have been previously reported in Chapters 3 and 4 [7-11].

8.3 Elemental Factors Applicable to Device Process

Table 8-1: Summary of PJE results for several III-V compound semiconductors.

			(001) orientation
Materials	Saturation value (ML)	Growth temp. (°C)	Sources
AlAs	2	500	TMAl + AsH_3
GaAs	1	500	TMGa + AsH_3
GaP	1	500	TMGa + PH_3
InP	0.5	350	TMIn + PH_3
InAs	1	350	TMIn + AsH_3

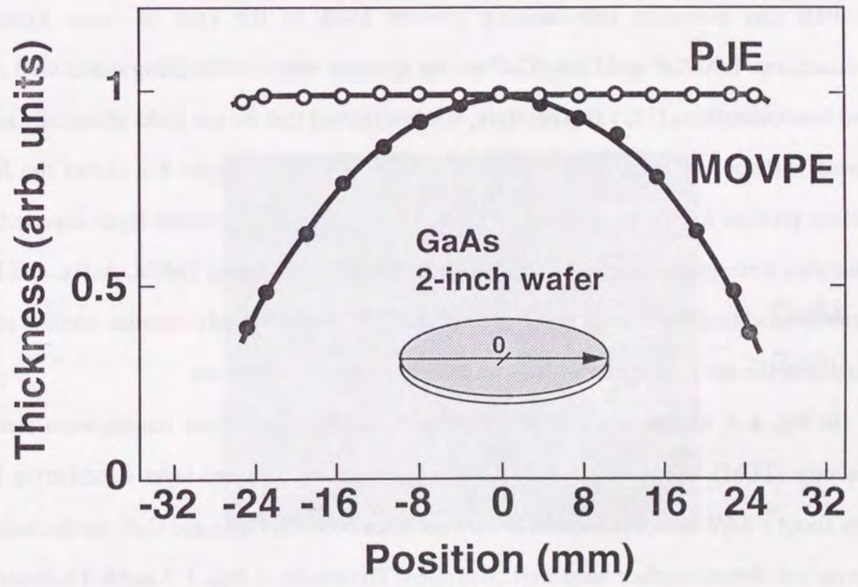

Figure 8-1. Comparison of thickness variations of GaAs epitaxial layes grown by PJE and MOVPE.

8.3.1 Thickness uniformity

PJE exhibits some important basic features useful in device fabrication. One of PJE's primary features is its exceptional thickness and interface controllability. Figure 8-1 compares the thickness variation of GaAs epitaxial layers grown by PJE and MOVPE on 2-inch wafers [8]. The growth thickness was normalized with the thickness at the center of wafers. In this experiment, we performed PJE and MOVPE in the same reactor without rotating the substrates. TMGa and AsH_3 were used as sources in both MOVPE and PJE. The wide variation in the MOVPE profile probably reflects the gas flow pattern in the reactor. This is because growth is controlled by the "mass-transport-limited process" in MOVPE. In contrast, the thickness variation of the PJE-grown layers was within 1.5%, which was comparable to the accuracy of thickness measurement using a stylus profilometer (DEKTAK). Thus, the inherent self-limiting nature of PJE enables us to grow extremely uniform epitaxial layers automatically over most of the substrate surface.

8.3.2 Interface controllability

PJE can maintain self-limiting growth even in the case of some kinds of heterostructures. InAs/InP and GaAs/GaP are the systems where self-limiting works well at the strained heterointerfaces [12, 13]. Therefore, it is considered that we can make atomically abrupt interfaces without any need for the precise control of growth. Figure 8-2 shows the X-ray diffraction profiles for the three kinds of GaAs/GaP short-period strained-layer superlattices. The samples were grown on GaAs (001) substrates at 500°C using TMGa, AsH_3, and PH_3. The growth conditions have been reported in detail [13]. We observed numerous satellite peaks. The angles of the satellites agree with those calculated using Bragg's law.

In Fig. 8-3, we showed a (110) cross-sectional high-resolution transmission electron microscopy (TEM) image of $(GaAs)_4(GaP)_2$ short-period strained-layer superlattice [14]. Despite about a 3.6% lattice mismatch at the interfaces between GaAs and GaP, the thickness of each layer and heterointerface were well controlled. The results in Figs. 8-2 and 8-3 indicate that the self-limited, monolayer growth is not just an average value, but that the growth is really controlled layer-by-layer on a monatomic scale.

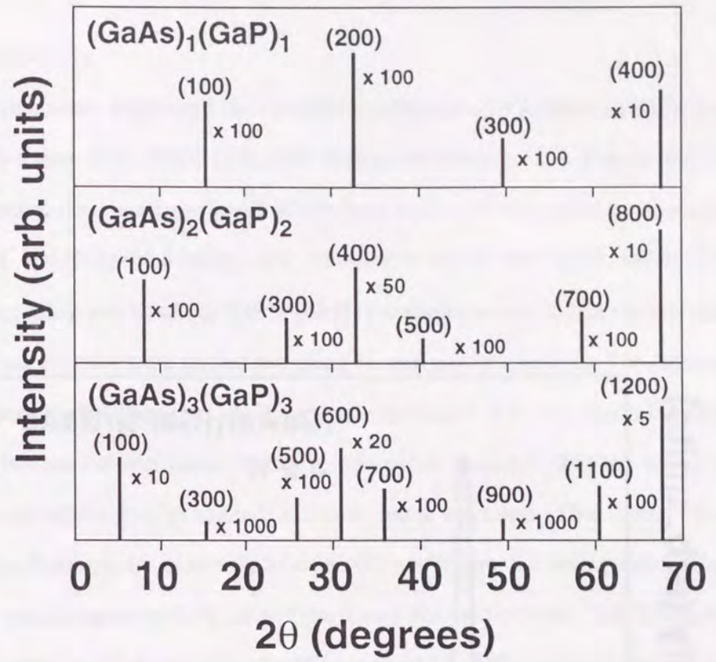

Figure 8-2. X-ray diffraction profiles of $(GaAs)_m(GaP)_n$ strained-layer superlattices.

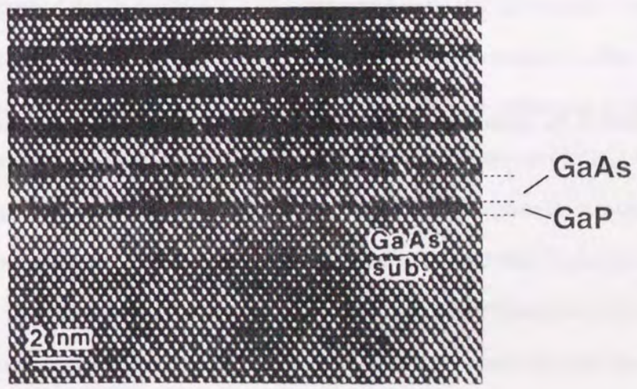

Figure 8-3. (110) cross-sectional TEM image of $(GaAs)_4(GaP)_2$ superlattice.

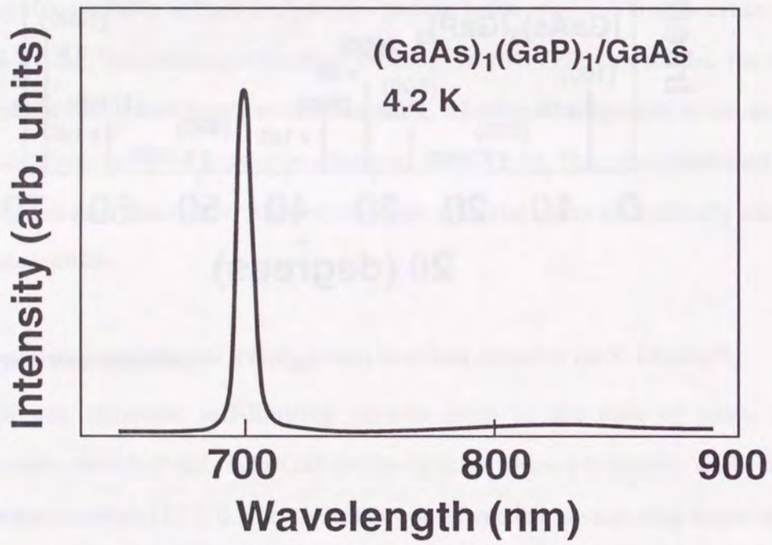

Figure 8-4. PL spectrum from a $(GaAs)_1(GaP)_1$ superlattice grown on GaAs (001), measured at 4.2 K.

8.3.3 Band engineering

We have already confirmed the successful fabrication of a $(GaAs)_1(GaP)_1$ superlattice by X-ray diffraction [13], TEM [14], and Raman scattering [15]. Figure 8-4 shows the photoluminescence (PL) spectrum at 4.2 K obtained from a $(GaAs)_1(GaP)_1$ superlattice grown on GaAs (001). We observed a strong, new emission at λ=700 nm, which was not observed in the $GaAs_{0.5}P_{0.5}$ alloy and $(GaAs)_n(GaP)_n$ ($n \geq 2$). Detailed analyses of the optical transition of the monolayer superlattice were carried out using PL and photoreflectance. The emission peak at 700 nm was seen to be the direct excitonic recombination [16, 17]. Since the $GaAs_{0.5}P_{0.5}$ ternary alloy has an indirect band structure, this result indicates that the formation of the monolayer superlattice has produced a direct band structure. The direct band gap of $(GaAs)_1(GaP)_1$, if coherently grown on a GaAs (001) substrate, has been predicted by Dandrea *et al.* [18] Our result experimentally proved the theory for the first time. This is a good example in which the superior thickness and interface control by PJE produced the unprecedented, exciting materials with new band structures.

8.3.4 Low-temperature growth and high-concentration doping

8.3.4.1 Se doping into GaAs

Growth can be carried out at relatively low temperatures by PJE. Since PJE uses pure surface reactions, there is no need to activate gas-phase chemical reactions. The surface migration of the adsorbed species, especially group-III species, might be enhanced by alternate supply of sources just as in migration-enhanced epitaxy (MEE) [19]. Because of these reasons, we can obtain smoother and superior epitaxial layers even at low growth temperatures. Considering the growth temperature dependence of selenium (Se) doping into GaAs, the doping concentration generally increases when the temperature decreases [20]. Therefore, PJE allows us to achieve high-concentration n-type doping of Se into GaAs and lower redistribution of the impurity atoms. Figure 8-5 shows the room temperature (300 K) electron concentration and the Hall mobility of Se-doped GaAs as a function of the injected H_2Se mole fraction in the reactor. These data were measured from the Se-doped GaAs epilayers grown on the semi-insulating

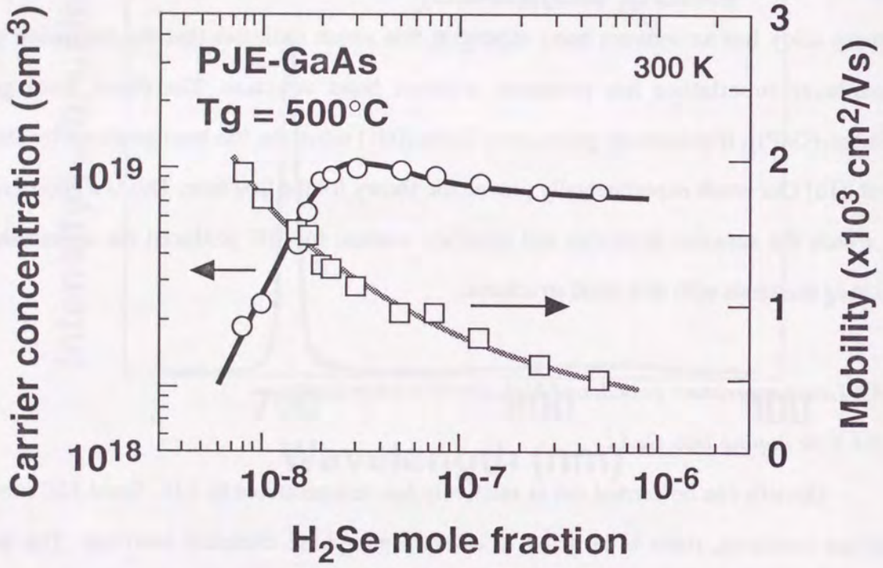

Figure 8-5. Carrier concentration of Se-doped GaAs grown by PJE as a function of H_2Se mole fraction.

(001) GaAs substrates, using Van der Pauw's method. The gas sequence for the growth of GaAs was 2 s TMGa, 0.5 s H_2 purge, 5 s AsH_3, and 0.5 s H_2. The partial pressures of TMGa and AsH_3 in the reactor were 2.1 Pa and 64 Pa. The thickness of epitaxial layers was 100 nm. For doping, H_2Se was supplied continuously throughout the growth. It should be noted that the maximum electron concentration obtained is as high as $1x10^{19}$ cm^{-3}. In addition, the surface morphology of all the Se-doped GaAs was specular. More detailed Se doping results of PJE-grown GaAs have been reported elsewhere [21].

8.3.4.2 Be doping into InGaAs

Lowering the growth temperature is very effective in doping the elements of high-vapor pressure, and is also effective in suppressing the solid diffusion of the dopants. In addition, the two-dimensional growth mode of PJE makes the surface morphology very smooth at low temperatures. Thus, these two features seem to be very useful for growth of extremely highly doped layers with good surface morphology. These features are attractive for making $In_{0.53}Ga_{0.47}As$/InP HBTs, where the growth of heavily p-type doped, thin $In_{0.53}Ga_{0.47}As$ with good crystalline quality is a key to success. Generally the p-type dopants such as zinc (Zn) and Be have a serious problem in that they easily diffuse among the III-V crystals. In spite of the promising behavior of carbon (C) acceptors in GaAs due to their small diffusion coefficient and high-concentration doping [22-24], its electrical activation efficiency is limited to be low, and is unstable in $In_{0.53}Ga_{0.47}As$ due to the deactivated mechanism by the incorporated hydrogen (H) atoms in the crystal [25, 26]. Therefore, the lowering the growth temperature seems to be a unique way to reduce the redistribution and increase the doping level for acceptors in $In_{0.53}Ga_{0.47}As$ [27]. In this section, we show the PJE growth of $In_{0.53}Ga_{0.47}As$ and the Be doping into $In_{0.53}Ga_{0.47}As$ layers. The results of HBT will be reported in a later section.

The growth kinetics of PJE-$In_{0.53}Ga_{0.47}As$ and the detailed growth conditions have been reported previously [28, 29]. $In_{0.53}Ga_{0.47}As$ growth by PJE was done at as low as 350°C, using TMIn, TEGa, and AsH_3. TMIn with TEGa, and AsH_3 were alternately supplied as shown in Fig. 8-6. As a source of Be, we used diethylberyllium (DEBe) [30]. We could not observe clear self-limiting growth of $In_{0.53}Ga_{0.47}As$ using these sources. Therefore, the

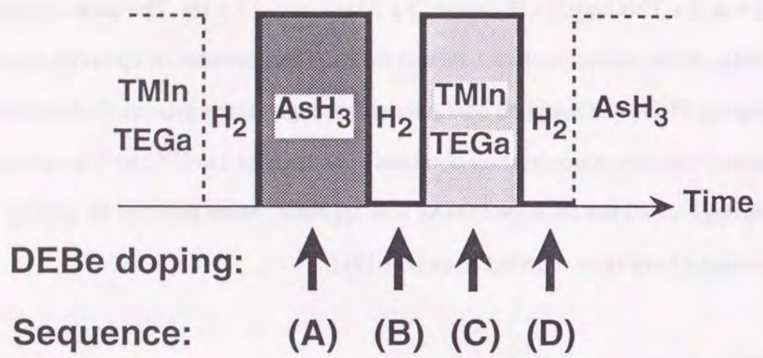

Figure 8-6. Gas sequence to grow InGaAs and the Be doping timing.

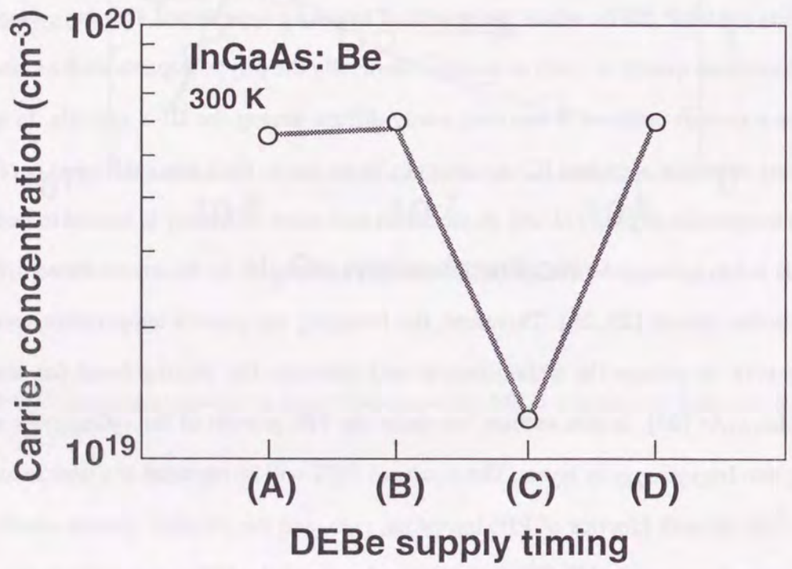

Figure 8-7. Carrier concentration of Be-doped InGaAs grown by PJE under different doping timings.

growth of $In_{0.53}Ga_{0.47}As$ cannot be regarded as the real PJE. We can, however, expect the advantage mentioned above, similar to the real PJE with self-limiting. We believe that such a "quasi-PJE (ALE)" technique is technically important.

Nishizawa *et al.* have carried out detailed studies on the gas sequence for impurity doping in GaAs grown by molecular layer epitaxy [31]. Also in our PJE, we can select several doping timings. We studied the appropriate timing of DEBe injection to clarify ways of making Be doping more efficient [29]. Figure 8-7 shows the carrier concentration of Be-doped $In_{0.53}Ga_{0.47}As$ grown by PJE for different doping timings. We found that a high carrier concentration was obtained, except when supplying DEBe with TMIn and TEGa.

Be atoms occupy the group-III sublattice sites of $In_{0.53}Ga_{0.47}As$ crystal, so it is strange that Be is less efficiently incorporated during the TMIn and TEGa exposure. This is probably due to the competitive adsorption process of DEBe at the growth surface. There is almost no difference in the carrier concentration among the other three types of doped timing. This implies that the Be incorporation by DEBe pyrolysis is not sensitive to the kinds of surface terminated atoms. We illustrated each situation of DEBe doping in Fig. 8-8. In PJE, the impurity incorporation would be controlled by surface adsorption, desorption, and decomposition kinetics of dopant sources. In timing (C), the competitive adsorption occurs among DEBe, TMIn, and TEGa. The number of gas-phase TMIn and TEGa molecules is much larger than that of DEBe. In addition, the adsorption lifetime of TMIn and TEGa is expected to be longer than that of H_2 or AsH_3. Therefore, from a statistical viewpoint, the TMIn and TEGa always cover the surface lattice sites, so the sticking probability of DEBe on the surface will be very small. This is the reason for the low Be doping level at the group-III exposure period. In contrast, in other timings, the Be doping level was the same. This is because the surface lifetimes of AsH_3 and H_2 will be so short that the surface lattice sites have a high probability of occupancy by DEBe. Therefore, the doping level will be high.

We found that the surface morphology of Be doped $In_{0.53}Ga_{0.47}As$ layers depended on the doped timing. Figure 8-9 shows the growth surfaces doped with H_2 purge (timing (B)) and with AsH_3 (timing (A)). Although the carrier concentrations were almost the same, a difference in surface morphology was observed. The surface became rough when the DEBe was supplied

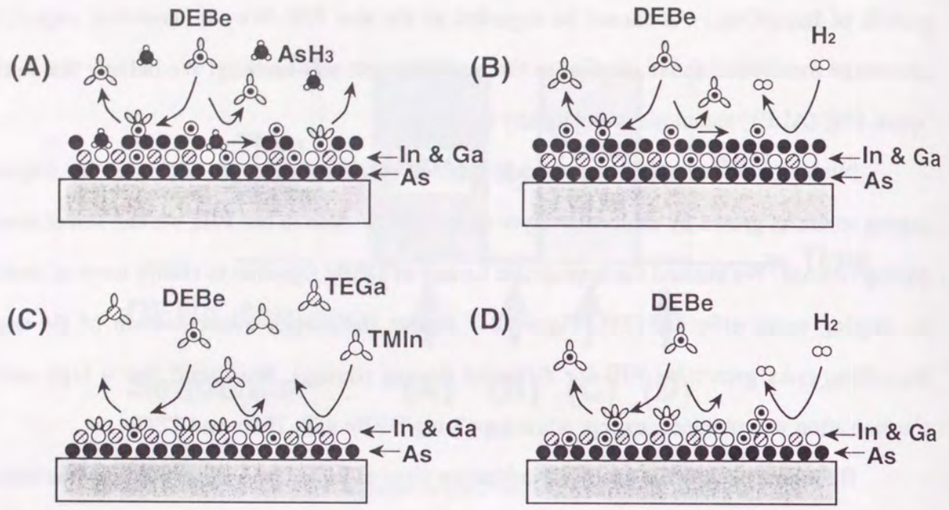

Figure 8-8. Illustration of Be doping by DEBe under different timings. In (A) and (B), DEBe will stick on top of surface As atoms and occupy the group-III sublattice sites. In (C), adsorption of DEBe will be suppressed due to the competition with TEGa and TMIn. Only DEBe at the vacant group-III sublattices will be incorporated. In (D), DEBe will be adsorbed on the surface and occupy the vacant, surface group-III lattice sites. Be might be remained on the group-III surface and be incorporated after the next As supply.

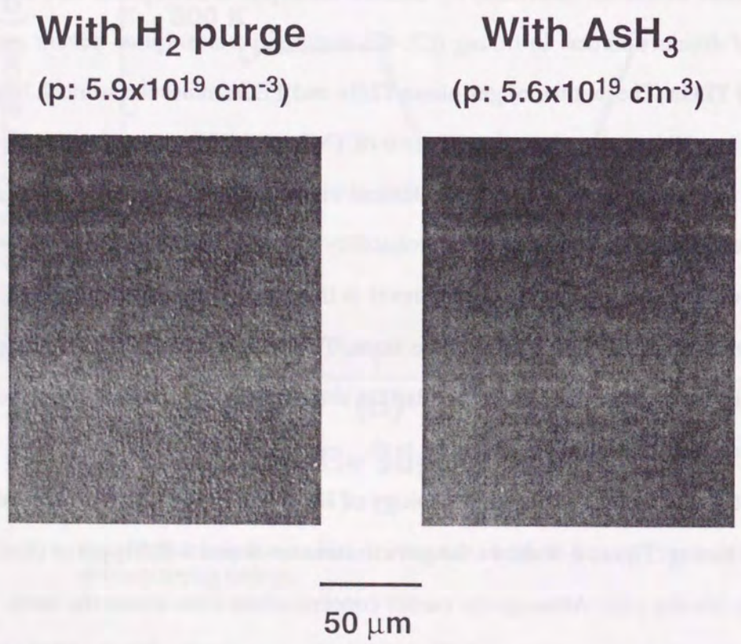

Figure 8-9. Surface morphologies of Be-doped InGaAs.

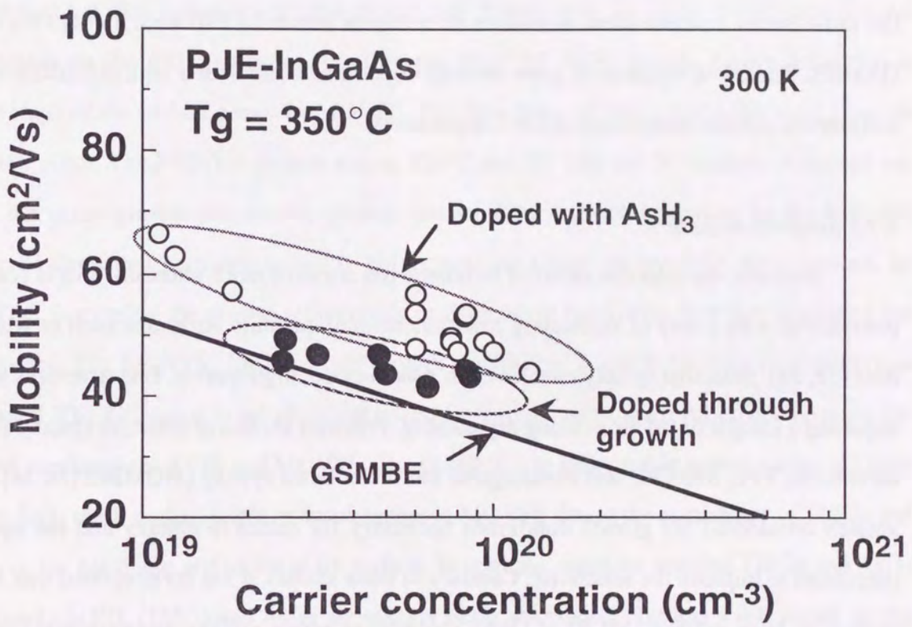

Figure 8-10. Hall mobilities as a function of carrier concentration in Be-doped InGaAs grown by PJE. The result reported for GSMBE is indicated by the solid line.

for H_2 purge durations. We always obtained good surface morphology when the DEBe was supplied during the AsH_3 period. The reason for this result is still unclear.

Figure 8-10 shows the Hall mobilities of p-type $In_{0.53}Ga_{0.47}As$ as a function of the carrier concentration. Compared to the results in which Be was doped continuously through growth, relatively high mobility materials were grown by doping with an AsH_3 pulse timing (A). The highest hole concentration we obtained was about $1x10^{20}$ cm^{-3}. The solid line indicates the experimental results obtained from gas-source molecular beam epitaxy (GSMBE) [27]. At the same carrier concentration, mobilities of epilayers grown by PJE were higher than that by GSMBE. Thus, PJE helps us to grow heavily doped materials with a high crystalline quality and smooth surface morphology at low temperatures.

8.3.5 Selective epitaxy

Recently, the selective epitaxial technique has attracted much attention. This is because it provides us with a way of fabricating low-dimensional quantum structures such as wires and dots [32, 33]. Selective epitaxy enables us to make buried, high-quality, fine structures without exposing a sample to the air or using dry etching. Previous studies of selective epitaxy focused on chloride VPE, MOVPE, and metalorganic molecular beam epitaxy (MOMBE) [34-36]. These studies considered the growth conditions necessary for selective epitaxy and the optimum precursors to improve the selectivity. Contrary to these studies, it has been reported that ALE or molecular layer epitaxy (MLE) of GaAs provides selective epitaxy and excellent thickness uniformity [37]. Preliminary results on GaAs growth by PJE also show that the thickness at the edge of SiO_2 mask opening is uniform, as expected from its self-limiting growth [8]. These attractive results might come from their peculiar gas sequence, that is, the alternate supply of TMGa and AsH_3.

In this section, we show the phenomenological results on GaAs selective epitaxy by PJE and try to reveal the mechanism related to the selectivity [6, 38].

8.3.5.1 Nucleation on mask

We compared GaAs selective growth in PJE with that in MOVPE. Figure 8-11(a) shows a Nomarski micrograph of a surface grown by PJE on a GaAs (001) substrate partially masked with SiO_2. We exposed the substrate alternately to TMGa and AsH_3 flows for 354 cycles. The gas sequence for PJE, *i.e.* AsH_3/ H_2/ TMGa/ H_2, was 10/ 1/ 3/ 1 s. The flow rates of H_2 through TMGa kept at 3.0°C and 10% AsH_3 were 30 sccm and 480 sccm. No deposits formed on the SiO_2 mask and a 120 nm-thick GaAs epitaxial layer formed at the openings, indicating perfect selective growth. The growth rate in this experiment was 1.2 ML/cycle, which is a little higher than the ideal monolayer-limited growth rate. We attribute the higher rate to excessive As adsorption on the (001) surface caused by the plentiful AsH_3 supply. Figure 8-11(b) is a micrograph of the surface grown by MOVPE. The flow rates of TMGa and AsH_3 were 10 sccm and 480 sccm. The MOVPE growth was at 500°C and 20 Torr for 20 minutes. Although we used the same growth precursors, growth temperature, and total pressure as for PJE, we observed deposited particles, probably polycrystalline GaAs, on the SiO_2 mask surface. In MOVPE, increasing the growth temperature or decreasing the TMGa flow rate improved the selectivity. For MOVPE, the range of growth conditions suitable for selective epitaxy is restricted. The difference in the observed selectivity originates from the difference between the growth mechanisms of PJE and MOVPE. The possibility to make stable growth nuclei of GaAs on the SiO_2 mask surface might be much higher in MOVPE due to the coexistence of TMGa and AsH_3 in the gas phase and on the mask surface. In contrast, since we supplied TMGa and AsH_3 alternately in PJE, TMGa and AsH_3 are quickly desorbed without forming stable nuclei on the mask. This leads to no deposition on the SiO_2 mask surface.

8.3.5.2 Growth rate enhancement at mask edge

We compared the thickness profiles of GaAs layers grown at the mask openings by PJE and MOVPE under the conditions described above (Fig. 8-12). We masked the (001) GaAs substrates with a 500-μm-wide SiO_2 line along the [110] or [1-10] direction. After growth, by removing the SiO_2 mask from the surface, we measured the profiles using a DEKTAK surface profiler. The deposited layer was flat at the SiO_2 edge in the PJE-grown sample as expected (Fig. 8-12(a)). Note that the growth rate was 1.25 ML/cycle. In the MOVPE-grown samples,

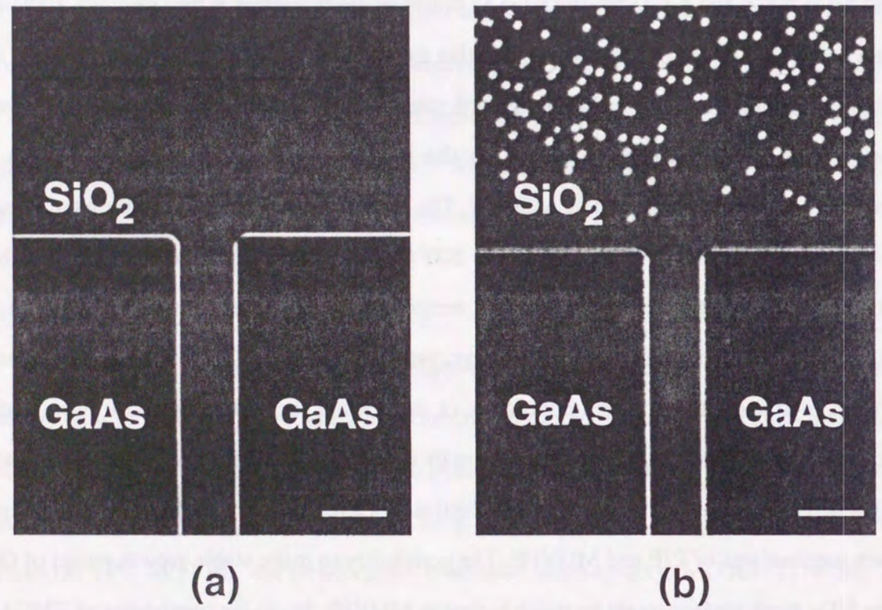

Figure 8-11. Nomarski micrograph of GaAs surface grown (a) by PJE and (b) by MOVPE. Marker represents 10 μm.

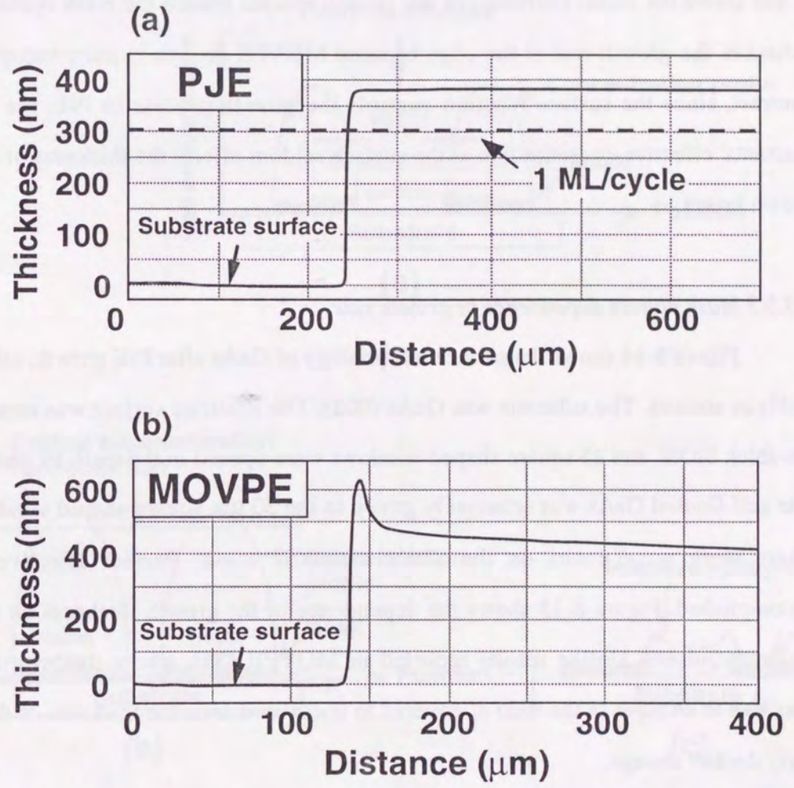

Figure 8-12. Thickness profiles of GaAs epilayers (a) by PJE and (b) by MOVPE. PJE growth was done with 1060 gas cycles. Note that the growth rate was 1.25 ML/cycle.

however, the growth rate was enhanced at the SiO_2 mask edge (Fig. 8-12(b)). We attribute the thickness nonuniformity in MOVPE to the lateral diffusion of the growth species in the gas phase.

Figure 8-13 illustrates the mechanism of MOVPE. The exclusive consumption of the growth reactants at the mask openings results in a concentration gradient in the lateral direction at and above the mask. Diffusion of the growth species toward the mask openings, therefore, enhances the growth rate at the edge because MOVPE growth is mass-transport limited. In contrast, since the surface reaction controls the growth process in PJE, the change in the reactants' effective concentration at the surface seldom affects the thickness of the selectively grown layers.

8.3.5.3 Mask pattern dependence of growth rate

Figure 8-14 shows the surface morphology of GaAs after PJE growth, using TMGa and AsH_3 as sources. The substrate was GaAs (001). The substrate surface was covered with 100-nm-thick SiON, and 25 square-shaped windows were opened in the mask by photolithography. The self-limited GaAs was selectively grown in the 30 μm square-shaped windows at 500°C. There were no deposits on the SiON dielectric mask. Perfect selective growth was accomplished. Figure 8-15 shows the dependence of the growth thickness on the size of the square windows. Unlike results reported in MOVPE [39], where the growth thickness is sensitive to changes in the ratio of covered to uncovered area, the thickness of the PJE-formed layer doesn't change.

8.3.5.4 Shape of selective-grown layers

To study the selective growth at the narrower openings in the mask, we carried out PJE growth of GaAs on substrates coated with SiO_2 about 120-nm-thick with stripes along [110] and [1-10]. Figure 8-16 shows scanning electron microscopy (SEM) pictures of a cross-section of selectively grown GaAs. We grew GaAs at 500°C by introducing TMGa and AsH_3 pulses alternately for 880 cycles. The pulse duration of TMGa and AsH_3 was 3 s and 10 s, respectively. The partial pressure of TMGa was 2.1 Pa and that of AsH_3 was 64 Pa. The H_2

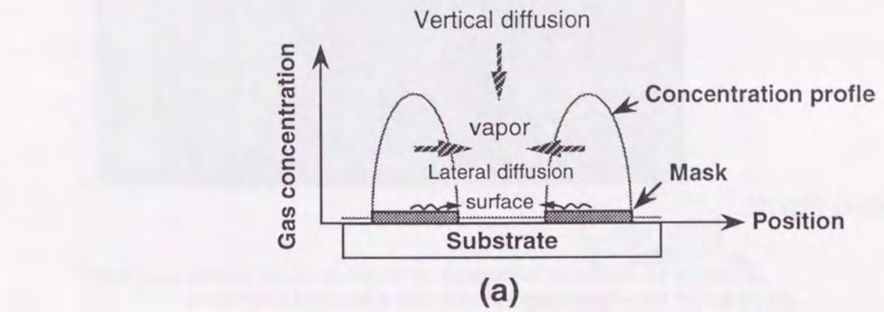

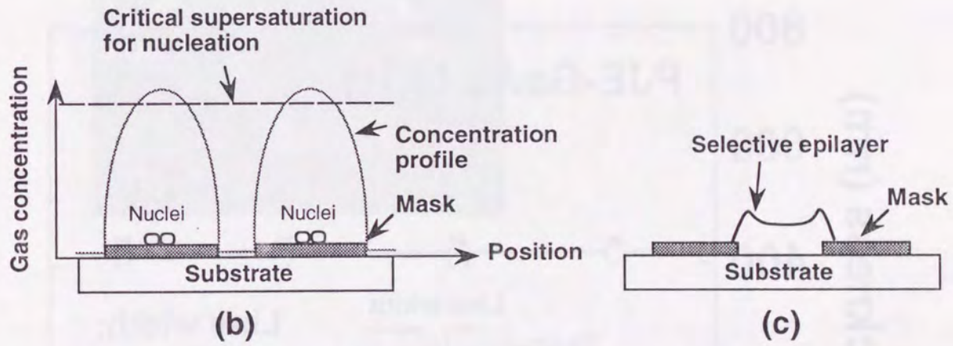

Figure 8-13. Mechanism of selective epitaxy during MOVPE. (a) The vertical and lateral diffusion of source species, (b) the mechanism of nucleation on the mask, and (c) the shape of selective epitaxy resulting from (a).

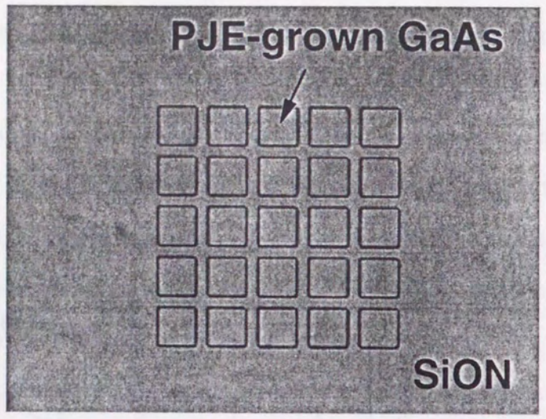

Figure 8-14. Nomarski micrograph of as-grown GaAs surface using PJE. A part of the substrate was covered with a patterned SiON mask.

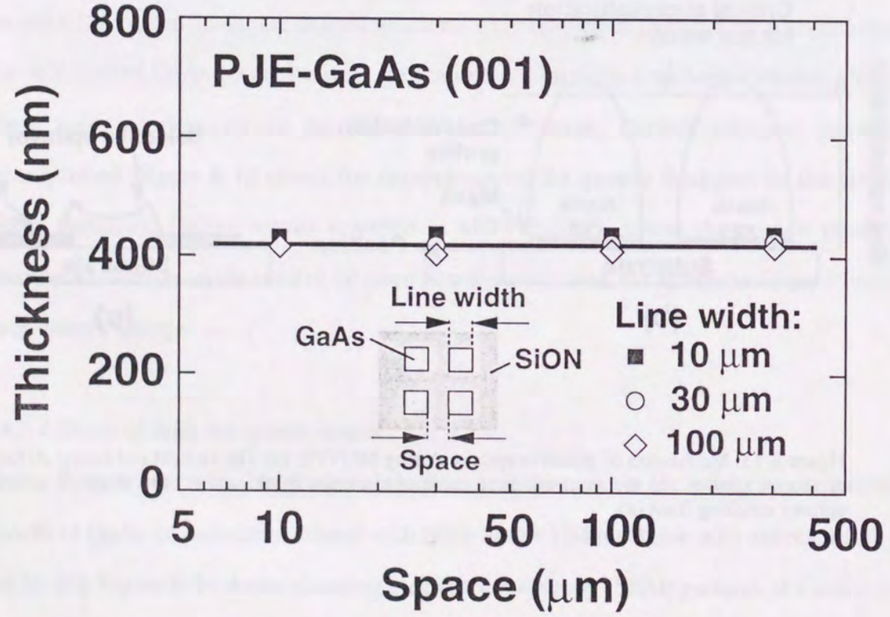

Figure 8-15. Dependence of PJE-grown GaAs thickness on the size of square windows in the SiON mask.

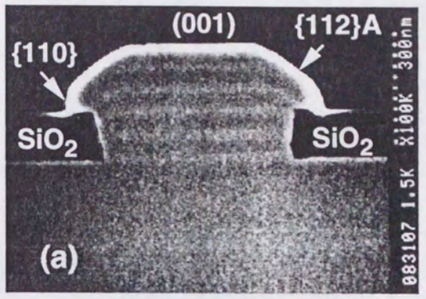

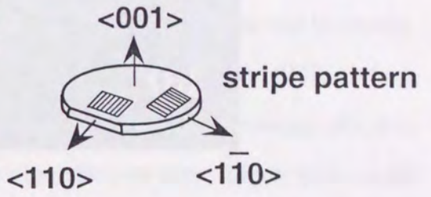

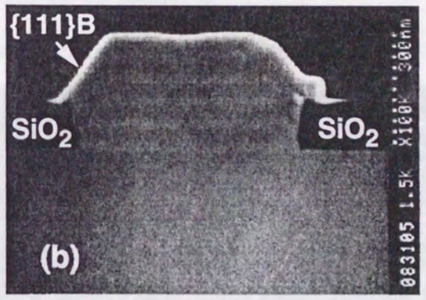

Figure 8-16. Cross-sectional SEM pictures of selectively grown GaAs by PJE. (a) (1-10) cross section at an opening width of 0.5 μm, (b) (110) cross section at a opening width of 0.6 μm.

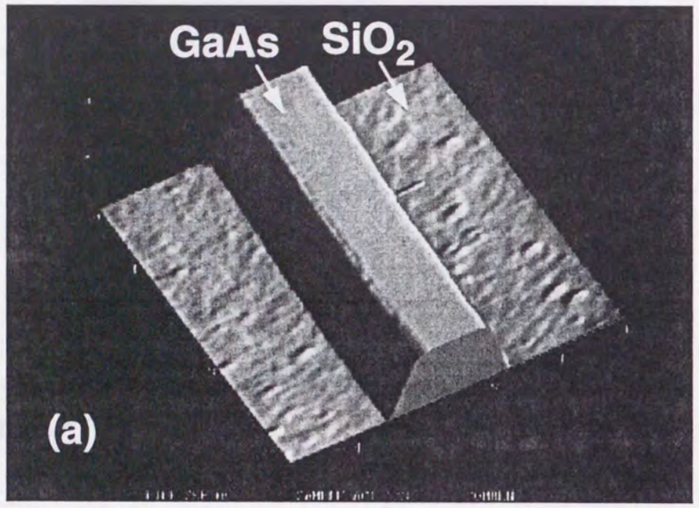

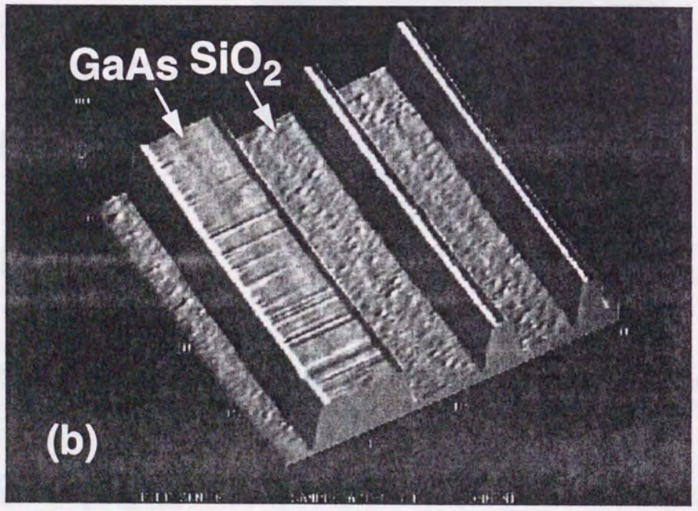

Figure 8-17. AFM images of selective GaAs layers. (a) A stripe toward <1-10> and (b) a stripe toward <110>.

purge duration was 1 s. To observe the path of the growth front, we periodically marked the epilayer with Se-doped layers. The selective growth could be achieved, even in these channels with submicron widths. The observed growth thickness was about 300 nm. Although this value was almost independent of the mask opening width, the growth thickness during a cycle of source gas exposure corresponded to about 1.2 ML/cycle. Our recent studies into PJE-grown GaAs (001) have shown that the growth rate is self-limited to about 1.2 to 1.3 ML/cycle for long exposure times and large partial pressures of AsH_3 [40]. We clarified that this was due, not to the gas-phase mixing reaction between TMGa and AsH_3, but to the excess As adsorption at the (001) surface. We speculate that the saturated growth rate above 1 ML/cycle will be closely related to the As-rich, c(4x4) or d(4x4) reconstruction of the MOVPE-GaAs (001) surface revealed by grazing incidence x-ray diffraction and reflectance difference spectroscopy [41, 42]. Since the growth over 1 ML/cycle is also a surface reaction, the growth rate dependence on the pattern size was almost negligible.

Looking more closely at Fig. 8-16, the (1-10) cross-sectional view in Fig. 8-16 (a) seems to be surrounded by (001), {112}A, {111}A, and {110} facets. We observed a lateral overgrowth of GaAs toward <110> on the SiO_2 layer. PJE growth proceeds, keeping a smooth top (001) surface even in the submicron openings. In contrast, at the (110) cross-section in Fig. 8-16 (b), the side walls of the structure were {111}B facets. The GaAs growth rate on {111}B facets seems to be low, judging from the small lateral overgrowth toward <1-10> on the SiO_2 mask. The top surface is not perfectly flat, and the layer is slightly thicker at the edges than in the center. Our growth experiments show that a H_2 purge time of 1 s is long enough to eliminate the gas-phase mixing. The reactants' mixture causing the MOVPE-like growth is therefore negligible. Since the growth thickness at the center is the same as that in Fig. 8-16 (a), the growth rate at the edges seems to be affected by the side wall facets.

The difference in the geometrical shape between the <110> and <1-10> stripes is observed in the images of atomic force microscope (AFM) as shown in Fig. 8-17.

8.3.5.5 Model for selective epitaxy

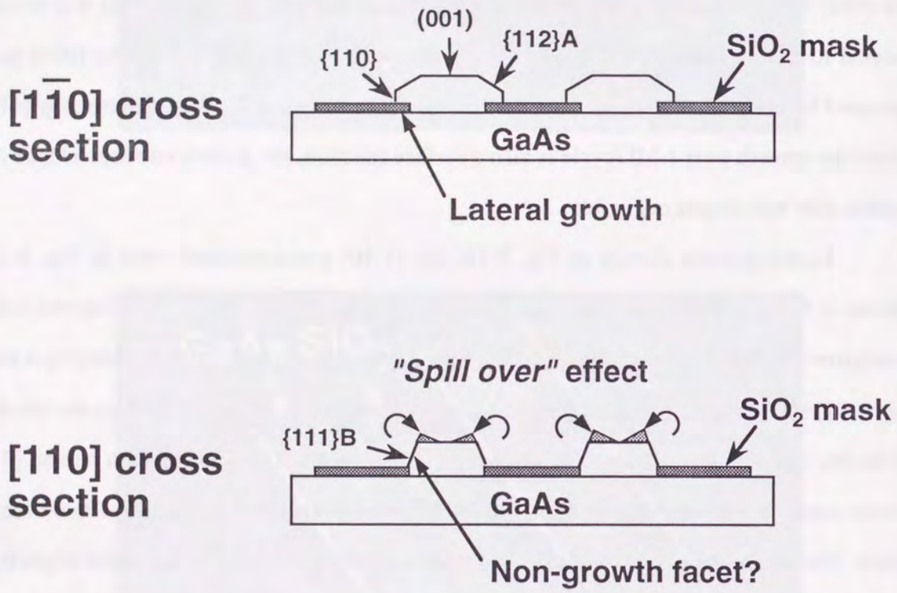

Figure 8-18. Illustration of GaAs facets grown by PJE.

The probable model is illustrated in Fig. 8-18. Ga species adsorbed on {111}B facets will migrate toward the (001) surface. Then, the Ga species will contribute to the growth of the (001) top surface, as in the *"spill over"* effect in MOVPE [43]. According to the selective adsorption model, which explains the self-limiting growth mechanism of PJE, the methylgallium molecules, $Ga(CH_3)_n$ (n=1-3), are not adsorbed and/or decomposed at the Ga-terminated surface of the (001) plane [7]. Hence, the result shows that the species migrating from (111)B to (001) will be atomic Ga. The TMGa molecules adsorbed on the {111}B facets will quickly decompose and release atomic Ga.

Thus, several kinds of growth facets have emerged for the selectively grown GaAs, although it is predicted that the conformable growth occurs in ALE. This is probably because growth conditions to obtain self-limited growth, such as gas sequences and appropriate growth temperatures, differ according to the crystal orientations. The growth rate of the non-planar selective epilayers is also different from the value on a planar substrate, due to the surface migration of growth species toward more favorable facets. Therefore, selective growth by PJE to make some low-dimensional structures requires further studies into growth mechanisms.

8.4 Practical Application

8.4.1 InGaAs/InP HBT

Making use of the low-temperature growth and high-concentration Be doping into PJE-grown InGaAs, we fabricate the $In_{0.53}Ga_{0.47}As$/InP heterojunction bipolar transistor (HBT) structures using a novel PJE/MOVPE hybrid growth process [6, 44]. We show that PJE is a key technology used for making a high-performance HBT.

The epitaxial layer structure for HBT is summarized in Table 8-2. In the growth procedure, the InP buffer layer, n^+-$In_{0.53}Ga_{0.47}As$ subcollector, and n-$In_{0.53}Ga_{0.47}As$ collector were grown by conventional MOVPE at 600°C. Then, the growth temperature was lowered to 350°C and a Be-doped p^+-$In_{0.53}Ga_{0.47}As$ base layer was grown by PJE. An undoped-$In_{0.53}Ga_{0.47}As$ spacer layer was grown by PJE at 350°C, or by MOVPE after raising the

growth temperature to 450°C. Finally, a Se-doped InP emitter layer and Se-doped n^+-$In_{0.53}Ga_{0.47}As$ contact layer were grown by MOVPE at 450°C. In preliminary experiments, we found significant Be diffusion toward the InP emitter in a structure without an undoped-$In_{0.53}Ga_{0.47}As$ spacer layer using the secondary ion mass spectroscopy (SIMS) analyses. The reason for the insertion of the undoped-$In_{0.53}Ga_{0.47}As$ between the p^+-$In_{0.53}Ga_{0.47}As$ base and the InP emitter is to suppress the Be diffusion. We compared ways of growing the undoped-$In_{0.53}Ga_{0.47}As$ spacer layer between PJE and MOVPE. However, we could not determine which is better for suppressing the Be diffusion into InP, because there is a trade-off between the growth temperature and the growth time. The growth of the InP emitter using MOVPE at 450°C clearly suppressed the Be diffusion. We found that shortening the growth time for the InP emitter by using MOVPE is more effective in reducing the Be diffusion than growing InP by PJE at 350°C. It takes longer to grow InP by PJE, because the growth rate is 0.5 ML/cycle.

To evaluate the effect of the spacer layer, we fabricated test structures with various thicknesses of the PJE-grown, undoped-$In_{0.53}Ga_{0.47}As$ spacer. The total thickness of the spacer (Δ) and the p^+-InGaAs base was kept at 50 nm (Table 8-2). Figure 8-19 shows the SIMS depth profiles of the test structures. In this experiment, a nominal $6x10^{19}$ cm^{-3} Be was doped into the $In_{0.53}Ga_{0.47}As$ region with a thickness of 50-Δ nm. When the p-type base layer was located adjacent to the emitter layer (Δ=0), a drastic diffusion of Be into InP was observed. The anomalous shape of the Be profile, similar to the previous report [45], implies a higher diffusion coefficient of Be in InP than in $In_{0.53}Ga_{0.47}As$ at this growth condition. In contrast, the diffusion was significantly reduced by the insertion of the undoped-$In_{0.53}Ga_{0.47}As$ spacer. As the thickness of the spacer layer increased, the degree of the Be diffusion into InP decreased. With Δ=20 nm, the redistribution of Be into InP was completely suppressed and the position of the p-n junction coincided with the position of the $In_{0.53}Ga_{0.47}As$/InP heterointerface. The undoped $In_{0.53}Ga_{0.47}As$ spacer became a p^+-layer due to the diffused Be during growth. As a result, a Be-doped $In_{0.53}Ga_{0.47}As$ with a thickness of 50 nm was formed, and the average Be-concentration became $4x10^{19}$ cm^{-3}. An HBT was fabricated using this

Table 8-2: Layer structure and growth conditions for InGaAs/InP HBT.

Layer	Material	Dopant and concentration (cm^{-3})	Thickness (nm)	Growth method and temperature
Cap	InGaAs	Se: 5E19	50	MOVPE, 450°C
Emitter	InP	Se:1E19, 1E20	25, 50	MOVPE, 450°C
	InP	Se:5E17, 2E18	50, 100	MOVPE, 450°C
Spacer	InGaAs	Undoped	Δ	MOVPE, 450°C or PJE, 350°C
Base	InGaAs	Be:6E19, 7E19	50-Δ	PJE, 350°C
Collector	InGaAs	Undoped	300	MOVPE, 600°C
Sub-collector	InGaAs	Se:5E18	350	MOVPE, 600°C
Buffer	InP	Undoped	300	MOVPE, 600°C

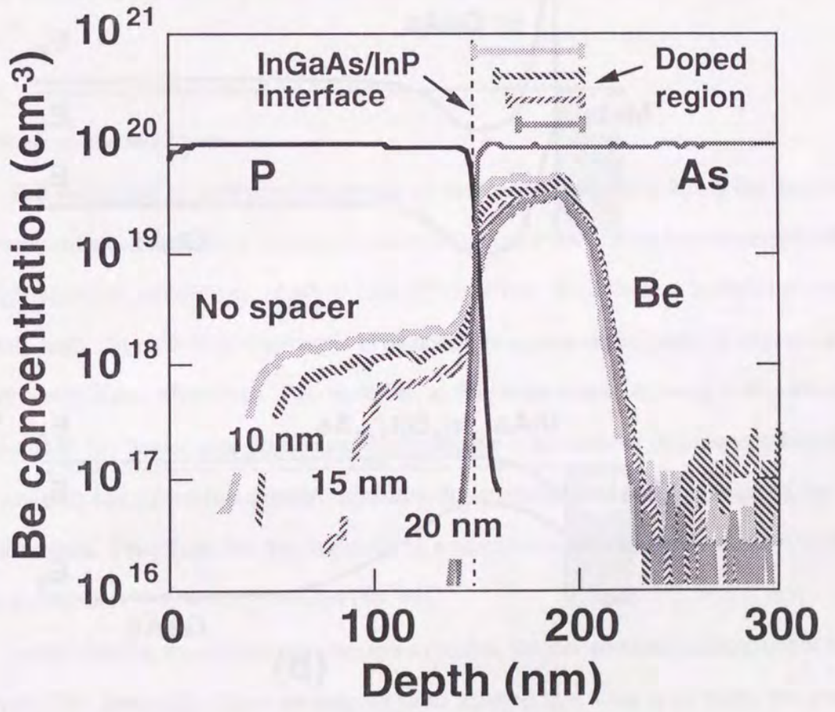

Figure 8-19. SIMS depth profiles of Be at InGaAs base and InP emitter region in the HBT structures. The thickness of the undoped-InGaAs spacer layer was varied.

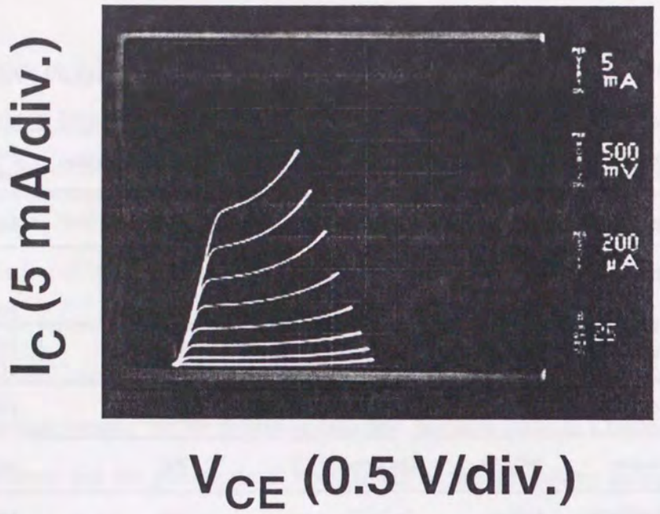

I_C (5 mA/div.)

V_{CE} (0.5 V/div.)

Figure 8-20. Common emitter I-V characteristics of a HBT with an InGaAs base layer doped at $7x10^{19}$ cm^{-3}.

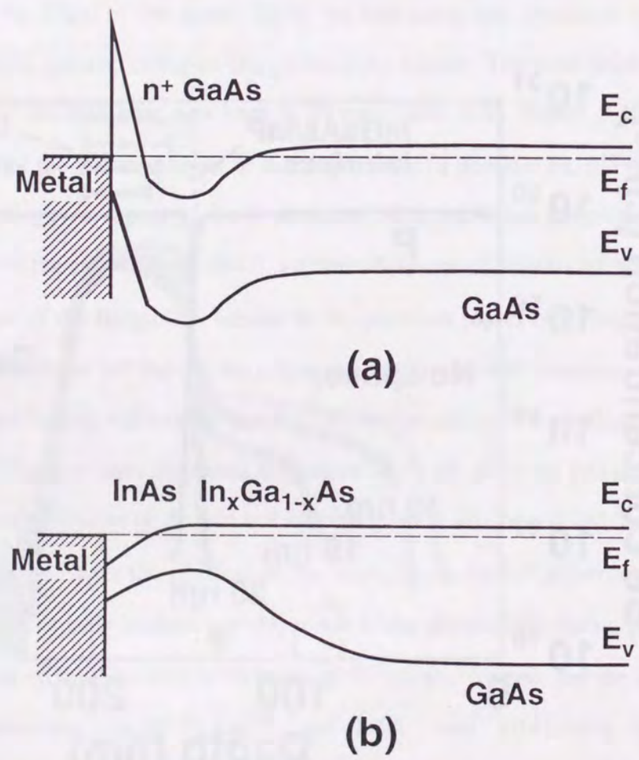

Figure 8-21. Band diagrams of typical two approaches to low-resistance ohmic contact to GaAs. E_c and E_v show the energies of conduction band edge and valence band edge, respectively. E_f shows the position of Fermi energy.

epitaxial structure with Δ=20 nm. For the device with a 5x20 μm emitter, DC current gain, β, was 47, at a V_{CE}=1.0 V and I_C=50 mA (which corresponds to J_C=$5x10^4$ A/cm^2).

We fabricated another HBT structure [46]. Here, we grew a 20-nm-thick, undoped-$In_{0.53}Ga_{0.47}As$ spacer layer using MOVPE at 450°C, on 30-nm-thick p^+-$In_{0.53}Ga_{0.47}As$ doped at $7x10^{19}$ cm^{-3} grown by PJE. Be diffusion during growth resulted in 50-nm-thick p^+-$In_{0.53}Ga_{0.47}As$ with a peak dopant concentration of $7x10^{19}$ cm^{-3}. The coincidence of the p-n junction with the $In_{0.53}Ga_{0.47}As$/InP heterointerface was confirmed by the SIMS depth profiles. Figure 8-20 shows the common-emitter I_C-V_{CE} characteristics of the fabricated HBT. The emitter size was 5x20 μm. The DC current gain was about 30.

Very recently, detailed results on $In_{0.53}Ga_{0.47}As$/InP HBT, where the 50-nm-thick $In_{0.53}Ga_{0.47}As$ base layer was doped with $1x10^{20}$ cm^{-3}, was reported by Shigematsu *et al.* [47]. They used the above-mentioned PJE/MOVPE hybrid process to make an HBT and obtained f_T of 161 GHz and f_{max} of 167 GHz. Their results show that the hybrid process using PJE and MOVPE is a promising technique for fabricating high performance $In_{0.53}Ga_{0.47}As$/InP HBTs.

8.4.2 Ohmic contacting layer

The reduction of parasitic resistance is very important to achieve the high-speed performance of electron devices such as metal semiconductor field effect transistors (MESFETs) and high electron mobility transistors (HEMTs). When the intrinsic switching speed is extremely high, the reduction of parasitic resistance has a great significance in suppressing the extrinsic delay time. Moreover, it is desirable to fabricate ohmic contacts with sub-micron dimensions as the device size decreases. However, the conventional technique using alloyed ohmic contacts has a poor fine-pattern capability due to the surface roughness called the *"ball-up"* phenomena. Therefore, the development of a novel non-alloyed ohmic contact with very low contact resistivity is strongly needed [48, 49].

In this section, we explain our attempts to realize the low resistance ohmic contacts to n-type GaAs [6]. Generally, there are two ways to achieve this. One is to make the Schottky barrier at the metal/GaAs interface thin by heavily doping into the GaAs surface (Fig. 8-21 (a)).

This leads to a high tunneling probability for electrons through the Schottky barrier. Another way is to insert a compositionally graded $In_xGa_{1-x}As$ layer (x=0-1) between the metal and n-type GaAs. This structure was proposed by Woodall [50] and the energy band diagram is shown in Fig. 8-21 (b). Because the surface Fermi level of InAs is pinned in the conduction band [50, 51], there is no barrier at the metal/InAs interface. In addition, due to the compositionally graded $In_xGa_{1-x}As$ layer, there are no Schottky barriers throughout the contact. An extremely low specific contact resistance of as little as $2x10^{-9}$ Ωcm^2 is predicted [50]. For fabricating these two kinds of structures, we used PJE.

8.4.2.1 InAs/InGaAs/GaAs graded layer

To make the surface layer having the compositional gradation in Fig. 8-21 (b), we used the PJE method. We used TMIn, TEGa, and AsH_3 as sources, and grew GaAs, $In_xGa_{1-x}As$, and InAs at 350°C. The n-type doping was done by flowing H_2Se throughout the growth. Here, we utilized the PJE's benefits for thickness controllability, the low temperature growth and the high doping concentration. It should be noted that the ohmic contacting layer can be formed in-situ at as low as 350°C. We showed the gas sequence for growing the layer in Fig. 8-22. We grew an $In_{xi}Ga_{1-xi}As$ layer, changing a pair of gas injection cycles for InAs (m_i) and GaAs (n_i). The growth rate in a pulse of GaAs and InAs was fixed at 0.5 ML/pulse. If we supply m InAs pulses and n GaAs pulses, the averaged composition of the InGaAs becomes $In_{0.5m}Ga_{0.5n}As_{(0.5m+0.5n)}$, or $In_{m/(m+n)}Ga_{n/(m+n)}As$. The thickness of each $In_{xi}Ga_{1-xi}As$ can be controlled by changing the repeated cycles of N_i.

Fig. 8-23 shows the scheme for growing an InAs/$In_xGa_{1-x}As$/GaAs structure. We grew the $In_xGa_{1-x}As$ (x=0-1) consisting of 7 steps of composition. The thickness of each compositional layer was about 15 to 16 nm with N_i=18. Therefore, the total thickness of the epilayer was about 100 nm. The H_2Se was flowed under the condition where Se was doped into GaAs with $9x10^{18}$ cm^{-3}.

To check the formation of the compositional graded layer, we studied the depth profile of atomic concentrations of In, Ga, and As using Auger electron microscopy (AES). Ar^+ sputtering, and measurements were repeated to detect the depth profile. The results are shown

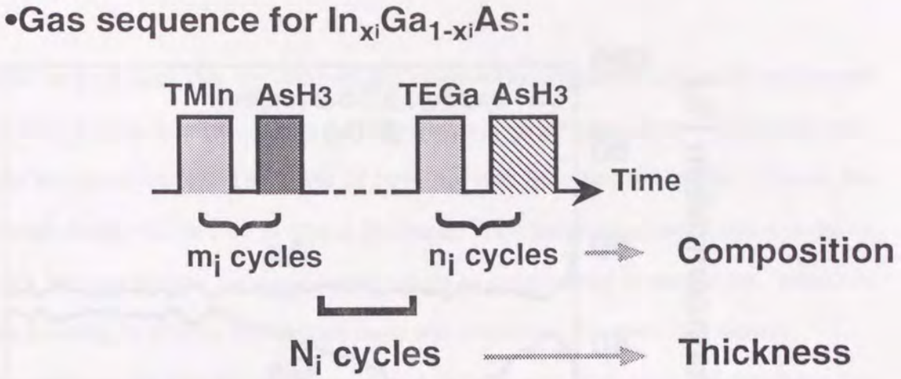

Figure 8-22. Gas sequence for growing composition-graded InGaAs on GaAs using PJE.

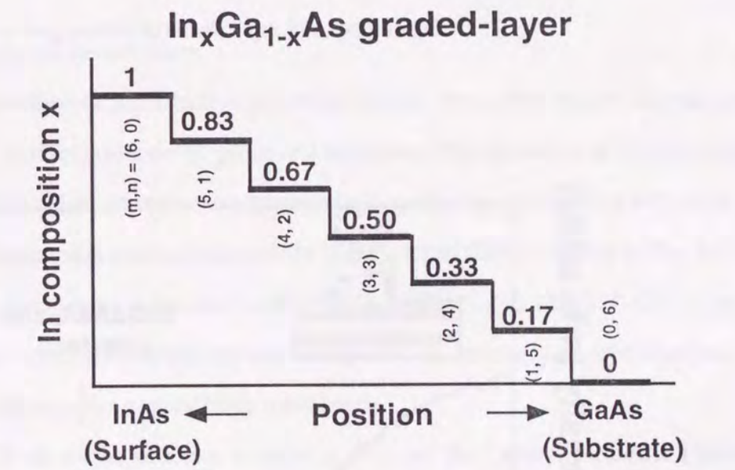

Figure 8-23. Scheme for growing composition-graded InGaAs on GaAs using PJE.

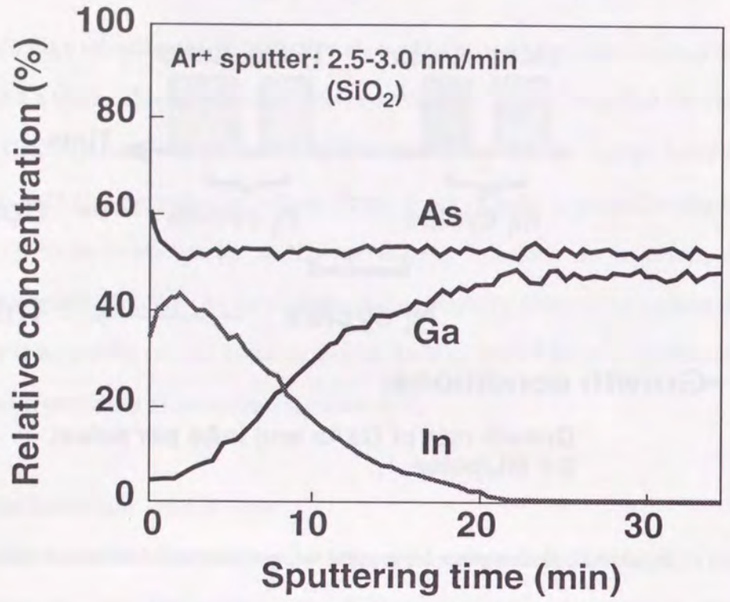

Figure 8-24. AES depth profile of InGaAs graded-layer.

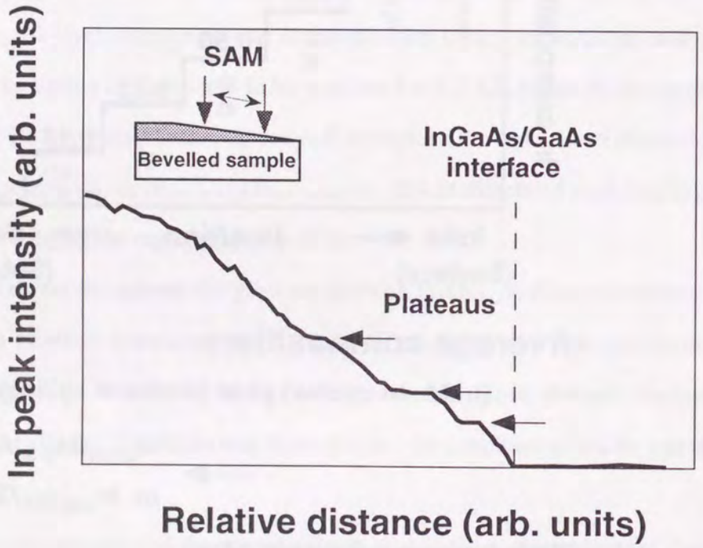

Figure 8-25. SAM profile of In for bevel-etched sample.

in Fig. 8-24. It is obvious that we obtained the compositional graded layer with our growth method of PJE. A more detailed analysis was done by scanning Auger microscope (SAM) after the sample was bevel-etched. The angle of beveling was less than 0.1° so as to detect the compositional change within a 15 to 16 nm thickness. The change of In composition is shown in Fig. 8-25. We can observe the step-like feature of In composition in our sample. Thus, our scheme for growing the composition graded layer was conducted in a controlled manner.

We evaluated the specific contact resistance of the grown layer using a transmission line method (TLM) [52]. The contact metal was 10 nm Ti/ 90 nm Pt/ 200 nm Au. The width of the contact metal was 100 μm and the distance between each metal contact was changed from 2 to 40 μm. The measured sheet resistance was 170 Ω/squares and the specific contact resistance, ρc, was in the range 10^{-7} to 10^{-8} Ωcm^2. This result indicates that the PJE is a very promising method for forming the compositional graded non-alloyed ohmic layer.

8.4.2.2 GaAs selective regrowth layer

As an application of the selective growth of GaAs, we tried to regrow low-resistance nonalloyed ohmic contact layers on the processed substrates. The formation of the contact layer using selective epitaxy is an attractive way to make high-performance transistors with small gate lengths. The band alignment corresponding to the highly doped GaAs is shown in Fig. 8-21 (a). Some researchers have reported the results obtained by MOVPE and ALE [53, 54]. To realize this method, a high-concentration doping and low growth temperatures are advantageous. PJE has merits also in these points as previously mentioned.

Figure 8-26 shows the structure we used to evaluate the contact resistance. The initial epilayer was grown by MBE on a semi-insulating GaAs (001) substrate, doped with Si to about $10^{18}cm^{-3}$. Boron (B) was implanted to isolate the epilayer into several sections. Then, a patterned SiON film was formed on the surface using plasma deposition followed by reactive ion etching. The Se-doped GaAs layer with a thickness of 100 nm was selectively regrown at 500°C by PJE. We used the growth condition giving $n=1x10^{19}$ cm^{-3}. Changing the distance L, between a pair of openings in the SiON mask from 5 to 20 μm, we measured the specific contact resistance, ρc, based on the TLM. We used evaporated AuGe/Au as the contact metal. A

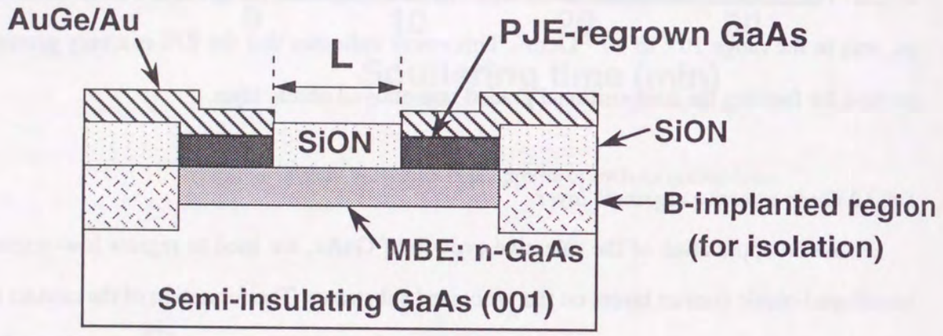

Figure 8-26. Sample structure for evaluating specific contact resistance, ρ_c. The Se-doped GaAs was selectively regrown by PJE on a patterned n-GaAs layer.

specific contact resistance of as low as $2x10^{-6}$ Ωcm^2 was obtained from TLM measurements without any thermal treatment. This value is quite promising for application in the conventional MESFETs.

8.5 Summary

We have reported three major factors of PJE in terms of the application to device processes. First, we showed the significant thickness uniformity and interface controllability of PJE. We grew a GaAs epitaxial layer with excellent uniformity within 1.5% on a 2-inch wafer. We successfully grew InAs/InP and GaAs/GaP short-period strained-layer superlattices which we could barely fabricate using other growth techniques. Second, making use of the low-temperature growth and heavy doping for PJE-grown $In_{0.53}Ga_{0.47}As$, we made the $In_{0.53}Ga_{0.47}As$/InP HBT structures by a novel PJE/MOVPE hybrid growth process. The performance of the fabricated HBT was fairly good, implying the possibility of a practical use for this new process. Finally, the selectively grown GaAs showed good results in PJE. We didn't observe any undesired deposits on the mask surface. The uniform growth occurred even at the narrow openings with submicron width. Moreover, we formed a nonalloyed contact layer using the selective regrowth of GaAs. The measured specific contact resistivity was low enough to be of use in a conventional MESFET. Through these studies, we found that the PJE is useful for some special applications in device fabrication.

REFERENCES (Chap. 8)

[1] T. Suntola, and M.J. Antson, Finnish Patent No. 52359 (1974) and US Patent No. 4058430 (1977).

[2] L. Niinistö and M. Leskela, Thin Solid Films **225** (1993) 130.

[3] S.P. DenBarrs, C.A. Beyler, A. Hariz, and P.D. Dapkus, Appl. Phys. Lett. **51** (1987) 1530.

[4] M. Hashemi, J. Ramdani, B.T. McDermott, K. Reid, and S.M. Bedair, Appl. Phys. Lett. **56** (1991) 964.

[5] A.C. Seabaugh, J.H. Luscombe, J.N. Randall, P.C. Colter, A. Dip, G.M. Eldallal, and S.M. Bedair, Thin Solid Films **225** (1993) 99.

[6] Y. Sakuma, M. Ozeki, N. Ohtsuka, Y. Matsumiya, H. Shigematsu, O. Ueda, S. Muto, K. Nakajima, and N. Yokoyama, Appl. Surf. Sci. **82/83** (1994) 46.

[7] M. Ozeki, K. Mochizuki, N. Ohtsuka, and K. Kodama, Appl. Phys. Lett. **53** (1988) 1509.

[8] M. Ozeki, K. Mochizuki, N. Ohtsuka, and K. Kodama, Thin Solid Films **174** (1989) 63.

[9] Y. Sakuma, K. Kodama, and M. Ozeki, Appl. Phys. Lett. **56** (1990) 827.

[10] Y. Sakuma, K. Kodama, and M. Ozeki, Jpn. J. Appl. Phys. **27** (1988) L2189.

[11] Y. Sakuma, M. Ozeki, and K. Nakajima, J. Cryst. Growth **130** (1993) 147.

[12] Y. Sakuma, M. Ozeki, K. Kodama, and N. Ohtsuka, J. Cryst. Growth **115** (1991) 324.

[13] M. Ozeki, K. Kodama, Y. Sakuma, N. Ohtsuka and T. Takanohashi, J. Vac. Sci. Technol. **B8** (1990) 741.

[14] O. Ueda, M. Ozeki, and T. Nakamura, Inst. Phys. Conf. Ser. **129** (1993) 405.

[15] K. Kodama, M. Ozeki, Y. Sakuma, and N. Ohtsuka, J. Appl. Phys. **69** (1991) 6713.

[16] T. Takanohashi and M. Ozeki, Jpn. J. Appl. Phys. **30** (1991) L956.

[17] T. Takanohashi and M. Ozeki, J. Appl. Phys. **71** (1992) 5614.

[18] R. G. Dandrea and A. Zunger, Appl. Phys. Lett. **57** (1990) 1031.

[19] Y. Horikoshi, M. Kawashima and H. Yamaguchi, Jpn. J. Appl. Phys. **25** (1986) L868.

[20] G.B. Stringfellow, J. Cryst. Growth **75** (1986) 91.

[21] T. Takanohashi, K. Mochizuki, and M. Ozeki, Inst. Phys. Conf. Ser. **106** (1990) 39.

[22] E. Tokumitsu, Y. Kudou, M. Konagai, and K. Takahashi, Jpn. J. Appl. Phys. **24** (1985) 1189.

[23] M. Weyers, N. Pütz, H. Heinecke, M. Heyen, H. Lüth, and P. Balk, J. Electron. Mater. **15** (1986) 57.

[24] C.R. Abernathy, S.J. Pearton, R. Caruso, F. Ren, and J. Kovalchik, Appl. Phys. Lett. **55** (1989) 1750.

[25] T.P. Chin, P.D. Kirchner, J.M. Woodall, and C.W. Tu, Appl. Phys. Lett. **59** (1991) 2865.

[26] S.A. Stockman, A.W. Hanson, S.M. Lichtenthal, M.T. Fresina, G.E. Hofler, K.C. Hsieh, and G.E. Stillman, J. Electron. Mater. **21** (1992) 1111.

[27] R.A. Hamm, M.B. Panish, R.N. Nottenburg, Y.K. Chen, and D.A. Humphrey, Appl. Phys. Lett. **54** (1989) 2586.

[28] Y. Sakuma, M. Ozeki, K. Kodama and N. Ohtsuka, J. Cryst. Growth **114** (1991) 31.

[29] N. Ohtsuka, K. Kodama, M. Ozeki, Y. Sakuma, J. Cryst. Growth **115** (1991) 460.

[30] J.D. Parsons, L.S. Lichtmann, F.G. Krajenbrink, and D.W. Brown, J. Cryst. Growth **77** (1986) 32.

[31] J. Nishizawa, H. Abe, and T. Kurabayashi, J. Electrochem. Soc. **136** (1989) 478.

[32] S. Tsukamoto, Y. Nagamune, M. Nishioka and Y. Arakawa, J. Appl. Phys. **71** (1992) 533.

[33] T. Fukui, S. Ando, Y. Tokura and T. Toriyama, Appl. Phys. Lett. **58** (1991) 2018.

[34] N. Vodjdani, M. Erman, and J.B. Theeten, J. Cryst. Growth **71** (1985) 141.

[35] K. Kamon, S. Takagishi, and H. Mori, J. Cryst. Growth **73** (1985) 73.

[36] E. Tokumitsu, Y. Kudou, M. Konagai, and K. Takahashi, J. Appl. Phys. **55** (1984) 3163.

[37] J. Nishizawa, H. Abe, and T. Kurabayashi, J. Electrochem. Soc. **132** (1985) 1197.

[38] Y. Sakuma, S. Muto, and N. Yokoyama, IEICE Trans. Electron. **E77-C** (1994) 1414.

[39] K. Hiriuma, T. Haga and M. Miyazaki, J. Cryst. Growth **102** (1990) 717.

[40] Y. Sakuma, S. Muto, K. Nakajima, and N. Yokoyama, Appl. Surf. Sci. **82/83** (1994) 239.

[41] F. J. Lamelas, P. H. Fuoss, P. Imperatori, D. W. Kisker, G. B. Stephenson, S. Brennan, Appl. Phys. Lett. **60** (1992) 2610.

[42] I. Kamiya, D. E. Aspnes, H. Tanaka, L. T. Florez, J. P. Harbison and R. Bhat, Phys. Rev. Lett. **8** (1992) 627.

[43] O. Kayser, J. Cryst. Growth **107** (1991) 989.

[44] Y. Matsumiya, Y. Sakuma, H. Shigematsu, O. Ueda, N. Yokoyama and K. Nakajima, in: Extended Abstracts of the 1993 International Conference on Solid State Devices and Materials, Makuhari (1993) 718.

[45] M. B. Panish, R. A. Hamm, D. Ritter, H. S. Luftman and C. M. Cottel, J. Cryst. Growth **112** (1991) 343.

[46] H. Shigematsu, H. Yamada, Y. Matsumiya, Y. Sakuma, H. Ohnishi, O. Ueda, T. Fujii, K. Nakajima and N. Yokoyama, in: Proc. 20th Int. Symp. on GaAs and Related Compounds (1993) 153.

[47] H. Shigematsu, T. Iwai, Y. Matsumiya, H. Ohnishi, O. Ueda, and T. Fujii, IEEE Electron Device Lett. **16** (1995) 55.

[48] T. Nittono, H. Ito, O. Nakajima, and T. Ishibashi, Jpn. J. Appl. Phys. **25** (1986) L865.

[49] T. Nittono, H. Ito, O. Nakajima, and T. Ishibashi, Jpn. J. Appl. Phys. **27** (1988) 1718.

[50] J.M. Woodall, J.L. Freeouf, G.D. Pettit, T. Jackson, and P. Kirchner, J. Vac. Sci. Technol. **19** (1981) 626.

[51] S.L. Wright, R.F. Marks, S. Tiwari, T.N. Jackson, and H. Baratte, Appl. Phys. Lett. **49** (1986) 1545.

[52] H.H. Berger, Solid-State Electron. **15** (1972) 145.

[53] A. Palevski, P. Solomon, T. F. Kuech and M. A. Tishler, Appl. Phys. Lett. **56** (1990) 171.

[54] M. M. Hashemi, F. E. Najjar, B. McDermott, J. S. Hills, L. Maynard, U. K. Mishra, J. R. Hauser and S. M. Bedair, J. Electron. Mater. **22** (1993) 179.

CHAPTER 9
Conclusions

Since the mid-1980s, there has been a trend toward the development of novel methods of growing III-V compound semiconductors in an atomically controlled fashion. Atomic layer epitaxy (ALE) is one of the candidates because it enables us to grow epitaxial layers in a self-limiting manner. We developed the pulsed-jet epitaxy (PJE) technique, which is an ALE variant, by modifying the low-pressure metalorganic vapor phase epitaxy (MOVPE). In this thesis, I have summarized our works on the PJE growth of III-V compounds in terms of both growth technology and the growth mechanism. The conclusions in each chapter are as follows.

In Chapter 1, the background and the purpose of our study were explained. First, to clarify the technological importance of ALE or PJE, the limitations and disadvantages of the well known previous techniques such as liquid-phase epitaxy, chloride or hydride vapor-phase epitaxy, MOVPE, and molecular beam epitaxy were discussed. Then, the principles of ALE and the self-limiting growth were revealed. To date, several methods have been proposed and demonstrated to achieve the clear self-limiting growth. I explained these reported ALE methods and revealed the inevitable problems in each method.

In Chapter 2, the fundamentals of PJE was reported. After explaining the PJE definition, the requirements for the distinct self-limiting were described in terms of the growth conditions and the growth apparatus. Although PJE is based on MOVPE, achieving clear self-limiting growth is difficult under the normal MOVPE growth conditions with conventional machines. It was clarified that the adopting of a fast gas stream in the reactor is indispensable for the self-limiting because it suppresses the gas-phase decomposition of group-III precursors. Special attention has to be paid to the design of reactors and the gas switching valves to ensure the laminar flow and to make the abruptly-switched gas pulses. I revealed that there exist some inherent advantages in PJE compared with other reported methods of ALE.

In Chapter 3, first, the results on the self-limiting homoepitaxial growth were shown for several III-V binary compounds: (001)-oriented GaAs, GaP, InP, and InAs. The experimental

results were compared between the horizontal reactor and the chimney reactor. I found several undesired, inevitable problems leading to the narrow "ALE window" in the horizontal configuration. Conversely, it was clarified that the chimney reactor is beneficial to achieving self-limiting over a wide rage of growth conditions due to the fast gas switching with laminar flow. Then, I showed the crystallographic dependence of the growth rates for GaAs and InP. In these results, it was shown that there exist several novel phenomena which imply the strong influence of surface As and P on the PJE growth kinetics. Furthermore, some electrical and optical properties of the PJE-grown GaAs epitaxial layers were shown. It was clarified that PJE allows us to grow high purity epitaxial layers under optimum growth conditions.

In Chapter 4, I explained the self-limiting growth mechanism. *In-situ* examination on the TMGa-exposed (or TMIn-exposed) growth surface using XPS revealed that the surface adsorbates causing the self-limiting are atomic Ga (or In). From the XPS experiments, a "selective-adsorption model" was deduced to explain the self-limiting growth process. With the rate equations based on the selective adsorption model, it was shown that GaAs growth kinetics can be well described. Furthermore, I reported growth experiments which strongly support the justice of the selective adsorption model.

In Chapter 5, the role of group-III precursors in the self-limiting growth was explained. As the Ga precursors, I employed TMGa, TEGa, EDMGa, TiBGa, and $GaCl_3$ and studied whether the growth is self-limiting. Although clear self-limiting was observed only with TMGa source, I found that the chemical ligands of Ga precursors have a significant effect on the selective adsorption and decomposition at the surface As atoms on the growth surface. A method to evaluate the site selectivity of Ga precursors at the surface lattice sites was proposed and it was shown that the degree of site selectivity of precursors is in good agreement with the tendency toward the self-limiting. The precursors' site selectivity in the chemical reactions at the surface was discussed from the viewpoint of the Lewis acid-base reaction and the polarization of both source molecules and GaAs crystal. Lastly, some novel approaches to achieving the self-limiting GaAs growth was reported. One is the use of TMGa and TEGa combination to deposit Ga. The other is the method to add CCl_4 after Ga deposition with TEGa over a monolayer coverage. I showed that these approaches have the possibility of attaining the self-

limiting at lower growth temperatures and in obtaining highly pure epitaxial layers over a wide range of growth conditions.

In Chapter 6, it was clarified that the growth rate during PJE is strongly affected by the adsorption and desorption of group-V atoms at the surface. First, the As or P desorption problem from InAs, GaAs and InP (001) surface was shown. It was found that, for the first time, the growth rate decreases when the H_2 purge time after supplying hydrides (AsH_3 and PH_3) increases. Conversely, the growth rate did not change by increasing the H_2 purge time after group-III metalorganics. This desorption of group-V atoms from the surface is derived from the PJE's gas sequence having a period without group-V overpressures. It was clarified that the only way to prevent the desorption of surface group-V atoms is to shorten the H_2 purge time period. Next, another important experimental fact was reported on GaAs (001) that the saturated growth rate during PJE slightly increases up to 1.2-1.3 ML/cycle with a sufficient AsH_3 supply. Results imply that adsorbed As atoms in excess of 1 ML exist on the growth surface and these also react with TMGa which leads to the growth rate of 1.2-1.3 ML/cycle. Similar problems related to As adsorption and desorption were observed on the substrates of other orientations: (011), (111)A, and (111)B GaAs. The experimental results were explained in terms of surface reconstructed structures and their surface stoichiometry. It was shown that the growth rate variations caused by the adsorption and desorption of group-V atoms are consistently explained by several reported surface reconstructions in an ultra-high vacuum (UHV) environment and the phase transition among them.

In Chapter 7, some experimental results on heteroepitaxial growth using PJE were shown. First, the heteroepitaxy of PJE between binary compounds were examined, where the thickness of epitaxial layer was beyond the so-called "critical thickness". I systematically studied how the self-limiting behavior is affected by the lattice mismatch and by the difference in surface free energy between the substrates and epitaxial layers. Next, the heteroepitaxy of ternary materials, such as InGaP and InGaAs, were studied. Unlike the simple homoepitaxial growth of binary materials, several novel phenomena were observed: In segregation toward surface due to immisibility of In and Ga, and compositional latching. These complicated phenomena seem to be derived from the surface strain due to the lattice mismatch between the

epitaxial layers and substrates. In spite of the complicated reactions at the surfaces and heterointerfaces, I succeeded in the growth of short-period superlattices for (InAs)(InP), (GaAs)(GaP), and ($In_xGa_{1-x}As$)(GaAs) systems. Thus, it was shown that PJE is a powerful method of obtaining atomically controlled heterointerfaces.

In Chapter 8, some applications of PJE to device processes were reported. First, the results on the significant thickness uniformity and interface controllability of PJE were shown. I was able to grow a GaAs epitaxial layer with excellent uniformity within 1.5% on a 2-inch wafer. I successfully grew InAs/InP and GaAs/GaP short-period strained-layer superlattices with good reproducibility. Second, making use of the low-temperature growth and heavy doping for PJE-grown $In_{0.53}Ga_{0.47}As$, $In_{0.53}Ga_{0.47}As$/InP heterojunction bipolar transistor (HBT) structures were grown by a novel PJE/MOVPE hybrid growth process. The performance of the fabricated HBT was fairly good, implying the possibility of a practical use for this new process. Finally, the selectively grown GaAs showed good results in PJE. Any undesired deposits were not observed on the mask surface. The uniform growth occurred even at the narrow openings with submicron width. Moreover, a nonalloyed contact layer was grown using the selective regrowth of GaAs. The measured specific contact resistivity was low enough to be of use in a conventional metal-semiconductor field effect transistor (MESFET). Through these results, it was shown that the PJE has some advantages in applying to the practical device fabrication.

Next, I'd like to consider some remaining problems. Solving these problems is important in making the PJE (or ALE) technique practical for use in the near future, as well as from a scientific viewpoint. I comment on the four items.

(1) From the technical point of view, it is essentially important to research and develop several kinds of new group-III precursors which provide the self-limited deposition. At present, there are severe problems of the narrow ALE window in the growth temperature range, of obtaining high pure epitaxial layers, and of the long gas sequence per cycle leading to a slow growth rate. If we eliminate the limitation of precursor variations, these bottlenecks will be less severe. Developing a growth technique to achieve self-limiting, which is based on the novel principle, is also an important subject to study.

(2) There is no guiding principle for the way to grow ternary or quaternary materials in a self-limiting manner. As described in the text, the segregation, islanding, and exchange reactions at interfaces are sometimes observed. A deep understanding of the mechanism of these phenomena is needed to establish the distinct self-limiting process for the alloy systems.

(3) The saturated growth thickness per cycle is related to the surface reconstructed structures and the surface stoichiometry. As a result, I believe that the self-limited growth rate does not always become 1 ML/cycle. Therefore, the control of structures of substrate's surface is also very important. An examination of the surface atomic structures, for example using scanning tunneling microscopy, will help us understand the self-limiting in more detail. Moreover, there is little information on the active surface reaction sites and the function of surface steps and kinks for the self-limiting growth at present. Research into these areas will also be necessary.

(4) More basic studies are needed to understand the self-limiting process and the surface chemical reaction more deeply. One is the study of the interaction between precursors and surface atoms, for example, using time resolved mass spectroscopy. The analyses on the residence time of molecules at the surface, their decomposition time constant and the products will elucidate the surface chemical reactions. The other is the study of the dynamical process of adsorbed atoms at the growth surface. It is interesting to know how the surface migration process of adatoms affects the self-limiting reactions.

I believe that studies into the above items will unveil the growth mechanism and help us develop the self-limiting process.

At the end of this thesis, I'd like to comment on the prospects for the future applications of the self-limiting process. As shown in the text, it is easy to control the thickness of the films even at extremely thin levels due to the self-regulated nature of the process. This enables us to grow the complicated structures needed for advanced electronic and optoelectronic applications such as heterojunction devices. A few examples using III-V semiconductors were shown in this thesis. In addition to the matrices, the doping process can be accurately controlled in a self-limiting manner. There is a possibility of controlling the occupied lattice sites by the dopant

atoms if the adsorption of dopants occurs in a manner showing well-defined surface reconstruction. One of the promising applications is for the metal-oxide-semiconductor (MOS) FET. To improve the characteristics of the MOSFET with small dimensions, it is essential to make highly-doped, ultra-shallow source/drain junctions. The random distribution of the dopants at the channel region is also a severe problem in a short-gate MOS structure, because it leads to the collapse of the reproducibility in transistor characteristics. ALE or PJE could possibly offer a breakthrough in making the source/drain junctions and in controlling the potential fluctuation for carriers induced by the random dopant distribution. Another application is in multilayered structures, such as Bragg reflectors for surface emitting optical devices. Multilayered X-ray mirrors are also a good target. In these structures, the extremely accurate film thicknesses and their periodicity is a key to the high reflectivity. Moreover, the ALE or PJE technique will be applicable to depositing some kinds of ultrathin insulating films such as SiO_2, Si_3N_4, and Al_2O_3. These materials are indispensable not only for high-performance capacitors but to the tunneling barriers of superconducting devices or recent single electron devices. ALE (PJE) will help us make these films with high uniformity and reproducibility.

Thus, there seem to be a lot of fields where the self-limiting process should be used. To make the ALE (PJE) applications real in the 21st century, we have to continue to expand the variety of the materials and develop appropriate growth techniques for them.

List of Publications and Presentations

*Papers (*Letter)*

1.* Y. Sakuma, K. Kodama, and M. Ozeki, *"Self-Limited Growth in InP Epitaxy by Alternate Gas Supply"*, Jpn. J. Appl. Phys. **27**, pp. L2189-L2191 (1988).

2.* Y. Sakuma, K. Kodama, and M. Ozeki, *"Atomic Layer Epitaxy of GaP and Elucidation for Self-Limiting Mechanism"*, Appl. Phys. Lett. **56**, pp. 827-829 (1990).

3. Y. Sakuma, M. Ozeki, N. Ohtsuka, and K. Kodama, *"Comparative Study of Self-Limiting Growth of GaAs using Different Ga-Alkyl Compounds: $(CH_3)_3Ga$, $C_2H_5(CH_3)_2Ga$, and $(C_2H_5)_3Ga$"*, J. Appl. Phys. **68**, pp. 5660-5664 (1990).

4. Y. Sakuma, M. Ozeki, K. Kodama, and N. Ohtsuka, *"Role of Interface Strain in Atomic Layer Epitaxy Growth Kinetics of $In_xGa_{1-x}As$"*, J. Cryst. Growth **114**, pp. 31-37 (1991).

5. Y. Sakuma, M. Ozeki, K. Kodama, and N. Ohtsuka, *"InAs/InP Short-Period Strained-Layer Superlattices Grown by Atomic Layer Epitaxy"*, J. Crystal Growth **115**, pp. 324-327 (1991).

6. Y. Sakuma, M. Ozeki, and K. Nakajima, *"Arsenic Desorption from the InAs (001) Growth Surface during Atomic Layer Epitaxy"*, J. Crystal Growth **130**, pp. 147-152 (1993).

7. Y. Sakuma, S. Muto, and N. Yokoyama, *"Selective Growth of GaAs by Pulsed-Jet Epitaxy"*, IEICE Trans. Electron. **E77-C**, pp. 1414-1419 (1994).

8. Y. Sakuma, M. Ozeki, N. Ohtsuka, Y. Matsumiya, H. Shigematsu, O. Ueda, S. Muto, K. Nakajima, and N. Yokoyama, *"Pulsed-jet Epitaxy: Application to Device Processes"*, Appl. Surf. Sci. **82/83**, pp. 46-56 (1994).

9. Y. Sakuma, S. Muto, K. Nakajima, and N. Yokoyama, *"A Solution to the Surface Arsenic Stoichiometric Problem at the GaAs (001) Growth Surface in Atomic Layer Epitaxy"*, Appl. Surf. Sci. **82/83**, pp. 239-249 (1994).

10. K. Kodama, M. Ozeki, Y. Sakuma, K. Mochizuki, and N. Ohtsuka, *"In Situ X-ray Photoelectron Spectroscopy for Atomic Layer Epitaxy of InP and AlAs"*, J. Crystal Growth **99**, pp. 535-539 (1990).

11. M. Ozeki, K. Kodama, Y. Sakuma, N. Ohtsuka, and T. Takanohashi, *"GaAs/GaP Strained-Layer Superlattices Grown by Atomic Layer Epitaxy"*, J. Vac. Sci. Technol. **B8**, pp. 741-746 (1990).

12. M. Ozeki, N. Ohtsuka, Y. Sakuma, and K. Kodama, *"Pulsed-Jet Epitaxy of III-V Compounds"*, J. Crystal Growth **107**, pp. 102-110 (1991).

13. N. Ohtsuka, K. Kodama, M. Ozeki, and Y. Sakuma, *"Extremely High Be Doping of InGaAs by Low Temperature Atomic Layer Epitaxy"*, J. Crystal Growth **115**, pp. 460-463 (1991).

14. K. Kodama, M. Ozeki, Y. Sakuma, and N. Ohtsuka, *"Raman Scattering of (GaAs)n(GaP)n Short-Period Superlattices Prepared by Pulsed Jet Epitaxy"*, J. Appl. Phys. **69**, pp. 6713-6715 (1991).

International Conferences (Proceedings)

1. Y. Sakuma, K. Kodama, and M. Ozeki, *"The Self-Limited Growth in InP Epitaxy by Alternate Gas Supply"*, The 20th International Conference on Solid State Devices and Materials, August, Tokyo, 1988; in Ext. Abst. of 20th Conference on SSDM, Tokyo, pp. 367-370 (1988).

2. Y. Sakuma, K. Kodama, M. Ozeki, and K. Mochizuki, *"Atomic Layer Epitaxy of GaP and InP, and Application to Heterostructures"*, The 31st Electronic Materials Conference, Boston, June, 1989.

3. M. Ozeki, K. Mochizuki, Y. Sakuma, N. Ohtsuka, and K. Kodama, *"Atomic Layer Epitaxy of III-V Compounds by Metalorganic and Hydride Sources"*, Int. Symp. GaAs and Related Compounds, Karuizawa, 1989; in Inst. Phys. Conf. Ser. **No. 106**: Chap. 2, pp. 31-38 (1989).

4. M. Ozeki, Y. Sakuma, K. Kodama, N. Ohtsuka, and T. Takanohashi, *"Growth Kinetics in Heteroepitaxy of III-V Compounds by Atomic Layer Epitaxy: GaAs/GaP SLS"*, Acta Polytechnica Scandinavica (Proc. of 1st Int. Symp. on Atomic Layer Epitaxy, ed. by Layri Ninisto), pp. 131-138, (1990).

5. K. Kodama, M. Ozeki, Y. Sakuma, and N. Ohtsuka, *"Growth Kinetics in Atomic Layer Epitaxy of III-V Compounds Using Metalorganic and Hydride Sources"*, Acta Polytechnica Scandinavica (Proc. of 1st Int. Symp. on Atomic Layer Epitaxy, ed. by Layri Ninisto), pp. 115-122, (1990).

6. Y. Sakuma, N. Ohtsuka, M. Ozeki, and K. Kodama, *"High Be Doping of $In_{0.53}Ga_{0.47}As$ Grown by Atomic Layer Epitaxy"*, 5th Workshop on Metalorganic Vapor Phase Epitaxy, Panama City, April, 1991.

7. Y. Sakuma, M. Ozeki, K. Kodama, and N. Ohtsuka, *"InAs/InP Short-Period Strained-Layer Superlattices Grown by Atomic Layer Epitaxy"*, The 7th International Conference on Vapor Growth and Epitaxy, Nagoya, July, 1991.

8. Y. Sakuma, M. Ozeki, O. Ueda, T. Ashino, and K. Nakajima, *"Fabrication of Atomically Abrupt InAs/InP Heterointerface by Atomic Layer Epitaxy, and Application to Strained-Layer Superlattices and Quantum Well Structures"*, 1st International Workshop on Quantum Functional Devices, Nasu Heights, May, 1992.

9. O. Ueda, Y. Sakuma, M. Ozeki, N. Ohtsuka, and K. Nakajima, *"High-Resolution TEM Evaluation of InAs/InP Strained Layer Superlattices Grown on InAs (001) Substrates by*

Atomic Layer Epitaxy", 11th Record of Alloy Semiconductor Physics and Electronics Symposium, pp. 463-470 (1992).

10. Y. Sakuma, M. Ozeki, O. Ueda, T. Ashino, *"Fabrication of Atomically-Controlled InAs/InP Hetero-Interface by Atomic Layer Epitaxy"*, The 3rd IUMRS International Conference on Advanced Materials, Tokyo, September, 1993; in Advanced Materials '93, VI/ Trans. Mat. Res. Soc. Jpn. **19A**, pp. 157-161 (1994).

11. Y. Sakuma, S. Muto, and K. Nakajima, *"A Study of Arsenic Adsorption and Desorption at GaAs(001) Growth Surface by Atomic Layer Epitaxy"*, 1st International Symposium on Control of Semiconductor Interfaces, Karuizawa, November, 1993.

12. O. Ueda, Y. Sakuma, M. Ozeki, N. Ohtsuka, K. Nakajima, *"High-Resolution TEM Evaluation of InAs/InP Strained Layer Superlattices Grown on (001) InAs Substrates by Atomic Layer Epitaxy"*, 1st International Symposium on Control of Semiconductor Interfaces, Karuizawa, November, 1993; in Proceedings of 1st ISCSI, pp. 531-536 (1993).

13. Y. Matsumiya, Y. Sakuma, H. Shigematsu, O. Ueda, N. Yokoyama, and K. Nakajima, *"A Novel Approach for the Fabrication of Highly Stable Be-Doped InGaAs/InP HBTs by ALE/MOVPE Hybrid Process"*, International Conference on Solid State Devices and Materials, Chiba, 1993; in Ext. Abst. of the 1993 International Conference on SSDM, pp. 718-720 (1993).

14. H. Shigematsu, H. Yamada, Y. Matsumiya, Y. Sakuma, H. Ohnishi, O. Ueda, T. Fujii, K. Nakajima and N. Yokoyama, *"ALE/MOCVD Grown InP/InGaAs HBTs with a Highly-Be-Doped Base Layer and Suppressed Diffusion"*, 20th Int. Symp. GaAs and Related Compounds, Freiburg, 1993; in Inst. Phys. Conf. Ser. **No. 136**: Chap. 3, pp. 153-158 (1993).

15. Y. Sakuma, M. Ozeki, N. Ohtsuka, Y. Matsumiya, H. Shigematsu, O. Ueda, S. Muto, K. Nakajima, and N. Yokoyama, *"Pulsed-jet Epitaxy: Application to Device Processes"*, 3rd International Symposium on Atomic Layer Epitaxy and Related Surface Processes, Sendai, May, 1994.

16. Y. Sakuma, S. Muto, K. Nakajima, and N. Yokoyama, *"A Solution to the Surface Arsenic Stoichiometric Problem at the GaAs (001) Growth Surface in Atomic Layer Epitaxy"*, 3rd International Symposium on Atomic Layer Epitaxy and Related Surface Processes, Sendai, May, 1994.